Fluid Modeling of the Plasma-Assisted Conversion of Greenhouse Gases to Value-Added Chemicals in a Dielectric Barrier Discharge

Christophe De Bie

PROMOTOR
prof. dr. Annemie Bogaerts

Universiteit
Antwerpen

Universiteit Antwerpen

Faculteit Wetenschappen

Departement Chemie

Fluid Modeling of the Plasma-Assisted Conversion of Greenhouse Gases to Value-Added Chemicals in a Dielectric Barrier Discharge

Fluid Modellering van de plasma-geassisteerde omzetting van broeikasgassen naar chemicaliën met toegevoegde waarde in een diëlektrische barrière ontlading

---

Proefschrift voorgelegd tot het behalen van de graad van

doctor in de wetenschappen: chemie

aan de Universiteit Antwerpen te verdedigen door

Christophe DE BIE

Promotor: prof. dr. Annemie Bogaerts   Antwerpen, 2016

Dit proefschrift werd geëvalueerd door de promotor, de voorzitter en de leden van de doctoraatsjury.

Promotor: prof. dr. Annemie Bogaerts (Universiteit Antwerpen)

Voorzitter: prof. dr. Pegie Cool (Universiteit Antwerpen)

Jury: prof. dr. Erik Neyts (Universiteit Antwerpen)

            prof. dr. Vera Meynen (Universiteit Antwerpen)

            dr. ir. Sabine Paulussen (VITO)

            dr. ir. Jan van Dijk (Technische Universiteit Eindhoven)

            prof. dr. ir. Gerard van Rooij (DIFFER)

Table of Contents

Chapter 1

Introduction

Socially, environmentally and economically a growing demand is being imposed for sustainability in the way energy resources are utilized. A global sustainable energy strategy that meets the increasing demand is based on an improvement of the energy efficiency of the current technologies and a more intensifying diversification of the energy resources with a huge preference for lower carbon resources.

1.1. Global Energy Demand

In 1974 the International Energy Agency (IEA) was established to promote energy security amongst its member countries (Belgium is a founding member) through collective response to physical disruptions in oil supply, and to provide authoritative research and analysis on ways to ensure reliable, affordable and clean energy for its 29 member countries and beyond.[1] The IEA annually publishes a World Energy Outlook which presents updated projections for the evolution of the global energy system, as well as detailed insights on the prospects for fossil fuels, renewables, the power sector and energy efficiency and analysis on trends in CO_2 emissions and fossil-fuel and renewable energy subsidies. The World Energy Outlook reports of 2014[2] and 2015[3] state that the energy use worldwide is set to grow by one-third to 2040, driven primarily by India, China, Africa, the Middle East, Southeast Asia and Latin America.

Pledges made prior to the 21st Conference of the Parties to the United Nations Framework Convention on Climate Change (COP21/CMP11; November-December, 2015) indicate that future energy policy intentions should result in a boost to lower-carbon fuels and technologies worldwide. As a result it is expected that the share of non-fossil fuels will increase from 19% of the global mix today to 25% in 2040. Therefore, the world's energy supply mix will be divided into four almost-equal parts by 2040: oil, gas, coal and low-carbon sources.[3] Although the demand for all fossil fuels is still increasing, natural gas, which is the least-carbon intensive, is the only one that sees its share rise by 2040. For instance, the share of oil will decrease from 34% in 2007 to 25% in 2040 and also the future use of coal, which resources are

abundant and which supply is secure, will be constrained if the global policy is to reduce the emission of carbon dioxide.[2-4]

A similar story can be found in the 23rd edition of the World Energy Resources Survey published in 2013 by the World Energy Council.[5] Formed in 1923, the Council is the UN-accredited global energy body, representing the entire energy spectrum, with more than 3000 member organizations located in over 90 countries and drawn from governments, private and state corporations, academia, NGOs and energy-related stakeholders.[6]

Globally, fossil fuel resources are still plentiful and will last for decades, but it becomes more difficult to recover them and there can be no guarantee that they will be exploited fast enough to meet the level of demand. The availability of energy resources is, however, of paramount importance to the society. Access to reliable, affordable commercial energy provides the basis for heat, light, mobility, communications and agricultural and industrial capacity in modern society and in this way energy stipulates the degree of civilization.[7] Besides, the transition of the energy market towards lower-carbon resources, also an enhancement in energy efficiency is very important in order to limit the world energy demand.

1.2. Reducing Greenhouse Gas Emissions

Furthermore, the recovery, production and use of fossil fuels are accompanied by the emission of greenhouse gases and contribute in this way to global warming. Climate change due to anthropogenic greenhouse gas emission is a growing concern for the global society. Anthropogenic

greenhouse gas emissions have increased since the pre-industrial era and have led to atmospheric concentrations of carbon dioxide (CO_2), methane (CH_4) and nitrous oxide (N_2O) that are unprecedented in at least the last 800,000 years. It is extremely likely that these greenhouse gas emissions have been the dominant cause of the observed global warming since the mid-20th century.[8]

Following the Synthesis Report on Climate Change[8] published by the Intergovernmental Panel on Climate Change[9] in 2014, a new international agreement on climate change was made at the 21st Conference of the Parties to the United Nations Framework Convention on Climate Change (COP21/CMP11; November-December, 2015), to keep global warming below 2°C. At the World Economic Forum 2016 Annual Meeting in Davos, Switzerland (January 2016), this new commitment to action on climate change was pointed out as one out of 10 key global challenges that matter to the world, stated as "Climate change: can we turn words into action?". The International Council of Chemical Associations (ICCA)[10], representing chemical manufacturers all over the world, and its member organization, i.e., the European Chemical Industry Council (Cefic)[11], which is the main European trade association for the chemical industry, strongly endorsed the international efforts to reach a binding global agreement at COP21. In the last decades, the chemical industry made its efforts to reduce greenhouse gas emissions, and today the European chemical industry uses less than half the energy it used back in 1990. Thus, its greenhouse gas emissions have fallen by 54% on 1990 levels, while its production grew by 70%. ICCA and Cefic believe that the chemical industry is also a pillar of tomorrow's low-carbon economy

by developing innovative solutions, which will be crucial to combating climate change.[10-11]

1.3.   Natural Gas - Methane (CH_4)

In a world in which fossil fuels make the day, natural gas has the most significant growth potential and so it becomes more and more an interesting alternative for crude oil as feedstock for the chemical industry. Table 1 gives an overview of the benefits and drawbacks of natural gas as an energy resource. Natural gas is currently the third most used energy resource in the world after crude oil and coal,[2-3] but the lifetime of gas resources is much longer than for oil and its lower carbon content makes natural gas the cleanest of all fossil-based fuels. Therefore, natural gas will continue making significant contribution to the world energy economy as it also is a flexible fuel. However, the exploration, development and transport of gas usually require significant upfront investment. In addition to power generation, natural gas is expected to play an increasing role as a transport fuel.[5]

Table 1. The benefits and drawbacks of natural gas.

(adopted from WER 2013 Survey[5])

Benefits	Drawbacks
Cleanest of fossil fuels	Fields increasingly off-shore and in remote areas
Flexible and efficient fuel for power generation	High upfront investment requirement for transport and distribution system
Increasing proved reserves (reassessments and shale gas)	Increasingly long supply routes and high cost of infrastructure

Natural gas is a mixture of hydrocarbons, of which methane (CH_4) is the principal component. Methane, which is also an important greenhouse gas, is an odorless, colorless, non-toxic gas which is lighter than air. It is currently mainly being used for home and industrial heating and for the generation of electrical power. On the other hand, methane is a greatly underutilized resource for the production of chemicals and liquid fuels, mainly because it is one of the most stable molecules.[12] Direct synthesis of hydrocarbons starting from methane is not yet feasible and the conventional indirect methods for partial and total oxidation of methane have poor yields and require high amounts of energy.[13] The utilization of natural gas as a chemical resource is currently limited to the production of synthesis gas (i.e., syngas: H_2 + CO) by steam reforming, which is a highly energy-intensive process.[14]

A sustainable process for the conversion of the abundant methane reserves into more value-added chemicals and fuels is therefore renowned as a challenge for the 21st century.[12] More in particular, the development of a process for the direct synthesis of higher hydrocarbons and oxygenates from methane in an energy-efficient way towards economy and environment would offer significant benefits, because this will circumvent the very expensive syngas step.[15]

1.4. Carbon Dioxide (CO$_2$)

Carbon Dioxide (CO$_2$), naturally present in the atmosphere as part of the natural circulation of carbon among the atmosphere, oceans, soil, plants, and animals, and thus being a vital gas for life on earth, is the primary greenhouse gas emitted through human activities.[16] It is a very stable molecule that requires a lot of energy to be activated for the majority of synthetic routes to produce chemicals. Therefore, a first objective in the mitigation of CO$_2$ emissions is the process of Carbon Dioxide Capture and Storage (CCS), as pointed out in a special report published in 2005 by the Intergovernmental Panel on Climate Change.[17] Nowadays, it is clear that aside from the reduction of CO$_2$ emissions to the atmosphere and the use of CCS for this purpose, also the energy efficient utilization of (captured) CO$_2$, as an important carbon resource to create products, will be a crucial step in order to achieve an economically viable low-carbon economy.

In 2011 Damiani et al.[18] published a perspective concerning the United States Department of Energy's R&D program, to reduce greenhouse gas emissions through the beneficial use of CO$_2$. A vision for smart CO$_2$ transformation in Europe, enabling the European industry to become more resource-efficient, sustainable and competitive, was published in November 2015. This vision document, designed as part of the Smart CO$_2$ Transformation (SCOT) project, is a collaborative European project focused on accelerating the market development of CO$_2$ utilization and supported by funding from the European Seventh Framework program.[16] Both documents stress the potential of CO$_2$ as a carbon resource and the importance of the transition into a world where CO$_2$ is used as feedstock for making many products. Damiani et al.[18] state the benefits of CO$_2$ utilization as follows: it can generate

revenue to offset capture costs associated with CCS, it contributes to CO_2 emissions reduction, and it reduces the demand for fossil fuels. In the SCOT vision document,[16] also three main reasons are listed why Europe should focus on CO_2 utilization: (i) it can be one of the major growth areas in Europe's future low-carbon circular economy, (ii) it can help to facilitate Europe's energy transition and (iii) it can contribute to achieving Europe's aims for decreasing carbon emissions. The goal is to identify and develop a range of novel technologies that can beneficially use CO_2. It is clear from both documents that the use of CO_2 for chemical production is one of the priority research areas concerning CO_2 utilization.

Today, CO_2 utilization is mainly limited to the direct use, i.e. without a conversion step, as an inert agent for food packaging, in carbonated drinks, in refrigeration systems, in fire extinguishers, as a solvent, and for enhanced oil recovery (particularly in the United States), as well as the indirect use for the chemical production of mainly urea, a small amount of methanol and an even smaller amount of a wide variety of other products.[16-18] Ongoing research on the conversion of CO_2 in value-added chemicals is primarily focusing on the formation of carbon monoxide (CO), methanol, polymers, urea, carboxylates, carbonates, olefins, etc.[16] Figure 1 gives an overview of the use of CO_2 and the research areas supported by the United States Department of Energy. In order to convert CO_2 into products, an energy source, such as heat or electricity, or material inputs, such as fly ash, hydrogen or epoxides, is required.[16] To become of added value, it is crucial that new CO_2 utilization processes have a lower carbon footprint than their equivalent classical processes using fossil fuel routes for the production of the same product.
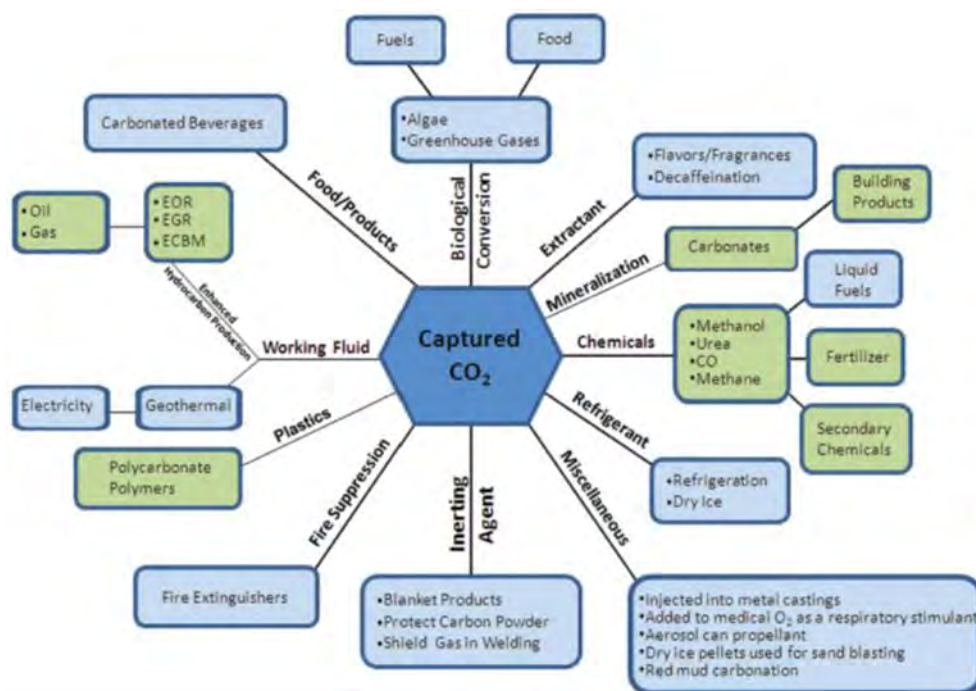
Figure 1. Overview of the use of CO_2. The research areas supported by the United States Department of Energy are shown in green.[18]

1.5. Value-Added Chemicals

The value-added chemicals of interest in this research are higher hydrocarbons, such as ethane (C_2H_6), ethylene (C_2H_4), acetylene (C_2H_2), propane (C_3H_8) and Propylene (C_3H_6), syngas, i.e., a mixture of carbon monoxide (CO) and hydrogen gas (H_2), also called synthesis gas, as well as oxygenates, such as methanol (CH_3OH) and formaldehyde (CH_2O).

C_2H_6 is mainly used in the chemical industry as a feedstock for the production of C_2H_4, which is considered as the most important feedstock in the chemical industry.[19] C_2H_4 is mainly used for the formation of polyethylenes, which are the world's most widely used plastics. Besides, it

also forms the basis for the formation of ethylene oxide, which is used in surfactants, and for the formation of ethylene glycol, which is applied as automotive antifreeze, as well as for many other applications. C_2H_2 is mainly utilized as a fuel source and as a chemical building block for the formation of ethylene and different polymerization products, which are applied in the plastic industry. C_3H_8 is the main component of liquefied petroleum gas (LPG), which is used as vehicle fuel. C_3H_6 forms the basis for the formation of polypropylene, which is typically used in the manufacturing of packaging and textiles.

Syngas is used as a fuel source or as an intermediate for the production of other chemicals. Classical processes, including steam reforming, partial oxidation and CO_2 reforming of methane, typically produce syngas with H_2/CO molar ratio greater than 3, less than 2 and less than 1, respectively.[20-21] The H_2/CO molar ratio from steam reforming (>3) is much higher than that required by the stoichiometry for many synthesis processes. A low H_2/CO molar ratio is desirable for many industrial synthesis processes, such as the Fischer Tropsch synthesis or the synthesis of valuable oxygenated chemicals. A H_2/CO ratio of about 2 is preferred for the formation of methanol out of syngas.[22] Methanol can even be produced from syngas with a H_2/CO molar ratio as low as 0.5, when the system can simultaneously carry out methanol synthesis and the water-gas-shift reaction.[20-21]

H_2 is mainly used for the processing of fossil fuels, the production of ammonia and methanol, and as fuel in fuel cells. Furthermore, it is used in the production of carbon steels, special metals and semiconductors. In the electronics industry, H_2 is employed as a reducing agent and as a carrier gas.[23]

CO is used to make a variety of chemicals such as acids, esters and alcohols, as well as for the reduction of ores and in the manufacture of metal carbonyls.[23]

Methanol is a primary liquid petrochemical, which is of great importance in the chemical and energy industries, because it can be easily stored and transported.[24] Methanol is one of the most commonly used raw materials in the chemical industry. More than one-third of it is used in the production of formaldehyde; the rest is mainly utilized to produce acetic acid and gasoline octane improvers. Additionally, the direct use of methanol as fuel in internal combustion engines and fuel cells opens up the possibility of methanol powered vehicles and consumer electronics.[25] Formaldehyde is a common building block for the synthesis of more complex compounds, which are used in a wide range of products.

Chapter 2

Plasma-Assisted Gas Conversion

The major difficulty for the direct conversion of methane and carbon dioxide into value-added chemicals is that both are very stable molecules that require a large amount of energy for activation of the stable C-H and C-O bonds, respectively. Conventional methods, which make use of a high temperature and pressure and a noble catalyst, require high amounts of energy. In the last decades, there is an increasing interest in using plasma technology for gas conversion. Atmospheric pressure non-thermal low-temperature plasmas can offer a distinct advantage, because they enable in a unique way gas phase reactions at ambient conditions.

2.1. What is a Plasma?

Plasmas are ionized gases. Hence, they consist of positive (and negative) ions and electrons, as well as neutral species. The ionization degree can vary from 100% (fully ionized gases) to very low values (e.g. 10^{-4}–10^{-6}; partially ionized gases).[26] A plasma is generated by supplying energy to a neutral gas, causing the formation of charge carriers. The charged species are considered to be balanced in the bulk of the plasma, giving plasmas the characteristic of quasi-neutrality. These unique properties make that the plasma state is often called the 'fourth state of matter', next to solid, liquid and gas. The name `plasma' was introduced in 1929 by Irving Langmuir who chose this name, because the multi-component, strongly interacting ionized gas reminded him of blood plasma.[27]

Almost all visible matter in the universe is in the plasma state. Examples of natural plasmas are the stars, the solar wind, the earth's ionosphere, the aurora borealis and lightning. Besides these astroplasmas, two main groups of laboratory plasmas can be distinguished, i.e. the high-temperature or fusion plasmas, and the so-called low-temperature plasmas or gas discharges. A subdivision can be made between plasmas which are in thermal equilibrium and those which are not in thermal equilibrium. Thermal plasmas are characterized by the fact that the temperature of all species in the plasma is the same. High temperatures are required to form these equilibrium plasmas, typically ranging from 4000 K to 20 000 K.[26] In non-thermal plasmas the temperature of the electrons is much higher than that of the heavy particles (ions, atoms, molecules). The most commonly used method to generate and sustain a low-temperature plasma is by applying a sufficiently high electric field to a neutral gas, which partially breaks it down, turning some atoms or

molecules into positive ions and generating free electrons. These charge carriers are accelerated by the electric field, and new charged particles may be created when these charge carriers collide with gas molecules or with the electrodes. The resulting avalanche of charged particles is eventually balanced by charge carrier losses, creating a steady-state plasma.[28]

There exists a wide variety of non-thermal gas discharge plasmas, each with its own characteristics and employed in a large range of applications. Based on the temporal behavior of the sustaining electric field, gas discharges can be classified as direct current (dc), alternating current (ac) or pulsed discharges.[28] An example of a non-thermal ac discharge is the dielectric barrier discharge (DBD), which is the type of plasma under study in this dissertation and will therefore be explained in more detail in the next section. An overview of the most important gas discharge plasmas and their applications can be found in Bogaerts et al.[26] and Conrads et al.[28]. Table 2 shows the most important gas discharges along with their parameters and possible applications.

Table 2. Plasma sources and their parameters.

(modified from Conrads et al.[28])

Physics	Pressure (mbar)	n_e (cm^{-3})	T_e (eV)	Application
Dielectric barrier discharge	1000	10^{14}	5	Ozone, microelectronics, chemistry
Corona	1000	10^{13}	5	Ozone, chemistry
Microwave	10-1000	10^{13}	1-2	Chemistry, microelectronics
Spark	1000-10^4	10^{17}	1	Chemistry, water treatment
Gliding arc	1000	10^{12}-10^{17}	1	Chemistry
Nanosecond pulsed	1000	10^{12}	5	Chemistry
DC glow	10^{-3}-100			
Cathode region			100	Sputtering, deposition
Negative glow		10^{12}	0.1	Chemistry, radiation
Positive column		10^{11}	1-10	Radiation
Hollow cathode	10^{-2}-800	10^{12}	0.1	Radiation, chemistry
Magnetron	10^{-3}			Sputtering
RF capacitive	10^{-3}-10	10^{11}	1-10	Microelectronics, sputtering
RF inductive	10^{-3}-10	10^{12}	1	Microelectronics, etching
Electron beam	10^{-2}-1	10^{12}	1	Microelectronics

2.2. Dielectric Barrier Discharge

A dielectric barrier discharge (DBD) or so-called silent discharge is an electrical discharge that is generated between two electrodes of which at least one is covered with a dielectric material made of glass, quartz, alumina, etc. The gap between the two electrodes is typically a few millimeters. An ac voltage with an amplitude from 1 kV to 100 kV and a frequency of a few Hz to MHz is usually applied to this kind of discharges. Typical electrode

arrangements of planar and cylindrical DBDs are shown in Figure 2. For gas conversion purposes mostly a cylindrical reactor is used. A DBD has the advantage, unlike other non-equilibrium discharges, that it can be operated at atmospheric pressure, while remaining at ambient temperature.
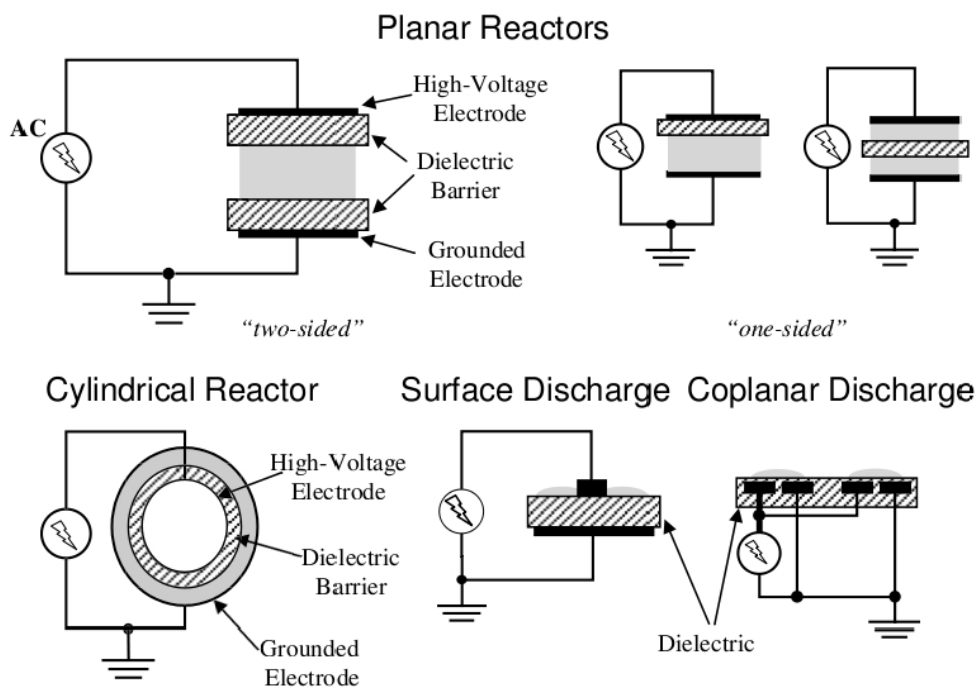
Figure 2. Typical electrode arrangements of barrier discharges.[29]

The first experimental investigations with a DBD were reported in 1857 by Werner von Siemens. The research was mainly focused on the generation of ozone by blowing air or oxygen through a narrow annular gap between two coaxial glass tubes in which a DBD was maintained by an alternating electric field of sufficient amplitude. The novelty of this setup was that the electrodes, which were made of tinfoil, were not in direct contact with the plasma, which

considerably increased their lifetime. In the following decades, ozone and nitrogen oxide formation in DBDs became an important research topic.[30]

Today, these silent discharge ozonizers are effective tools, and a large number of ozone installations based on plasma technology are being used worldwide for water treatment. DBDs are nowadays also used to pump CO_2 lasers, to generate excimer radiation in the UV and VUV spectral regions, in various thin-film deposition processes, and for plasma display panels. In recent years, DBDs are increasingly being used as reactor set-up for gas treatment or gas conversion, which is the objective of this dissertation. Detailed information on the history of a DBD and the wide variety of applications for which a DBD is used can be found in literature.[26, 28, 30-36]

2.3. Breakdown: The Initiation of Reaction Kinetics

In a DBD reactor typically operating at atmospheric pressure, a large number of short-living current filaments, so-called microdischarges, which are randomly distributed both in time and in space, appear during breakdown.[37] It can be presumed that the plasma is enclosed in the volume surrounded by these microdischarges. Three separate steps can be distinguished during the life cycle of one such filament: (i) the formation of the discharge, i.e., the electrical breakdown, (ii) the subsequent current pulse or transport of charge across the gap, and (iii) simultaneously the excitation of the atoms and molecules present, and thus the initiation of the reaction kinetics. The durations of these three steps are of different orders of magnitude. The local breakdown is usually completed within nanoseconds, the current transport takes typically 1-100 ns, while the chemistry can last from nanoseconds to

seconds.[31] Approximate time-scales for the different processes involved are given in Figure 3.

By applying an increasing voltage to the electrodes, breakdown is induced once the electric field inside the gap exceeds the corresponding reduced Paschen field of the gap. The Paschen voltage is given by the smallest constant voltage needed to initiate breakdown in the gap. This breakdown voltage depends on the gas composition and on the reactor configuration, i.e. the gas pressure and the gap width. The reduced Paschen field is obtained by dividing the Paschen voltage by the product of the gas pressure and the gap width.[31]

Each microdischarge has an almost cylindrical plasma channel and typically a diameter of the order of some 100 μm. They are usually very short-lived, on the order of 100 ns or less. Both the diameter and the duration depend upon the gas used and the pressure.[31] The number of microdischarges is proportional to the voltage applied on the electrodes.[37-38] The current flows entirely within the filaments and is limited by the dielectric barrier(s) between the electrodes. Thus, the dielectric serves a dual purpose. It limits the amount of charge and energy imparted to an individual microdischarge and, at the same time, it distributes the microdischarges over the entire electrode area. Typically the current density in the filaments is $100–1000$ A cm^{-2}, the electron density is 10^{14}-10^{15} cm^{-3}, and typical electron energies are in the range of 1-10 eV.[28, 30, 39] Typical charges transported by individual microdischarges are of the order of nC, and typical energies of the order of μJ.[40] Over long time periods, the microdischarges, which are randomly distributed by the way they are initiated, will thus evenly fill the available volume.

The exchange of energy between the accelerated electrons and the atoms and molecules occurs within the microdischarges. The fairly energetic

electrons collide with the gas molecules and excite them and thus transform some of their kinetic energy into internal energy of the gas molecules. Due to the high electron energy, this energy exchange can be very efficient. It is not unusual that 90% of the kinetic energy or more is transformed into stored energy.[31] Elastic losses are therefore very low, and initially very little energy is lost as heat.[31] The excited species formed in the microdischarge filaments can diffuse into the regions between the filaments, which are free of charged particles, and initiate the chemical reactions (see below) before the next discharge strikes at the same location. This separation of electron-producing regions and chemically active regions can be very beneficial.[39]

More information about the formation of these microdischarges and the characteristics of a DBD can be found in literature.[28, 30-31, 34, 37, 39-41]
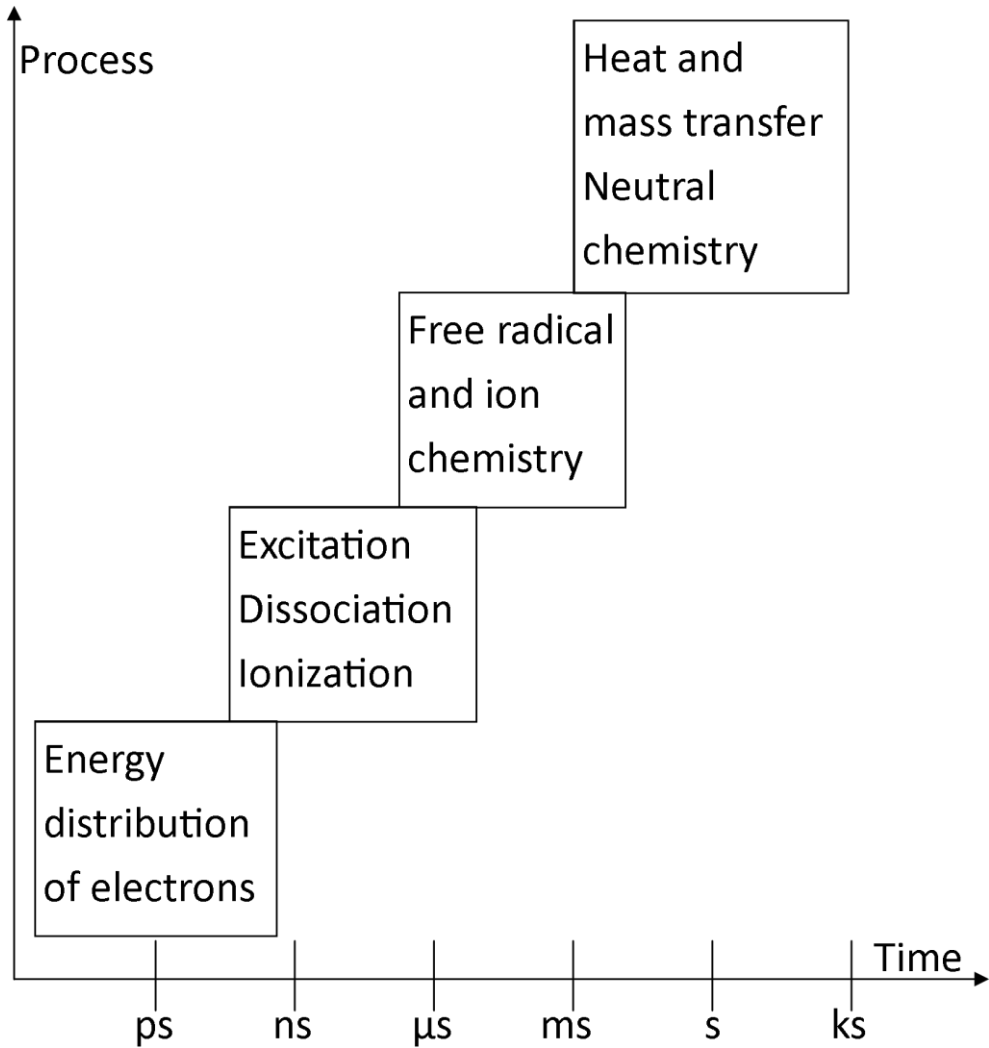
Figure 3. Time-scale of the relevant processes of a filamentary DBD.

(modified from Wagner et al.[29])

2.4. The Plasma Chemistry

The excited molecules can now, due to their high internal energy, either dissociate or initiate other reactions.[39] The main types of reactions occurring in the plasma are listed in Table 3, for an arbitrary gas (called A_2). Different plasma activation mechanisms cause vibrational and electronic excitation, as well as ionization and dissociation of species, and in this way gas conversion processes are induced. Reactive species in the discharge (free radicals, electrons, …) will cause decomposition of the molecules, initially present in the gas mixture, and afterwards recombination will lead to the formation of value-added and/or less hazardous end products. Every reaction is characterized by a few main characteristics, such as the reactants, the products, the pressure, the temperature, the heat of the reaction, and the rate coefficient.[39]

These plasma chemistry processes, taking place at atmospheric pressure and ambient temperature, make a DBD reactor of interest for the conversion of greenhouse gases to higher hydrocarbons, oxygenates and syngas. Nowadays a lot of research is carried out on the use of a DBD for the conversion of CH_4 and CO_2, as will be clear from the next chapters in this dissertation. However, there are still a lot of issues open for discussion. More specifically, a lot of research work still has to be performed with respect to improving the energy efficiency and the selectivities of the end products, in order to come to a sustainable industrial process, which is competitive with currently existing or other emerging technologies. In order to optimize such a process to become competitive, it is essential to understand the huge underlying plasma chemistry acting in the conversion processes. This is exactly the purpose of this PhD dissertation, where we try to obtain a better insight in

the plasma chemistry, by means of fluid modeling, as elaborated in the next chapter.

Table 3. Overview of the main plasma reactions for an arbitrary gas, called A_2.

(adopted from Eliasson et al.[39])

Electron/Molecular Reactions	
Excitation	$e^- + A_2 \rightarrow A_2^* + e^-$
Dissociation	$e^- + A_2 \rightarrow 2\,A + e^-$
Attachment	$e^- + A_2 \rightarrow A_2^-$
Dissociative Attachment	$e^- + A_2 \rightarrow A^- + A$
Ionization	$e^- + A_2 \rightarrow A_2^+ + 2\,e^-$
Dissociative Ionization	$e^- + A_2 \rightarrow A^+ + A + 2\,e^-$
Recombination	$e^- + A_2^+ \rightarrow A_2$
Detachment	$e^- + A_2^- \rightarrow A_2 + 2\,e^-$
Atomic/Molecular Reactions	
Penning Dissociation	$M^* + A_2 \rightarrow 2\,A + M$
Penning Ionization	$M^* + A_2 \rightarrow A_2^+ + M + e^-$
Charge Transfer	$A^\pm + B \rightarrow B^\pm + A$
Ion Recombination	$A^- + B^+ \rightarrow AB$
Neutral Recombination	$A + B + M \rightarrow AB + M$
Decomposition	
Electronic	$e^- + AB \rightarrow A + B + e^-$
Atomic	$A^* + B_2 \rightarrow AB + B$
Synthesis	
Electronic	$e^- + A \rightarrow A^* + e^-$, $A^* + B \rightarrow AB$
Atomic	$A + B \rightarrow AB$

Chapter 3

Fluid Modeling: An Insight in the Plasma Chemistry

Plasma modeling can offer the experimentalist the necessary information to understand the role of the different species in the immensity of chemical reactions taking place in the discharge gap. The aim of our research is to describe in detail the plasma chemistry in an atmospheric pressure DBD in different gas mixtures with CH_4 and/or CO_2, by means of a 1D fluid model. More information about the fluid model applied for this research can be found in this chapter.

3.1.   Motivation for Numerical Simulations

Experimental observations are the base for understanding natural phenomena. They lead to new theories and the discovery of proportionalities, which allows mathematical formulations of these theories. These descriptions can be tested and improved by additional observations up till the point where these observations become too difficult.[27] Obstacles for such observations are for example that the phenomenon happens too fast, or that the setup becomes too small or too large, or that the materials under study are very expensive or very dangerous, or that the phenomenon involves many different theoretical aspects at the same time, so that the link between theory and experiment is rather complicated.[27, 42]

Modeling or simulation of a phenomenon or experiment can offer here a solution to circumvent these issues. Models are used to theoretically interpret and predict experimental observations. In physics, the word "model" is used to indicate a system of equations, data, and assumptions, which gives a mathematical representation of all the major features of a certain physical phenomenon.[42] The equations used in the model can be solved exactly or numerically. The latter means that they have to be discretized in both space and time, so that by choosing an appropriate initial condition and by respecting the boundary conditions, the described system is recalculated again and again, so that it iteratively evolves into the desired converged solution. Both the exact and the numerical solutions of these equations have their advantages and disadvantages, but in general, numerical methods are increasingly being used, because they are able to describe enormously complex systems and they can be defined much more generally than the exact solutions.[27]

Also in the field of gas discharges and plasma technology numerical simulations are a useful tool to describe the discharge physics or the plasma chemistry. There exist various useful theoretical descriptions to describe the physics and chemistry in the gas discharges studied in this dissertation. Different possible simulation methods for this purpose, such as an analytical approach, a kinetic approach, a fluid model or a hybrid model, as well as their advantages and disadvantages, are discussed by Martens[27]. In order to describe the DBD plasma under study in this work, we decided to adopt a fluid model for the reasons given in next section.

3.2. The Fluid Approach

In a fluid model the various discharge species (electrons, molecules, radicals, ions) are described in terms of average, hydrodynamic quantities, such as density, momentum and energy.[27] The space and time variation of these quantities is described by fluid equations, which are derived by taking the velocity moments of the Boltzmann equation. The Boltzmann equation[43] describes the evolution of the density $f(\vec{r},\ \vec{v},\ t)$ of a single particle species in the phase space spanned by configuration space $\vec{r}$ and velocity space $\vec{v}$. Often the Boltzmann equation is written as:

$$\frac{\partial f}{\partial t} + \vec{v} \cdot \frac{\partial f}{\partial \vec{r}} + \vec{a} \cdot \frac{\partial f}{\partial \vec{v}} = \left(\frac{\partial f}{\partial t}\right)_c \qquad (1)$$

where $\vec{a}$ is the acceleration of the particle and $(\partial f = \partial t)_c$ is the change of the distribution function f due to collisions.[27] More detailed information on the continuity equations for density, momentum and energy obtained from the Boltzmann equation is given below. Surface processes are accounted for in

the boundary conditions of the fluid equations. Usually the fluid equations are coupled to macroscopic Maxwell equations, such as Poisson's equation, which describes the effect of space charge on the electric field. In this way, a complete, self-consistent description of the discharge is obtained. Note that the assumptions made in this approach can only be applied over a limited range of discharge conditions. Detailed information on this can be found in Hagelaar[42]. However, for the DBD under study, the fluid approach is very useful and quite reliable. A great advantage of fluid models is that they can simulate the time evolution of a discharge in one or two spatial dimensions within a manageable period of computation time, i.e., a few hours, even for a complex plasma chemistry, as illustrated in the next chapters. On the other hand, in a fluid model each type of species is considered as one group, and therefore a fluid model cannot describe the behavior of the species individually. Furthermore, it is supposed that the plasma must have a high enough density so that it resembles a continuum.[27] It is assumed that the species are more or less in equilibrium with the electric field, i.e., the energy gain due to the electric field is more or less balanced by the energy loss due to collisions, which is not always the case, e.g., for energetic electrons in a plasma. In addition, a fluid model requires input data on macroscopic properties of the species, which are based on assumptions of the particle energy distribution function.[42] Moreover it is not so easy to describe filaments in a DBD by means of a fluid model.

3.3. Plasimo's MD2D: The Fluid Model Applied

The model employed in this study is a one-dimensional fluid model, called Plasimo's MD2D.[44-45] Originally, MD2D was developed to describe the behavior of microdischarges in display technology, such as plasma addressed liquid crystal (PALC) and plasma display panel (PDP) technology.[42, 46-48] Later the model was transformed and extended by Brok and van Dijk, and incorporated into Plasimo.[49] In this way the model has previously been used for investigating the breakdown phenomena in fluorescent lamps,[49-51] the discharge characteristics of the plasma needle used for biomedical applications,[52] the behavior of DBDs at low pressure[53] and the characteristics of DBDs used as ionization source in analytical spectrochemistry.[54-56]

Analogous to other fluid models used for the description of low temperature plasmas,[43, 57-60] the MD2D fluid model is based on a set of balance equations derived from the Boltzmann transport equation (see previous section).

The first equation is the particle continuity equation, which describes the continuity of each type of species p incorporated in the model, in terms of its density n_p, flux $\vec{\Gamma}_p$ and source S_p as a function of time and space:

$$\frac{\partial n_p}{\partial t} + \vec{\nabla} \cdot \vec{\Gamma}_p = S_p \qquad\qquad (2)$$

The source term S_p is obtained by considering the volume reactions in which species p are produced or lost.

The second equation is the drift-diffusion equation, which describes the flux $\vec{\Gamma}_p$ of each type of species p by means of the summation of a drift component

(only for the charged species), driven by the electric field $\vec{E}$, and a diffusion component, caused by the gradient of the density:

$$\vec{\Gamma}_p = \pm\mu_p \vec{E} n_p - D_p \vec{\nabla} n_p \tag{3}$$

μ_p and D_p denote here the mobility and diffusion coefficient of species p.

For the electrons also the electron energy balance equation is solved. The assumption that the energy is directly related to the local electric field is not valid for electrons, because they have a much lower mass compared with the heavy particles. Electron parameters are therefore expressed as a function of the average energy $\bar{\varepsilon}$ which results from the following balance equation:

$$\frac{\partial(n_\varepsilon)}{\partial t} + \vec{\nabla} \cdot \vec{\Gamma}_{\bar{\varepsilon}} = S_{\bar{\varepsilon}} \tag{4}$$

$S_{\bar{\varepsilon}}$ is again a source term, which depends on the heating by the electric field and on the energy gained or lost in the various reactions. n_ε is the electron energy density:

$$n_\varepsilon = n_e \bar{\varepsilon} \tag{5}$$

and $\vec{\Gamma}_{\bar{\varepsilon}}$ denotes the electron energy flux:

$$\vec{\Gamma}_{\bar{\varepsilon}} = \frac{5}{3}\bar{\varepsilon}\,\vec{\Gamma}_e + q \tag{6}$$

where q is the heat flux, which is assumed to be proportional to the gradient of the electron mean energy:

$$q = -\frac{5}{3}n_e D_e \nabla \bar{\varepsilon} \tag{7}$$

Substitution of equation (7) and equation (3) for $\vec{\Gamma}_e$ transforms equation (6) into a drift-diffusion equation for the electron energy flux:

$$\vec{\Gamma}_{\bar{\varepsilon}} = -\frac{5}{3}\mu_e\vec{E}n_e\bar{\varepsilon} - \frac{5}{3}n_eD_e\vec{\nabla}\bar{\varepsilon} \qquad (8)$$

The first term is called the hydrodynamic flux of enthalpy and the second term is the heat conduction flux.

This set of partial differential equations is coupled to the Poisson equation, which delivers the electric field distribution:

$$\vec{\nabla} \cdot \left(\varepsilon_m\vec{\nabla}\varphi\right) = -\vec{\nabla} \cdot \left(\varepsilon_m\vec{E}\right) = -\sum_p q_p n_p \qquad (9)$$

φ is here the electric potential as a function of time and space, ε_m is the permittivity of the medium (i.e. the plasma and the dielectrics) and q_p is the charge of species p. This Poisson equation is not only solved within the plasma, but also inside the dielectrics of the DBD plasma, where it reduces to:

$$\nabla^2\varphi = 0 \qquad (10)$$

because no charges are present inside the dielectrics.

The effect of charge accumulation on the surface of the dielectric materials is considered using Gauss's law:

$$\varepsilon_{dielectric}\vec{E}_{dielectric} \cdot \overrightarrow{u_n} - \varepsilon_{gas}\vec{E}_{gas} \cdot \overrightarrow{u_n} = \sigma \qquad (11)$$

where $\vec{E}_{dielectric}$ and $\vec{E}_{gas}$ are the electric field inside the dielectric and in the gas, respectively, $\overrightarrow{u_n}$ is the unit vector normal to the wall, where the charge accumulation occurs. σ is the surface charge density on the dielectric, calculated from the charged particle fluxes directed to the surface.

Furthermore, at the open boundaries of the reactor, where the gas enters and leaves the reactor, homogeneous Neumann boundary conditions are employed, meaning that the derivatives of the plasma quantities in the

direction perpendicular to these boundaries are set to zero; this applies to the densities of all the active species, the electron energy density and the electric potential. At the physical boundaries, i.e., the electrodes and the dielectric, the boundary conditions for n_p and n_e are given by the expressions for the flux densities $\vec{\Gamma}_p$ and $\vec{\Gamma}_e$. These boundary conditions are determined by the reflection coefficients and the secondary electron emission coefficients of the different species included in the model. Besides, the correct electrode properties and dielectric properties are defined in the model. Detailed information about the boundary conditions used in this fluid model can be found in Mihailova et al.[61].

The coupled differential equations are solved by the so-called "modified strongly implicit method",[62] using an extra stabilization method,[42] until convergence is reached over the discharge cycles. The electron transport parameters and rate coefficients are not updated with each iteration, but they are updated whenever the densities of the molecules change a few percent. A more detailed description of the physics used in the model and of the numerical methods that are used is reported by Hagelaar[42] and by Brok et al.[49].

Because the aim of our research is to determine the conversion of the inlet gases and the yields of the reaction products, calculations are carried out for a residence time up to 20 s. To limit the calculation time, the fluid model is used to follow all species as a function of time with a maximal time step in the order of 10 ns, until a periodic steady state is reached for the charged species. This takes typically 2 ms or 20 ac periods. Subsequently, the time averaged electron density, electron energy and rate coefficients of electron impact reactions are calculated and taken as a constant input for a reduced fluid

model, in which the electron energy balance equation and the Poisson equation are not solved. In this second part, the conversion of the molecules is calculated with a larger time step in the order of 100 μs. Back-coupling to the short time step calculations is carried out regularly, to update the electron energy and density and the rate coefficients of the electron impact reactions if necessary. This decoupling of the model into charged species kinetics and neutral chemistry kinetics allows to increase the calculation speed with a factor of 10^4. Typically, the calculations carried out in this PhD work take about 2 or 3 days on today's personal computers.

3.4. The Reactor Set-Up under Study

The numerical model is applied to an atmospheric pressure cylindrical DBD (see Figure 4). The reactor consists of two coaxial electrodes. The inner electrode (stainless steel) has an outer diameter of 22 mm. The outer electrode (chrome) has a diameter of 29.3 mm and at the inside it is in contact with a dielectric tube made of alumina. The alumina tube has an inner diameter of 26 mm and a wall thickness of 1.6 mm, leading to a discharge gap of 2 mm between both cylinders, i.e., the region where the gas flows through the reactor. The outer electrode is powered, whereas the inner electrode is grounded. The background gas temperature is 300 K and assumed to be constant in time and uniform in space. This is justified, because in a DBD there is only local heating due to the discharge filaments. However, the latter only take a very small fraction of the reactor volume for several nanoseconds, with a repetition in the microseconds scale, yielding a volume-corrected filament frequency of about 0.01% per discharge period.[63] Thus overall, the gas heating

is very limited. Furthermore, often a water jacket is used in experiments to cool the reactor and keep the reactor temperature constant at about 300 K.[25, 64-68] The total length of the reactor in the experiment is 120 mm. A residence time of 20 s corresponds for this set-up to a gas flow rate of about 0.05 L·min^{-1}. More detailed information on the reactor set-up under study has been reported by Paulussen et al.[68]

In the model, however, only a segment of 1.5 mm long is considered. This is done to limit the calculation time and to avoid having to deal with filament formation in the reactor, as this cannot yet be simulated with the present model. On the other hand, by using 3 grid cells, instead of 1, in the axial direction, it is possible to describe the boundary conditions (see Section 3.3.) in a proper way in both the axial and the radial direction.
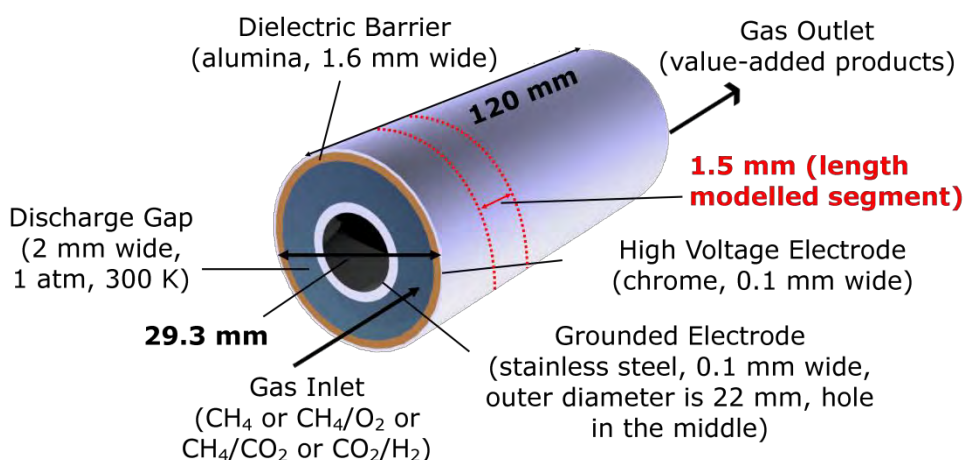
Figure 4. Schematic diagram of the reactor under study.

It needs to be realized that the effect of gas flow in the reactor is not modeled explicitly. Indeed, the real reactor can be considered as a kind of plug flow reactor, hence the concentration of the species varies as a function of the position in the reactor when the gas flows through. However, in the model this can be approximated by considering the reactor as a batch reactor, where the concentration of the species varies as a function of the residence time. Indeed, the variation of the concentrations as a function of time in a batch reactor is the same as the variation as a function of position in a plug flow reactor. In other words, the effect of gas flow is accounted for by studying the time variation of the species concentrations, where the residence time is calculated as the reactor volume divided by the gas flow rate.

3.5. Transport and Wall Interaction Coefficients

The species and reactions included in the different gas mixtures under study in this dissertation will be discussed in Chapter 4 for pure CH_4, in Chapter 5 for CH_4/O_2 and CH_4/CO_2, and in Chapter 6 for CO_2/H_2. Here we will discuss the determination of their transport coefficients for diffusion and mobility (only for the charged species), their sticking coefficients and their secondary electron emission coefficients, as this determination is generally valid for the different chapters.

The diffusion coefficient D_{ij} ($m^2 \cdot s^{-1}$) of the neutral species j in the background gas i is obtained by the Chapman-Enskog equation:[69-70]

$$D_{ij} = \frac{3k_bT\sqrt{\frac{4\pi k_bT}{2m_{ij}}}}{16p\pi\sigma_{ij}^2\Omega_D(\Psi)} \tag{12}$$

where k_b is the Boltzmann constant, T is the background gas temperature (K), p is the total pressure (Pa), m_{ij} is the reduced mass (kg), σ_{ij} is the characteristic length (m) and Ω_D is the dimensionless diffusion collision integral. This collision integral, which is a function of the dimensionless temperature Ψ, is given by

$$\Omega_D = \frac{A}{\Psi^B} + \frac{C}{e^{D\Psi}} + \frac{E}{e^{F\Psi}} + \frac{G}{e^{H\Psi}} \tag{13}$$

where Ψ equals k_bT/ε_{ij}, A = 1.06036, B = 0.15610, C = 0.19300, D = 0.47635, E = 1.03587, F = 1.52996, G = 1.76474 and H = 3.89411.[69] σ_{ij} and ε_{ij} are calculated by

$$\sigma_{ij} = \frac{\sigma_i+\sigma_j}{2} \tag{14}$$

$$\varepsilon_{ij} = \sqrt{\varepsilon_i\varepsilon_j} \tag{15}$$

with σ (m) and ε (J) being the characteristic length and energy for every species in the 12-6 Lennard-Jones potential. These Lennard-Jones parameters were reported for most of the neutral species by Reid et al.[69] and by Svehla[71] and for the other species they were obtained by linear interpolation.

Finally the diffusion coefficient D_j of the species j in the entire gas mixture, i.e., the sum of all background gases i, is obtained from the different D_{ij}-values using Blanc's law:[72]

$$\frac{p_{tot}}{D_j} = \sum_i \frac{p_i}{D_{ij}} \tag{16}$$

with p_{tot} the total pressure and p_i the partial pressure of the background gas i.

The ion mobility $\mu_{i,j}$ (m^2·V^{-1}·s^{-1}) of an ion j in the background gas i is calculated using the low electric field Langevin mobility expression:[72]

$$\mu_{i,j} = 0.515\frac{T}{p\sqrt{m_{ij}\alpha_i}} \qquad (17)$$

with T again the background gas temperature (K), p the gas pressure (Pa), m_{ij} the reduced mass (amu) and α_i the polarizability (Å^3) of the background gas, which was obtained from Böttcher et al.[73] Afterwards the mobility coefficient μ_j of the ion j in the entire gas mixture can be obtained in a similar way as the diffusion coefficient according to Blanc's law.

The mobility of the electrons and the rates of their collision reactions are described as parameters depending on the mean electron energy. These dependencies are calculated using the external Boltzmann solver Bolsig+,[74] which creates lookup tables for the mean electron energy, the electron mobility and the reaction rate coefficients as function of the reduced electric field. Accordingly, the electron mobility and the rate coefficients can be used as a function of the mean electron energy, which is calculated with the electron energy balance equation (see Section 3.3.).

From the ion mobility μ_j, the ion diffusion coefficient D_j of an ion j can directly be obtained using the Einstein relation, in order to remain consistent with the physical approximations used in the model:

$$D_j = \frac{k_b T_{ion}}{e}\mu_j \qquad (18)$$

where k_b is again the Boltzmann constant, T_{ion} is the ion temperature (K), which is assumed to be equal to the background gas temperature, and e is the

elementary charge. The Einstein relation is also used to obtain the electron diffusion coefficient from the electron mobility.

The sticking coefficients for the different higher hydrocarbon radicals are based on reported values by Bohmeyer et al.[75] and by Eckert et al.[76] Although the reported sticking coefficients are defined for somewhat different conditions, a good indication of the trend of the coefficients can be deduced. The sticking coefficients for the oxygen containing radicals were assumed to be one. The sticking probabilities for the various molecules and the ions were assumed to be zero and one, respectively. Note that the description of the surface reactions in the model is currently limited to this rough approximation and therefore the calculated densities of the radicals and molecules might be overestimated. The calculated densities of the ions, on the other hand, might be underestimated, although this is not so likely, as sticking equal to one is quite realistic for the ions, because they are indeed mostly neutralized upon arrival at the walls. For the ions, also secondary electron emission is considered when they collide with the reactor wall. A secondary electron emission coefficient of 0.05 was assumed and a corresponding energy of 5 eV.

3.6. Definitions of Conversion, Yield and Selectivity

Besides typical plasma characteristics, such as species densities, rates of the various reactions, electron energy, etc., the model can also calculate the conversion of the inlet gases, as well as the yields and selectivities of the reaction products, which is of interest for the application of gas conversion, investigated in this PhD thesis. The definitions of the conversions X, the yields Y and the selectivities S are as follows. The definitions can be slightly different, depending on the gas or gas mixture under study. Therefore, the gases or gas mixtures to which these specific definitions apply, are given between brackets.

$$X_{CH_4/CO_2/O_2/H_2} = \frac{n_{CH_4/CO_2/O_2/H_2,converted}}{n_{CH_4/CO_2/O_2/H_2,feed}} \times 100\% \tag{19}$$

$$Y_{H_2} = \frac{n_{H_2}}{2 \times n_{CH_4,feed}} \times 100\% \quad (CH_4, CH_4/O_2, CH_4/CO_2) \tag{20}$$

$$Y_{C_xH_yO_z} = \frac{x \times C_xH_yO_z}{n_{CH_4,feed}} \times 100\% \ (CH_4, CH_4/O_2) \tag{21}$$

$$Y_{C_xH_yO_z} = \frac{x \times C_xH_yO_z}{n_{CH_4,feed} + n_{CO_2,feed}} \times 100\% \ (CH_4/CO_2) \tag{22}$$

$$Y_{C_xH_yO_z} = \frac{x \times C_xH_yO_z}{n_{CO_2,feed}} \times 100\% \ (CO_2/H_2) \tag{23}$$

$$Y_{H_2O} = \frac{n_{H_2O}}{2 \times \left(n_{CH_4,feed} + n_{O_2,feed}\right)} \times 100\% \quad (CH_4/O_2) \tag{24}$$

$$Y_{H_2O} = \frac{n_{H_2O}}{2 \times \left(n_{CH_4,feed} + n_{CO_2,feed}\right)} \times 100\% \quad (CH_4/CO_2) \tag{25}$$

$$S_{H_2} = \frac{n_{H_2}}{2 \times n_{CH_4,converted}} \times 100\% \quad (CH_4, CH_4/O_2, CH_4/CO_2) \tag{26}$$

$$S_{C_xH_yO_z} = \frac{x \times C_xH_yO_z}{n_{CH_4,converted}} \times 100\% \ (CH_4, CH_4/O_2) \qquad (27)$$

$$S_{C_xH_yO_z} = \frac{x \times C_xH_yO_z}{n_{CH_4,converted} + n_{CO_2,converted}} \times 100\% \ (CH_4/CO_2) \qquad (28)$$

$$S_{C_xH_yO_z} = \frac{x \times C_xH_yO_z}{n_{CO_2,converted}} \times 100\% \ (CO_2/H_2) \qquad (29)$$

$$S_{H_2O} = \frac{n_{H_2O}}{2 \times (n_{CH_4,converted} + n_{O_2,converted})} \times 100\% \ (CH_4/O_2) \qquad (30)$$

$$S_{H_2O} = \frac{n_{H_2O}}{2 \times (n_{CH_4,converted} + n_{CO_2,converted})} \times 100\% \ (CH_4/CO_2) \qquad (31)$$

In these definitions the parameter x denotes the stoichiometric balance coefficient, which corresponds also to the index in the compound name of C_xH_y or $C_xH_yO_z$. Furthermore, note that the yield and selectivity of CO are calculated with $Y_{C_xH_yO_z}$ and $S_{C_xH_yO_z}$, respectively, with y = 0, and that the yield and selectivity of the higher hydrocarbons (C_xH_y) are calculated with $Y_{C_xH_yO_z}$ and $S_{C_xH_yO_z}$, respectively, with z = 0.

3.7. Aim and Outline of the PhD Dissertation

The aim of this dissertation is to come to a better understanding of the huge plasma chemistry governing gas conversion processes in a DBD using numerical simulations. More specifically, the goal is to develop a reliable chemistry set for the description of the gas phase chemistry in pure CH_4, CH_4/O_2, CH_4/CO_2 and CO_2/H_2 gas discharges by 1D fluid modeling. In this way, calculation results can be obtained on the densities of the different plasma species, the conversions of the inlet gases, the yields and selectivities of the end products and the dominant reaction pathways for each of the gas mixtures studied. This allows us to determine whether or not a specific gas mixture is suitable for the production of a specific end-product of interest. Our calculation results are validated with reported results in literature and for pure CH_4 also with some experiments for the reactor set-up under study. Based on these results, we hope to clarify whether a sustainable competitive industrial process for gas conversion in a DBD can be developed in the future.

In the next chapters, the construction of the chemistry sets, as well as the obtained results for the different gas mixtures studied, are described. In **Chapter 4**, the fluid model is applied to describe the conversion of pure CH_4 into higher hydrocarbons. **Chapter 5** concerns the fluid modeling of the gas phase chemistry for partial oxidation (CH_4/O_2) and for dry reforming (CH_4/CO_2) of methane, focusing on the formation of oxygenates and syngas. In **Chapter 6**, the aim is to investigate the potential of the hydrogenation of carbon dioxide (CO_2/H_2) in a DBD using a fluid model.

Finally, in **Chapter 7,** a general conclusion is given, as well as an outlook for the future.

Chapter 4

The Conversion of CH$_4$ into Higher Hydrocarbons

The fluid model described in previous chapter is applied here to the conversion process of methane into higher hydrocarbons. The spatially averaged densities of the various plasma species as a function of time are discussed. Besides, the conversion of methane and the yields of the reaction products as a function of the residence time in the reactor are shown and compared with experimental data. Higher hydrocarbons (C$_2$H$_y$ and C$_3$H$_y$) and hydrogen gas are typically found to be important reaction products. Furthermore, the main underlying reaction pathways are determined.

4.1. Introduction

As discussed in Chapter 1, a sustainable process for the conversion of the abundant methane reserves into more value-added chemicals and fuels is renowned as a challenge for the 21st century. More in particular, the development of a process for the direct synthesis of higher hydrocarbons and oxygenates from methane in an energy-efficient way would offer significant benefits, because this will circumvent the very expensive syngas step. In this chapter the plasma chemistry governing the conversion of pure CH$_4$ into higher hydrocarbons (C$_x$H$_y$) is discussed.

Experimental results on the conversion in a pure methane plasma found in literature show that the typical end products are H$_2$ and higher hydrocarbons, mostly C$_2$H$_6$ and in a lower content C$_3$H$_8$, C$_2$H$_4$ and C$_2$H$_2$.[13, 77-80] Modeling results on gas phase physics and chemistry in different kinds of methane containing discharges have been investigated extensively during the past thirty years.[20, 81-109] A minority of them concerns the modeling of the plasma as a gas conversion reactor in pure CH$_4$.[92, 103] Up to now, these numerical studies mostly concerned zero-dimensional simulations largely based on specific empirical input so that semi-empirical simulations were obtained, which are only valid for the experimental set-up under study. Only Yang[92] used a more generic method to describe the gas conversion in a pure methane plasma, which can be generally used for this kind of gas discharges. In this paper again a 0D model was used, the plasma chemistry presented was limited and the presented results were rather preliminary.

In order to achieve our goal, i.e., to describe in detail the plasma chemistry in an atmospheric pressure DBD in different gas mixtures with CH$_4$ and/or CO$_2$,

we started by developing a 1D fluid model for an atmospheric pressure DBD in pure methane. In this chapter we present our most important results on the conversion of CH$_4$ into higher hydrocarbons. First of all, the spatially averaged densities of the various plasma species as a function of time will be discussed. Furthermore, the conversion of CH$_4$, and the yields and selectivities of the reaction products will be shown. Finally, the main underlying reaction pathways for the conversion of CH$_4$ into higher hydrocarbons will be pointed out.

4.2. Species Included in the Model

In order to describe the chemistry in a pure methane plasma, 36 different species (electrons, molecules, ions and radicals) are taken into account in the model. The selection of species is based on other modeling studies for methane discharges under various conditions.[70, 81, 110] In addition to the feed gas CH$_4$, also H$_2$ and some higher order neutral molecules C$_2$H$_6$, C$_2$H$_4$, C$_2$H$_2$, C$_2$, C$_3$H$_8$ and C$_3$H$_6$ are considered in the model, as it was shown in literature that they are formed in the plasma at high densities.[78, 80] High densities of C$_2$H$_2$ in the discharge may lead to polymerization and in order to deal with this, in a first attempt the polymerization product C$_4$H$_2$ is also included in the model. Furthermore, 11 radical species and 16 ionic species are taken into account corresponding to the products of dissociation and ionization reactions, respectively, of these high density molecules.

A methane plasma has a very strong electropositive character.[70] The negative ion densities are about one order of magnitude lower than the electron and the positive ion densities[82-83] and therefore, negative ions are

not incorporated in the model. Although some vibrational excitation reactions are included in the model, vibrationally excited species are not taken into account separately in order to limit the number of species and reactions, and because vibrationally excited species are considered to be of minor importance in a DBD.[111-112] Also rotationally and electronically excited species are not taken into account in the model. Indeed, the electron energy required for rotational excitations is negligible compared with this for vibrational excitations,[70, 110] and all electronically excited states of methane lead to dissociation.[113] Therefore, it is also assumed here that the electronically excited states for the higher order neutrals lead to dissociation. An overview of the different species taken into account in the model can be found in Table 4.

Table 4. Overview of the species included in the model, besides the electrons.

Molecules	Ions	Radicals
CH$_4$	CH$_5^+$, CH$_4^+$, CH$_3^+$, CH$_2^+$, CH$^+$, C$^+$	CH$_3$, CH$_2$, CH, C
C$_2$H$_6$, C$_2$H$_4$, C$_2$H$_2$, C$_2$, C$_3$H$_8$, C$_3$H$_6$	C$_2$H$_6^+$, C$_2$H$_5^+$, C$_2$H$_4^+$, C$_2$H$_3^+$, C$_2$H$_2^+$, C$_2$H$^+$, C$_2^+$	C$_2$H$_5$, C$_2$H$_3$, C$_2$H, C$_3$H$_7$, C$_3$H$_5$
H$_2$	H$_3^+$, H$_2^+$, H$^+$	H
C$_4$H$_2$		

4.3. Reactions Included in the Model

A consistent set of 367 gas phase reactions involving the 36 defined species was built to describe the plasma chemistry in the discharge gap. These gas phase reactions can be divided into four groups: 100 electron-neutral, 35 electron-ion, 92 neutral-neutral and 140 ion-neutral reactions. The electron-

neutral reactions include 6 momentum transfer, 15 vibrational excitation, 47 ionization and 32 dissociation reactions. The electron-ion reactions are all dissociative recombination reactions, because volume recombination is an important process at atmospheric pressure, which is logical because of the high densities. An overview of the reactions considered in the model is given in the Appendices.

The rates of the different reactions are calculated in the model from the densities of the colliding species and the corresponding reaction rate coefficients. For the electron-neutral and electron-ion reactions, an energy dependent reaction rate coefficient is used. The Boltzmann solver Bolsig+[74] (see previous chapter) is used to create the lookup tables for the rate coefficients of the electron-neutral reactions based on the energy dependent collision cross sections for these reactions. The references for the cross sections can be found in Table A.1. of the Appendices. The lookup tables for the electron-ion dissociative recombination reactions are built using the functions in combination with the branching ratios for the different channels of which a detailed overview is given in Table A.2. of the Appendices. The neutral-neutral and ion-neutral reactions are defined in the model with a constant reaction rate coefficient, for a fixed pressure and temperature of 1 atm and 300 K, respectively. The constant rate coefficients and the corresponding references for the neutral-neutral and ion-neutral reactions are summarized in Table A.3. and Table A.4. of the Appendices, respectively. Note that the rate coefficient of the recombination reaction of CH$_3$ with C$_2$H$_5$ resulting in the formation of C$_3$H$_8$ was estimated based on the matching between experimental results and our calculation results. The values reported in literature for this reaction are either too low[114] (i.e., 5.60 x 10^{-11} cm^3·s^{-1},

which is equal to 2.29 x 10^{-30} cm^6·s^{-1} as adjusted for a three-body collision by dividing by the density of the background gas) or too high[115] (i.e., 1.87 x 10^{-23} cm^6·s^{-1}). Therefore, a rate coefficient of 1x10^{-28} cm^6·s^{-1} is assumed in the model.

4.4. Operating Conditions

The calculations are carried out at a fixed applied voltage of 6 kV and a frequency of 10 kHz, which are typical operating conditions applied in the experiments.[68] Experiments are performed for this DBD set-up to validate the calculated results. The analysis of the reaction product mixture is done by gas chromatography. A Trace GC from Thermo is equipped with two analysis channels. A first channel contains a thermal conductivity detector (TCD) to analyze the outcome of two serial installed packed columns: a Hayesep Q (80-100, 2m*1/8" Siltek) and a Molsieve 5A (80-100, 3m*1/8"). The second channel has a flame ionization detector (FID) installed after a RTX-1 capillary column (5μ, 25m*0.53mm).

4.5. Results and Discussion

4.5.1. Densities of the Plasma Species

Figure 5 illustrates the calculated periodic behavior of the spatially averaged electron density on a linear (a) and on a logarithmic (b) scale as a function of time, for four periods of the applied voltage. The applied voltage as a function of time is also plotted. It is clear that multiple breakdowns in the gas appear each half period following the applied voltage. The difference in the electron

density behavior for the positive and the negative polarity of the applied voltage is due to the dissimilarity in surface dimensions and properties of the inner and outer electrode (only one of the electrodes is covered by a dielectric, see Figure 4). The overall spatially and time averaged electron density amounts to 10^{17} m^{-3}. The overall spatially and time averaged electron energy was calculated to be about 2 eV.
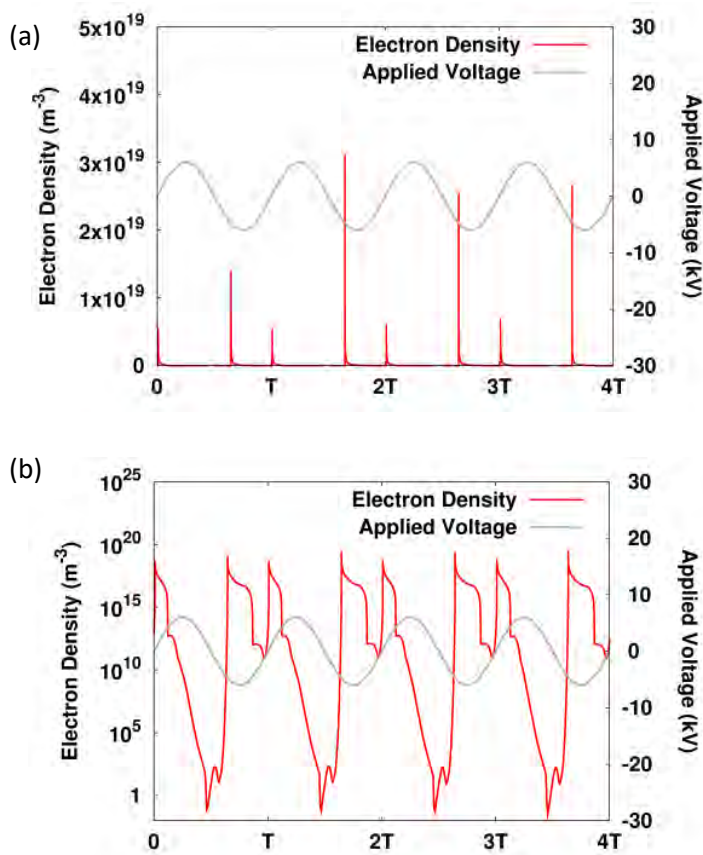
Figure 5. Spatially averaged electron density, on a linear (a) and a logarithmic (b) scale, as a function of time, as well as the applied voltage for four periods of time.

Note that the present model cannot deal with filament formation in the reactor. Therefore, the presented electric behavior corresponds to a DBD treated as a homogeneous glow discharge. Of course, this behavior is quite different from the experimental behavior, but we believe that the rest of our calculation results, such as conversion and yields, and the reaction pathways, are still valid.

The spatial variation of the electron density, total ion density and electron energy, taken at the maximum of its time profile, is depicted in Figure 6. It is clear that in the bulk plasma, the electron and ion densities are in the order of 10^{18} m^{-3}, and they are more or less equal to each other, providing charge neutrality in the bulk. However, close to the electrodes, the electron density drops to zero, and the total positive ion density is several orders of magnitude higher than the electron density, providing a net positive space charge. This behavior is typical for the sheath formation in a DBD.[116] A different behavior is observed in the pre-sheath near the inner (grounded) electrode, where the ion density drops one order of magnitude, while near the dielectric barrier at the outer (powered) electrode, the ion density rises one order of magnitude. This different behavior is attributed to the fact that at this particular moment in time the powered electrode (covered by the dielectric barrier) is the cathode, which attracts the ions, while the grounded electrode is the anode, which repels the ions. Due to the acceleration of the electrons in the high electric field in the sheath, these electrons have an increased energy there.
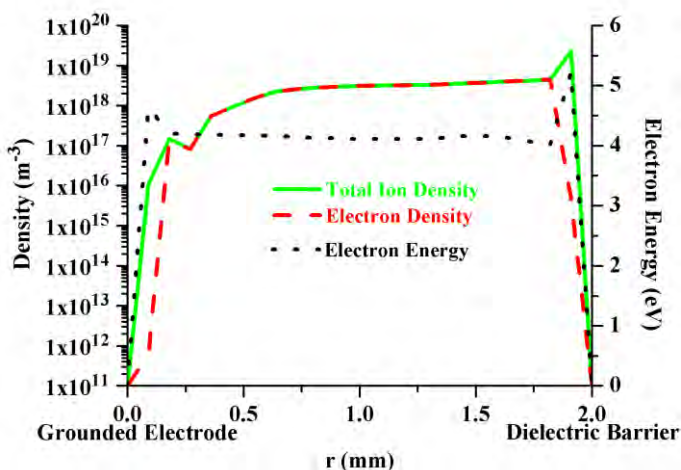
Figure 6. Calculated spatial profiles of the electron and total ion density (left axis) and electron energy (right axis) in the gap between both electrodes, taken at the maximum of their time profile. The inner (grounded) electrode is at the left, whereas the outer (powered) electrode with the dielectric layer is at the right.

Collisions of the electrons with the background gas molecules lead to the formation of radicals and ions. The number densities of these radicals and ions exhibit the same periodic behavior as the electron density. Figure 7 shows the spatially averaged radical densities as a function of time. In case of the radicals this periodic trend is superimposed on a rising or declining trend which acts over a longer time-scale until periodic steady state is reached. The variation through a period, i.e. the difference between the minimum and maximum value in one period, varies from less than one order of magnitude for C_2H_5, C_2H_3, C_3H_7, C_3H_5 and H, to several orders of magnitude for CH_3, CH_2, CH, C and C_2H. This can be explained by the fact that, except for C_2H, this last group of radicals is directly formed from the background gas CH_4 by electron impact dissociation, which is not the case for the higher order radicals. The overall spatially and time averaged radical densities vary from about 10^{12} m^{-3}

for the less abundant radicals to about 10^{20} m^{-3} for the most abundant radicals. The most abundant radicals are H, CH$_3$, CH$_2$, C$_2$H$_5$ and C$_2$H$_3$. The overall spatially and time averaged ion densities vary from almost zero to the order of 10^{16} m^{-3} for the most important ions (CH$_5^+$, C$_2$H$_5^+$, C$_2$H$_4^+$, C$_2$H$_3^+$).
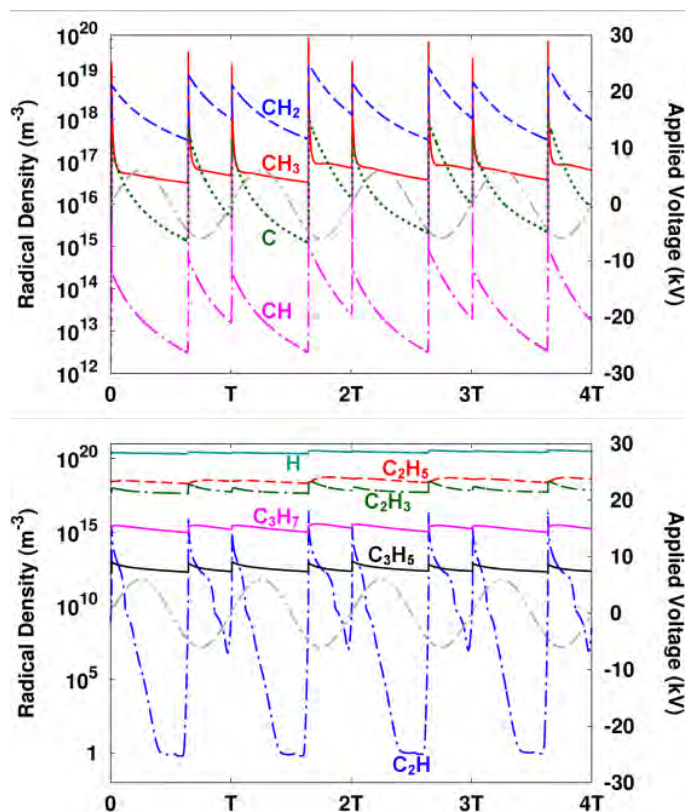
Figure 7. Spatially averaged radical densities as a function of time, as well as the applied voltage for four periods of time.

Recombination of the radicals leads to the formation of higher order hydrocarbons and hydrogen gas. The spatially averaged densities of these molecules do not exhibit this periodic behavior. Indeed, their densities behave more or less independent from the applied voltage, since they are only indirectly correlated with the electron density and electron energy by the

densities of the radicals from which they are formed (see discussion about the reaction pathways in Section 4.5.3.). The net production of these higher hydrocarbon molecules and hydrogen gas is higher than their net consumption, and as result a gradual increase in the densities is observed each half period of the applied voltage. In contrast, the net consumption of CH_4 is higher than its net production, and therefore a gradual decrease in the CH_4 density is observed each half period. Therefore, it is more interesting to look to the variation of the molecule densities on a longer time-scale.
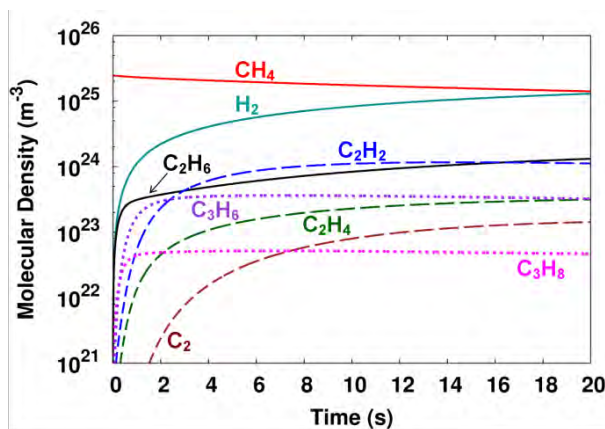
Figure 8. Spatially averaged molecular densities as a function of the residence time.

Figure 8 illustrates the spatially averaged molecule densities as a function of the residence time in the plasma reactor. Note that a residence time of 20 s corresponds to a gas flow rate of 0.05 L·min^{-1} for the experimental set-up under study. The density of the background gas methane is initially 2.45 x 10^{25} m^{-3}, but is decreasing due to dissociation and ionization reactions governing the conversion process. As a result, H_2, C_2H_6, C_2H_4, C_2H_2, C_2, C_3H_8 and C_3H_6 are formed and are also present in the discharge at high densities, as shown in Figure 8. It appears that the production is most pronounced in the first 1 to 2 s

and that the densities of the higher hydrocarbons and H$_2$ molecules do not significantly change anymore for a longer residence time. However, the logarithmic scale is a bit misleading and the conversion still continues, as will be illustrated in Section 4.5.2. below. The spatially averaged densities vary between 10^{22} m^{-3} and 10^{25} m^{-3} for the different molecules. H$_2$ seems to be formed at the highest density, and after 20 s, its density is comparable to the CH$_4$ density. As far as the higher hydrocarbon species are concerned, it appears from Figure 8 that C$_2$H$_6$ and C$_2$H$_2$ are formed with the highest density, which is only about one order of magnitude lower than the CH$_4$ density after 20 s. As a result of the polymerization of C$_2$H$_2$, also C$_4$H$_2$ is formed with a density of 10^{24} m^{-3}. At first sight, this density seems rather high. This can be explained by the fact that C$_4$H$_2$ is considered in the model as the sum of all higher polymerized species. Moreover, in the model no loss mechanism for C$_4$H$_2$ is included and the sticking probability of C$_4$H$_2$ is defined zero, as for the other molecules (see Section 3.5. above).

4.5.2. Conversion, Yields and Selectivities

Figure 9(a) illustrates the calculated conversion of CH$_4$ and the yields of the reaction products, i.e., H$_2$ and the summation over all C$_2$H$_y$ and C$_3$H$_y$ hydrocarbons, as a function of residence time in the reactor (solid lines). The measured conversion and yields of these products, for similar operating conditions, are depicted with dashed lines.

As expected, both the conversion and the various yields increase as a function of residence time. After 20 s, only 40% of CH$_4$ is converted and the H$_2$ and C$_2$H$_y$ molecules are formed with the highest yields. Reasonable

agreement is reached between calculated and experimental results, taking into account the complexity of the plasma chemistry. The calculated and measured CH_4 conversion and C_3H_y yield agree within 5 %. However, the differences are significant for the H_2 yield and the C_2H_y yield, although they show at least similar trends between calculated and experimental values. A possible explanation for these significant differences is given below when the selectivities of H_2 and C_2H_2 are discussed. The calculated and measured carbon and hydrogen balances are plotted in Figure 9(b), and show an agreement within 20 %. A possible explanation for the differences between the calculated and the measured balances is the uncertainty of the used sticking coefficients. The carbon balance drops slightly as a function of residence time, due to sticking at the walls in the form of solid carbon. After a residence time of 20 s, roughly 20% of the carbon atoms is left in the reactor.

In Figure 9(c) the calculated (solid lines) and measured (dashed lines) selectivities of the individual reaction products are plotted as a function of the conversion of CH_4. From the higher hydrocarbons, C_2H_6 (dark blue) has the highest selectivity, both in the calculated and the measured results. The selectivity is especially high (100% in the calculations) at very low conversion of CH_4. This is because when the discharge is ignited, electron impact dissociation of CH_4 leads to the formation of H_2 and CH_3. This methyl radical will immediately initiate the recombination reactions towards C_2H_6, which in turn is converted later in new radicals and the other higher hydrocarbons. A more thorough discussion on the dominant reaction pathways can be found in the next section. However, this very low conversion is not interesting from an applications point of view. The typical selectivity, in the range of 10-40% CH_4 conversion, is around 20-30%.
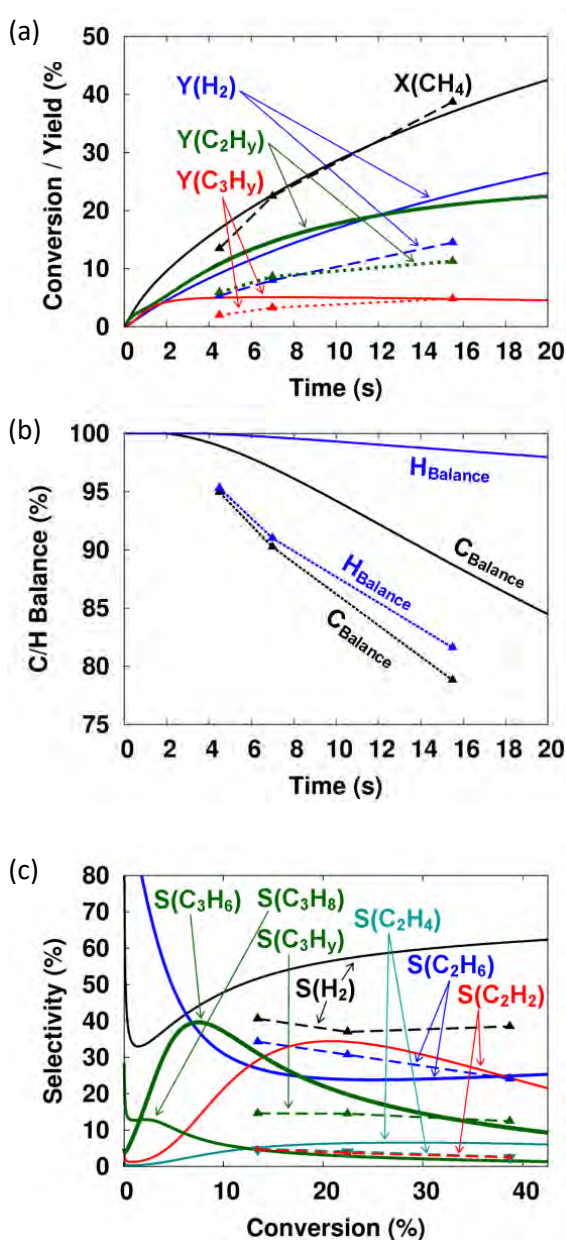
Figure 9. (a) Calculated (solid lines) and experimental (dashed lines) conversion of CH$_4$ and yields of the reaction products, as a function of residence time in the reactor. In (b) the calculated (solid lines) and measured (dashed lines) carbon-balances and hydrogen-balances are illustrated. In (c) the calculated (solid lines) and experimental (dashed lines) selectivities of the individual hydrocarbon reaction products are plotted as a function of the conversion of CH$_4$. Note that the selectivity of C$_3$H$_6$ could not be measured.

The experimental results show that C$_2$H$_4$ (dark cyan, dashed) and C$_2$H$_2$ (red, dashed) have a much lower selectivity than C$_2$H$_6$. The calculated selectivity of C$_2$H$_4$ (dark cyan, solid) is in good agreement with the experiment (i.e., in the order of 5-10%), but the calculated selectivity of C$_2$H$_2$ (red, solid) is too high compared to the experimental results. A possible reason might be that the further polymerization of C$_2$H$_2$ molecules into higher molecules is underestimated in the model. Indeed, dust formation appears to be important in acetylene plasmas. In previous models by our group,[117-119] these polymerization reactions were studied in detail by an extensive chemistry set, including neutral, positive and negative ion pathways. However, in the present model, the polymerization is only treated by one chemical reaction (i.e., C$_2$H insertion; see Section 4.5.3. below), in order not to further complicate our plasma chemistry set, which is already huge. Therefore, the obvious overestimated C$_2$H$_2$ selectivity in our model is probably attributed to the underestimation of C$_2$H$_2$ polymerization. Moreover, the overestimated C$_2$H$_2$ formation explains why the calculated yield of the overall C$_2$H$_y$ fraction is higher than the measured values (Figure 9(a)).

The calculated and measured yields of the summation over all C$_3$H$_y$ molecules are in an almost perfect agreement (Figure 9(a)). The sum of the calculated selectivities of C$_3$H$_8$ (dark green, solid) and C$_3$H$_6$ (light green, solid) is in reasonable agreement with the total measured selectivity of C$_3$H$_y$ (green, dashed). However, it is not possible to compare the calculated selectivities of the different compounds, as the measured peaks of the different C$_3$H$_y$ molecules overlap in the chromatogram.

Besides the higher hydrocarbons, H$_2$ is also formed as a main end product in the discharge. The calculated yields and selectivities of H$_2$ are a bit higher than

the measured values. This is probably because the production of H$_2$ by electron impact dissociation of C$_2$H$_6$ and C$_3$H$_8$ (see next section for the most important consumption and production pathways of H$_2$) is assumed a bit too high in the model.

As mentioned above, the formation of C$_4$H$_2$ by polymerization reactions of C$_2$H$_2$ species is also included in the model. However, as C$_4$H$_2$ could not be measured in the experiments, it is treated as a loss of carbon in the model, in order to match the calculated and measured carbon balances. The calculated yield of C$_4$H$_2$ after 20s amounts to 13.75 %.

Reported results in literature based on experiments on the conversion of methane into higher hydrocarbons, at similar conditions, show similar trends, namely the end products were mainly H$_2$ and C$_2$H$_y$ (mostly C$_2$H$_6$) as well as, to a lower extent, some higher hydrocarbons (C$_3$H$_y$, C$_4$H$_y$, …).[13, 78, 80]

4.5.3. Dominant Reaction Pathways

(a) Electron impact reactions with CH$_4$: the formation of radicals and ions

As soon as the sinusoidal voltage is applied to the reactor and the discharge is ignited, electron impact ionization and dissociation of CH$_4$ occurs, and this results in the consumption of CH$_4$ and the creation of new species (electrons, ions, radicals). The formation of new electrons and ions in the plasma is important in order to sustain the discharge. The most important channels for electron impact ionization of CH$_4$ are:

$$e^- + CH_4 \rightarrow 2e^- + CH_4^+ \tag{R1}$$

$$\text{e}^- + \text{CH}_4 \rightarrow 2\text{e}^- + \text{CH}_3^+ + \text{H} \qquad\qquad \text{(R2)}$$
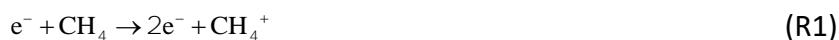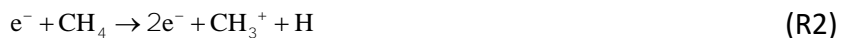
Our calculations point out that reaction (R1) is responsible for 66% of the total electron impact ionization of CH$_4$, while reaction (R2) is responsible for 33%, which is in good agreement with the results reported by Yang.[92]

The dissociation of CH$_4$ leads to the formation of radicals. It is of special interest when studying the gas conversion process, because these radicals are important reagents in the production of higher order hydrocarbons. The most important channels for consumption of CH$_4$ are electron impact dissociation reactions, more specifically:

$$\text{e}^- + \text{CH}_4 \rightarrow \text{e}^- + \text{CH}_3 + \text{H} \qquad\qquad \text{(R3)}$$

$$\text{e}^- + \text{CH}_4 \rightarrow \text{e}^- + \text{CH}_2 + \text{H}_2 \qquad\qquad \text{(R4)}$$

$$\text{e}^- + \text{CH}_4 \rightarrow \text{e}^- + \text{CH} + \text{H}_2 + \text{H} \qquad\qquad \text{(R5)}$$

Our calculations point out that reaction (R3) is responsible for 79% of the total electron impact dissociation of CH$_4$, while reactions (R4) and (R5) are responsible for 15% and 5%, respectively. Similar results were reported by Yang.[92]

(a)

(b)

(c)
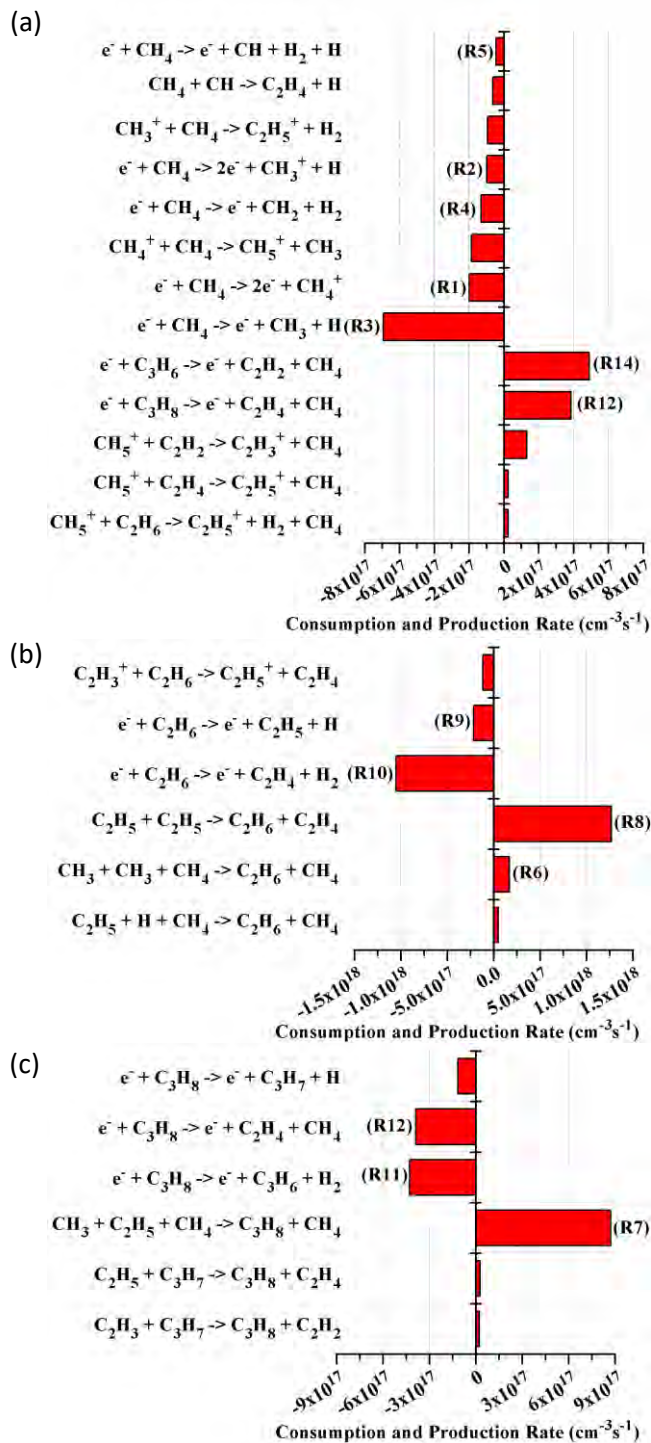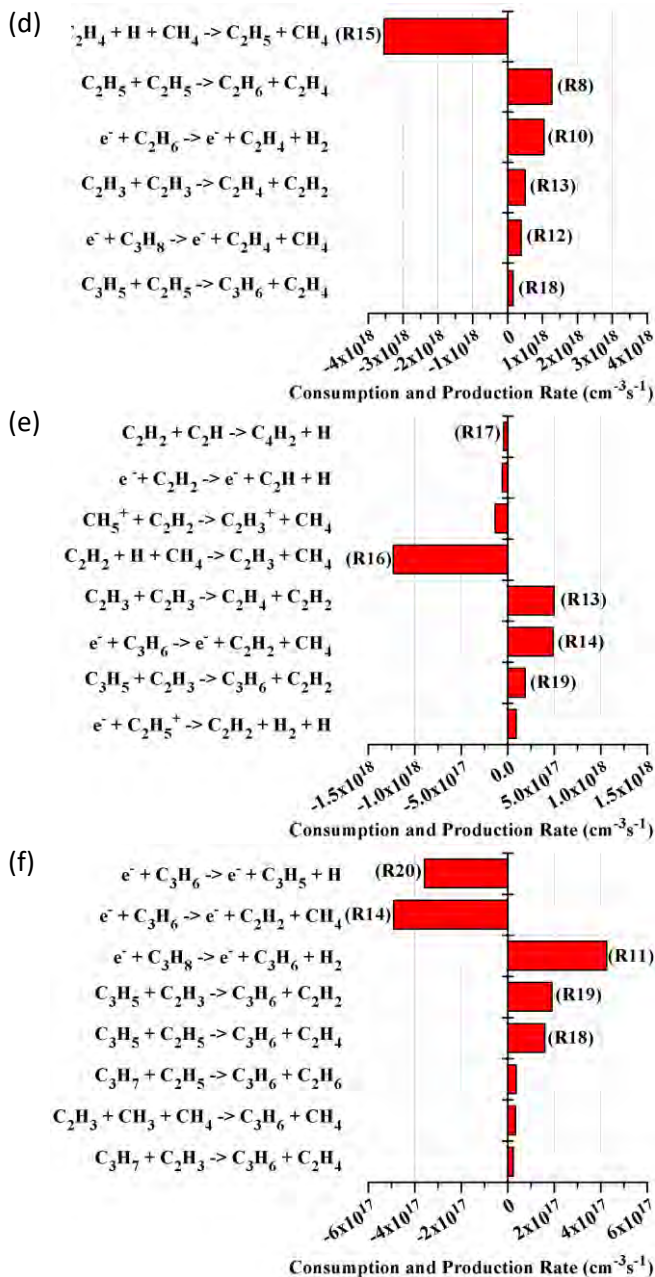
Figure 10. Calculated time-averaged reaction rates of the dominant reaction pathways for the production and consumption of CH$_4$ (a), C$_2$H$_6$ (b), C$_3$H$_8$ (c), C$_2$H$_4$ (d), C$_2$H$_2$ (e) and C$_3$H$_6$ (f). The production rates are plotted as positive values (i.e., right-hand side of the figures), whereas the consumption rates are defined as negative values (i.e., left-hand side of the figures). The most important pathways are labeled, and the labels correspond to the reactions given in the text.

The dominant reactions for CH_4 consumption (and production) are depicted in Figure 10(a). It is clear that the electron impact dissociation reaction to CH_3 (i.e., reaction (R3)) is by far the dominant consumption process of CH_4, followed by electron impact ionization to CH_4^+ (i.e., reaction (R1)). Besides the electron impact ionization and dissociation reactions, also some neutral-neutral and ion-neutral reactions are important for the consumption of CH_4 (see Figure 10(a)).

Note that electron impact vibrational excitation of CH_4 is also an important process. However, in the model these vibrational excitation reactions are only considered as an energy loss for the electrons (i.e., the vibrationally excited species are not taken into account separately) and therefore these reactions are not included in Figure 10(a) since they neither entail consumption or production of CH_4. In literature it is reported that a similar result is obtained whether the vibrationally excited species are taken into account or not, because in that case the electron impact excitation to CH_4^* is balanced by the de-excitation of CH_4^* on the reactor wall.[92]

It can also be deduced from Figure 10(a) that the most important pathways for the regeneration of CH_4 are based on electron impact dissociation of higher hydrocarbons, such as C_3H_6 and C_3H_8 (see below).

(b) The recombination of CH_3: the formation and loss of C_2H_6 and C_3H_8

The most important radical produced out of CH_4 is CH_3, which is mainly formed by reaction (R3) above. This radical will initiate the recombination reactions towards higher hydrocarbons such as C_2H_6 and especially C_3H_8:

$$CH_3 + CH_3 + CH_4 \rightarrow C_2H_6 + CH_4 \tag{R6}$$

$$CH_3 + C_2H_5 + CH_4 \rightarrow C_3H_8 + CH_4 \tag{R7}$$

The most important pathways for the production and consumption of ethane (C$_2$H$_6$) and propane (C$_3$H$_8$) are illustrated in Figures 10(b) and 10(c), respectively. It is clear that reaction (R7) is the dominant production process for C$_3$H$_8$ (see Figure 10(c)), but reaction (R6) is only responsible for about 11% of the C$_2$H$_6$ production. Indeed, as is apparent from Figure 10(b), C$_2$H$_6$ is mainly (83%) formed by the recombination of two C$_2$H$_5$ radicals:

$$C_2H_5 + C_2H_5 \rightarrow C_2H_6 + C_2H_4 \tag{R8}$$

This results from the fact that the overall averaged density of C$_2$H$_5$ (7 x 10^{20} m^{-3}) is three orders of magnitude higher than the CH$_3$ density, while the rate coefficient of reaction (R6) (i.e., 1.56 x 10^{-38} m^6 s^{-1}, or 3.82 x 10^{-13} m^3 s^{-1} for a CH$_4$ gas density of 2.446 x 10^{25} m^{-3}) is five orders of magnitude higher than the rate coefficient of reaction (R8) (i.e., 2.41 x 10^{-18} m^3 s^{-1}). Taking into account that the rates of both reactions depend on the square of the concentrations of CH$_3$ and C$_2$H$_5$, respectively, it is clear that the rate of reaction (R8) is almost one order of magnitude higher than the rate of reaction (R6).

Electron impact dissociation reactions are the most important loss processes for both C$_2$H$_6$ and C$_3$H$_8$, leading to the formation of C$_2$H$_4$, C$_2$H$_5$ and C$_3$H$_6$:

$$e^- + C_2H_6 \rightarrow e^- + C_2H_5 + H \tag{R9}$$

$$e^- + C_2H_6 \rightarrow e^- + C_2H_4 + H_2 \tag{R10}$$

$$e^- + C_3H_8 \rightarrow e^- + C_3H_6 + H_2 \tag{R11}$$

$$e^- + C_3H_8 \rightarrow e^- + C_2H_4 + CH_4 \tag{R12}$$
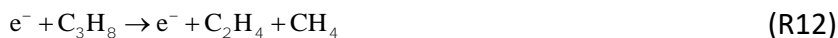
Especially reaction (R10) is important as loss process for C_2H_6 (see Figure 10(b)), whereas both reactions (R11) and (R12) contribute nearly equally to the loss of C_3H_8 (see Figure 10(c)).

(c) The formation and loss of higher order unsaturated hydrocarbons: C_2H_4, C_2H_2 and C_3H_6

The most important pathways for the production and consumption of C_2H_4, C_2H_2 and C_3H_6 are plotted in Figures 10(d), 10(e) and 10(f), respectively. The production of C_2H_4 occurs mainly by the recombination of two C_2H_5 radicals (i.e., reaction (R8) above) and by electron impact dissociation of C_2H_6 (i.e., reaction (R10) above). Also electron impact dissociation of C_3H_8 (i.e., reaction (R12) above) and the recombination of two C_2H_3 radicals (reaction (R13)) contribute to some extent:

$$C_2H_3 + C_2H_3 \rightarrow C_2H_4 + C_2H_2 \tag{R13}$$

The latter reaction, as well as the electron impact dissociation of C_3H_6, are mainly responsible for the production of C_2H_2:

$$e^- + C_3H_6 \rightarrow e^- + C_2H_2 + CH_4 \tag{R14}$$

Hydrogen attachment reactions are the most important loss processes for both C_2H_4 and C_2H_2, leading to the formation of C_2H_5 and C_2H_3 radicals, respectively:

$$C_2H_4 + H + CH_4 \rightarrow C_2H_5 + CH_4 \tag{R15}$$

$$C_2H_2 + H + CH_4 \rightarrow C_2H_3 + CH_4 \tag{R16}$$

Note in Figure 10(e) also the occurrence of the polymerization reaction of C$_2$H$_2$ resulting in the formation of C$_4$H$_2$:

$$C_2H_2 + C_2H \rightarrow C_4H_2 + H \tag{R17}$$

Finally, the production of C$_3$H$_6$ occurs mainly by electron impact dissociation of C$_3$H$_8$ (i.e., reaction (R11) above) and to a lower extent also by the recombination of C$_3$H$_5$ radicals with either C$_2$H$_5$ or C$_2$H$_3$:

$$C_3H_5 + C_2H_5 \rightarrow C_3H_6 + C_2H_4 \tag{R18}$$

$$C_3H_5 + C_2H_3 \rightarrow C_3H_6 + C_2H_2 \tag{R19}$$

The loss of C$_3$H$_6$ is mainly attributed to electron impact dissociation reactions, leading to the formation of either C$_2$H$_2$ (reaction (R14) above) or C$_3$H$_5$:

$$e^- + C_3H_6 \rightarrow e^- + C_3H_5 + H \tag{R20}$$
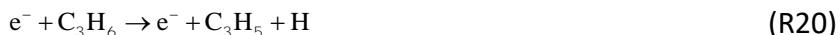
(d) The role of C$_2$H$_5$: an important radical in the conversion process

Our calculations predict that C$_2$H$_5$ is present in the discharge at rather high density (see Figure 7), and it plays a significant role in the production and loss of the various hydrocarbon molecules. Therefore, the most important pathways for the production and consumption of this radical are illustrated in Figure 11. C$_2$H$_5$ is mainly (94%) formed by hydrogen attachment to C$_2$H$_4$ (reaction (R15)) and to a lower extent (6%) also by electron impact dissociation of C$_2$H$_6$ (reaction (R9)). The loss of C$_2$H$_5$ is mainly attributed to

radical recombination by reactions (R8), (R7) and (R18), which contribute for 51%, 35% and 6%, respectively. As these reactions result in the formation of C_2H_4, C_2H_6, C_3H_6 and C_3H_8, this means that the equilibrium established between C_2H_4, C_2H_5, and C_2H_6, which relies on the accuracy of the rate coefficients considered, plays a crucial role.
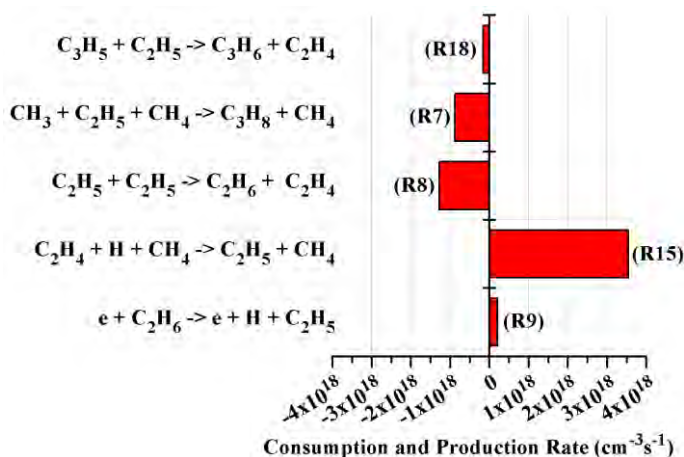

Figure 11. The dominant reaction pathways for the production and consumption of C_2H_5. The time-averaged production rates are plotted as positive values (i.e., right-hand side of the figure), whereas the time-averaged consumption rates are defined as negative values (i.e., left-hand side of the figure). The most important pathways are labeled, and the labels correspond to the reactions given in the text.

(e) The formation and loss of H_2

The most important pathways for the production and consumption of H_2 are illustrated in Figure 12. H_2 is mainly used for the processing of fossil fuels, the production of ammonia and methanol, and as fuel in fuel cells. As appears from Figure 12, H_2 is mainly produced by electron impact dissociation of hydrocarbon molecules. The dissociation reaction of C_2H_6 (reaction (R10)) appears to be the dominant production mechanism, with a contribution of 56%, whereas the dissociation of C_3H_8 (reaction (R11)) and CH_4 (reaction (R4))

contribute for 23% and 7%, respectively. Electron impact dissociation is also the dominant loss process for H$_2$:

$$e^- + H_2 \rightarrow e^- + H + H \qquad\qquad\qquad\qquad (R21)$$
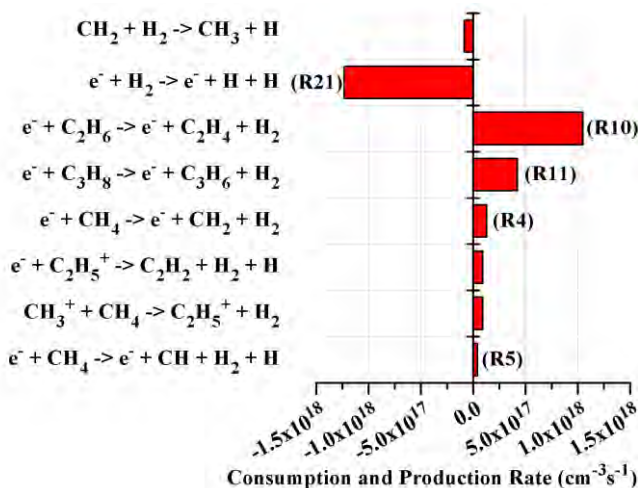
Figure 12. The dominant reaction pathways for the production and consumption of H$_2$. The time-averaged production rates are plotted as positive values (i.e., right-hand side of the figure), whereas the time-averaged consumption rates are defined as negative values (i.e., left-hand side of the figure). The most important pathways are labeled, and the labels correspond to the reactions given in the text.

(f) Summary of the dominant pathways governing the conversion of CH$_4$ into C$_X$H$_Y$ and H$_2$

Finally, Figure 13 gives a schematic overview of the dominant reaction pathways for the conversion of CH$_4$ into higher hydrocarbons and hydrogen gas. Electron impact dissociation of CH$_4$ resulting in the formation of the methyl radical (CH$_3$) starts the conversion process (R3). This methyl radical will initiate recombination reactions towards higher hydrocarbons such as C$_2$H$_6$ and C$_3$H$_8$ (R6, R7). Subsequently, a play of dissociation and recombination

leads to the conversion towards the other, unsaturated hydrocarbons. Finally, dissociation of CH$_4$ and the higher hydrocarbons also results in the formation of H$_2$.
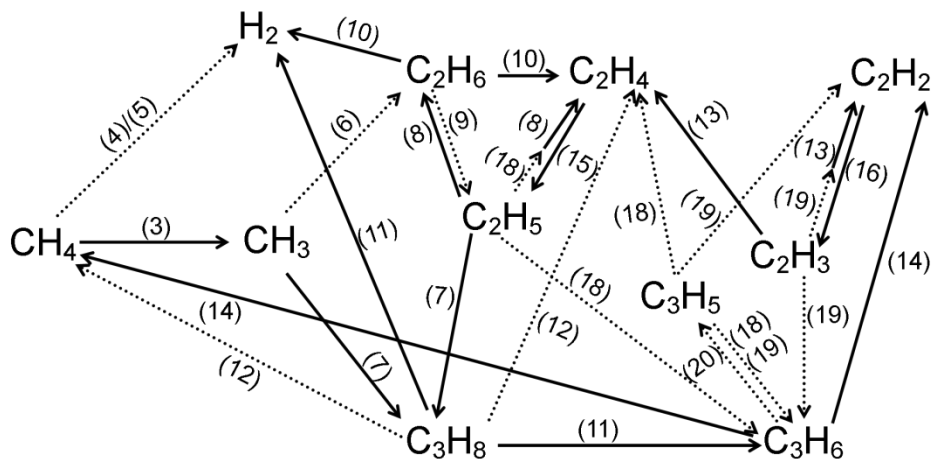
Figure 13. Schematic overview of the dominant reaction pathways for the conversion of CH$_4$ into higher hydrocarbons and hydrogen gas. The most important pathways are depicted with a solid line, less important channels are represented by a dashed line. The labels correspond to the reactions given in the text. Note that C$_4$H$_2$ is not mentioned as it is considered as the sum of all higher polymerized species and also no loss mechanism for it is included in the model.

4.6. Conclusion

In this chapter, a detailed plasma chemistry is presented for the conversion of CH$_4$ into higher hydrocarbon molecules in a DBD reactor. The densities of the various plasma species have been studied as a function of the residence time. The spatially averaged densities of the electrons, ions and radicals show a periodic behavior as a function of time, following the applied voltage. The spatially averaged densities of the molecules do not exhibit a periodic behavior. Indeed, their densities are characterized by a gradual reduction (CH$_4$) or increase (higher hydrocarbon molecules and H$_2$) each half period

following the maximum of the applied voltage, which results in a more notable decreasing or increasing trend over a longer time-scale.

The density of the background gas, methane, is decreasing due to dissociation (and ionization) reactions governing the conversion process. The calculated and measured conversions of CH$_4$ as a function of the residence time are illustrated. The dissociation of CH$_4$ leads to the formation of CH$_3$, which is the most important radical in the gas phase chemistry. This methyl radical will initiate the recombination reactions towards higher hydrocarbons. As a result, these molecules are also present in the discharge at high densities.

The calculated and measured yields and selectivities of these higher hydrocarbons (C$_2$H$_6$, C$_2$H$_4$, C$_2$H$_2$, C$_3$H$_8$ and C$_3$H$_6$) and of H$_2$ are depicted and a reasonable agreement between our calculation results and the measurements is established. C$_2$H$_6$ and H$_2$ are the main reaction products of the conversion of CH$_4$.

Furthermore, the underlying plasma chemistry of the conversion process is analyzed and the dominant reaction pathways for the consumption of CH$_4$ and for the production and loss of the various end products are pointed out. It is found that electron impact dissociation of CH$_4$ resulting in the formation of the methyl radical (CH$_3$) initiates the conversion process. Recombination of CH$_3$ with either another CH$_3$ radical or with a C$_2$H$_5$ radical will lead to the formation of C$_2$H$_6$ and C$_3$H$_8$. Dissociation of these higher hydrocarbons leads directly to the formation of other hydrocarbons, but also indirectly by the formation of new radicals, which can subsequently also recombine towards these higher order hydrocarbons. In other words, the conversion of CH$_4$ is a play of dissociation and recombination reactions leading to a diverse mixture of higher hydrocarbons.

Chapter 5

The Conversion of CH$_4$/O$_2$ and CH$_4$/CO$_2$ into Oxygenates and Syngas

The fluid model described in Chapter 3 is applied here to describe the gas phase chemistry for partial oxidation and for dry reforming of methane. The spatially averaged densities of the various plasma species are presented as a function of time and initial gas mixing ratio. Besides, the conversion of the inlet gases and the selectivities of the reaction products are calculated. Syngas, higher hydrocarbons and higher oxygenates are typically found to be important reaction products. Furthermore, the main underlying reaction pathways for the formation of syngas, methanol, formaldehyde and other higher oxygenates are determined.

5.1. Introduction

In order to convert CH_4 into oxygenates and syngas, the presence of a co-reactant is required. This co-reactant has an important influence on the selectivities of the desired end products. Co-reactants reported in literature for the conversion of methane are oxygen[13, 25, 64-67, 85, 99, 105-106, 120-134], carbon dioxide[14, 20-21, 64, 93, 107-109, 135-184], hydrogen[67, 185-186], steam[165, 168, 187], nitrogen[188] and others[104, 189-192]. When focusing on the formation of oxygenates and syngas, most research is performed on the partial oxidation with oxygen [13, 25, 65-67, 85, 99, 105-106, 120-134] and on dry reforming (CO_2 reforming)[14, 20-21, 93, 107-109, 135-164, 166-167, 169-184]. In this chapter a modeling study for the conversion of CH_4 in the presence of O_2 or CO_2 into higher oxygenates and syngas will be discussed.

Of course, oxygen is very effective for low temperature plasma activation of methane. However, a possible drawback is an excessive oxidation, resulting in the formation of CO_2 and a wide variety of oxygenates. Therefore, the use of CO_2 as a milder oxidant can sometimes be more preferable, depending on the desired end product(s). Moreover, with CO_2 as a co-reactant the two most important greenhouse gases are converted in the process. Current interests in CO_2 utilization include hydrogenation of CO_2 (see also Chapter 6) and the reforming of CH_4 by CO_2.

Experimental results on the conversion in CH_4/O_2[13, 25, 65-67, 85, 99, 105-106, 120-134] and CH_4/CO_2[14, 20-21, 93, 107-108, 135-164, 166-167, 169-170, 173-176, 180, 182-184] plasmas show that the typical end products are C_xH_y, H_2 and CO, and to a lower extent also CH_3OH, CH_2O and other higher oxygenates (acids, alcohols, aldehydes, esters, ketones, …). The H_2/CO ratio and the yield of higher hydrocarbons and oxygenates seems to be very dependent on the CH_4/O_2 or CH_4/CO_2 feed ratio.

In most papers the focus is largely on the formation of C_xH_y and syngas. Only a few papers explicitly focus on the formation of CH_3OH, CH_2O and other higher oxygenates.[14, 25, 64-67, 105-107, 121-122, 126-127, 129, 133-134, 137, 143, 147, 158, 162, 173, 175]

Modeling results on the plasma chemistry in CH_4/O_2 and CH_4/CO_2 mixtures reported in literature mostly originate from zero-dimensional simulations, largely based on specific empirical input, which is only valid for the experimental set-up under study.[20, 25, 85-86, 89, 93, 99, 101, 104-107, 109] Zhou et al. used a semi-empirical kinetic model to simulate the accumulated chemical action of many microdischarges in CH_4/O_2[85] and CH_4/CO_2[20] gas mixtures. Besides the densities of the inlet gases and main products, the pathways for formation of methanol in CH_4/O_2 and syngas in CH_4/CO_2 were briefly discussed. Nair et al.[99], Matin et al.[101], Agiral et al.[25], Goujard et al.[105] and Zhou et al.[106] used a semi-empirical kinetic model to simulate the conversion in a CH_4/O_2 non-thermal plasma. Agiral et al.[25] briefly discussed the mechanisms of the gas-to-liquid process governing the formation of oxygenates. Goujard et al.[105] performed calculations for two different temperatures and discussed the main underlying pathways for the formation of higher oxygenates at these temperatures. Kraus et al.[104] and Luche et al.[89] used a semi-empirical kinetic model to simulate the conversion in a CH_4/CO_2 and a CH_4/air non-thermal plasma, respectively. Goujard et al. applied a simplified global kinetic model to study the helium dilution effect on CO_2 reforming of CH_4 in a DBD.[107] Within our group PLASMANT, Snoeckx et al. performed a computational study ranging from the nanoseconds to seconds time-scale for the conversion of CH_4 and CO_2 into value-added chemicals in a DBD.[109] A zero-dimensional chemical kinetics model was applied to study the plasma chemistry in a 1:1 CH_4/CO_2 gas mixture. The calculations were first

performed for one microdischarge pulse and its afterglow. Subsequently, long time-scale simulations were carried out, corresponding to real residence times in the plasma, assuming a large number of consecutive microdischarge pulses. The conversion of CH_4 and CO_2 as well as the selectivity of the formed products were calculated and compared to experiments for a range of different powers and gas flow rates. In a follow-up paper, this model was applied to a wide range of conditions, including gas mixing ratio, gas residence time, power and frequency, to investigate which conditions give rise to the best conversion and energy efficiency.[181] Machrafi et al. performed calculations for a 1:1 CH_4/CO_2 gas mixture[108] by means of a so-called 3D "Incompressible Navier-Stokes" model with strongly reduced kinetic mechanism, in order to determine the velocity fields. This model was combined with a convection-diffusion model in order to study the behavior of the inlet gases. Qualitative densities were shown, as it was not possible to have a huge kinetic precision using a 3D model. Wang et al. conducted a density functional theory (DFT) study to investigate the reaction mechanisms for the synthesis of oxygenates and higher hydrocarbons from CH_4 and CO_2 using cold plasmas.[94] The main dissociation routes of the reactants were analyzed and the formation of various products, including syngas, higher hydrocarbons and oxygenates, was discussed. Istadi et al. developed a hybrid artificial neural network-genetic algorithm to simulate and optimize a catalytic–DBD plasma reactor in a CH_4/CO_2 gas mixture.[97] The effects of the CH_4/CO_2 feed ratio, total feed flow rate, discharge voltage and reactor wall temperature on the conversion of the inlet gases and the selectivities of the main products were investigated. Recently, Janeco et al.[178] performed a study on the electron kinetics in $He/CH_4/CO_2$ mixtures, including the contribution of H_2 and CO formed in the discharge, as an initial step to model the reforming

of natural gas for syngas production in a DBD. The electron Boltzmann equation for a swarm in the hydrodynamic regime was solved in mixtures of $He/CH_4/CO_2/CO/H_2$. The method used in this work takes into account nonconservative terms and the full angular dependency of the electron velocity distribution function.

In order to achieve our goal, i.e., to describe in detail the plasma chemistry in an atmospheric pressure DBD in different CH_4/O_2 and CH_4/CO_2 gas mixtures, the 1D fluid model used to describe the plasma chemistry for an atmospheric pressure DBD in pure methane (see Chapter 4) was extended. Unlike in most of the above-cited papers, we focus in detail on the main underlying pathways governing the conversion to higher oxygenates, and moreover, we make a comparison of those pathways between a mixture with O_2 and a mixture with CO_2.

In this chapter we present the most important results on the partial oxidation and the dry reforming of CH_4 into syngas, higher oxygenates and higher hydrocarbons. First, the spatially averaged electron and radical densities as a function of time will be illustrated. Furthermore, the densities of the reaction products for a range of different initial gas mixing ratios, as well as the conversion of the inlet gases, will be discussed. Finally, the main underlying reaction pathways for the formation of syngas, methanol and formaldehyde, which appear to be the main oxygenates produced, will be pointed out.

5.2.   Species Included in the Model

The chemistry in a CH$_4$/O$_2$ and CH$_4$/CO$_2$ gas mixture is described by 75 species (electrons, molecules, ions and radicals). As mentioned above, the model for pure CH$_4$ (see Chapter 4) is extended. O$_2$ and CO$_2$ are included as extra feed gases. Furthermore, CO, H$_2$O, CH$_2$O, CH$_3$OH and some other higher oxygenates are considered in the model, as they might be formed in the plasma. Note that formic acid (HCOOH) and acetic acid (CH$_3$COOH), which were experimentally found, are not included in the model as the rate constants for the formation and loss processes for these molecules are not well known. Similar to the model for pure CH$_4$, the radical and ionic species corresponding to the formation products of dissociation, ionization and attachment reactions of the molecules are also taken into account. Although some vibrational and electronic excitation reactions are included in the model, vibrationally and electronically excited species are not taken into account separately, in order to limit the number of species and reactions (see also Chapter 4). Also rotationally excited species are not taken into account in the model. Indeed, the electron energy required for rotational excitations is negligible compared with this for vibrational excitations.[70, 110] Table 5 presents an overview of the different species taken into account in the model.

Table 5. Overview of the species included in the model, besides the electrons.

Molecules	CH$_4$, C$_2$H$_6$, C$_2$H$_4$, C$_2$H$_2$, C$_2$, C$_3$H$_8$, C$_3$H$_6$, C$_4$H$_2$, H$_2$, O$_3$, O$_2$, CO$_2$, CO, H$_2$O, H$_2$O$_2$, CH$_2$O, CH$_3$OH, C$_2$H$_5$OH, CH$_3$CHO, CH$_2$CO, CH$_3$OOH, C$_2$H$_5$OOH
Ions	CH$_5^+$, CH$_4^+$, CH$_3^+$, CH$_2^+$, CH$^+$, C$^+$, C$_2$H$_6^+$, C$_2$H$_5^+$, C$_2$H$_4^+$, C$_2$H$_3^+$, C$_2$H$_2^+$, C$_2$H$^+$, C$_2^+$, H$_3^+$, H$_2^+$, H$^+$, O$_4^+$, O$_2^+$, O$^+$, O$_4^-$, O$_3^-$, O$_2^-$, O$^-$, CO$_2^+$, CO$^+$, H$_3$O$^+$, H$_2$O$^+$, OH$^+$, H$^-$, OH$^-$
Radicals	CH$_3$, CH$_2$, CH, C, C$_2$H$_5$, C$_2$H$_3$, C$_2$H, C$_3$H$_7$, C$_3$H$_5$, H, O, OH, HO$_2$, CHO, CH$_2$OH, CH$_3$O, C$_2$H$_5$O, C$_2$HO, CH$_3$CO, CH$_2$CHO, CH$_3$O$_2$, C$_2$H$_5$O$_2$

5.3. Reactions Included in the Model

The 75 species can interact with each other through a large number of reactions. 1019 gas phase reactions, including 157 electron-neutral, 48 electron-ion, 476 neutral-neutral and 338 ion-ion or ion-neutral reactions, are considered. An overview of the reactions is given in the Appendices.

Like in Chapter 4, the rates of the different reactions are calculated from the densities of the colliding species and the corresponding reaction rate coefficients. The electron-neutral and electron-ion reactions are again treated by energy dependent reaction rate coefficients. The rate coefficients of the electron-neutral reactions are obtained from look-up tables calculated with the Boltzmann solver Bolsig+[74], based on the energy dependent collision cross sections for these reactions. The references for the cross sections can also be found in Table A.1. of the Appendices. The lookup tables for the electron-ion dissociative recombination reactions are built using the functions in combination with the branching ratios for the different channels, of which a detailed overview is given in Table A.2. of the Appendices. The neutral-neutral and ion-neutral reactions are again defined in the model with a constant reaction rate coefficient at a pressure and temperature of 1 atm and 300 K, respectively. These rate coefficients and their corresponding references are summarized in Table A.3. and Table A.4. of the Appendices, respectively.

5.4. Operating Conditions

The calculations are carried out for a gas residence time up to 20s, at a fixed applied voltage of 5 kV and a frequency of 10 kHz. The CH_4/CO_2 molar ratio is

varied in the range of 5-80% CO_2, while the CH_4/O_2 molar ratio is varied from 10 to 30% O_2. The CH_4/CO_2 molar ratio can be varied in a much wider range than the CH_4/O_2 molar ratio, because the latter approaches the upper flammability or explosion limit when the mole fraction of CH_4 in pure O_2 reaches 61 mole%.[193]

5.5.   Results and Discussion

5.5.1.   Densities of the Plasma Species

Figure 14 illustrates the periodic behavior as a function of time of the spatially averaged electron density for a 70/30 (a) and 90/10 (b) CH_4/O_2 gas mixture and for a 70/30 (c) and 90/10 (d) CH_4/CO_2 gas mixture, on a logarithmic scale, for four periods of the applied voltage. The applied voltage as a function of time is also plotted, for the sake of clarity. In the 70/30 CH_4/O_2 mixture, breakdown in the gas appears once each period following the applied voltage, while in the 90/10 CH_4/O_2 mixture and the 70/30 CH_4/CO_2 mixture, a breakdown appears each half period, and in the 90/10 CH_4/CO_2 mixture, even more breakdowns occur (see below). The electron density behavior is different for the positive and the negative polarity of the applied voltage, which is due to the dissimilarity in surface dimensions and properties of the inner and outer electrode (i.e., only the outer electrode is covered by a dielectric), as was also discussed in Section 4.5.1. above.
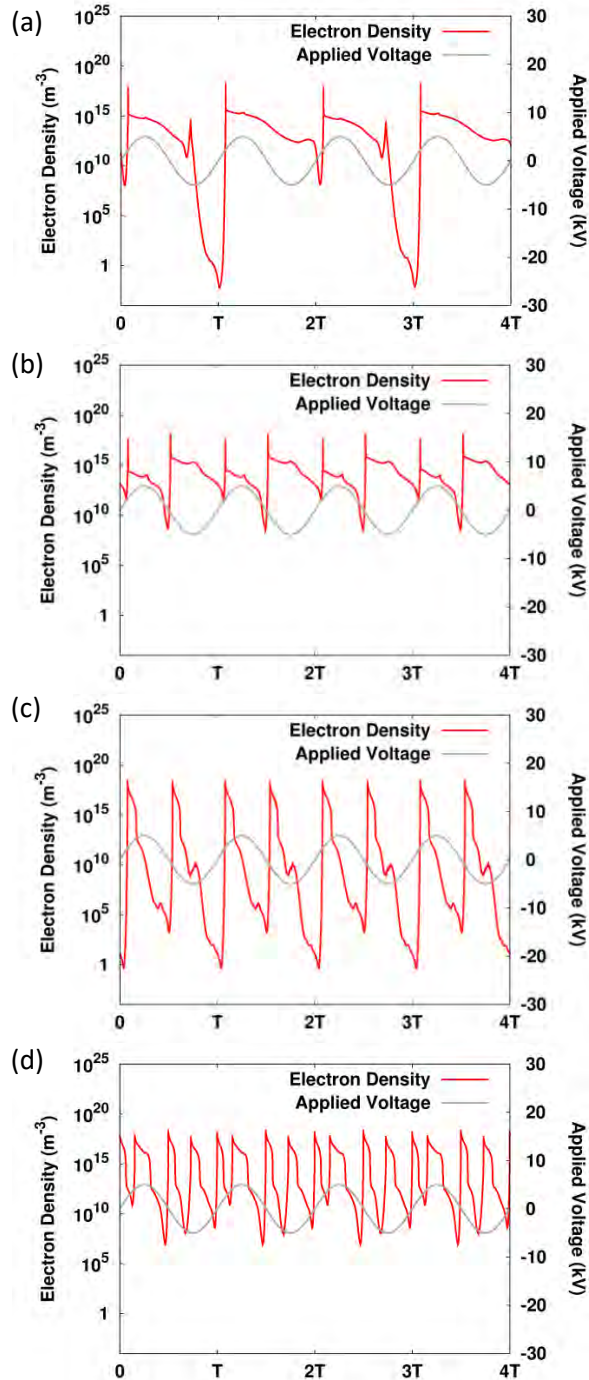
Figure 14. Spatially averaged electron density on a logarithmic scale for a 70/30 (a) and 90/10 (b) CH_4/O_2 gas mixture and for a 70/30 (c) and 90/10 (d) CH_4/CO_2 gas mixture, as a function of time, for four periods of the applied voltage. The applied sinusoidal voltage is also presented, for the sake of clarity.

As mentioned above, in the mixtures with CO_2 twice as many breakdowns appear, compared to the corresponding mixtures with O_2. The figures (a ↔ c, b ↔ d) also illustrate the different periodical behavior. Furthermore, the number of breakdowns is also twice as large for the mixtures with 90 % CH_4 (b and d) compared to the corresponding mixtures with 70 % CH_4 (a and c). The same behavior was also observed for the current profiles and the charging of the electrodes, and can be attributed to the different degree of electronegativity of the various gas mixtures and mixing ratios (see below).

It is also clear from the figures that for the mixtures with 90 % CH_4 (b and d) the minimum electron density is much higher than for the mixtures with 70 % CH_4 (a and c). Nevertheless, the overall spatially and time averaged electron density is almost the same for either 90% or 70% CH_4, and amounts to ca. 10^{15} m^{-3} for the CH_4/O_2 mixture and to ca. 10^{16} m^{-3} for the CH_4/CO_2 mixture. This is one and two orders of magnitude lower than the calculated value of 10^{17} m^{-3} for a pure CH_4 plasma (see Section 4.5.1.), and the reason for this is given below.

The overall spatially and time averaged mean electron energy in the CH_4/O_2 and CH_4/CO_2 gas mixtures was calculated to be about 1.6 eV and 2.1 eV, respectively, compared to about 2 eV in pure CH_4 (see Section 4.5.1.). These differences in electron density and mean electron energy between CH_4/O_2 and CH_4/CO_2 can be attributed to the fact that CH_4/O_2 gives rise to an electronegative plasma in contrast to CH_4/CO_2 and pure CH_4. Indeed, the (positive and negative) ion density is three orders of magnitude higher than the electron density in CH_4/O_2, while in CH_4/CO_2 the electron density is in the same order of magnitude as the positive ion density and one order of magnitude higher than the negative ion density. This can be explained

because in CH_4/O_2 the electrons are more easily trapped by attachment reactions with O_2, and moreover, the higher energy electrons are more frequently consumed in ionization and dissociation reactions, as the threshold energies for these reactions are much lower in CH_4/O_2[194-195] than in CH_4/CO_2[196]. Thus, the CH_4/O_2 plasma is most electronegative, containing the highest negative ion density, and this explains the lower (spatially and time averaged) electron density than in the CH_4/CO_2 plasma (which still contains some negative ions), and especially compared to the pure CH_4 plasma (which virtually does not contain negative ions).

The number densities of the radicals and ions, produced by collisions of the electrons with the gas molecules, exhibit the same periodic behavior as the electron density, as is illustrated in Figure 15 for the radicals, for a 70/30 CH_4/O_2 (a, b) gas mixture and a 70/30 CH_4/CO_2 (c, d) gas mixture. However, this periodic trend is superimposed on a rising or declining trend, acting over a longer time-scale until periodic steady state is reached.
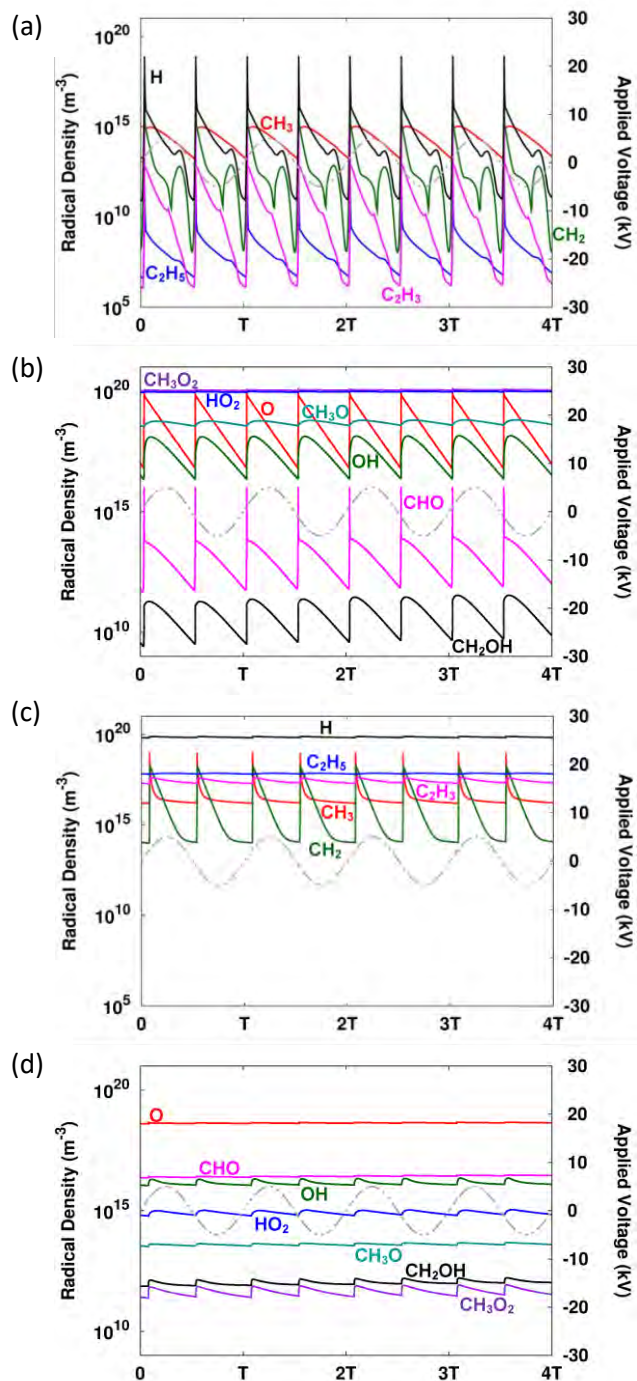
**Figure 15. Spatially averaged radical densities (left axis) as a function of time for a 70/30 CH_4/O_2 (a, b) gas mixture and for a 70/30 CH_4/CO_2 (c, d) gas mixture, as well as the applied sinusoidal voltage (gray, right axis) for four periods of the applied voltage.**

It is clear from Figure 15 that the densities of some radicals, such as O, OH, CHO, CH_2OH, C_2H_5, C_2H_3 and H in the CH_4/O_2 gas mixture, and CH_3 and CH_2 in both gas mixtures, vary over several orders of magnitude throughout a period. This is because their formation or loss (e.g., H radicals are consumed in reactions with O_2) is strongly dependent on electron impact dissociation of one of the inlet gases. On the other hand, the densities of radicals which are not directly formed by electron impact dissociation of one of the inlet gases, such as C_2H_5, C_2H_3, H, O, OH, CHO, CH_2OH in the CH_4/CO_2 gas mixture, and HO_2, CH_3O and CH_3O_2 in both gas mixtures, vary by less than one order of magnitude throughout a period. The overall spatially and time averaged radical densities vary from about 10^8 m^{-3} for the less abundant radicals, to about 10^{19} m^{-3} for the most abundant radicals. The most abundant radicals in the CH_4/O_2 gas mixture are O, OH, HO_2, CH_3O and CH_3O_2, while H, O, CH_3, CH_2, C_2H_5 and C_2H_3 are mostly abundant in the CH_4/CO_2 gas mixture (see also below). This will determine the different reaction pathways for the formation of the oxygenates in the CH_4/O_2 and CH_4/CO_2 gas mixtures, as will be elaborated in Section 5.5.3. below.

Figure 16 shows the spatially and time averaged radical densities as a function of the initial gas mixing ratio in both the CH_4/O_2 and CH_4/CO_2 gas mixtures. It is clear that the mixtures with CO_2, at an identical initial fraction of CH_4, yield higher densities of C_xH_y, H, CHO and CH_2OH radicals than the mixtures with O_2, while the densities of O, OH, HO_2, CH_3O and CH_3O_2 are higher in the mixtures with O_2 than in the mixtures with CO_2. This can be explained because the net formation of C_xH_y directly or indirectly from CH_4 is higher in the mixtures with CO_2. Furthermore, the formed H, CHO and CH_2OH radicals immediately react with O_2 into HO_2, CO and CH_2O, respectively, and

therefore the net formation of H, CHO and CH_2OH is higher in the mixtures with CO_2. Likewise, the O, OH, HO_2, CH_3O and CH_3O_2 radicals are directly or indirectly formed from O_2 (see Section 5.5.3. below), which explains their higher density in the CH_4/O_2 mixtures. Upon rising initial fraction of CO_2 between 5 and 80 %, the densities of the C_xH_y radicals and of the H atoms drop by half an order to one order of magnitude, due to the fact that these radicals are directly or indirectly formed out of CH_4. A similar trend is observed upon rising fraction of O_2. On the other hand, the densities of O, OH and other O-containing radicals increase by half an order to several orders of magnitude upon rising fraction of CO_2 in the gas mixture, which can be explained by the fact that these radicals are directly or indirectly formed out of CO_2. For the same reason, the densities of the O and OH radicals slightly increase upon rising fraction of O_2 in the gas mixture, while the other O-containing radicals decrease by half an order to several orders of magnitude. The latter can be explained by the fact that a higher inlet fraction of O_2 leads towards full oxidation of CH_4 (see also Figure 17 below).

The ion densities also exhibit a similar periodic behavior as the electrons, which is logical, as they are mostly formed by electron impact ionization or by (dissociative) attachment from the inlet gases, for the positive and negative ions, respectively. The most abundant ions in the CH_4/O_2 gas mixtures are CH_5^+, $C_2H_5^+$, O_4^+, H_3O^+, O_2^-, O_4^- and OH^-, while CH_5^+, $C_2H_5^+$ and OH^- are the most abundant ions in the CH_4/CO_2 gas mixtures. Their spatially and time averaged densities are in the order of 10^{17} m^{-3} and 10^{16} m^{-3} for the CH_4/O_2 and CH_4/CO_2 gas mixtures, respectively. This is typically 2 or 3 orders of magnitude lower than the spatially and time averaged densities of the most abundant radicals in both gas mixtures, indicating that the ions play a minor role in the plasma

chemistry (see Section 5.5.3. below). Therefore, we do not go in further detail on the ion densities.
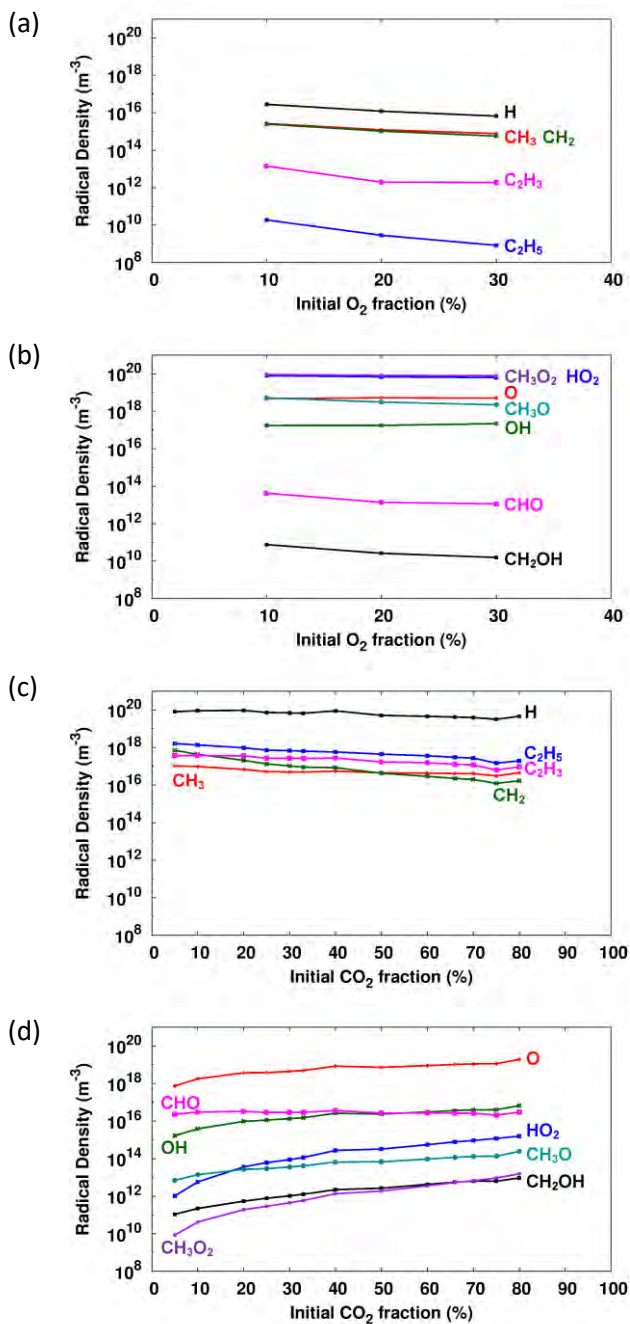
**Figure 16. Spatially and time averaged radical densities as a function of the initial gas mixing ratio for the CH_4/O_2 (a, b) and CH_4/CO_2 (c, d) gas mixtures.**

CH_4/O_2
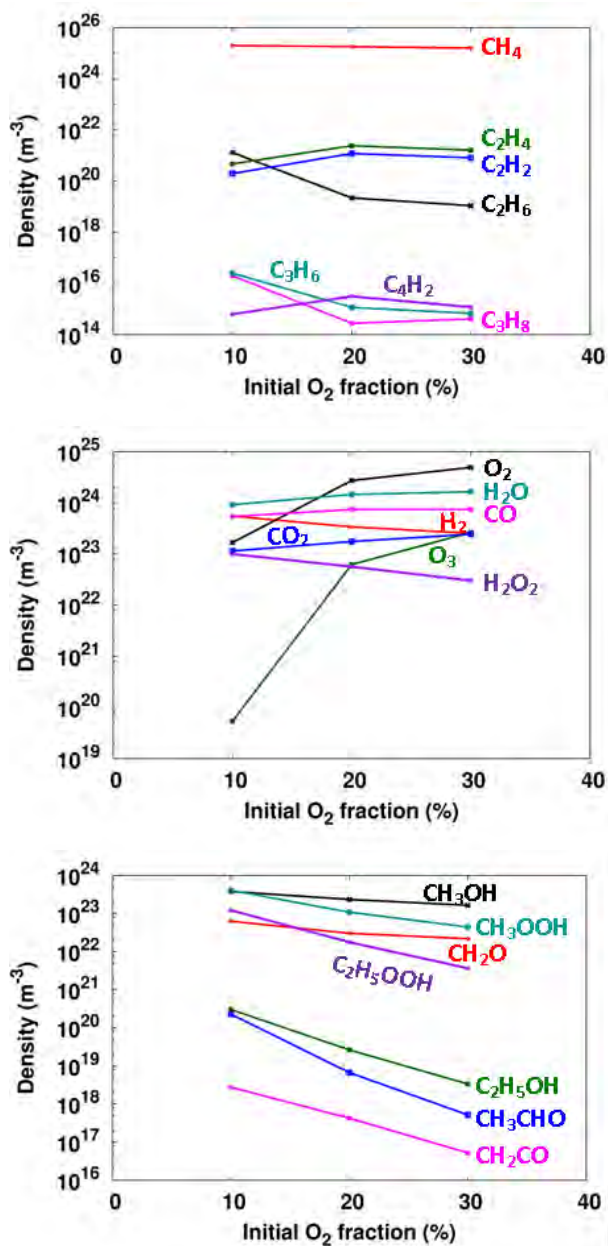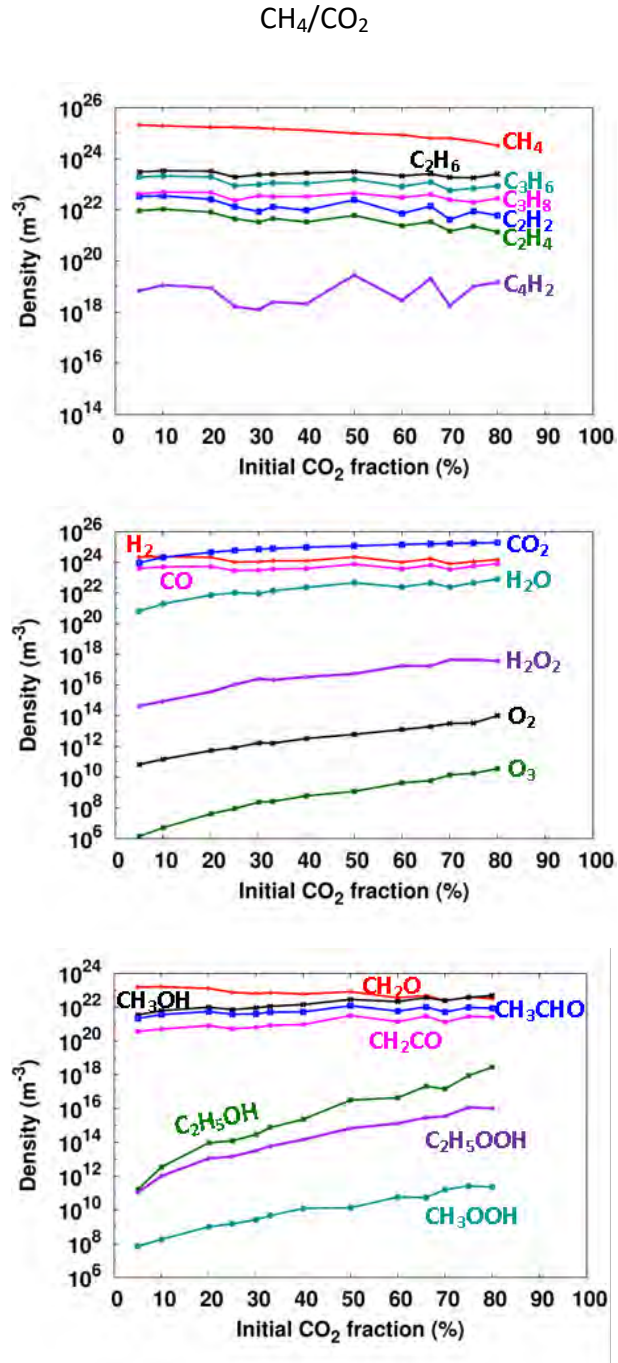
CH_4/CO_2

Figure 17. Spatially averaged molecule densities as a function of the initial gas mixing ratio, after a residence time of 5 seconds, for the CH_4/O_2 (left panel) and CH_4/CO_2 (right panel) gas mixtures.

The molecules do not exhibit such a periodic behavior as the electrons, as they are not directly correlated with the electron density and electron energy, because they are typically formed by recombination of the radicals (see Section 5.5.3. below). The densities of the molecules formed from the inlet gases, i.e., H_2, CO, higher order hydrocarbons and oxygenates, exhibit a rising trend as a function of time, during each half period of the applied voltage, because their net production is higher than their net consumption. The inlet gases, on the other hand, have a higher net consumption, so they are characterized by a gradual decrease in their densities during each half period. It appears that the conversion is most pronounced in the first few seconds and that the densities of the molecules do not significantly change anymore for a longer residence time. Below, we present the densities as a function of time, but here we first focus on the densities of the different end products as a function of the initial gas mixing ratio after a certain residence time.

Figure 17 illustrates the densities of the various molecules as a function of the initial gas mixing ratio, after a residence time of 5 seconds, for the CH_4/O_2 (left panel) and CH_4/CO_2 (right panel) gas mixtures. A residence time of 5 s corresponds to a gas flow rate of 0.2 L·min^{-1} for the plasma reactor under study. It is clear that the densities of the higher hydrocarbons (C_xH_y), as well as H_2, CH_2O (formaldehyde), CH_3CHO (acetaldehyde) and CH_2CO (ketene or ethenone) are higher in the mixtures with CO_2, while the densities of O_3, H_2O, H_2O_2 (hydrogen peroxide), CH_3OH (methanol), C_2H_5OH (ethanol), CH_3OOH (methyl hydroperoxide) and C_2H_5OOH (ethyl hydroperoxide) are higher in the mixtures with O_2. CO is formed at high density in both gas mixtures and therefore the H_2/CO ratio is higher than 1 in the mixtures with CO_2 and lower

than 1 in the mixtures with O_2. Note that in the gas mixtures with O_2 as a co-reactant also a significant amount of undesired CO_2 is formed.

These results are in good agreement with reported results in literature on the formation of oxygenates in CH_4/O_2 and CH_4/CO_2 in discharges at similar conditions. Larkin et al.[64-67] discussed the formation of CO, CO_2, CH_3OH, CH_2O, HCOOH (formic acid) and CH_3COOH (acetic acid) in CH_4/O_2 in a plasma reactor surrounded by a water cooling jacket to increase the formation of liquid oxygenates. They also showed that in the presence of enough O_2 the selectivity of C_xH_y will remain low. Okumoto et al.[121-122] made use of dilution gases to enhance the formation of oxygenates in CH_4/O_2 and reported the formation of C_xH_y, CO, CO_2, H_2, H_2O, CH_3OH, CH_2O and CH_3CHO. Nozaki et al.[126, 133-134], Goujard et al.[105] and Agiral et al.[25] carried out experiments for CH_4/O_2 gas mixtures in a microplasma reactor, which was immersed into a water bath maintained near room temperature, to enhance the condensation of liquid components on the cooled reactor wall. Furthermore, they intermittently injected distilled water in addition to the inlet gases in order to wash out these liquid components and they collected all condensable components at the end of the reactor by a cold trap. They found that if oxygen was totally consumed, so after a long residence time, or when the inlet oxygen fraction was excessively high, the main products were CO, CO_2 and H_2O. Besides, also the formation of H_2, C_xH_y, HCOOH, H_2O_2, CH_3OOH, CH_3OH and CH_2O were reported, and the concentration of CH_3OH was much higher than that of CH_2O without the cooling, which is in good agreement with our results. However, the selectivity of CH_2O and HCOOH drastically increased when cooling the reactor. Indarto et al.[127, 129] discussed the formation of H_2, CO, CO_2, H_2O, C_xH_y and CH_3OH in CH_4/O_2 and found that a

proper selection of catalyst can drastically enhance the yield and selectivity of CH_3OH. Our results are also in reasonable agreement with the results reported by Zhou et al.[106] comparing the use of a single and a double dielectric plasma reactor for the direct oxidation of CH_4 to H_2O_2 and oxygenates, where the double dielectric reactor favored the formation of these products.

The conversion of CH_4 in the presence of CO_2 is much less reported. Zou et al.[14] discussed the formation of CO, H_2, C_xH_y, H_2O, CH_2O, CH_3OH, C_2H_5OH, HCOOH, CH_3COOH and other alcohols, acids, aldehydes, ketones and esters in CH_4/CO_2 in the presence of starch. It was shown that the selectivity of C_xH_y was much higher than for the oxygenates, which is in good agreement with our results. Kozlov et al.[137], Zhang et al.[147] and Scarduelli et al.[162] reported the formation of a variety of hydrocarbons and oxygenates in CH_4/CO_2. Li et al.[143] found that CH_3COOH and C_2H_5OH were the major oxygenates among other alcohols and acids formed in CH_4/CO_2, but of course their selectivities were much lower than those for C_xH_y and CO. Sentek et al.[158] discussed the formation of H_2, CO, C_xH_y and alcohols in a CH_4/CO_2 plasma in the presence of a catalyst. Finally, Goujard et al.[107] studied the effect of helium dilution on the formation of CO, C_xH_y, CH_2O and CH_3OH in CH_4/CO_2.

The flexible adaptation of the H_2/CO ratio in a DBD by altering the inlet gas mixing ratio is an advantage compared to classical processes, including steam reforming, partial oxidation, and CO_2 reforming, which typically produce syngas with H_2/CO molar ratio greater than 3, less than 2 and less than 1, respectively.[20-21] The H_2/CO molar ratio from steam reforming (>3) is much higher than that required by the stoichiometry for many synthesis processes. A low H_2/CO molar ratio (in the order of 2) is desirable for many industrial

synthesis processes, such as the Fischer Tropsch synthesis or the synthesis of valuable oxygenated chemicals. Methanol can even be produced from syngas with a H_2/CO molar ratio as low as 0.5, when the system can simultaneously carry out methanol synthesis and the water-gas-shift reaction.[20-21]

If the initial fraction of O_2 increases from 10 to 30%, the densities of C_2H_6, C_3H_6, C_3H_8, H_2, H_2O_2, CH_2O, CH_3OH and CH_3OOH decrease up to one order of magnitude, and the densities of C_2H_5OH, CH_3CHO, CH_2CO and C_2H_5OOH decrease even with several orders of magnitude. Meanwhile, the densities of C_2H_4, C_2H_2, C_4H_2, CO_2, CO and H_2O increase up to one order of magnitude and the density of O_3 increases with several orders of magnitude, pointing towards full oxidation of CH_4. In other words, if higher oxygenates, such as CH_2O and CH_3OH, are the desired end products of the gas conversion of CH_4, it is appropriate to make use of CH_4/O_2 gas mixtures with a not too high fraction of O_2. These results are in reasonable agreement with reported research on the effect of the initial gas mixing ratio in similar discharges in CH_4/O_2 by Larkin et al.[65-66], Okumoto et al.[122] and Zhou et al.[106].

Likewise, increasing the initial fraction of CO_2 from 5 to 80% results in a drop of the densities of C_xH_y, H_2, and CH_2O up to one order of magnitude, while the densities of CO, CH_3OH, CH_3CHO and CH_2CO increase up to one order of magnitude and the densities of O_2, O_3, H_2O, H_2O_2, C_2H_5OH, CH_3OOH and C_2H_5OOH increase even with several orders of magnitude. In other words, the ideal gas mixing ratio for CH_4/CO_2 gas mixtures depends on the desired higher oxygenate to be formed. Since the H_2 density drops and the CO density increases upon rising initial fractions of O_2 and CO_2, the H_2/CO molar ratio will significantly decrease, which is interesting, in view of the desired stoichiometry for industrial synthesis processes (cf. above). These results are

again in reasonable agreement with literature studies on the effect of the initial gas mixing ratio in similar discharges in CH_4/CO_2 by Zou et al.[14], Li et al.[143] and Zhang et al.[147].

Note that the trends illustrated in Figure 17 correspond to a residence time of 5 seconds; however, the different molecules might have their maximum densities at a different residence time for the different gas mixtures studied, so the trends depicted in Figure 17 are not necessarily the same at other residence times. Besides, the gas composition in the CH_4/O_2 gas mixtures completely changes at the moment when O_2 is fully consumed, which happens after 5.6s and 15.2s, in the case of 10 and 20% O_2, respectively (see Figure 19 below). To make this more clear, we show in Figure 18 the characteristic density profiles as a function of the residence time, as we have observed for the different molecules, for a 90/10 CH_4/O_2 (a) and a 90/10 CH_4/CO_2 (b) gas mixture.

In the mixture with O_2 we can distinguish six different density profiles:

1. H_2 and CO show a continuously rising trend.

2. The higher hydrocarbons (C_xH_y), ethanol (C_2H_5OH) and ketene (CH_2CO) have negligible values up to 5.6s, followed by a strong increase up to an equilibrium value after 10s.

3. O_3 exhibits a maximum within 1s, and then reacts away within 3 s.

4. CO_2, H_2O and methanol (CH_3OH) show a steady increase to a maximum at around 6-8s, followed by a very slow decrease.

5. Hydrogen peroxide (H_2O_2), methyl hydroperoxide (CH_3OOH) and ethyl hydroperoxide (C_2H_5OOH) go over a maximum at 4-6s and then decrease rapidly.

6. Finally, formaldehyde (CH_2O) and acetaldehyde (CH_3CHO) also reach a maximum at 4-6s, but after a fast drop, their density increases again after 8s.

Except for the profile of O_3 (no. 3), which has already reacted away after 4s, the effect of O_2 being fully consumed after 5.6s can be observed in the changes of the density profiles of all different molecules at this moment of time. Indeed, the densities of the higher hydrocarbons, for instance, start rising at that time, because in the absence of O_2, the CH_4 will mainly be converted into higher hydrocarbons, while the densities of the oxygenates typically show a (sharp) drop in time, when O_2 is fully depleted.

In the mixture with CO_2 four different density profiles can be distinguished:

1. H_2, CO, ethane (C_2H_6) and methanol (CH_3OH) exhibit a steady rise as a function of time.
2. Ethylene (C_2H_4), acetylene (C_2H_2), C_4H_2, H_2O, formaldehyde (CH_2O), acetaldehyde (CH_3CHO) and ketene (CH_2CO) go over a maximum at around 6-8s.
3. Propane (C_3H_8), propene (C_3H_6) and ethanol (C_2H_5OH) rise rapidly, but reach an equilibrium density after 2s.
4. O_2, O_3, hydrogen peroxide (H_2O_2), methyl hydroperoxide (CH_3OOH) and ethyl hydroperoxide (C_2H_5OOH) reach a maximum within 5 ms, and then react rapidly away.

Thus it is clear that the higher hydrocarbons and oxygenates (no. 2 and no. 3) can be formed at rather high density, but they react away again after a longer residence time towards H_2 and CO, respectively, which explains why H_2 and CO show a continuously rising trend. Besides H_2 and CO, also C_2H_6 and CH_3OH exhibit a steady rise (no. 1) as their formation is strongly connected to

the dissociation products of CH$_4$, in particular the CH$_3$ and CH$_2$ radicals. Finally, O$_2$, O$_3$ and the different peroxides are only present at very low densities, and for a very short time, as they are formed as an intermediate in the direct or indirect formation of CO.

An identical behavior is observed for all these species in the other gas mixing ratios of CH$_4$ with O$_2$ and CO$_2$.
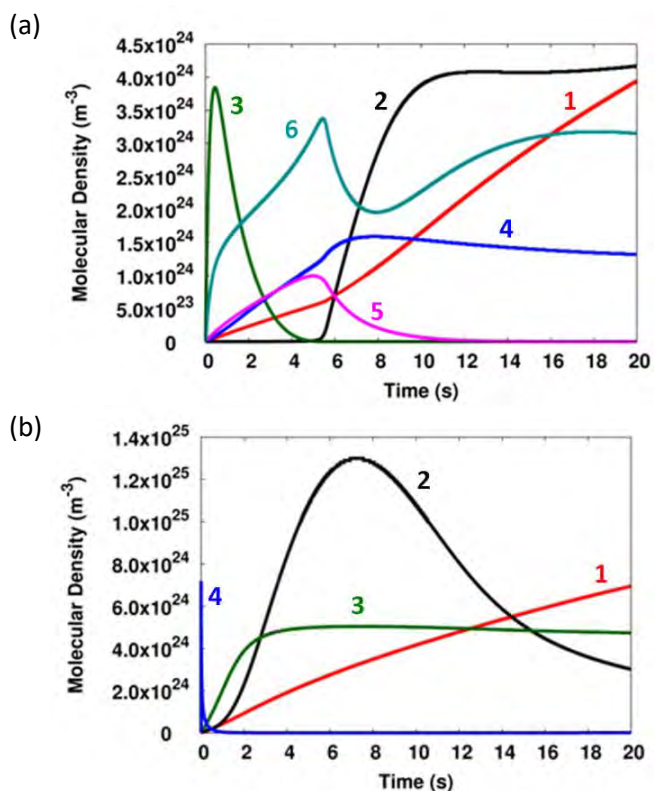
Figure 18. Spatially averaged molecule densities as a function of the residence time, for the 90/10 CH$_4$/O$_2$ gas mixture (a) and the 90/10 CH$_4$/CO$_2$ gas mixture (b). The labels of the curves characterize some specific molecules (see text). For panel (a): 1 = H$_2$ (density divided by 10), 2 = C$_2$H$_6$, 3 = O$_3$ (density multiplied by 10), 4 = CO$_2$, 5 = H$_2$O$_2$, 6 = CH$_2$O (density multiplied by 5). For panel (b): 1 = H$_2$, 2 = C$_2$H$_4$ (density multiplied by 1000), 3 = C$_3$H$_8$ (density multiplied by 100), 4 = O$_2$ (density multiplied by 10^{10}).

5.5.2.   Conversion, Yields and Selectivities

Figure 19 shows the conversion of CH_4 and O_2 (a) and of CH_4 and CO_2 (b) as a function of residence time for different gas mixing ratios. The conversion of CH_4 after 20s is around 20% in all considered mixtures with O_2, while in pure CH_4, a conversion of 40% was calculated after 20s (see Section 4.5.2.). This is logical, because in the CH_4/O_2 mixture a considerable fraction of the energy is also consumed by O_2. O_2 is indeed converted very quickly, and the time for full conversion depends on the initial fraction of O_2, i.e., full conversion is reached faster in the case of a lower O_2 initial fraction (see Figure 19(a)), which is logical.

In the CH_4/CO_2 gas mixture, the conversion of both CH_4 and CO_2 strongly depends on the initial gas mixing ratio. No clear trend can be observed from Figure 19(b), because the initial gas mixing ratio strongly affects the discharge characteristics and therefore the conversion of the inlet gases. The effect of the initial gas mixing ratio on the conversion will be discussed below. Our calculations predict a maximum conversion of 68% for CH_4 and 55% for CO_2 after a residence time of 20s in a 20/80 and a 95/5 CH_4/CO_2 gas mixture, respectively (not shown in Figure 19(b)). It is logical that a higher CH_4 conversion is reached at a lower initial CH_4 fraction in the gas mixture, and vice versa for CO_2, because these conditions yield a higher co-reactant concentration, which contributes to a more efficient conversion.

(a)   CH$_4$/O$_2$
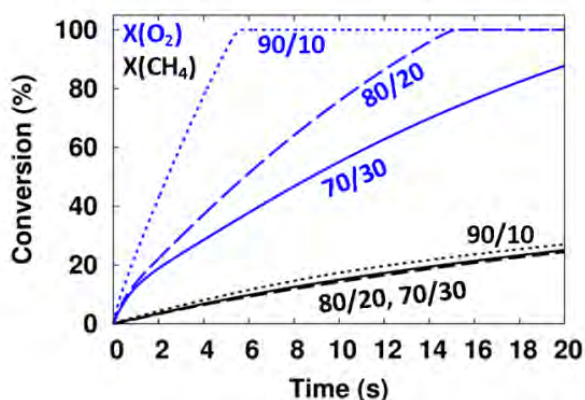
(b)   CH$_4$/CO$_2$
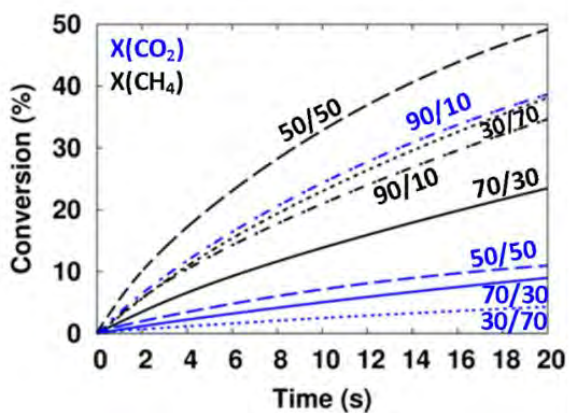
Figure 19. Conversion of CH$_4$ (black) and O$_2$ (a, blue) or CO$_2$ (b, blue) as a function of residence time.

When comparing the conversion of CH$_4$ in both the CH$_4$/O$_2$ and the CH$_4$/CO$_2$ gas mixtures with the same gas mixing ratios, it is clear that at a 70/30 gas mixing ratio, the CH$_4$ conversion is equal (i.e., around 20%) in both gas mixtures, while at the 80/20 and 90/10 gas mixing ratios, the CH$_4$ conversion was found to be slightly higher in the mixtures with CO$_2$ than in the mixtures with O$_2$. This can be explained because the loss (by electron impact dissociation and ionization) of CH$_4$ is about a factor 2 higher in CH$_4$/CO$_2$ than in CH$_4$/O$_2$ due to the fact that much more electrons are consumed by electron impact reactions with O$_2$ than with CO$_2$ (cf. the electronegative character,

explained in Section 5.5.1. above). However, the lower consumption of CH_4 in the CH_4/O_2 gas mixture is partially compensated by the increasing importance of the reaction with OH when the initial fraction of O_2 in the gas mixture increases. Furthermore, in the CH_4/CO_2 gas mixture, the production (or regeneration) of CH_4 is around 50% of the CH_4 consumption when the initial fraction of CO_2 is in the range of 10-30%, while in the CH_4/O_2 mixture, the CH_4 production is decreasing with increasing O_2 initial fraction, from 30% of the CH_4 consumption in 90/10 CH_4/O_2 to 8% in 70/30 CH_4/O_2 (i.e. one order of magnitude lower than in 70/30 CH_4/CO_2). In other words, the much lower regeneration of CH_4 in the 70/30 CH_4/O_2 mixture than in the 70/30 CH_4/CO_2 mixture compensates enough for the lower consumption of CH_4 in the 70/30 CH_4/O_2 mixture than in the 70/30 CH_4/CO_2 mixture. This effect, together with the increasing importance of the reaction with OH radicals, results in an almost equal net conversion of CH_4 in both gas mixtures at a 70/30 gas mixing ratio (see more details in Section 5.5.3. and Figure 21 below).

Figure 20 shows the conversion of CH_4, O_2 and CO_2 as a function of the initial gas mixing ratio, for both the CH_4/O_2 and CH_4/CO_2 gas mixtures, after a residence time of 5s. The CH_4 conversion is roughly independent from the initial O_2 or CO_2 fraction up to 30-40%, with a value of about 10%, but it increases for higher initial CO_2 fractions, especially above 70%. Indeed, at higher initial CO_2 fractions, the conversion of CH_4 rises due to the increasing importance of the reaction of CH_4 with CO_2^+, which becomes the most important channel for consumption of CH_4, while at lower initial CO_2 fractions electron impact dissociation of CH_4 is the most important loss channel (see also Section 5.5.3. and Figure 21 below). For the same reason, the conversion of O_2 and CO_2 increases with decreasing initial O_2 or CO_2 fraction, because of

the additional loss reactions with CH$_4$ molecules (or CH$_4$-derived species). For instance, in the 70/30 CH$_4$/O$_2$ mixture, a three-body reaction with O radicals is the most important loss process for O$_2$, while in the 90/10 CH$_4$/O$_2$ mixture, the most important loss processes for O$_2$ are three-body reactions with CH$_3$ or H radicals (see also Section 5.5.3. and Figure 22 below). Likewise, in the CH$_4$/CO$_2$ mixtures with high initial CO$_2$ fractions, electron impact ionization of CO$_2$ is the most important loss channel, while at lower initial CO$_2$ fractions, the reaction of CO$_2$ with CH$_2$ radicals is the most important loss channel for CO$_2$ (see again Section 5.5.3. and Figure 22 below).
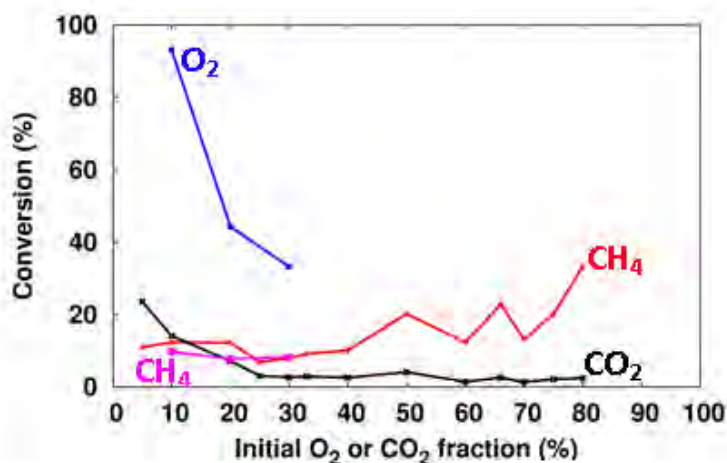
Figure 20. Conversion of CH$_4$, O$_2$ and CO$_2$ as a function of the initial O$_2$ or CO$_2$ fraction in the gas mixture, for a residence time of 5 seconds. The CH$_4$ conversion in the CH$_4$/CO$_2$ mixture is depicted in red, while the CH$_4$ conversion in the CH$_4$/O$_2$ mixture is presented in pink.

As was also clear from Figure 19, the O$_2$ conversion is much higher than the CO$_2$ conversion, which is only in the order of 20% at low CO$_2$ fractions, and even below 3% at higher CO$_2$ fractions. This is because the threshold energies for electron impact ionization and dissociation are much lower for O$_2$ than for

CO_2. The CH_4 conversion is comparable to the CO_2 conversion at low CO_2 fractions, i.e., around 10%, but it rises to 35% at high CO_2 fractions. Finally, it is worth to mention that Figure 20 illustrates the conversion, relative to the amount of CH_4, CO_2 or O_2 present in the mixture. The absolute (or effective) conversion of CH_4 is of course higher at a higher initial CH_4 fraction, and vice versa for the absolute CO_2 and O_2 conversions, which is logical, as there is more of these gases initially present in the gas mixture.

Besides the conversion of CH_4, CO_2 and O_2, we are especially interested in the yields and selectivities of the formed value-added chemicals. Table 6 shows the maximum yields of H_2, CO, formaldehyde (CH_2O) and methanol (CH_3OH), as well as the gas mixtures and residence times for which these maximum values were obtained. Also the corresponding selectivities are presented. Note that the sum of the selectivities does not have to be equal to 100%, because in the CH_4/CO_2 mixture, the selectivities of CO, CH_2O and CH_3OH are calculated with respect to both the CH_4 and CO_2 conversion, while the H_2 selectivity is only calculated with respect to the CH_4 conversion. Similarly in the case of the CH_4/O_2 mixture, the selectivities of CO, CH_2O and CH_3OH are calculated with respect to the CH_4 conversion, while the H_2 selectivity is calculated with respect to twice the CH_4 conversion, resulting in a difference of a factor 2 (see Section 3.6.).

Table 6. Overview of the maximum yields for some important end products in both the CH_4/O_2 and CH_4/CO_2 gas mixtures, as well as the corresponding gas mixing ratio and residence time at which these maximum yields are obtained. The corresponding selectivities of these end products are also listed.

		H_2	CO	CH_2O	CH_3OH
CH_4/O_2	Yield (%)	9	10	0.3	4
	Mixture	90/10	70/30	90/10 and 80/20	80/20
	Residence Time (s)	20	20	5.4 and 14.9	20
	Selectivity (%)	33	39	3 and 2	15
CH_4/CO_2	Yield (%)	34	10	0.9	0.4
	Mixture	20/80	20/80	90/10	25/75
	Residence Time (s)	20	20	10.3	20
	Selectivity (%)	50	52	4	2

It is clear that syngas is the main product in both gas mixtures, but the H_2/CO molar ratio is somewhat different, as was also discussed in Section 5.5.1. above. In the CH_4/O_2 mixture, the H_2 yield reaches a maximum at 10% O_2 fraction, while the CO yield reaches a maximum at 30% O_2 fraction, which is logical. In the CH_4/CO_2 mixture, the maximum H_2 and CO yields are both reached at 80% CO_2. For H_2, this can be explained because, although the absolute formation of H_2 is of course lower at a higher initial CO_2 fraction, its yield becomes higher as the latter is calculated with respect to the initial CH_4 density, which is obviously lower at higher initial CO_2 fraction. For CO, electron impact dissociation of CO_2 is the most important production channel, and the highest density and yield of CO are found at the highest initial CO_2 fraction. Note that at lower initial CO_2 fractions, the most important production channel of CO is the reaction of CH_2 radicals with CO_2, but this

reaction does not lead to a higher CO density (see also Section 5.5.3. and Figure 24 below). The H_2/CO molar ratio in the case of the 20/80 CH_4/CO_2 gas mixture is around 1.5, which is desirable for many industrial synthesis processes (cf. above). At higher CH_4/CO_2 gas mixing ratios, the H_2/CO molar ratio rises to about 5, because the H_2 density increases, while the CO density decreases upon higher CH_4 fraction in the mixture.

The maximum yields of CH_2O and CH_3OH are clearly lower than the maximum H_2 and CO yields. This is especially true in the CH_4/CO_2 mixtures, where both yields are below 1%. In this case, the highest CH_2O yield is obtained at 90% CH_4 fraction, while the highest CH_3OH yield is reached at 25% CH_4. In the CH_4/O_2 mixtures, the highest CH_2O yield is also below 1%, but the maximum CH_3OH yield reaches a value of 4%, which is not negligible. Nevertheless, a really selective production process towards CH_2O or CH_3OH seems not feasible in a DBD plasma, at least not at the conditions under study. For this purpose, a catalyst will need to be integrated into the plasma region.

Finally, it is clear from Table 6 that the highest yields are not necessarily reached at the longest residence time. Indeed, the H_2, CO and CH_3OH yields reach their maximum at 20s residence time, pointing out that their densities are still rising as a function of time (cf. Figure 18 above), while the CH_2O yield clearly reaches its maximum at a shorter residence time (see also Figure 18 above), and the exact value depends on the gas mixture and gas mixing ratio, as appears from Table 6. This indicates that, when the production of formaldehyde is targeted, the optimal residence time should be carefully selected.

Indeed, similar results were reported in literature. Okumoto et al.[122] stated that CH_3OH and CH_2O are in fact intermediate products in the oxidation of CH_4 and are easily decomposed or converted to CO, CO_2 and H_2O. In other words, the formation of oxygenates is strongly dependent on the initial gas mixing ratio, the residence time and a variety of other parameters. Okumoto et al. found that 15 vol.% of O_2 showed optimum performance for the formation of CH_3OH and CH_2O in CH_4/O_2.[122] Note that the authors made use of dilution gases to enhance the formation of oxygenates. Also Zou et al.[14] discussed the existence of an optimum feed composition to attain the maximum selectivity of the desired oxygenates. They obtained the highest total selectivity of oxygenates at a CH_4 concentration of 35 vol.% in CH_4/CO_2 in the presence of starch with the highest selectivities of alcohols, such as CH_3OH, and acids when the CO_2 fraction in the feed increases to 74 vol.%, and the highest selectivity of CH_2O at a higher CH_4 concentration of about 50 vol.%. These findings are in reasonable agreement with our results.

5.5.3. Dominant Reaction Pathways

We will now discuss the dominant reaction pathways for the conversion of the inlet gases into syngas, higher order hydrocarbons and oxygenates for a 70/30 CH_4/CO_2 gas mixture and for a 70/30 CH_4/O_2 gas mixture.

(a) Electron impact dissociation of CH_4, CO_2 and O_2: initiating the conversion process

As soon as the discharge is ignited, electron impact ionization and dissociation of the inlet gases occurs, resulting in the creation of new species (electrons, ions, radicals), as discussed in Section 5.5.1. above. The formation of new electrons and ions in the plasma enables to sustain the discharge, while the formation of radicals is important for the production of syngas, higher order hydrocarbons and oxygenates.

The dominant reactions for CH_4 consumption (and production) for a 70/30 CH_4/CO_2 gas mixture and a 70/30 CH_4/O_2 gas mixture are depicted in Figure 21(a) and Figure 21(b), respectively. Electron impact dissociation, yielding the formation of CH_3, CH_2 or CH radicals, are important channels for CH_4 consumption in both gas mixtures, with relative contributions of about 33%, 6% and 2% in CH_4/CO_2 and 34%, 7% and 2% in CH_4/O_2. In the 70/30 CH_4/O_2 gas mixture, the reaction with OH radicals, forming CH_3 radicals and H_2O, also contributes for about 19% to the loss of CH_4. This reaction is negligible in the CH_4/CO_2 mixture, due to the much lower OH radical density in that case (see Figure 15 above). Furthermore, also electron impact ionization and reactions with ions or radicals contribute to the loss of CH_4, accounting in total for about 20%, 31% and 6%, respectively, in CH_4/CO_2 and for about 15%, 21% and 22% (including the 19% of the reaction with OH), respectively, in CH_4/O_2.

(a)

(b)
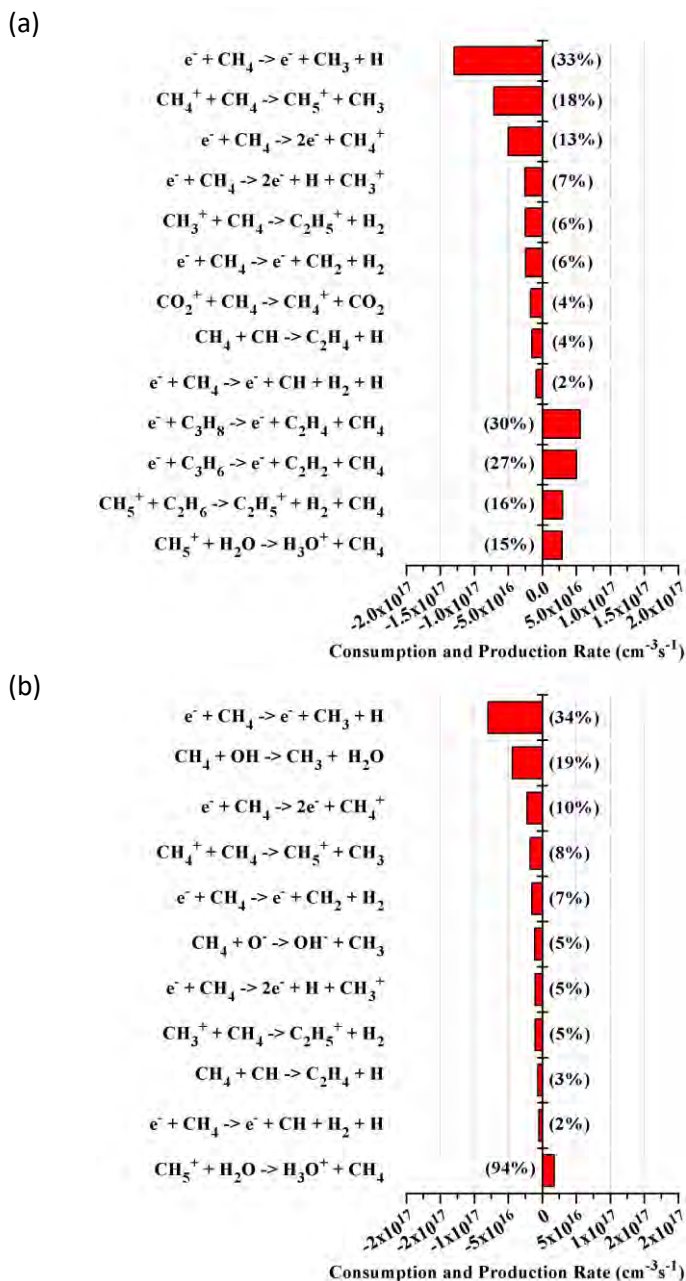
Figure 21. Time-averaged reaction rates of the dominant reaction pathways for the consumption and production of CH_4, for a 70/30 CH_4/CO_2 gas mixture (a) and a 70/30 CH_4/O_2 gas mixture (b). The consumption rates are defined as negative values (i.e., left-hand side of the figures), while the production rates are plotted as positive values (i.e., right-hand side of the figures). The relative contributions of these consumption and production processes to the overall consumption and production of CH_4 are also indicated.

It should be noted that electron impact vibrational excitation of CH_4 is also important, but this process is only considered in our model as an energy loss for the electrons, and not as a chemical loss process for CH_4, because the vibrationally excited species are not taken into account separately in our model (see Section 5.2.).

The most important pathways for the production (or regeneration) of CH_4 in the mixture with CO_2 are based on electron impact dissociation of higher hydrocarbons, such as C_3H_8 and C_3H_6, while in the mixture with O_2 these reactions appear negligible, and a charge transfer process of CH_5^+ with H_2O is the most important production process.

Finally, it is clear from Figure 21 that the total production (or regeneration) rate of CH_4 in the 70/30 CH_4/CO_2 gas mixture is almost one order of magnitude higher than in the 70/30 CH_4/O_2 gas mixture, while the consumption rate in both gas mixtures is in the same order of magnitude. However, the total loss rate is still a factor 2 higher than the total production rate in the CH_4/CO_2 mixture, and even a factor 12 higher in the CH_4/O_2 mixture, resulting in a clear loss of CH_4.

At a higher initial CO_2 fraction, the reactions of CH_4 with CO_2^+ and CH_4^+ become the most important channels for the consumption of CH_4 (see also Section 5.5.2.), accounting both for about 29% in 20/80 CH_4/CO_2, while the electron impact dissociation reaction yielding the formation of CH_3 only contributes for about 15% at these conditions. The most important pathway for the production (or regeneration) of CH_4 then becomes the charge transfer process of CH_5^+ with H_2O, with a contribution of 32%. A decrease of the initial fraction of CO_2 results in an increase of the contributions of the electron impact dissociation reactions for the consumption of CH_4 and also an increase

of the contributions of the electron impact dissociations of C_3H_8 and C_3H_6 for the regeneration of CH_4. A decrease of the initial fraction of O_2 to 10% results in a drastic decrease of the contribution of the reaction with OH radicals (3%). Electron impact dissociation yielding the formation of CH_3 remains the most important loss channel in this case, with a contribution of 42%. Meanwhile, the contribution of the charge transfer process of CH_5^+ with H_2O, the most important production process of CH_4, decreases from 94% in 70/30 CH_4/O_2 to 38% in 90/10 CH_4/O_2, as electron impact dissociation of C_3H_8 and C_3H_6 becomes more important, like in the mixtures with CO_2.

   The dominant reactions for CO_2 consumption (and production) for a 70/30 CH_4/CO_2 gas mixture and for O_2 consumption (and production) for a 70/30 CH_4/O_2 gas mixture are depicted in Figure 22(a) and Figure 22(b), respectively. The most important channel for consumption of CO_2 at this gas mixing ratio is the reaction with CH_2 radicals, contributing for about 48% to the CO_2 loss, followed by electron impact dissociation and ionization, which contribute for 16% and 30% to the total consumption of CO_2, respectively. At lower CO_2 fractions, the contribution of the first process will even increase to 77% for a 90/10 CH_4/CO_2 gas mixture. On the other hand, at higher CO_2 fractions in the gas mixture, the latter two processes will become gradually more important. For a 20/80 CH_4/CO_2 gas mixture, electron impact ionization and dissociation contribute for 52% and 27%, respectively, while the reaction with CH_2 radicals contributes for 9%. It is worth to mention that the reaction with CH_2 radicals is also the most important pathway for the production of CH_2O and CO in the 70/30 CH_4/CO_2 gas mixture (see below).

(a)

(b)
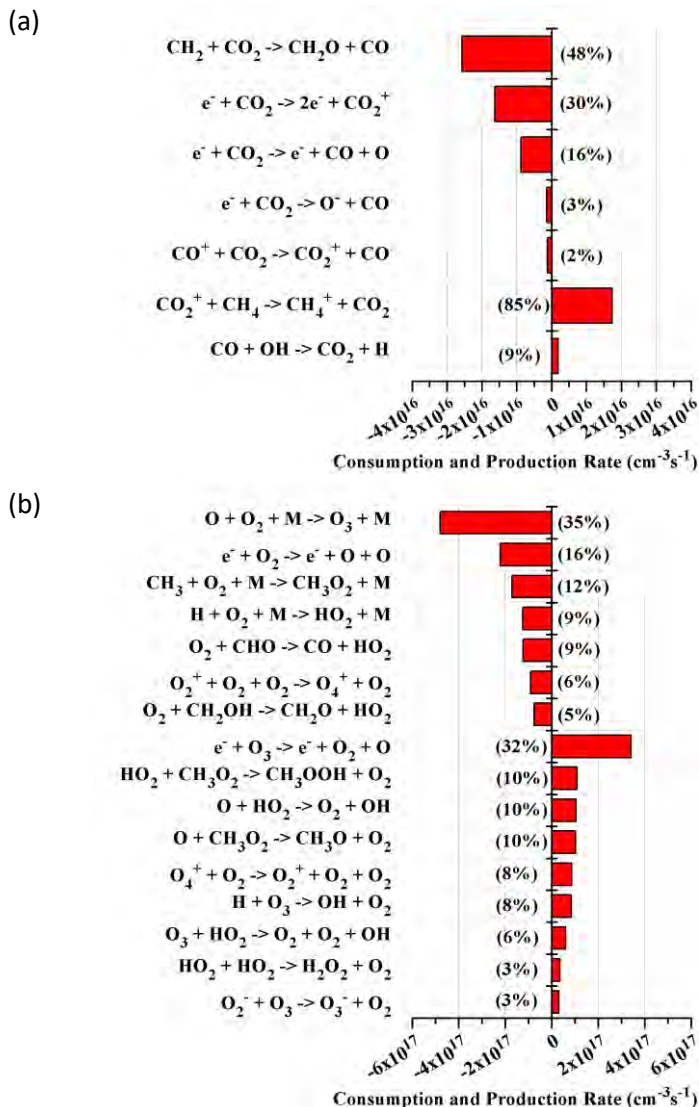
Figure 22. Time-averaged reaction rates of the dominant reaction pathways for the consumption and production of CO_2 for a 70/30 CH_4/CO_2 gas mixture (a) and for the consumption and production of O_2 for a 70/30 CH_4/O_2 gas mixture (b).

The most important channels for consumption of O_2 are three-body collisions with O, CH_3 or H radicals, with either CH_4, O_2, H_2O or CO_2 as third body (denoted as M in Figure 22(b)), as well as electron impact dissociation of O_2 and a chemical reaction with CHO radicals. The three-body reaction with O

radicals, forming O_3, is the most important loss process, with a contribution of 36%. However, almost all the O_3 will be decomposed back to O_2 by electron impact dissociation, so that the net contribution of this reaction will be lower.

Electron impact dissociation of O_2 yields the formation of O radicals, while the reactions with CH_3, H and CHO yield among others the formation of CH_3O_2 and HO_2. The O and HO_2 radicals will react further into OH (see below), which is an important species for the consumption of CH_4 (see above), while CH_3O_2 plays an important role in the formation of CH_3OH and CH_3OOH (see below). When the initial fraction of O_2 decreases to 10%, the three-body collisions with CH_3 and H radicals become more important for the consumption of O_2, with contributions of 29% and 25%, respectively. Meanwhile, the contribution of electron impact dissociation of O_2 decreases to 11% and the three-body collision with O radicals decreases drastically to 10%.

The most important production mechanism for CO_2 in the CH_4/CO_2 gas mixtures is a charge transfer process between CO_2^+ and CH_4, while electron impact dissociation of O_3 (see above) is the most important production process for O_2 in a 70/30 CH_4/O_2 gas mixture. As a result of the lower production of O_3 (see above) in a 90/10 CH_4/O_2 gas mixture, the reaction of HO_2 radicals with CH_3O_2 radicals towards CH_3OOH is the most import process for regeneration of O_2 in this mixture, with a contribution of 33%. However, the rates for regeneration of CO_2 and O_2 are again a factor 2.6 and 1.3 lower than their corresponding loss rates, so that there is a net consumption of CO_2 and O_2.

(b) Recombination of CH_3 radicals: the formation of C_xH_y vs. the formation of CH_3O_2

The most important species produced from CH_4 are the CH_3 radicals (see above). Figure 23(a) and Figure 23(b) show the dominant reactions for CH_3 consumption and production, again for a 70/30 CH_4/CO_2 gas mixture and a 70/30 CH_4/O_2 gas mixture, respectively. In the 70/30 CH_4/CO_2 mixture, the CH_3 radicals will mainly recombine towards higher hydrocarbons, such as C_2H_6 and C_3H_8, which contribute for 48% and 46% to the consumption of CH_3, respectively. On the other hand, in the 70/30 CH_4/O_2 gas mixture, these reactions are negligible compared to the three-body recombination reaction with O_2 molecules, forming CH_3O_2 radicals (see Figure 23(b)). This is in good agreement with Nozaki et al.[134] and Goujard et al.[105], who also discussed the importance of the formation of CH_3O_2 in the methane partial oxidation mechanism towards the formation of CH_3OH. Furthermore, this result explains the lower densities for the higher hydrocarbons in the gas mixtures with O_2 as co-reactant (see Figure 17 (a, b) above). The formation and loss mechanisms of the higher hydrocarbon molecules in both gas mixtures are similar to the case of pure CH_4 (see Section 4.5.3.), and will therefore not be discussed here.

At higher initial fraction of CO_2, the recombination of CH_3 towards C_2H_6, C_3H_8 and CH_4 will contribute for 57%, 22% and 19% to the consumption of CH_3, respectively. On the other hand, at a lower initial fraction of CO_2, the recombination towards C_3H_8 will become more important than the recombination to C_2H_6. In a 90/10 CH_4/O_2 gas mixture, thus a lower O_2 content, the recombination towards C_2H_6 and C_3H_8 becomes more important, with contributions of 38% and 30%, respectively, while the three-body

recombination with O_2 molecules, forming CH_3O_2 radicals, contributes for 29% to the consumption of CH_3.

(a)

(b)
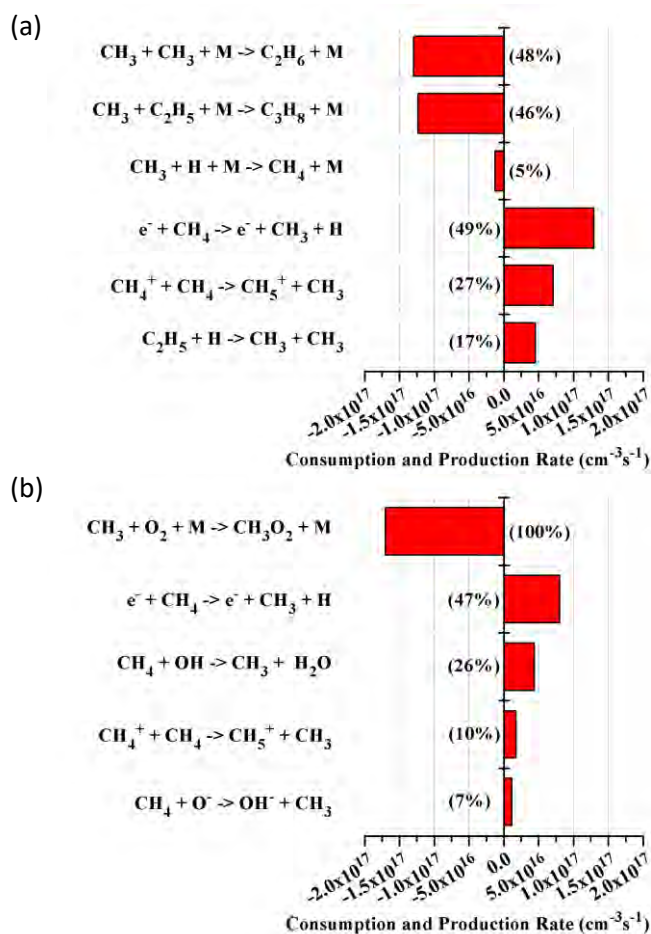
Figure 23. Time-averaged reaction rates of the dominant reaction pathways for the consumption and production of CH_3, for a 70/30 CH_4/CO_2 gas mixture (a) and for a 70/30 CH_4/O_2 gas mixture (b).

(c) Formation of syngas

In Figure 24(a) and Figure 24(b) the most important channels for production and loss of CO in a 70/30 CH_4/CO_2 and a 70/30 CH_4/O_2 gas mixture are illustrated, respectively.

As already mentioned above, the reaction of CO_2 with CH_2 radicals is the most important channel for the production of CO in a 70/30 CH_4/CO_2 gas mixture, with a relative contribution of 37% (see Figure 24(a)). Two other important production mechanisms are the reaction of C_2H_5 with CHO, as well as electron impact dissociation of CO_2, which contribute for 28% and 13% to the total formation of CO in a 70/30 CH_4/CO_2 gas mixture. In the 70/30 CH_4/O_2 gas mixture, on the other hand, 90% of the CO formation occurs through the reaction of O_2 molecules with CHO radicals. It is thus clear that the chemistry yielding CO formation is completely different in both gas mixtures. Note that in a 20/80 CH_4/CO_2 gas mixture, electron impact dissociation of CO_2 becomes the most important channel for the production of CO.

The same applies to the loss of CO. Indeed, electron impact dissociation and ionization, as well as reactions with H radicals, are the most important loss processes for CO in the CH_4/CO_2 gas mixture, while the reaction with OH radicals is the most important loss process for CO in the CH_4/O_2 gas mixture. However, it is clear from Figure 24 that the total rate for CO formation is a factor 5 and 2.6 higher than the total loss rate, in the CH_4/CO_2 and CH_4/O_2 gas mixtures, respectively.

(a)

(b)
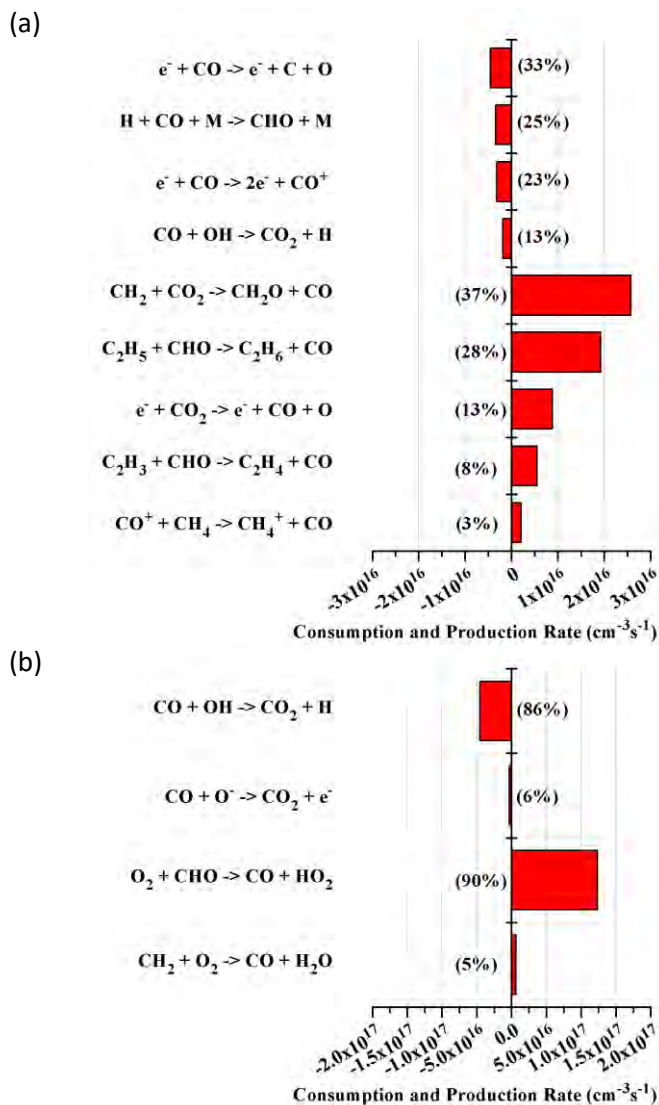
Figure 24. Time-averaged reaction rates of the dominant reaction pathways for the consumption and production of CO, for a 70/30 CH_4/CO_2 gas mixture (a) and a 70/30 CH_4/O_2 gas mixture (b).

Figure 25(a) and Figure 25(b) show the dominant reactions for production and loss of H_2 in a 70/30 CH_4/CO_2 and a 70/30 CH_4/O_2 gas mixture, respectively.

In the 70/30 CH_4/CO_2 gas mixture, electron impact dissociation of C_2H_6 and C_3H_8 are the most important formation channels of H_2, while electron impact dissociation of CH_4 only contributes for 12% (i.e., 8% (towards $CH_2 + H_2$) + 3% (towards $CH + H_2 + H$) + 1% (towards $C + 2H_2$, not shown in Figure 25(a)). In the 70/30 CH_4/O_2 gas mixture, however, electron impact dissociation of CH_4 is clearly most important. Indeed, the higher hydrocarbons are of lower importance in this case (see Figure 17(a, b) above). However, when the initial fraction of O_2 decreases, electron impact dissociation of C_2H_6 and C_3H_8 become the most important formation channels of H_2. Furthermore, electron impact dissociation is the most important loss process for H_2 in both the CH_4/CO_2 and the CH_4/O_2 gas mixture. In the CH_4/CO_2 mixture, the total loss rate is a factor 2 lower than the total production rate, while in the CH_4/O_2 mixture, it is a factor 4 lower. Nevertheless, the overall H_2 production is still much more pronounced in the CH_4/CO_2 mixture than in the CH_4/O_2 mixture (with a total rate of 1.8×10^{17} $cm^{-3}s^{-1}$ vs 4.5×10^{16} $cm^{-3}s^{-1}$; see Figure 25), and this explains the higher H_2 density, as well as the higher H_2/CO molar ratio, in the CH_4/CO_2 mixture. The reason for the higher H_2 production in the CH_4/CO_2 mixture is the higher formation of higher hydrocarbons (see above), which represent additional formation channels for H_2, as is clear from Figure 25(a).

(a)

(b)
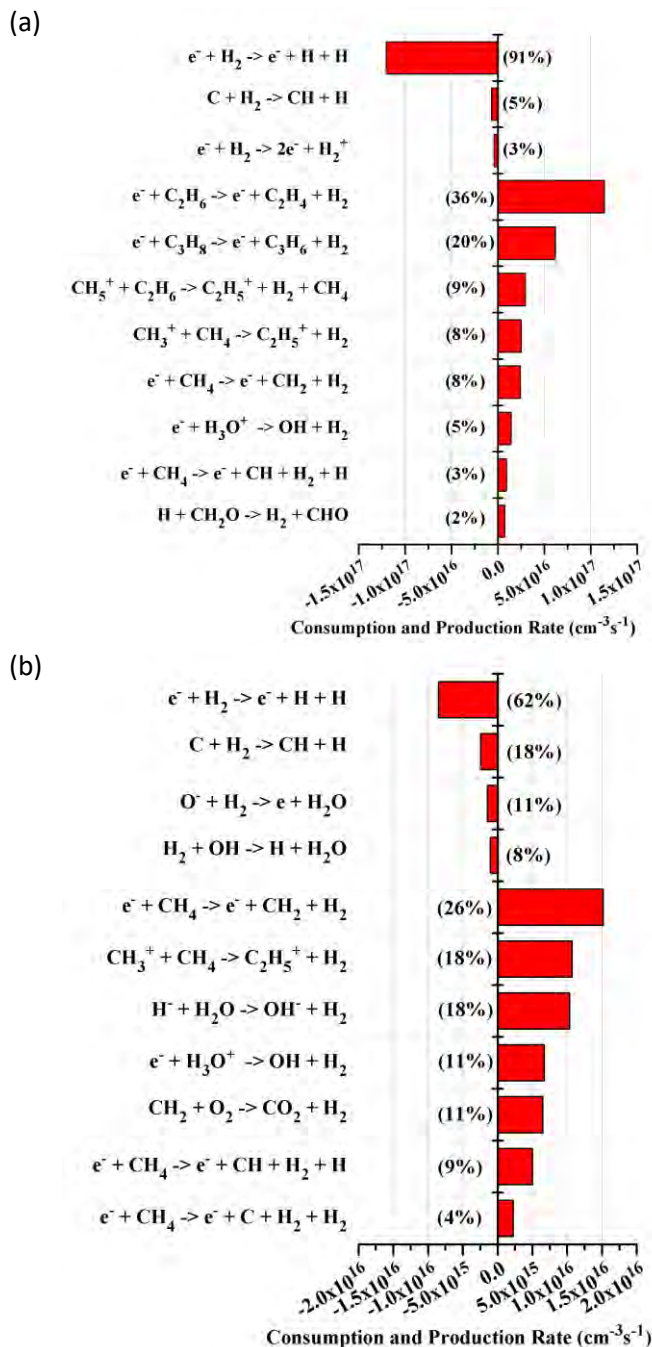
Figure 25. Time-averaged reaction rates of the dominant reaction pathways for the consumption and production of H_2, for a 70/30 CH_4/CO_2 gas mixture (a) and a 70/30 CH_4/O_2 gas mixture (b).

(d) Formation of methanol and formaldehyde

Figure 26(a) and Figure 26(b) illustrate the dominant reactions for production and loss of CH_3OH in a 70/30 CH_4/CO_2 and a 70/30 CH_4/O_2 gas mixture, respectively, while in Figure 27(a) and Figure 27(b) the dominant reactions for production and loss of CH_2O in a 70/30 CH_4/CO_2 and a 70/30 CH_4/O_2 gas mixture are illustrated, respectively.

In the 70/30 CH_4/CO_2 gas mixture, the production of methanol occurs almost entirely through the three-body reaction between the CH_3 and OH radicals, while in the 70/30 CH_4/O_2 gas mixture, methanol is almost entirely formed by the reaction between H_2O and CH_3O radicals. Indeed, the rate of the three-body reaction between the CH_3 and OH radicals is one order of magnitude higher in CH_4/CO_2 than in CH_4/O_2 (1.1 x 10^{15} $cm^{-3}s^{-1}$ vs 1.6 x 10^{14} $cm^{-3}s^{-1}$), but the rate of the reaction between H_2O and CH_3O radicals is four orders of magnitude higher in CH_4/O_2 than in CH_4/CO_2 (8.5 x 10^{16} $cm^{-3}s^{-1}$ vs 1.4 x 10^{12} $cm^{-3}s^{-1}$). When comparing the overall production rates in Figure 26, it is clear that the total CH_3OH production rate is almost two orders of magnitude higher in the CH_4/O_2 mixture than in the CH_4/CO_2 mixture, explaining the higher CH_3OH density and yield in the CH_4/O_2 mixture (see Figure 17 and Table 6 above).

As already mentioned above, the reaction between CO_2 and CH_2 radicals is the most important channel for the production of formaldehyde in the 70/30 CH_4/CO_2 gas mixture, while in the 70/30 CH_4/O_2 gas mixture, formaldehyde is mainly produced by the reactions of O_2 with CH_2OH and CH_3O, with relative contributions of 64% and 23%, respectively. The total production rate of CH_2O is a factor 4 higher in the CH_4/O_2 mixture than in the CH_4/CO_2 mixture, but the total loss rate of CH_2O is a factor 4.6 higher in the CH_4/O_2 mixture than in the

CH_4/CO_2 mixture, explaining the higher CH_2O density and yield in the CH_4/CO_2 mixture (see Figure 17 and Table 6 above).

(a)

(b)
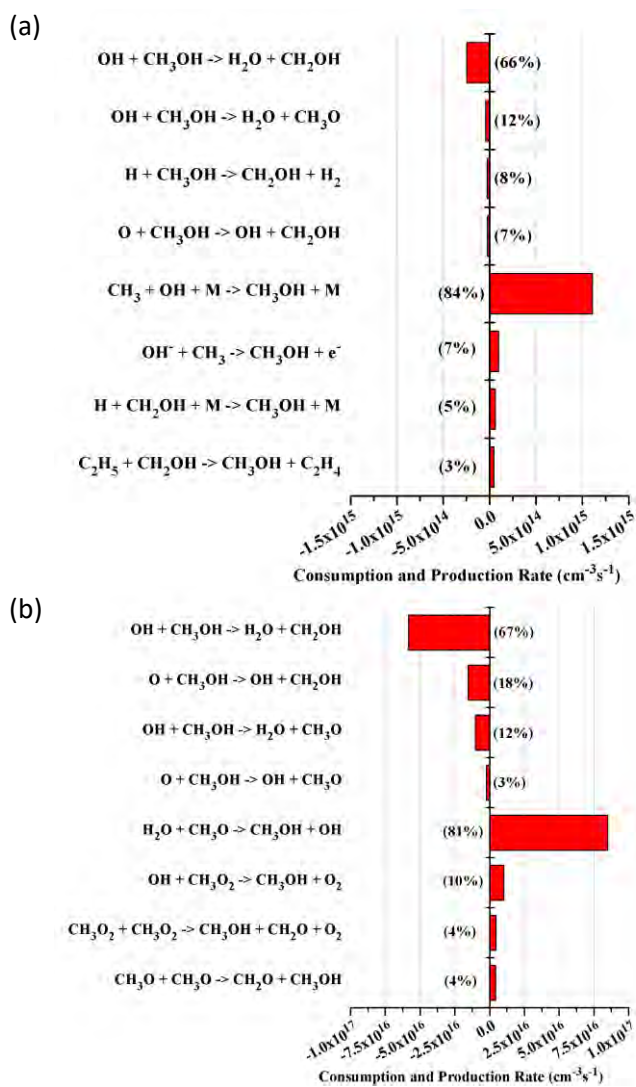
Figure 26. Time-averaged reaction rates of the dominant reaction pathways for the consumption and production of CH_3OH, for a 70/30 CH_4/CO_2 gas mixture (a) and a 70/30 CH_4/O_2 gas mixture (b).

(a)

(b)
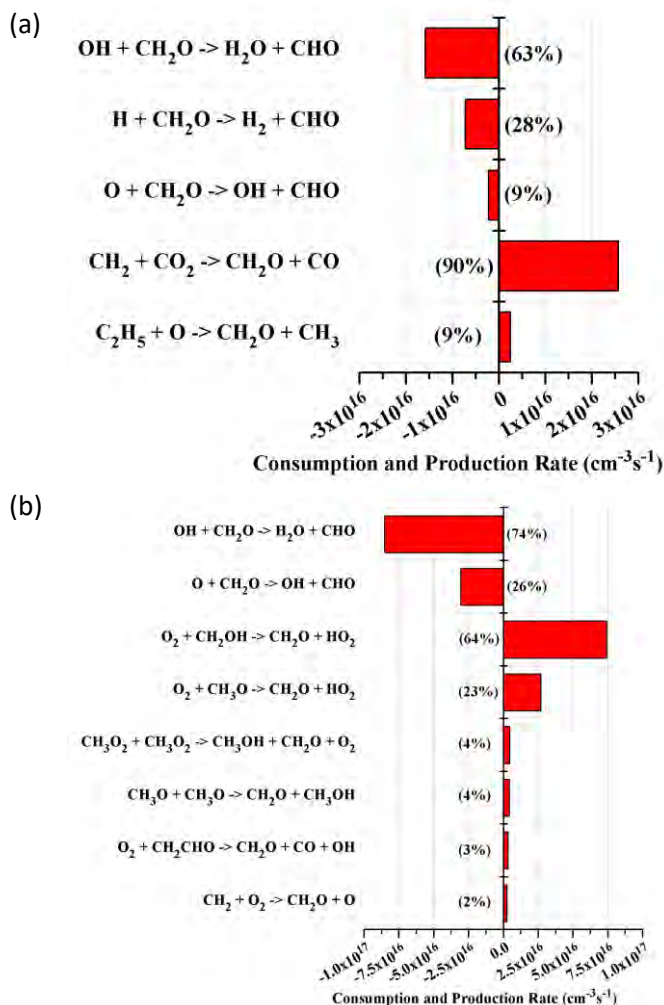
Figure 27. Time-averaged reaction rates of the dominant reaction pathways for the consumption and production of CH_2O, for a 70/30 CH_4/CO_2 gas mixture (a) and a 70/30 CH_4/O_2 gas mixture (b).

The most important loss process in both gas mixtures for both methanol and formaldehyde is the reaction with OH radicals. The overall loss rates are again typically lower than the overall production rates.

Note that for the 70/30 CH_4/O_2 gas mixture the degradation of methanol leads to the formation of CH_2OH (Figure 26(b)), which subsequently reacts to

formaldehyde (Figure 27(b)). The degradation of formaldehyde leads to the formation of CHO, which is subsequently converted to CO (Figure 24(b)). In other words, the formation processes of three of the desired end products (CH_3OH, CH_2O and CO) are dependent on each other in the 70/30 CH_4/O_2 gas mixture, which is in good agreement with the findings of Larkin et al.[65]. The development of a catalyst that activates or inhibits one of the reactions influencing the balance between these molecules should make it possible to favor selectively the formation of one of them.

(e) Summary of the dominant pathways governing the conversion of CH_4 into higher oxygenates

Figure 28 summarizes the dominant reaction pathways for the conversion of CH_4 and CO_2 into higher oxygenates in a 70/30 CH_4/CO_2 gas mixture. The conversion process starts with electron impact dissociation of CH_4, yielding the formation of the CH_3 radicals. The CH_3 radicals will recombine towards higher hydrocarbons, such as C_2H_6 and C_3H_8. Subsequently, a number of dissociation and recombination reactions leads to the conversion towards the other, unsaturated hydrocarbons, and dissociation of CH_4 and the higher hydrocarbons also yields the formation of H_2. The reaction mechanisms towards H_2 and the higher hydrocarbons in the CH_4/CO_2 mixture are exactly the same as in the case of pure CH_4, and thus, more details can be found in Section 4.5.3. above. However, in the CH_4/CO_2 mixture, the CH_3 radicals can also form methanol (CH_3OH) and CH_3O_2 radicals, albeit to a lower extent. Moreover, the CH_2 radicals, which are also formed by electron impact dissociation of CH_4, react with the CO_2 molecules, to form formaldehyde (CH_2O) and CO. Finally, the O atoms, created from electron impact

dissociation of CO_2, initiate the formation of other oxygenates, like acetaldehyde (CH_3CHO), which also reacts further into CH_3CO radicals, which can subsequently be converted into ketene (CH_2CO). However, this reaction path is not so important, because of the limited formation of O radicals compared to CO and CH_2O out of the CO_2 molecules. H_2, CO, ethane (C_2H_6), propene (C_3H_6) and CH_2O are the main end products of the conversion of CH_4 and CO_2 in a 70/30 CH_4/CO_2 gas mixture (see also Figure 17 above).

For a schematic overview of the dominant reaction pathways for the conversion of CH_4 into higher hydrocarbons: see Section 4.5.3. above.
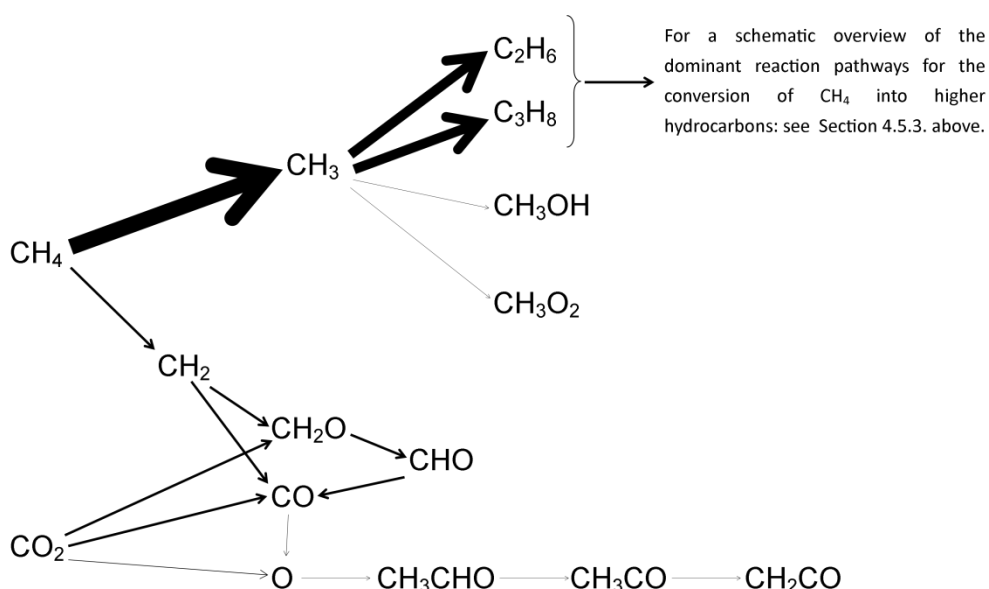
Figure 28. Schematic overview of the dominant reaction pathways for the conversion of CH_4 and CO_2 into higher oxygenates in a 70/30 CH_4/CO_2 gas mixture. The thickness of the arrows is linearly proportional to the rate of the net reaction.

The dominant reaction pathways for the conversion of CH_4 and O_2 into higher oxygenates in a 70/30 CH_4/O_2 gas mixture are schematically illustrated in Figure 29. Again, electron impact dissociation of CH_4 results in the formation of CH_3 radicals. The latter can recombine into methanol or higher hydrocarbons, but more important is the recombination into CH_3O_2 radicals,

which form either CH$_3$O radicals or methyl hydroperoxide (CH$_3$OOH). The CH$_3$O radicals yield the formation of methanol, which can react further into formaldehyde through the CH$_2$OH radicals, and formaldehyde can further be converted into CO through the CHO radicals (see above). Furthermore, formaldehyde is also partially converted into water. The O$_2$ molecules are converted into HO$_2$ radicals, O atoms and CO. They are also converted into O$_3$ molecules, but the O atoms and O$_3$ molecules quickly react back into O$_2$ molecules at a somewhat larger rate, so there is a net formation of O$_2$ molecules out of O$_3$ (see the direction of the arrow in Figure 29). This delicate balance between O$_2$, O and O$_3$ was also discussed in detail in Aerts et al.[197] CO can be further oxidized into CO$_2$, which is of course undesired. The O atoms are also converted into CH$_3$O and OH radicals, which can again form water. The most important products in this CH$_4$/O$_2$ mixture are H$_2$O, CO, CO$_2$, H$_2$, O$_3$, CH$_3$OH, methyl hydroperoxide (CH$_3$OOH) and hydrogen peroxide (H$_2$O$_2$) (see also Figure 17 above). The reaction scheme revealed by our model for the conversion of CH$_4$ and O$_2$ into higher oxygenates is in good agreement with the proposed mechanisms for partial oxidation of CH$_4$ by Goujard et al.[105] and Zhou et al.[106].
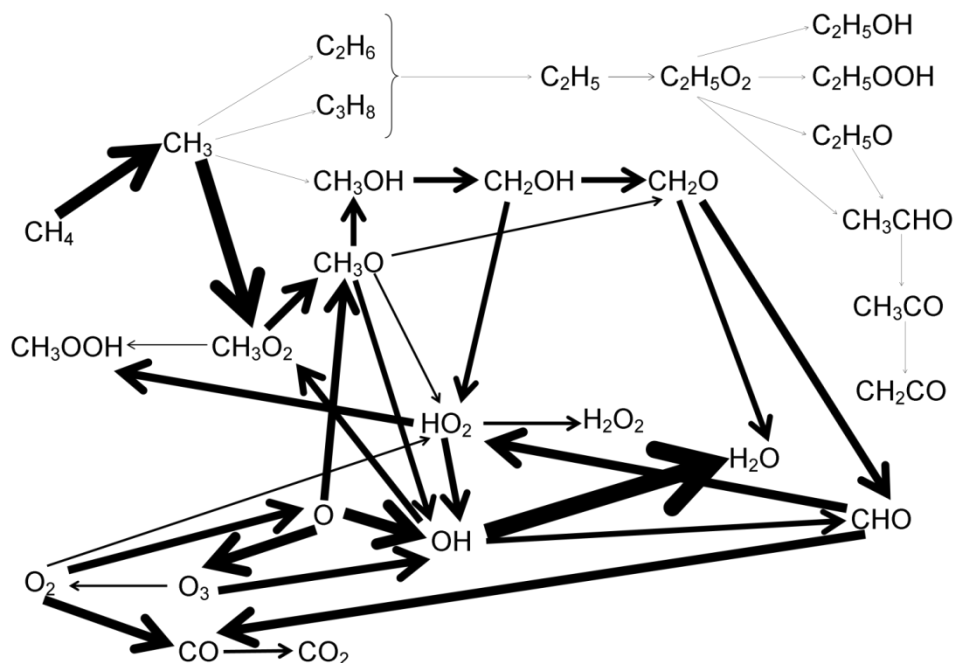
Figure 29. Schematic overview of the dominant reaction pathways for the conversion of CH_4 and O_2 into higher oxygenates in a 70/30 CH_4/O_2 gas mixture. The thickness of the arrows is linearly proportional to the rate of the net reaction.

5.6. Conclusion

In this chapter, we have presented the detailed plasma chemistry in a DBD plasma for the conversion of CH_4 in the presence of O_2 or CO_2 into syngas, higher hydrocarbons and higher oxygenates. We have studied the densities of the various plasma species as a function of residence time and gas mixing ratio. The spatially averaged densities of the electrons, ions and radicals exhibit a periodic behavior as a function of time, following the sinusoidal applied voltage, while the spatially averaged molecule densities do not show a periodic behavior. While the densities of some molecules steadily rise as a function of residence time, the densities of other molecules go over a

maximum, or show a plateau after some time. This is important to realize, as a careful selection of the residence time can entail a higher production of some targeted molecules. We have also presented the densities of all molecules as a function of the initial gas mixing ratio. The mixtures with CO_2 favor the formation of H_2, CH_2O, CH_3CHO and CH_2CO, while the densities of H_2O_2, CH_3OH, C_2H_5OH, CH_3OOH and C_2H_5OOH are higher in the mixtures with O_2. CO is formed at high density in both gas mixtures. Note that in the gas mixtures with O_2 as co-reactant also a significant amount of undesired CO_2 is formed.

The calculated conversions of the inlet gases as a function of residence time and initial gas mixing ratio are also illustrated. The conversion of CH_4 is roughly independent from the initial O_2 or CO_2 fraction (up to 30-40% CO_2), but it increases for higher initial CO_2 fractions, especially above 70%. The conversion of O_2 and CO_2 both decrease with increasing initial O_2 or CO_2 fraction. However, the O_2 conversion is much higher than the CO_2 conversion.

Finally, the underlying plasma chemistry of the conversion process is analyzed in detail, and the dominant reaction pathways for the consumption of CH_4, O_2 and CO_2 and the production and loss of the dominant end products, i.e., CO, H_2, CH_3OH and CH_2O, are discussed. Electron impact dissociation of the inlet gases initiates the conversion process. The recombination of CH_3 radicals plays a crucial role and it was shown that this recombination leads to the formation of higher hydrocarbons in the mixtures with CO_2, while CH_3O_2 radicals are favored in the mixtures with O_2. In the CH_4/CO_2 mixture, also CH_2 radicals play a role, which can be converted into formaldehyde and CO molecules. In the CH_4/O_2 mixture, the CH_3O_2 radicals lead among others to the formation of methanol, which can react further into formaldehyde and the latter can form CO.

Our results are in reasonable agreement with reported results from literature for similar CH_4/O_2 and CH_4/CO_2 discharges. Moreover, our model provides additional information, mainly on the comparison between the formed end products in CH_4/O_2 and CH_4/CO_2 gas mixtures and on the different pathways leading to these products. In this way, the model can help to determine the most suitable feed gas ratio, residence time, co-reactant and other plasma parameters, to obtain the highest yield and/or selectivity of a desired oxygenate. However, as a lot of different products are typically formed in a plasma, the development of a catalyst, which increases the selective formation of some desired oxygenates, will be crucial. Furthermore, besides the conversion, yield and selectivity of specific products, also the energy efficiency of the discharge is critical, to determine whether or not plasma technology can compete with conventional technologies.

Chapter 6

The Hydrogenation of CO$_2$

The fluid model described in Chapter 3 is applied here to describe the plasma chemistry governing the hydrogenation of carbon dioxide. The spatially averaged densities of the most important end products formed in the CO$_2$/H$_2$ mixture are determined as a function of the initial gas mixing ratio. CO and H$_2$O are found to be present at the highest densities, and to a lower content also CH$_4$, C$_2$H$_6$, CH$_2$O, CH$_3$OH, O$_2$ and some other higher hydrocarbons and oxygenates. The main underlying reaction pathways for the conversion of the inlet gases and the formation of CO, CH$_4$, CH$_2$O and CH$_3$OH are pointed out for various gas mixing ratios. The CO$_2$ conversion and the production of value-added products is found to be quite low, also in comparison to a CO$_2$/CH$_4$ mixture, and this can be explained by the model.

6.1. Introduction

Current research on the use of plasma for CO_2 conversion includes the splitting of pure CO_2 into CO and O_2[38, 68, 111, 197-218], and the direct synthesis of higher hydrocarbons, syngas and oxygenates through the reforming of CH_4 by CO_2[14, 20-21, 64, 93, 107-109, 135-184] (see Chapter 5) or the hydrogenation of CO_2[219-222]. However, application of the latter is up to now limited because of the high cost of hydrogen.[136]

Recently, the interest in the development of new sustainable industrial processes for the direct hydrogenation of CO_2 into CH_3OH is increasing because of the potential of CH_3OH in a growing hydrogen economy. Moreover, this hydrogenation process is a well-known reaction in catalysis research. In this chapter a modeling study for the hydrogenation of CO_2 in a DBD plasma will be discussed.

Experimental and modeling investigations on the plasma chemistry in CO_2/H_2 mixtures reported in literature are very rare. Eliasson et al.[219] investigated the hydrogenation of CO_2 to CH_3OH in a DBD with and without the presence of a catalyst. Experimentally the effects of combining a catalyst with a discharge on the yield of CH_3OH were analyzed for different reaction parameters, such as the gas temperature, the pressure, the inlet gas mixing ratio, the electric power and the flow rate of the feed gas. Furthermore, a simplified semi-empirical kinetic model was used to simulate the accumulated chemical action of many microdischarges, in order to calculate the CH_3OH yield in the CO_2/H_2 discharge. A radical reaction mechanism was proposed for the formation of CH_3OH. Liu et al.[223] discussed in a review paper the use of non-thermal plasmas for CO_2 utilization, including the hydrogenation of CO_2

to form CH_3OH in a DBD, referring thereby to the work of Eliasson et al[219]. Hayashi et al.[220] discussed the decomposition of CO_2 in the presence of H_2 or water vapor by a non-thermal plasma, produced by a surface discharge at atmospheric pressure. CO, CH_4, dimethyl ether (C_2H_6O), formic acid (HCOOH) and water vapor were detected as end products of a gas mixture of 50% CO_2 and 50% H_2. Kano et al.[221] studied the reforming of CO_2 by H_2 to CH_4 and CH_3OH by using a radio frequency impulse low-pressure discharge under different discharge parameters. CH_4, CO, CH_3OH and water vapor were found as end products. Recently Zeng et al.[222] investigated the plasma-catalytic CO_2 hydrogenation in a coaxial packed-bed DBD at low temperatures and atmospheric pressure. The performance of different γ-Al_2O_3 supported metal catalysts on the conversion of CO_2 was studied. The reverse water-gas shift reaction, i.e. the formation of CO and H_2O, as well as carbon dioxide methanation, i.e. the formation of CH_4 and H_2O, have been reported as the dominant reaction processes. The results also show that the H_2/CO_2 molar ratio significantly affects the conversion of CO_2 and the yields of CO and CH_4.

In this chapter we present the most important results on the conversion of CO_2, in the presence of H_2, into CO, higher hydrocarbons and higher oxygenates. The chemistry set is almost the same as used for the CH_4/O_2 and CH_4/CO_2 gas mixtures (see Chapter 5 above and Section 6.2. below). The formation of a variety of higher hydrocarbons and higher oxygenates in CO_2/H_2 for different gas mixing ratios is calculated, as well as the conversion of the inlet gases. These results will be compared with the experimental observations from the papers mentioned above on CO_2/H_2 gas discharges, as well as with earlier calculated results with the same model for a CH_4/CO_2 gas mixture (see Chapter 5). Furthermore, the main underlying pathways

governing the conversion of CO_2 with H_2, into the main reaction products, i.e., CO, CH_4, CH_2O and CH_3OH, are discussed in order to explain the product formation in the different gas mixing ratios and to reveal why some oxygenates are formed while others seem not to be formed.

6.2. Species Included in the Model

As mentioned above, the chemistry set used for the CO_2/H_2 gas mixture is almost identical to the one constructed for the CH_4/O_2 and CH_4/CO_2 gas mixture, except for some adaptations of the third body species in the neutral-neutral three-body collision reactions, where CO_2 and H_2 are now included as third body instead of CH_4, O_2, CO_2 and H_2O, with the same rate coefficients. In total, 75 species (electrons, molecules, ions and radicals) are included in the model, as presented in Table 5 above. Note that dimethyl ether (CH_3OCH_3) and formic acid (HCOOH), which were experimentally found by Hayashi et al.[220], as mentioned above, are not included in the model as the rate constants for the formation and loss processes for these molecules are not well known. As a consequence, our model will not be able to make predictions on the formation of these products. We expect that these species would anyway play a minor role in the chemistry, especially as intermediates. They might be potential end products, but we don't expect their densities to be higher than e.g., CH_4, CH_3OH and CH_2O, and certainly much lower than e.g., CO.

6.3. Reactions Included in the Model

As mentioned in Chapter 5, the 75 species included in the model interact with each other in 963 gas phase reactions, including 157 electron-neutral, 48 electron-ion, 420 neutral-neutral and 338 ion-ion or ion-neutral reactions. Detailed information on the construction of the chemistry set and the transport coefficients and wall interaction coefficients used in the model can be found in Section 5.3. and Section 3.5., respectively.

6.4. Operating Conditions

The calculations are again carried out for a gas residence time up to 20s, at a fixed applied voltage of 5 kV and a frequency of 10 kHz, like in the previous chapter. The CO$_2$ fraction in the CO$_2$/H$_2$ mixture is varied from 10 to 90%.

6.5. Results and Discussion

6.5.1. Densities of the Plasma Species

The spatially averaged electron density and the densities of the radicals and ions produced in the plasma exhibit periodic behavior as a function of time, following the period of the applied sinusoidal voltage. The overall spatially and time averaged electron density for all CO$_2$/H$_2$ gas mixtures under study amounts to ca. 10^{15} m^{-3}, while the overall spatially and time averaged mean electron energy varies between 1.9eV and 2.7 eV. These results are similar to the values calculated in pure CH$_4$ (see Section 4.5.1.) and in the CH$_4$/O$_2$ and

CH$_4$/CO$_2$ gas mixtures (see Section 5.5.1.). More information on the periodic behavior of the electron density, and of the various ion densities, can thus be found in Section 4.5.1. and in Section 5.5.1. above.

Figure 30 illustrates the periodic behavior of the most important radical densities for a 50/50 CO$_2$/H$_2$ gas mixture, on a logarithmic scale, for four periods of the applied voltage. The periodic trend is here superimposed on a rising or declining trend, acting over a longer time-scale until periodic steady state is reached. The most abundant radicals are H, O, OH, HO$_2$, CHO, CH$_3$ and CH$_2$, with overall spatially and time averaged densities up to about 10^{20} m^{-3}. Most of these radicals do not vary a lot as a function of time within one period, except for the CH$_2$ radicals. This is because the formation of all these radicals proceeds in a quite similar way, i.e. either directly or indirectly related to electron impact dissociation of the inlet gases. However, CH$_2$ is rapidly destructed in reactions with CO$_2$, one of the inlet gases, which is thus present at high density, explaining the significant drop in the CH$_2$ density as a function of time, while H, O, OH, HO$_2$, CHO and CH$_3$ react away through collisions with other radicals or molecules at lower densities. The most abundant radicals will determine the different reaction pathways for the formation of different end products (see below). Compared to our previous results for the CO$_2$/CH$_4$ mixture (see Section 5.5.1.), the higher order hydrocarbon radicals, such as C$_2$H$_5$ and C$_2$H$_3$, as well as the oxygenate radicals, such as CH$_3$O, CH$_2$OH and CH$_3$O$_2$, are formed to a lower extent in CO$_2$/H$_2$, which is logical, as there is no hydrocarbon precursor (CH$_4$) in the inlet gas mixture, resulting in a lower overall carbon fraction than in CO$_2$/CH$_4$.
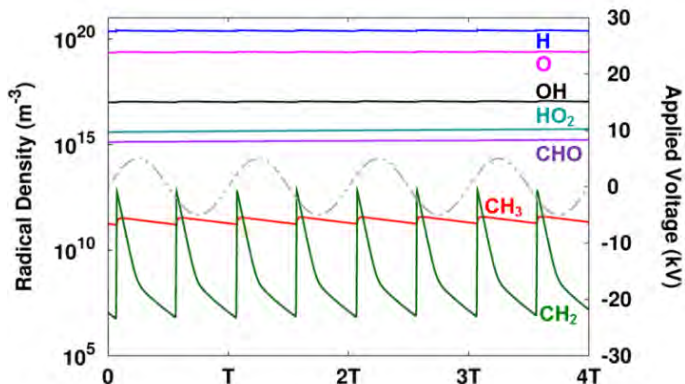
Figure 30. Spatially averaged radical densities (left axis) as a function of time for a 50/50 CO$_2$/H$_2$ gas mixture, on a logarithmic scale, as well as the applied sinusoidal voltage (gray, right axis) for four periods of the applied voltage.

The spatially and time averaged densities of the most abundant radicals in CO$_2$/H$_2$ are plotted in Figure 31 as a function of the initial CO$_2$ content in the mixture. Upon rising the initial fraction of CO$_2$ between 10 and 90 %, the densities of the H, CH$_3$ and CH$_2$ radicals drop by one order of magnitude, because these radicals are directly or indirectly formed out of H$_2$. On the other hand, the densities of O, OH, HO$_2$ and CHO, as well as the other O-containing radicals (not shown), increase by one order to several orders of magnitude upon rising the inlet fraction of CO$_2$, as they are directly or indirectly formed out of CO$_2$.

The most abundant ion in the CO$_2$/H$_2$ gas mixture is H$_3$O$^+$, with a spatially and time averaged density in the order of 10^{15} m^{-3}, hence comparable to the electron density (cf. above). The other ion densities are two or even more orders of magnitude lower, and thus the ion densities are much lower than the spatially and time averaged densities of the most abundant radicals, indicating that the ions play a minor role in the plasma chemistry (see also

Section 6.5.3. below). Therefore, we do not go in further detail on the ion densities.
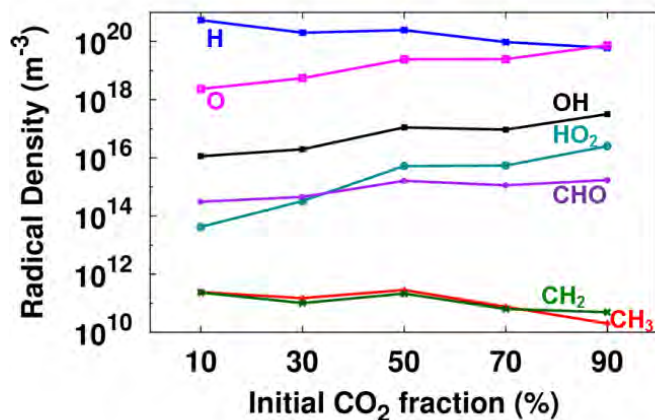
Figure 31. Spatially and time averaged radical densities as a function of the initial CO$_2$ fraction in the CO$_2$/H$_2$ gas mixture.

The densities of the stable molecules do not exhibit a periodic behavior like the electrons and the radicals. The reason is that their formation rates are typically much larger than their loss rates, in contrast to the radials and ions. The densities of the molecules formed during the hydrogenation of CO$_2$, i.e., CO, higher order hydrocarbons and oxygenates, exhibit a rising trend as a function of time, because their net production is higher than their net consumption. This will continue until periodic steady state will be reached. Indeed, when the densities of the reaction products rise, the rates of their consumption reactions will rise as well, until a balance is reached between production and consumption. The inlet gases, on the other hand, have a higher net consumption, so their densities show a gradual decrease as a function of time again until periodic steady state will be reached. The

conversion is most pronounced in the first few seconds, and afterwards the densities of the molecules do not significantly change anymore for a longer residence time, as is clear from Figure 32, for both CO_2 and H_2, and the most abundant products.
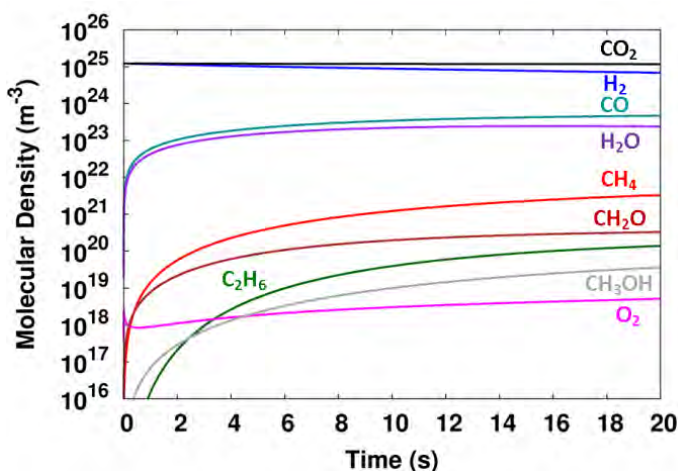
Figure 32. Spatially averaged molecular densities as a function of the residence time for a 50/50 CO_2/H_2 gas mixture.

Figure 33 illustrates the densities of the various molecules in the CO_2/H_2 gas mixture as a function of the initial CO_2 fraction, after a residence time of 5 seconds. The most abundant reaction products are CO, H_2O, CH_4, CH_2O, C_2H_6, O_2 and CH_3OH (more or less in order of decreasing density). This is in good agreement with the end products reported by Eliasson et al.[219], i.e. CH_4 and CH_3OH, Hayashi et al.[220], i.e. CO and CH_4, Kano et al.[221], i.e. CO, CH_4 and CH_3OH, and Zeng et al.[222], i.e. CO and H_2O as major products, a small amount of CH_4 and traces of C_2H_6, for similar CO_2/H_2 discharges. Note that Hayashi et al.[220] also detected the formation of dimethyl ether and formic acid, which are not included in our model as mentioned above. However, our model provides

us more insight in the formation of other higher hydrocarbons and oxygenates. The densities of CO and H_2O, which are by far the most abundant products, are almost not influenced by the inlet fraction of CO_2 (see Figure 33(a)). For H_2O, a maximum is obtained at an initial CO_2 fraction of 50%. This can be explained because H_2O is formed out of the collision of OH and H radicals. From Figure 31 it is clear that the H density decreases while the OH density increases with increasing initial CO_2 fraction, resulting in an optimum ratio at an inlet concentration of 50% CO_2. Furthermore, as will be clear from Section 6.5.2. below, the CO_2 conversion drops upon increasing initial CO_2 fraction in the mixture, and thus, the same applies to the yield of CO. On the other hand, a higher initial CO_2 fraction in the mixture allows for more CO_2 to be converted, and as both effects compensate each other, the effective CO_2 conversion remains constant, explaining why the CO density is constant for all CO_2/H_2 gas mixtures (see Figure 33(a)).

On the other hand, the densities of O_2, H_2O_2 and O_3 increase by several orders of magnitude upon increasing initial fraction of CO_2, which is logical, as they are directly formed out of the CO_2 splitting products (O and O_2). The densities of the higher hydrocarbons (C_xH_y) generally drop upon increasing initial fraction of CO_2, which can be explained by the higher conversion of CO_2 at lower initial fraction of CO_2 (see Section 6.5.2. below) resulting in higher densities of CH_2 and CH_3 radicals, as is clear from Figure 31 above, which are the building blocks for the higher hydrocarbons. However, an optimum seems to be reached for the 50/50 CO_2/H_2 gas mixture (see Figure 33(b)). Indeed, these higher hydrocarbons need the C from CO_2 as their building block, but they also need the H originating from H_2, and therefore an equal presence of both inlet gases seems to be preferable.

The same is true for the densities of CH_2O and CH_3OH and the other oxygenates, as is clear from Figure 33(c), although the hydroperoxides (CH_3OOH and C_2H_5OOH) generally increase with rising initial fraction of CO_2. Compared to our previous results on the formation of higher hydrocarbons and oxygenates in CH_4/O_2 and CH_4/CO_2 mixtures (see Section 5.5.1.), it is clear that except for CO and H_2O, the densities of the most important end products are now several orders of magnitude lower. The reason for this is that the conversion of CO_2 is very low in all gas mixtures (see Section 6.5.2. below), while CH_4 as C building block was more easily converted (see Section 5.5.2. above), and therefore, the crucial radicals in the formation process of higher hydrocarbons and oxygenates, such as CH_2 and CH_3, can be produced at a much higher density in mixtures with CH_4 than in the CO_2/H_2 mixture under study here. Note that the trends illustrated in Figure 33 correspond to a residence time of 5 seconds; however, the different molecules might have their maximum densities at a different residence time for the different gas mixing ratios studied (see also Section 5.5.1.); therefore the trends depicted in Figure 33 are not necessarily the same at other residence times.

Altering the inlet gas mixing ratio also affects the H_2/CO (syngas) ratio. A variable H_2/CO molar ratio is useful, as it allows the mixture to be used for various industrial synthesis processes (see Section 5.5.1.). The H_2/CO ratio, as obtained from our calculations, decreases with increasing initial CO_2 fraction, which is logical. It ranges from 54 (at 10% CO_2), which is not useful for industrial synthesis processes, to 3 (at 90% CO_2), which can be of interest as this is similar to the molar ratio produced by steam reforming (see Section 5.5.1.).
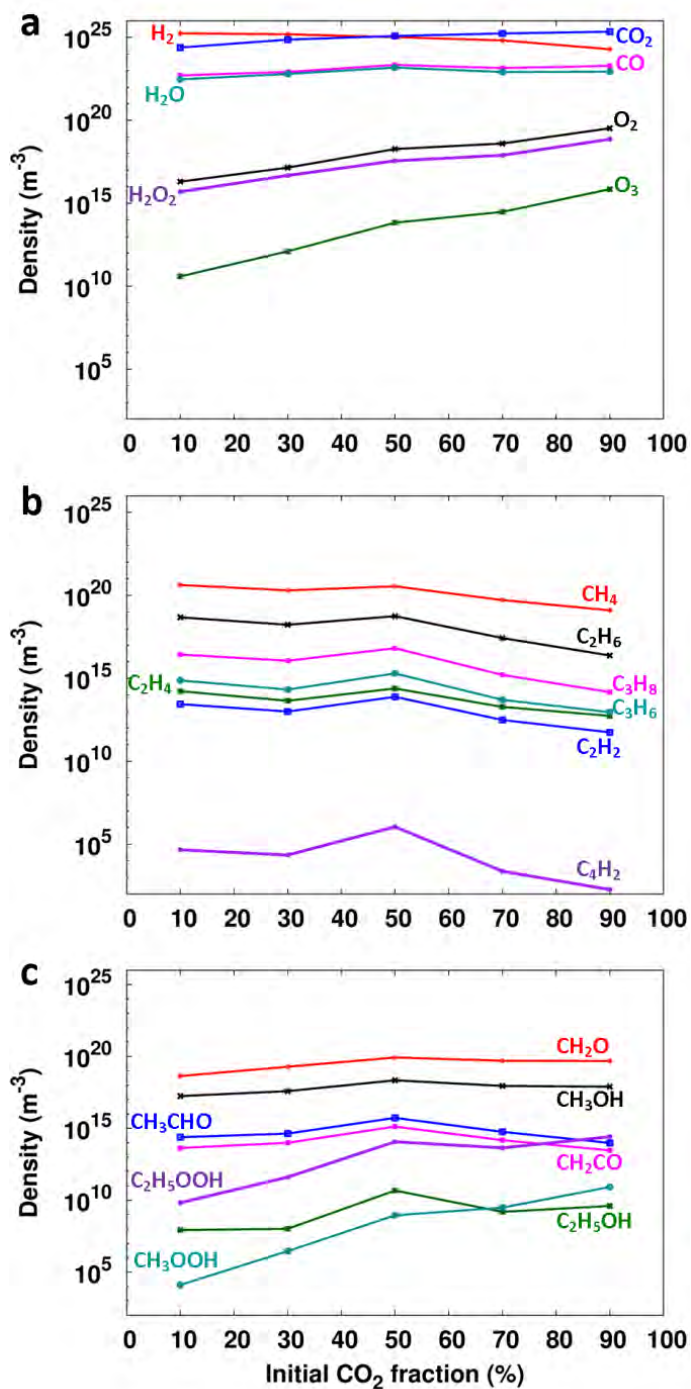
Figure 33. Spatially averaged molecule densities as a function of the initial CO_2 fraction in the CO_2/H_2 gas mixture, after a residence time of 5 seconds.

6.5.2. Conversion, Yields and Selectivities

Table 7 shows the maximum conversions of the inlet gases, i.e. CO_2 and H_2, and the maximum yields and corresponding selectivities of CO and CH_4, for different CO_2/H_2 gas mixtures. These maximum values are in all cases obtained for a residence time of 20s. The conversion of CO_2 clearly decreases with increasing initial CO_2 fraction in the mixture, from 7% at 10% CO_2 in the mixture to roughly 2% at 90% CO_2 in the mixture. This trend is in good agreement with the results of Zeng et al.[222], who reported that the conversion of CO_2 increases almost linearly with the increase of the H_2/CO_2 molar ratio at a fixed flow rate. A similar trend was also observed in CO_2/CH_4 (see Section 5.5.2. above), but the conversion of CO_2 was a factor 3 higher at a high initial CH_4 fraction (i.e., 90%) compared to a high initial H_2 fraction of 90%. This can be explained because CH_2, which is a direct dissociation product of CH_4, is much more abundant in CO_2/CH_4 than in CO_2/H_2, and thus provides an extra and very important loss process for CO_2 in a CO_2/CH_4 mixture (see Section 5.5.). The H_2 conversion is significantly larger, i.e., between 30 and 60 %, but no clear trend can be observed as a function of gas mixing ratio, because the discharge characteristics are strongly affected by the initial gas mixing ratio. As CO is directly produced by electron impact dissociation of CO_2 (see Section 6.5.3. below), the yield of CO shows the same trend as the conversion of CO_2, with values of only 2-6 %. Moreover, CO is the only C containing molecule directly produced out of CO_2 and therefore the selectivity of CO is in all cases around 90%. CH_4 is only formed with a selectivity above 1% at a low initial CO_2 fraction, i.e. a high initial H_2 fraction, which is logical. The yields of C_2H_6, CH_2O and CH_3OH are one or two orders of magnitude lower than the yield of CH_4, while the yields of other higher hydrocarbons and oxygenates are even more

negligible, which is of course the direct result of the rather low conversion of CO_2 in all gas mixing ratios. Note that also some sticking of the C atoms and hydrocarbon species at the walls occurs, which explains why the sum of the selectivities is not equal to 100 %. This formation of a C-containing layer on the electrodes was indeed also experimentally observed in the DBD reactor under study for a pure CO_2 discharge.[214, 224]

Table 7. Overview of the maximum conversions of the inlet gases, i.e. CO_2 and H_2, and the maximum yields and corresponding selectivities of CO and CH_4 for different CO_2/H_2 gas mixtures. All values are noted as percentage.

Initial CO_2 fraction	X (CO_2)	X (H_2)	Y (CO) - S (CO)	Y (CH_4) - S (CH_4)
10	7.0	64	6 - 86	0.2 - 2.2
30	3.6	33	3 - 90	0.03 - 0.9
50	4.4	44	4 - 87	0.03 - 0.6
70	2.1	33	2 - 89	0.003 - 0.2
90	1.9	58	2 - 92	0.0003 - 0.02

6.5.3. Dominant Reaction Pathways

To better explain the above trends, and to find out how the densities of the most important products can be optimized, it is crucial to obtain a better insight in the underlying reaction chemistry. Therefore, we will now discuss the dominant reaction pathways for the conversion of the inlet gases into the most important value-added products, i.e., CO, CH_4, CH_3OH and CH_2O, for the entire range of gas mixing ratios.

(a) Dissociation of CO_2 and H_2

The dominant reactions for CO_2 consumption (and production), as well as the time-averaged total production rate, total loss rate and net loss rate, as a function of the initial CO_2 fraction in the gas mixture are depicted in Figure 34. Although the consumption of CO_2 is mostly relevant in this work, we also show the production processes, because part of the CO_2 dissociation products will again recombine into the formation of CO_2. However, the total loss rate is larger than the total production rate, as is clear from Figure 34, thus leading to a net loss of CO_2 (i.e., conversion into other products). Furthermore, the total formation and loss rate generally increase upon larger initial CO_2 fraction in the mixture, which is logical. The most important channel for consumption of CO_2 is electron impact ionization towards CO_2^+. However, CO_2^+ immediately reacts back towards CO_2 upon charge transfer with H_2O molecules. Therefore, the most important reaction for consumption of CO_2 is effectively electron impact dissociation towards CO. This result was also obtained in earlier simulations carried out in our group for pure CO_2 splitting.[197] Furthermore, the relative importance of the various consumption and production processes is more or less independent from the gas mixing ratio, as is clear from Figure 34.
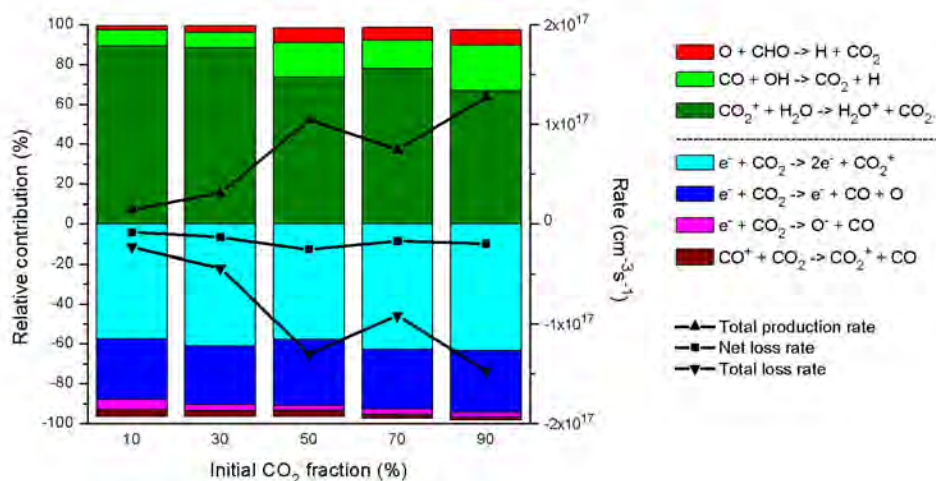
Figure 34. Relative contributions of the various production and consumption processes of CO_2 (left axis), as well as the time-averaged total production rate, total loss rate and net loss rate (right axis), as a function of the initial CO_2 fraction in the CO_2/H_2 gas mixture. The production rates are defined as positive values, while the consumption rates are plotted as negative values.

In Figure 35 the most important reactions for consumption (and production) of H_2 are shown. At an initial CO_2 inlet fraction of 10%, electron impact dissociation is the most important loss process for H_2, but part of the H atoms will recombine back into H_2, or react with CHO radicals into H_2 and CO. At an inlet fraction of 90% CO_2 the reaction of H_2 with H_2O^+ towards H_3O^+ becomes the most important loss mechanism. However, the latter is not due to the high absolute rate of this reaction, but rather because the rate of electron impact dissociation drops. Indeed, it is clear from Figure 35 that the total loss rate of H_2 is much lower at 90% than at 10% CO_2 content, because there is of course less H_2 in the mixture. Nevertheless, from comparing Figure 34 and Figure 35 it is clear that the net consumption of H_2 is much higher than the net consumption of CO_2. Indeed, the net loss rate of H_2 drops from

7×10^{17} cm^{-3} s^{-1} at 10% CO_2 to 7×10^{16} cm^{-3} s^{-1} at 90% CO_2, while the net loss rate of CO_2 is virtually constant around 10^{16} cm^{-3} s^{-1} for all gas mixing ratios. This explains also why the conversion of H_2 is much higher than the conversion of CO_2 (see Section 6.5.2. above).
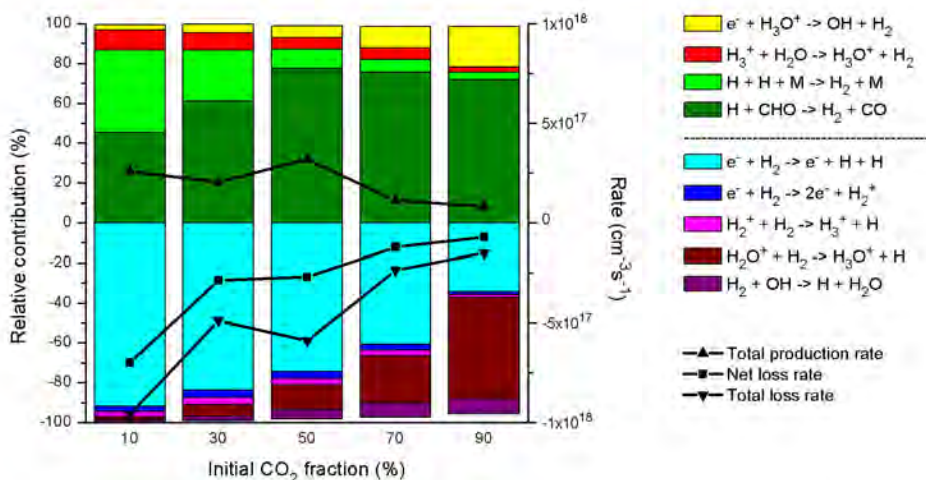
Figure 35. Relative contributions of the production and consumption processes of H_2 (left axis), as well as the time-averaged total production rate, total loss rate and net loss rate (right axis), as a function of the initial CO_2 fraction in the CO_2/H_2 gas mixture.

(b) Formation of CO, CH_4, CH_2O and CH_3OH

In Figure 36 the most important channels for the production (and loss) of CO are illustrated as a function of the initial CO_2 fraction in the gas mixture. The most important production process appears to be the reaction between H atoms and CHO radicals, forming H_2 and CO, but this reaction is counterbalanced by the most important loss process, i.e., the recombination of H with CO into CHO radicals. Therefore the most important effective

reaction for the formation of CO is electron impact dissociation of CO_2. On average there is a net formation of CO, with a rate in the order of 10^{16} cm^{-3}s^{-1}, slightly increasing upon higher initial CO_2 fraction in the mixture, which is logical.
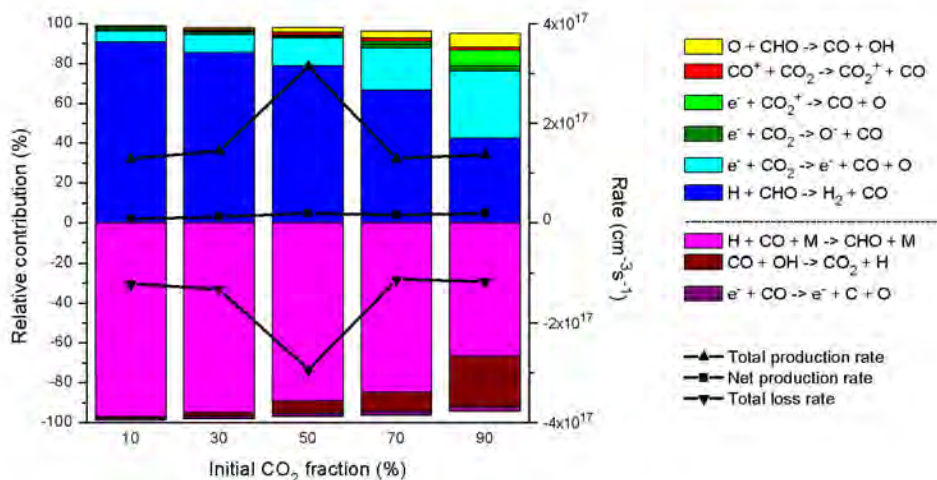
Figure 36. Relative contributions of the production and consumption processes of CO (left axis), as well as the time-averaged total production rate, total loss rate and net production rate (right axis), as a function of the initial CO$_2$ fraction in the CO$_2$/H$_2$ gas mixture.

The most important reactions for production (and loss) of CH$_4$ are depicted in Figure 37 as a function of the initial CO_2 fraction in the gas mixture. The production of CH$_4$ seems to be driven by only two reactions, i.e., the three-body recombination reaction between CH$_3$ and H radicals, and at a lower initial fraction of CO_2 also the charge transfer reaction between CH$_5^+$ and H$_2$O. However, the latter reaction is partially balanced by the loss of CH$_4$ via a charge transfer reaction with H$_3^+$. At a higher initial CO_2 fraction, the charge transfer reaction with CO$_2^+$ becomes the most important loss mechanism for

CH_4. A similar trend is observed for the net production rate of CH_4 as a function of the initial CO_2 fraction as for the net loss rate of H_2 (see Figure 35 above). Indeed, the dissociation of H_2 leads to the formation of H radicals which are needed for the formation of CH_4. An optimum is obtained for an initial CO_2 fraction of 10%, as is logical, and can be explained by the maximum densities found for the CH_3 and H radicals, as shown in Figure 31 above.
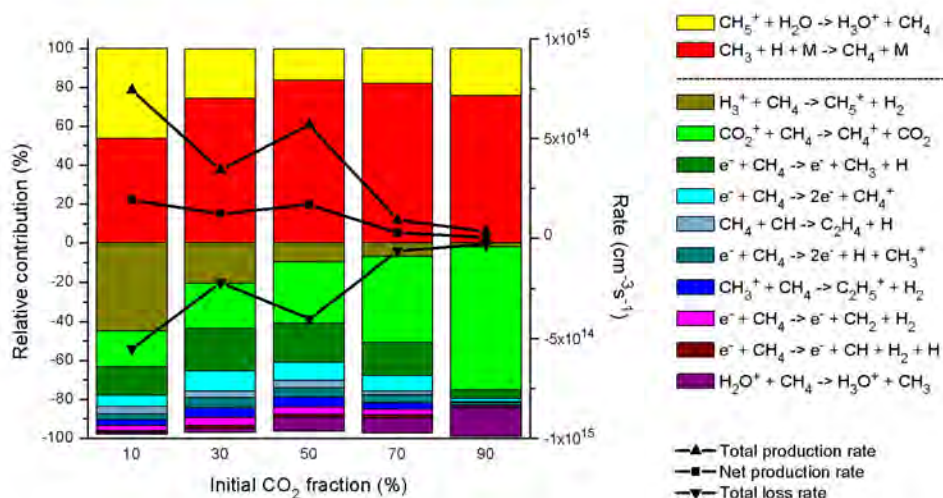
Figure 37. Relative contributions of the production and consumption processes of CH_4 (left axis), as well as the time-averaged total production rate, total loss rate and net production rate (right axis), as a function of the initial CO_2 fraction in the CO_2/H_2 gas mixture.

Figure 38 and Figure 39 show the dominant reactions for production (and loss) of CH_2O and CH_3OH, respectively, as a function of the initial CO_2 fraction in the gas mixture. The reaction between CO_2 and CH_2 radicals appears to be the most important channel for the production of formaldehyde at low initial CO_2 fractions, as was also observed for a CO_2/CH_4 mixture (see Section 5.5.3.). At higher initial CO_2 fractions, CH_2O is also formed to some extent out of two

CHO radicals. Furthermore, CH$_2$O is mainly lost upon collision with H atoms, yielding CHO and H$_2$, although the collisions with O atoms or OH radicals, yielding CHO and OH or H$_2$O, respectively, become gradually more important at higher CO$_2$ fractions, which is logical.

The total formation and loss rates reach a clear maximum at 50% CO$_2$ in the mixture, which is explained by the fact that at these conditions an optimum ratio of CH$_2$ (see maximum in Figure 31 above) and CO$_2$ is present in the gas mixture. As the total formation and loss rates are more or less equal to each other, the net formation rate of CH$_2$O is very low, and increases from 10^{11} to 10^{13} cm^{-3}s^{-1} upon rising CO$_2$ fraction. This explains why the CH$_2$O density rises slightly upon increasing CO$_2$ fraction in the mixture, as illustrated in Figure 33 above.
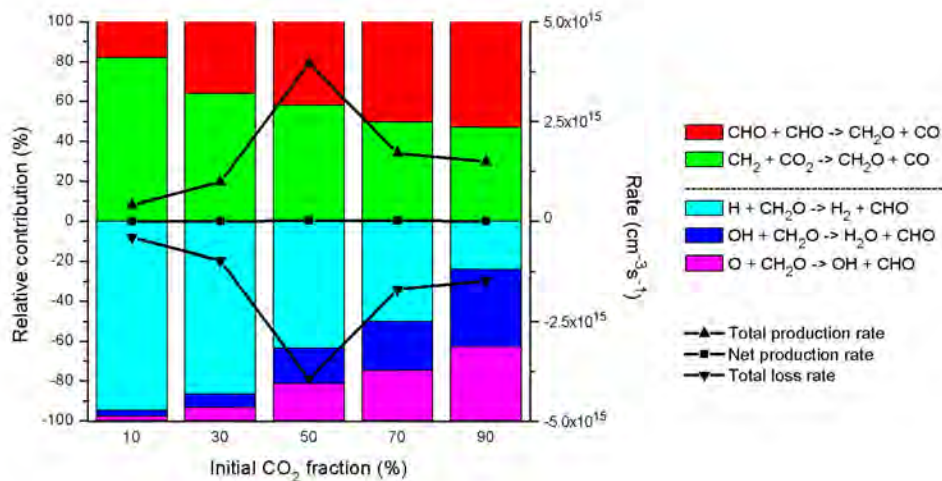
Figure 38. Relative contributions of the production and consumption processes of CH$_2$O (left axis), as well as the time-averaged total production rate, total loss rate and net production rate (right axis), as a function of the initial CO$_2$ fraction in the CO$_2$/H$_2$ gas mixture.

As is clear from Figure 39, the most important channel for the production of methanol, as predicted by our model, is the three-body reaction between CH$_3$ and OH radicals, like was also the case in the CO$_2$/CH$_4$ mixture studied before (see Section 5.5.3.). However, different from the CO$_2$/CH$_4$ mixture, the three-body reaction between CH$_2$OH and H radicals is now also an important production channel. Most of the CH$_3$OH produced, is also consumed again upon collision with either H atoms, OH radicals or O atoms, so the net formation rate of CH$_3$OH varies from 10^{11} to 10^{12} cm^{-3}s^{-1}. An optimum production of CH$_3$OH is again observed at 50/50 CO$_2$/H$_2$, because at these conditions an optimum ratio of CH$_3$ and OH (see Figure 31 above) is present in the gas mixture, and this explains why the CH$_3$OH density reaches a maximum at this mixing ratio, as shown in Figure 33 above.
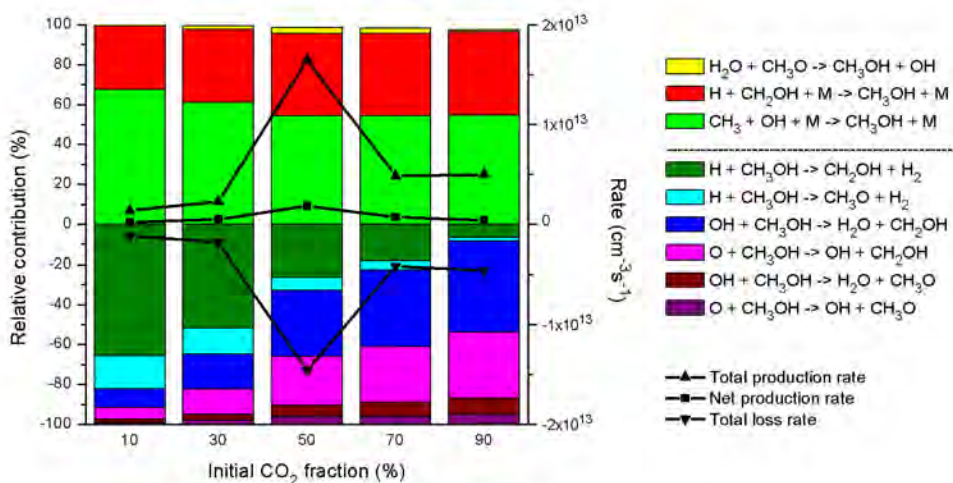
Figure 39. Relative contributions of the production and consumption processes of CH$_3$OH (left axis), as well as the time-averaged total production rate, total loss rate and net production rate (right axis), as a function of the initial CO$_2$ fraction in the CO$_2$/H$_2$ gas mixture.

(c) Overall reaction mechanism for the hydrogenation of CO_2 into valuable products

Figure 40 summarizes the dominant reaction pathways for the conversion of CO_2 and H_2 in a 50/50 CO_2/H_2 gas mixture. Note that the thickness of the arrow lines is proportional to the rates of the net reactions. The conversion starts with electron impact dissociation of CO_2, yielding CO and O radicals. Simultaneously, and much more pronounced, is the electron impact dissociation of H_2, resulting in the formation of H radicals (cf. the thickness of the arrow line). Radical recombination reactions of the O and H radicals lead to the formation of OH radicals, which recombine further into H_2O, and this explains why H_2O is also formed at relatively high density, as shown in Figure 33 above. However, this is of course of lesser interest than CO as valuable product.

CO will partially react back into CO_2, mainly through the formation of CHO radicals. Note that in this gas mixture, the major reaction from CO back into CO_2 indeed proceeds through CHO, as the rate of the reaction (CO + H + M → CHO + M) is in the order of 10^{17} cm^{-3} s^{-1}, and the rate of the subsequent formation of CO_2 through the reaction (CHO + O → CO_2 + H) is about 7×10^{15} cm^{-3} s^{-1}, while the rate of the direct reaction (CO + O + M → CO_2 + M) is only in the order of 10^{15} cm^{-3} s^{-1}. The H atoms thus contribute significantly to the back reaction of CO into CO_2. It is clear from the thick arrow line from H to CHO in Figure 40 that the formation of CHO out of CO and H indeed occurs at a very high rate. The reason why the arrow line from CO to CHO is much thinner is because CHO also reacts back into CO upon collision with H (CHO + H → CO + H_2), so the net reaction from CO to CHO is smaller than the net reaction from H to CHO. Furthermore, electron impact dissociation of CO

results in the formation of C radicals, which react further into CH, CH_2, C_2HO and CH_3 radicals in several successive radical recombination reactions. The formed CH_2 radicals react with CO_2 into the formation of CH_2O, as was also shown in Figure 38 above. The CH_3 radicals easily form CH_4, which is much more favored (i.e., the rate is one order of magnitude larger) than the formation of CH_3OH out of CH_3. CH_4 partially reacts further into higher hydrocarbons (C_xH_y).

From the reaction scheme, it is clear that a lot of subsequent radical reactions are necessary for the formation of (higher) hydrocarbons and oxygenates, such as CH_4, C_2H_6, CH_2O and CH_3OH, which explains the very low yields and selectivities of these end products (see Section 6.5.2. above). Indeed, the lack of direct formation of CH_2 and CH_3 in CO_2/H_2, which is important in CO_2/CH_4 gas mixtures (see Section 5.5.), combined with the very low conversion of CO_2, which is again due to the absence of CH_2 as important collision partner for the loss of CO_2, makes a CO_2/H_2 mixture under the present conditions less interesting for the formation of higher hydrocarbons and oxygenates than a CO_2/CH_4 mixture. This is especially true because H_2 itself is a useful product, while CH_4, besides being a fuel itself, also greatly contributes to global warming, and thus, the simultaneous conversion of CO_2 and CH_4 will reduce the concentration of two greenhouse gases. Moreover, CO_2/CH_4 mixtures are available from biomass installations, and their simultaneous conversion can be seen as a direct valorization of biogas, instead of the energy intensive biogas upgrading to a CH_4-rich gas by removing CO_2. Another possibly interesting H-source to be added to a CO_2 plasma to produce value-added chemicals, could be water, and the combined CO_2/H_2O conversion could even mimic the natural photosynthesis process.

However, recent investigations have illustrated that this gas mixture is also not able to produce oxygenates above the ppm range in a DBD plasma.[225]

Nevertheless, we still believe a CO$_2$/H$_2$ mixture can be of interest for producing CO, to obtain gas mixtures with a specific H$_2$/CO ratio. In order to produce specific oxygenated compounds, however, we believe that a catalyst should be added to the plasma.[226] This was also demonstrated by Eliasson et al.[219], who reported much higher methanol yields in the presence of a catalyst in the plasma, and by Zeng et al.[222], who found that the combination of a plasma with a catalyst enhances the conversion of CO$_2$ by 7-36 %, as well as the yield and energy efficient production of CO.
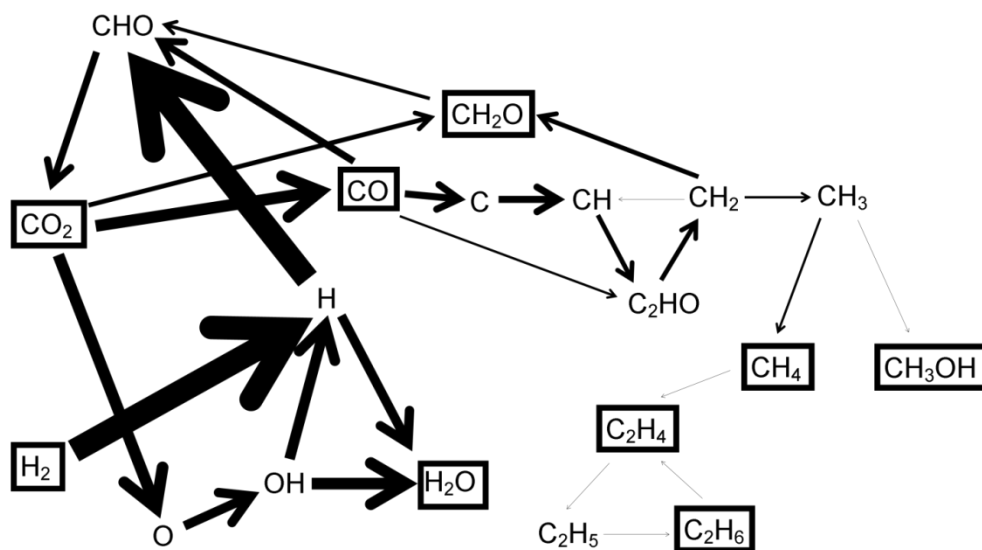
Figure 40. Dominant reaction pathways for the conversion of CO$_2$ and H$_2$ into various products, in a 50/50 CO$_2$/H$_2$ gas mixture. The thickness of the arrow lines is proportional to the rates of the net reactions. The stable molecules are indicated with black rectangles.

6.6. Conclusion

A 1D fluid modeling study for the hydrogenation of CO$_2$ in a DBD plasma was carried out for different CO$_2$/H$_2$ gas mixing ratios. The densities of the various plasma species as a function of the residence time and the gas mixing ratio were discussed. The spatially averaged densities of the electrons, radicals and ions produced in the plasma exhibit periodic behavior as a function of time, following the period of the sinusoidal applied voltage. The most abundant radicals are H, O, OH, HO$_2$, CHO, CH$_3$ and CH$_2$. The densities of the molecules formed during the hydrogenation of CO$_2$, i.e., CO, higher order hydrocarbons and oxygenates, exhibit a rising trend as a function of time, because their net production is higher than their net consumption. The most abundant reaction products are CO, H$_2$O and CH$_4$, and to a lower extent also CH$_2$O, C$_2$H$_6$, O$_2$ and CH$_3$OH. This is in good agreement with reported results from literature for similar CO$_2$/H$_2$ discharges. Altering the inlet gas mixing ratio did not drastically affect the densities of the formed higher hydrocarbons and oxygenates, as the conversion of CO$_2$ was found to be very low in all gas mixing ratios. We have also presented the calculated conversions of the inlet gases and the maximum yields and corresponding selectivities of the main reaction products. It is clear that the conversion of CO$_2$ is rather low (i.e., in the order of 2-7 %) in all gas mixtures, and much lower than in a CO$_2$/CH$_4$ mixture, where typical conversions in the order of 3-20 % are obtained at similar conditions. The reason is the abundance of CH$_2$ radicals in the latter mixture, which significantly contribute to the loss of CO$_2$, but their density is very low in the CO$_2$/H$_2$ mixture. The H$_2$ conversion was calculated to be about 30-60 %, depending on the gas mixing ratio. CO was found to be the only value-added end product with a high selectivity. Finally,

the underlying plasma chemistry governing the conversion of CO_2 and H_2 into the various products was analyzed in detail. The dominant reaction pathways for the consumption of CO_2 and H_2 and the production and loss of some interesting end products, i.e., CO, CH_4, CH_2O and CH_3OH, were discussed. It is clear from our results that a higher conversion of CO_2, as well as a higher density of CH_3 and CH_2 radicals, would be necessary in order to obtain higher yields of the desired end products. For the conditions under study, only CO is formed at an acceptable level. Thus, it is clear that a CO_2/H_2 mixture is not very suitable for the production of other value-added chemicals besides CO, and that a CO_2/CH_4 mixture is more appropriate, because of the presence of CH_2 and CH_3 radicals. The use of a catalyst can possibly increase the formation of some desired oxygenates, as is indeed also shown by Eliasson et al.[219] and Zeng et al.[222].

Chapter 7

General Conclusion and Outlook for the Future

7.1. General Conclusion

We have studied the plasma chemistry for gas conversion in a DBD plasma, in pure CH_4, as well as in CH_4/O_2, CH_4/CO_2 and CO_2/H_2 mixtures, which are used for partial oxidation of CH_4, dry reforming of CH_4 and CO_2 hydrogenation, respectively. More specifically, we have calculated the densities of the various plasma species, created in these gas mixtures, as a function of residence time and gas mixing ratio. C_2H_6 and H_2 are found to be the main reaction products of the conversion of pure CH_4 into higher hydrocarbons in a DBD reactor. Partial oxidation of CH_4 favors the formation of H_2O_2, CH_3OH, C_2H_5OH, CH_3OOH and C_2H_5OOH, while the densities of H_2, CH_2O, CH_3CHO and CH_2CO are higher for the dry reforming of CH_4. CO is formed at high density in both gas mixtures. Note that in the gas mixtures with O_2 as co-reactant also a significant amount of undesired CO_2 is formed. The most abundant reaction products for the hydrogenation of CO_2 in a DBD plasma are CO, H_2O and CH_4, and to a lower extent also CH_2O, C_2H_6, O_2 and CH_3OH. It is illustrated that a careful selection of the residence time and gas mixing ratio can entail a higher production of some targeted molecules.

From the calculated densities, the conversions of the inlet gases and the yields and selectivities of the end products as a function of residence time and initial gas mixing ratio can be obtained. The conversion of CH_4 after 20s is around 20% in all considered mixtures with O_2, while in pure CH_4, a conversion of 40% was calculated after 20s. A maximum conversion of 68% for CH_4 and 55% for CO_2 in CH_4/CO_2 is predicted by our calculations. In contrast, the conversion of CO_2 was found to be very low in CO_2/H_2 for all gas mixing ratios (i.e., in the order of 2-7 %). Altering the inlet gas mixing ratio in CO_2/H_2 did not drastically affect the densities of the formed higher

hydrocarbons and oxygenates. Therefore, it is clear that a CO_2/H_2 mixture is not very suitable for the production of other value-added chemicals besides CO.

The dominant reaction pathways for the consumption of the inlet gases and the production and loss of the dominant end products are also discussed. These results explain in detail why the formation of some molecules is favored in one gas mixture, while other molecules are predominantly formed in another gas mixture. They also point out the reason for the rather low conversion in CO_2/H_2 compared to the conversion in CH_4/CO_2, i.e., the lack of CH_2 radicals in CO_2/H_2. Schematic overviews at the end of each chapter summarize the dominant reaction pathways for the conversion of the inlet gases into various compounds, in the different gas mixtures.

Reasonable agreement between our calculation results and the measurements for pure CH_4 is established. Furthermore, our results on the partial oxidation and dry reforming of CH_4 and on the hydrogenation of CO_2 are in good agreement with reported results from literature for similar CH_4/O_2, CH_4/CO_2 and CO_2/H_2 discharges. Moreover, the model can help to obtain more insight into the most suitable feed gas ratio, residence time, co-reactant and other plasma parameters, to obtain the highest yield and/or selectivity of a desired oxygenate.

7.2.   Outlook for the Future

In this PhD dissertation, we only focused on the conversion, yields and selectivities, but another crucial parameter to determine whether a sustainable competitive industrial process for gas conversion in a DBD can be established, is the energy efficiency of the conversion process. The latter was not studied in the present PhD dissertation, but it is known that a DBD plasma has a rather low energy efficiency for gas conversion, as studied in other PhD dissertations within our group PLASMANT.[109, 181, 197, 227-229] To improve the energy efficiency, a (dielectric) packing can be included in the DBD reactor, enhancing the electric field, and thus the electron temperature, thereby increasing the electron impact reaction rates, yielding a higher conversion for the same input power, and thus a higher energy efficiency. The effect of introducing a dielectric packing in a DBD reactor is currently being investigated by fluid modeling in another PhD dissertation within our group PLASMANT,[212, 230] as well as experimentally,[212] in collaboration with the group LADCA.

Furthermore, a packed bed DBD reactor is also very suitable to introduce a catalyst in the plasma. Our calculation results indicate that the latter will indeed be crucial to improve the selectivities of the desired end products, by acting on one or more of the underlying gas-phase reactions, which will be needed to make this DBD plasma conversion competitive for industrial applications. Plasma catalysis is also being studied within the group PLASMANT, both by computer modeling and experiments, the latter in collaboration with LADCA.

Finally, our specific modeling results on the plasma chemistry can be further improved by including vibrational excitation levels, so that the model can also be applied to other types of plasma reactors, like a microwave or gliding arc discharge (which are known to have a higher energy efficiency, and which are also being studied within our group PLASMANT), or by including other value-added compounds in the model, such as dimethyl ether and formic acid. However, it will be crucial to find reliable data to describe the formation or loss of these species. On the other hand, a reduction of the chemistry set based on a sensitivity analysis is also worth to perform, to be able to simulate the plasma conversion by 2D fluid models, and account for the specific features of a plasma reactor, such as the occurrence of filaments in a DBD.

Summary

The world primary energy demand is set to grow by one-third to 2040. Globally, fossil fuel resources are still plentiful and will last for decades, but it becomes more difficult to recover them and there can be no guarantee that they will be exploited fast enough to meet the level of demand. The availability of energy resources is, however, of paramount importance to the society. Access to reliable, affordable commercial energy provides the basis for heat, light, mobility, communications and agricultural and industrial capacity in modern society and in this way energy stipulates the degree of civilization. Therefore, socially, environmentally and economically, a growing need is being imposed for a global sustainable energy strategy, based on an improvement of the energy efficiency of the current technologies and a more intensifying diversification of the energy resources, with a huge preference for lower carbon resources. Future energy policy intentions indicate a boost to lower-carbon fuels and technologies worldwide, resulting in an increasing share of non-fossil fuels and natural gas, which is the least-carbon intensive fossil fuel, within the global energy mix up to 2040, while the share of oil and coal is decreasing.

Besides this, climate change due to anthropogenic greenhouse gas emission is a growing concern for the global society. Anthropogenic greenhouse gas emissions have increased since the pre-industrial era and have led to atmospheric concentrations of carbon dioxide (CO_2), methane (CH_4) and nitrous oxide (N_2O) that are unprecedented in at least the last 800,000 years. At the 21st Conference of the Parties to the United Nations Framework Convention on Climate Change (COP21/CMP11; November-December, 2015) a new international agreement, which is strongly endorsed by the chemical

industry, on climate change was made, in order to keep global warming below 2°C.

The conversion of methane, the principal component of natural gas, and carbon dioxide to value-added chemicals and fuels has still a significant growth potential. Currently, both resources are greatly underutilized for the production of chemicals and liquid fuels, mainly because they are very stable molecules. More in particular, the development of a process for the direct synthesis of higher hydrocarbons, syngas and oxygenates, such as methanol and formaldehyde, from methane and/or carbon dioxide in an energy-efficient way would offer significant benefits.

Atmospheric pressure non-thermal plasmas, such as dielectric barrier discharges (DBDs), can offer here a distinct advantage because a DBD has the unique characteristic that it combines an ambient bulk gas temperature and the presence of highly energetic electrons with an electron temperature between 5000 and 20000 K at an electron density of about 10^{14} cm^{-3}, and so it enables gas phase reactions at ambient conditions.

A DBD is an electrical discharge that is generated between two electrodes of which at least one is covered with a dielectric material made of glass, quartz, alumina, etc. The gap between the two electrodes is typically a few millimeters. An ac voltage with an amplitude from 1 kV to 100 kV and a frequency of a few Hz to MHz is usually applied to this kind of discharges. Different plasma activation mechanisms will act, causing vibrational and electronic excitation, as well as ionization and dissociation of species, and in this way gas conversion processes are induced.

These processes always involve a huge underlying plasma chemistry and in order to optimize such a process, it is indispensable to get notion of the play of the different species in the immensity of chemical reactions. Fluid modeling can provide here the necessary information to obtain insight in the gas phase chemistry taking place in the discharge gap.

The aim of this dissertation was to describe in detail the plasma chemistry in an atmospheric pressure cylindrical DBD, used as a chemical reactor for gas conversion in different gas mixtures with CH_4 and/or CO_2, by means of a 1D fluid model. The model applied in this study is called Plasimo's MD2D. It is based on the continuity and flux equations for each type of species treated, the electron energy equation and the Poisson equation. This set of coupled partial differential equations is solved by the so-called modified strongly implicit method.

More specifically, the goal was to develop a reliable chemistry set for the description of the gas phase chemistry in pure CH_4, CH_4/O_2, CH_4/CO_2 and CO_2/H_2 gas discharges. In order to achieve our goal, we started by developing a 1D fluid model for an atmospheric pressure DBD in pure methane, and extended this model in a later stage to describe the plasma chemistry in the other gas mixtures. A large number of different plasma species (i.e., electrons, molecules, radicals, ions) are included in our model, as well as a comprehensive set of chemical reactions, into which these species participate. For the electron-induced reactions, cross sections as a function of the electron energy were defined as input for the Boltzmann solver BOLSIG+, which provides the energy dependent electron transport coefficients and rate coefficients of the electron reactions, whereas the ion-neutral and neutral-

neutral reactions were characterized by a constant reaction rate coefficient for the working pressure and temperature of 1 atm and 300 K, respectively.

In this way, calculation results could be obtained for the densities of the different plasma species, the conversions of the inlet gases, the yields and selectivities of the end products and the dominant reaction pathways for each of the gas mixtures studied. This allows us to determine whether or not a specific gas mixture is suitable for the production of a specific end-product of interest. Our calculation results were validated with reported results in literature, and for pure CH_4 also with some experiments for the reactor set-up under study.

In all gas mixtures, the spatially averaged densities of the electrons, ions and radicals exhibit a periodic behavior as a function of time, following the sinusoidal applied voltage, while the spatially averaged molecule densities do not show a periodic behavior. It is illustrated that a careful selection of the residence time and gas mixing ratio can entail a higher production of some targeted molecules.

Higher hydrocarbons (C_2H_y and C_3H_y) and hydrogen gas are typically found as end products for the conversion of pure CH_4. A reasonable agreement between our calculation results and the measurements is established. It is found that electron impact dissociation of CH_4, resulting in the formation of the methyl radical (CH_3), initiates the conversion process. Recombination of CH_3 with either another CH_3 radical or with a C_2H_5 radical will lead to the formation of C_2H_6 and C_3H_8. Dissociation of these higher hydrocarbons leads directly to the formation of other hydrocarbons, but also indirectly by the formation of new radicals, which can subsequently also recombine towards these higher order hydrocarbons. In other words, the conversion of CH_4 is a

play of dissociation and recombination reactions leading to a diverse mixture of higher hydrocarbons.

Dry reforming of CH_4 in a DBD favors the formation of H_2, CH_2O, CH_3CHO and CH_2CO, while the densities of H_2O_2, CH_3OH, C_2H_5OH, CH_3OOH and C_2H_5OOH are higher for the partial oxidation of CH_4 in a DBD. CO is formed at high density in both gas mixtures, i.e., CH_4/O_2 and CH_4/CO_2. In the gas mixtures with O_2 as co-reactant, also a significant amount of undesired CO_2 is formed. Electron impact dissociation of the inlet gases initiates the conversion process. The recombination of CH_3 radicals again plays a crucial role and it was shown that this recombination leads to the formation of higher hydrocarbons in the mixtures with CO_2, while CH_3O_2 radicals are favored in the mixtures with O_2. In the CH_4/CO_2 mixture, also CH_2 radicals play a role, which can be converted into formaldehyde and CO molecules. In the CH_4/O_2 mixture, the CH_3O_2 radicals lead among others to the formation of methanol, which can react further into formaldehyde and the latter can form CO. Our results are in reasonable agreement with reported results from literature for similar CH_4/O_2 and CH_4/CO_2 discharges. Moreover, our model provides additional information, mainly on the comparison between the formed end products in CH_4/O_2 and CH_4/CO_2 gas mixtures and on the different pathways leading to these products.

The most abundant reaction products for the hydrogenation of CO_2 in a DBD are CO, H_2O and CH_4, and to a lower extent also CH_2O, C_2H_6, O_2 and CH_3OH. This is in good agreement with reported results from literature for similar CO_2/H_2 discharges. Altering the inlet gas mixing ratio did not drastically affect the densities of the formed higher hydrocarbons and oxygenates, as the conversion of CO_2 was found to be very low (i.e., in the order of 2-7 %) in all

gas mixtures, and much lower than in a CO_2/CH_4 mixture, where typical conversions in the order of 3-20 % are obtained at similar conditions. The reason is the abundance of CH_2 radicals in the latter mixture, which significantly contribute to the loss of CO_2, but their density is very low in the CO_2/H_2 mixture. It is clear that a CO_2/H_2 mixture is not very suitable for the production of other value-added chemicals besides CO, at least in a pure DBD, and that the combination with a catalyst will be needed for the selective production of some value-added compounds, not only in the CO_2/H_2 mixture, but in a DBD plasma in general.

Samenvatting

De wereldwijde vraag naar primaire energie zal naar verwachting met een derde groeien tegen 2040. Hoewel fossiele brandstoffen wereldwijd nog overvloedig aanwezig zijn, wordt het steeds moeilijker om ze te ontginnen en is er geen garantie dat ze snel genoeg gewonnen zullen worden om aan de vraag naar energie tegemoet te komen. De beschikbaarheid van energiebronnen is echter van het grootste belang voor onze maatschappij. De toegang tot betrouwbare, betaalbare commerciële energie vormt de basis voor warmte, licht, mobiliteit, communicatie en agrarische en industriële capaciteit in een moderne maatschappij, en op deze manier bepaalt energie de ontwikkelingsgraad van een maatschappij. Daarom is er vanuit sociaal, ecologisch en economisch oogpunt een groeiende behoefte aan een wereldwijde strategie voor duurzame energie, door middel van een verbetering van de energie-efficiëntie van de huidige technologieën en een toenemende verscheidenheid aan energiebronnen, met een grote voorkeur voor energiebronnen met een lager koolstofgehalte. Beleidsintenties inzake energie wijzen op een algemene verschuiving naar brandstoffen en technologieën met een lager koolstofgehalte. Dit leidt ertoe dat het aandeel aan niet-fossiele brandstoffen en aardgas, de minst koolstofintensieve fossiele brandstof, binnen de wereldwijde energiemix zal blijven groeien in de komende decennia, terwijl olie en steenkool minder belangrijk worden.

Daarnaast is er de toenemende bezorgdheid over de gevolgen van de klimaatverandering voor de samenleving. De antropogene uitstoot van broeikasgassen, welke aan de basis ligt van de klimaatverandering, is gestegen sinds het pre-industriële tijdperk. Daardoor is de atmosferische concentratie van koolstofdioxide (CO_2), methaan (CH_4) en lachgas (N_2O) toegenomen tot

waarden die ongezien zijn in de laatste 800.000 jaar. Tijdens de 21ste Conferentie van Partijen over het Klimaatverdrag (COP21/CMP11, november-december 2015) werd een nieuwe internationale overeenkomst gemaakt over klimaatverandering, welke wordt onderschreven door de chemische industrie. Er werd hierbij afgesproken om de opwarming van de aarde onder de 2 °C te houden.

De omzetting van methaan, het hoofdbestanddeel van aardgas, en koolstofdioxide in chemicaliën en brandstoffen met toegevoegde waarde heeft nog steeds een aanzienlijk groeipotentieel. Momenteel worden beide grondstoffen sterk onderbenut voor de productie van chemicaliën en vloeibare brandstoffen, vooral omdat het beiden zeer stabiele moleculen zijn. Vooral de ontwikkeling van een energie-efficiënt en duurzaam proces voor de directe vorming van hogere koolwaterstoffen, syngas en zuurstofhoudende verbindingen, zoals methanol en formaldehyde uit methaan en/of koolstofdioxide zou perspectieven bieden.

Atmosferische niet-thermische plasma's, zoals diëlektrische barrière ontladingen (DBDs), kunnen hier een duidelijk voordeel bieden, daar in een DBD de temperatuur van het bulkgas relatief laag blijft (tussen kamertemperatuur en 200 °C) terwijl elektronen gevormd worden, die zeer energetisch zijn en een temperatuur hebben variërend tussen 5000 en 20.000 K, bij een elektronendichtheid van circa 10^{14} cm^{-3}. Dit maakt reacties mogelijk die thermodynamisch niet zouden kunnen optreden bij deze lage gastemperaturen. Als dusdanig kunnen plasmaprocessen de nadelen van de hoge temperatuur, die vereist is bij conventionele katalytische processen, vermijden.

Een DBD is een elektrische ontlading die wordt gegenereerd tussen twee elektroden waarvan er ten minste één is bedekt met een diëlektricum, gemaakt van bv. glas, kwarts, aluminiumoxide, enz. De afstand tussen de twee elektroden is typisch enkele millimeters. Doorgaans wordt een wisselspanning met een amplitude van 1 kV tot 100 kV en een frequentie van enkele Hz tot MHz over de elektroden aangelegd, waarna in de ontladingsruimte een plasma gecreëerd zal worden. Verschillende plasma-activatiemechanismen treden op en dit leidt tot vibrationele en elektronische excitatie, ionisatie en dissociatie van de gasdeeltjes en dusdanig tot gasconversie.

Een waaier aan deeltjes en reacties is betrokken in deze gasconversie processen. Het is dan ook cruciaal om een inzicht te krijgen in deze onderliggende plasmachemie, indien men dergelijk proces wenst te optimaliseren. Fluid modellering kan hier de nodige informatie aanreiken om een inzicht te krijgen in de gasfase chemie in zulk een DBD.

Het opzet van dit doctoraat was om in detail de plasmachemie in een cilindrische DBD bij atmosfeerdruk, gebruikt als een chemische reactor voor gasconversie, te beschrijven aan de hand van een 1D fluid model, voor verschillende gasmengsels met CH_4 en/of CO_2. Het model dat gebruikt werd in dit onderzoek is Plasimo's MD2D. Een fluid model is gebaseerd op de snelheidsmomenten van de Boltzmann transportvergelijking. De nulde, eerste en tweede momenten van deze vergelijking geven namelijk de behoudsvergelijkingen van respectievelijk deeltjesdichtheid, hoeveelheid van beweging en energiedichtheid. De behoudsvergelijking voor hoeveelheid van beweging wordt hier echter benaderd door de eenvoudigere drift-diffusie vergelijking. De behoudsvergelijking van deeltjesdichtheid en de drift-diffusie vergelijking worden opgesteld voor elke deeltjessoort, terwijl de

energiebalansvergelijking enkel opgesteld wordt voor de elektronen. Deze vergelijkingen worden ten slotte gekoppeld aan de Poisson vergelijking om de elektrische potentiaalverdeling zelfconsistent te kunnen berekenen uit de dichtheden van elektronen en ionen. Aangezien deze set van vergelijkingen sterk gekoppeld is, moeten deze vergelijkingen ook simultaan worden opgelost.

Meer bepaald was het het doel om een betrouwbare chemieset op te stellen voor de beschrijving van de gasfase chemie in zuiver CH_4, CH_4/O_2, CH_4/CO_2 en CO_2/H_2 gasontladingen. Om ons doel te bereiken, zijn we begonnen met het ontwikkelen van een 1D fluid model voor een DBD bij atmosfeerdruk in zuiver methaan. In een volgende stap hebben we dit model dan uitgebreid om de plasmachemie in de andere gasmengsels te kunnen beschrijven.

Zulk een reactieset bestaat uit een groot aantal verschillende soorten plasmadeeltjes (elektronen, moleculen, radicalen, ionen) en hun bijhorende reacties. Voor de deeltjes dienen diffusiecoëfficiënten, mobiliteitscoëfficiënten, stickingcoëfficiënten en secundaire elektronen emissiecoëfficiënten gedefinieerd te worden in het model. Voor de reacties met elektronen werden cross secties als functie van de elektronenenergie gedefinieerd als input voor de Boltzmann solver BOLSIG+, die energie-afhankelijke elektron transport- en snelheidscoëfficiënten van de elektron-reacties bepaalt. De reacties tussen neutrale deeltjes en tussen neutrale deeltjes en ionen werden gedefinieerd met een constante reactiesnelheidscoëfficiënt voor 1 atmosfeer en 300 K.

Op deze manier konden de dichtheden van de verschillende plasmadeeltjes, de omzettingen van de inlaatgassen, de rendementen en de selectiviteiten

van de eindproducten en de belangrijkste reactiepaden berekend worden voor elk van de in dit onderzoek beschouwde gasmengsels. Daardoor konden we bepalen of een bepaald gasmengsel geschikt is voor de productie van een specifiek beoogd eindproduct. Onze resultaten werden gevalideerd aan de hand van gerapporteerde waarden in de literatuur voor gelijkaardige ontladingen, alsook aan de hand van experimenten uitgevoerd in de plasmareactor beschouwd in dit onderzoek, in het geval van zuiver CH_4.

De ruimtelijk gemiddelde dichtheden van de elektronen, ionen en radicalen vertonen in elk van de gasmengsels periodisch gedrag in functie van de tijd. Dit is in tegenstelling tot de ruimtelijk gemiddelde dichtheden van de moleculen, welke een dalende of stijgende trend vertonen. Een zorgvuldige keuze van de verblijftijd en de gassamenstelling kan leiden tot een hogere productie van bepaalde gewenste eindproducten.

Hogere koolwaterstoffen (C_2H_y en C_3H_y) en waterstofgas zijn de belangrijkste eindproducten voor de conversie van zuiver CH_4. Een redelijke overeenkomst tussen onze berekeningen en de metingen werd verkregen. Het blijkt verder dat botsingen van elektronen met CH_4 leiden tot de dissociatie van CH_4 in methylradicalen (CH_3) welke het gasconversie proces zullen initiëren. Recombinatie van CH_3 met een ander CH_3 radicaal of een C_2H_5 radicaal leidt tot de vorming van C_2H_6 en C_3H_8. Dissociatie van deze hogere koolwaterstoffen leidt direct en indirect (via nieuwe recombinatiereacties) tot de vorming van andere koolwaterstoffen. De omzetting van CH_4 is met andere woorden een spel van dissociatie- en recombinatiereacties, die leiden tot een divers mengsel van hogere koolwaterstoffen.

'Dry reforming' van CH_4 in een DBD leidt tot de vorming van H_2, CH_2O, CH_3CHO en CH_2CO, terwijl partiële oxidatie van CH_4 resulteert in de vorming

van H_2O_2, CH_3OH, C_2H_5OH, CH_3OOH en C_2H_5OOH. De dichtheid van CO is hoog in zowel CH_4/O_2 als CH_4/CO_2. In de gasmengsels met O_2 als co-reactant wordt ook een aanzienlijke hoeveelheid ongewenst CO_2 gevormd. Elektron impact dissociatie van de gasmoleculen initieert het conversieproces. De recombinatie van CH_3 radicalen speelt wederom een cruciale rol. Er werd aangetoond dat deze recombinatie leidt tot de vorming van hogere koolwaterstoffen in het mengsel met CO_2, terwijl CH_3O_2 radicalen bij voorkeur gevormd worden in de mengsels met O_2. In de CH_4/CO_2 gasmengsels spelen ook de CH_2 radicalen een belangrijke rol, waarbij er via botsingen met CO_2 formaldehyde en CO gevormd worden. De CH_3O_2 radicalen in de CH_4/O_2 gasmengsels leiden onder andere tot de vorming van methanol, dat verder kan reageren tot formaldehyde en dit kan dan weer verder reageren tot CO. Er is een redelijke overeenstemming tussen onze resultaten en gerapporteerde resultaten uit de literatuur voor soortgelijke CH_4/O_2 en CH_4/CO_2 ontladingen. Bovendien levert ons model extra informatie, voornamelijk wat betreft de vergelijking van de gevormde eindproducten tussen CH_4/O_2 en CH_4/CO_2 gas gasmengsels en de verschillende reactiepaden verantwoordelijk voor de vorming van deze producten.

De belangrijkste reactieproducten voor de hydrogenatie van CO_2 in een DBD zijn CO, H_2O en CH_4, en in mindere mate ook CH_2O, C_2H_6, O_2 en CH_3OH. Dit komt goed overeen met de gerapporteerde resultaten uit de literatuur voor soortgelijke CO_2/H_2 ontladingen. Het veranderen van de initiële gasverhouding heeft geen grote invloed op de dichtheid van de gevormde hogere koolwaterstoffen en zuurstofhoudende verbindingen, daar de omzetting van CO_2 zeer laag bleek (in de orde van 2-7%) in alle gasmengsels, en dus veel lager is dan deze in een CO_2/CH_4 mengsel, waarbij omzettingen in

de orde van 3-20% worden verkregen bij soortgelijke omstandigheden. De reden is de grotere aanwezigheid van CH_2 radicalen in het CO_2/CH_4 gasmengsel, die aanzienlijk bijdragen tot de afbraak van CO_2. Het is duidelijk dat een CO_2/H_2 mengsel niet erg geschikt is voor de productie van andere chemicaliën met toegevoegde waarde behalve dan CO, tenminste voor een DBD plasma, en dat de combinatie met een katalysator nodig zal zijn voor de selectieve productie van specifieke waardevolle componenten, niet enkel in het CO_2/H_2 mengsel, maar ook meer algemeen in een DBD plasma.

List of Peer-Reviewed Publications

Paulussen, S.; Verheyde, B.; Tu, X.; **De Bie, C.**; Martens, T.; Petrovic, D.; Bogaerts, A.; Sels, B. Conversion of Carbon Dioxide to Value-Added Chemicals in Atmospheric Pressure Dielectric Barrier Discharges. Plasma Sources Sci. Technol. 2010, 19, 034015.

Bogaerts, A.; **De Bie, C.**; Eckert, M.; Georgieva, V.; Martens, T.; Neyts, E.; Tinck, S. Modeling of the Plasma Chemistry and Plasma-Surface Interactions in Reactive Plasmas. Pure Appl. Chem. 2010, 82, 1283-1299.

De Bie, C.; Martens, T.; van Dijk, J.; Paulussen, S.; Verheyde, B.; Corthals, S.; Bogaerts, A. Dielectric Barrier Discharges Used for the Conversion of Greenhouse Gases: Modeling the Plasma Chemistry by Fluid Simulations. Plasma Sources Sci. Technol. 2011, 20, 024008.

De Bie, C.; Verheyde, B.; Martens, T.; van Dijk, J.; Paulussen, S.; Bogaerts, A. Fluid Modeling of the Conversion of Methane into Higher Hydrocarbons in an Atmospheric Pressure Dielectric Barrier Discharge. Plasma Process. Polym. 2011, 8, 1033-1058.

Aerts, R.; Tu, X.; **De Bie, C.**; Whitehead, J. C.; Bogaerts, A. An Investigation into the Dominant Reactions for Ethylene Destruction in Non-Thermal Atmospheric Plasmas. Plasma Process. Polym. 2012, 9, 994-1000.

De Bie, C.; van Dijk, J.; Bogaerts, A. The Dominant Pathways for the Conversion of Methane into Oxygenates and Syngas in an Atmospheric Pressure Dielectric Barrier Discharge. J. Phys. Chem. C 2015, 119, 22331-22350.

De Bie, C.; van Dijk, J.; Bogaerts, A. CO_2 Hydrogenation in a Dielectric Barrier Discharge Plasma Revealed. J. Phys. Chem. C 2016, 120, 25210–25224.

Bogaerts, A.; **De Bie, C.**; Snoeckx, R.; Kozák, T. Plasma Based CO_2 and CH_4 Conversion: A Modeling Perspective. Plasma Process. Polym. 2017, DOI 10.1002/ppap.201600070.

List of Conference Contributions

De Bie, C.; Martens, T.; Bogaerts, A.; Brok, W. J. M.; van Dijk, J., Description of the Detailed Plasma Chemistry of a DBD in a Mixture of CH_4 and O_2 Using a 2D Fluid Model. **Poster Presentation** at the *19th Europhysics Conference on the Atomic and Molecular Physics of Ionized Gases*, Granada, Spain, 15-19 July 2008.

De Bie, C.; Martens, T.; Petrović, D.; Mihailova, D.; van Dijk, J.; Bogaerts, A., The Conversion of CH_4 into Higher Hydrocarbons in an Atmospheric Pressure Dielectric Barrier Discharge Described Using a Two Dimensional Fluid Model. **Talk** at the *6ème Édition des Journées Rencontres des Jeunes Chimistes*, Namur, Belgium, 19-20 March 2009.

De Bie, C.; Martens, T.; van Dijk, J.; van der Mullen, J. J. A. M.; Bogaerts, A., Description of the Plasma Chemistry in an Atmospheric Pressure CH_4 Dielectric Barrier Discharge Using a Two Dimensional Fluid Model. **Talk** at the *4th International Congress on Cold Atmospheric Pressure Plasmas*, Ghent, Belgium, 22-24 June 2009.

De Bie, C.; Martens, T.; Petrović, D.; Mihailova, D.; van Dijk, J.; Bogaerts, A., The Plasma Chemistry in an Atmospheric Pressure CH_4 Dielectric Barrier Discharge Described Using a Two Dimensional Fluid Model. **Talk** at the *19th International Symposium on Plasma Chemistry*, Bochum, Germany, 27-31 July 2009.

De Bie, C.; Martens, T.; Bogaerts, A., Description of the Plasma Chemistry in an Atmospheric Pressure CH_4/O_2 Dielectric Barrier Discharge Using a Fluid Model. **Poster Presentation** at the *11th European Conference on High-Technology Plasma Processes*, Brussels, Belgium, 27 June - 2 July 2010.

De Bie, C.; Martens, T.; van Dijk, J.; Bogaerts, A., Fluid Modeling of the Conversion of CH_4 in the Presence of O_2 or CO_2 into Methanol and Syngas in an Atmospheric Pressure Dielectric Barrier Discharge. **Poster Presentation** at the *20th Europhysics Conference on the Atomic and Molecular Physics of Ionized Gases*, Novi Sad, Serbia, 13-17 July 2010.

De Bie, C.; Corthals, S.; Verheyde, B.; Martens, T.; van Dijk, J.; Sels, B.; Paulussen, S.; Bogaerts, A., Determination of the Dominant Reaction Pathways Governing the Oxidation of Methane in an Atmospheric Pressure Dielectric Barrier Discharge. **Talk** at the *20th International Symposium on Plasma Chemistry*, Philadelphia, United States of America, 24-29 July 2011.

De Bie, C.; Martens, T.; van Dijk, J.; Corthals, S.; Verheyde, B.; Sels, B.; Paulussen, S.; Bogaerts, A., Modeling of the Plasma Chemistry in a DBD Reactor Used for Greenhouse Gas Conversion into Value-Added Chemicals. **Invited Talk** at the *4th Central European Symposium on Plasma Chemistry*, Zlatibor, Serbia, 22-25 August 2011.

De Bie, C.; Verheyde, B.; Corthals, S.; Martens, T.; van Dijk, J.; Paulussen, S.; Sels, B.; Bogaerts, A., Modelling Study on the Oxidation of Methane in an Atmospheric Pressure Dielectric Barrier Discharge. **Poster Presentation** at the *30th International Conference on Phenomena in Ionized Gases*, Belfast, United Kingdom, 28 August - 2 September 2011.

De Bie, C.; Bogaerts, A., Modelling for a Better Insight in the Plasma-Assisted Conversion of Greenhouse Gases. **Invited Talk** at the *Plasma-assisted catalysis: recent advances and perspectives*, Antwerp, Belgium, 28 November 2011.

Appendices - Overview of the Reactions in the Model

Note: This set is applicable for the CH_4/CO_2, CH_4/O_2 and CO_2/H_2 mixtures, as well as for pure CH_4, where of course only the reactions with CH_4 and CH_x species are included. The reactions included in the model for pure CH_4 are indicated with a gray shadow.

Table A.1. Electron impact reactions with the various molecules and radicals, included in the model. These reactions are treated by energy-dependent cross sections (or rate coefficients), and the references where these cross sections (or rate coefficients) were adopted from, are also included. For the vibrational and electronic excitations, several individual excitations are included, as indicated by the number between brackets.

CH_4											
Momentum Transfer	e^-	$+$	CH_4	$\rightarrow$	e^-	$+$	CH_4				[231]
Vibrational Excitation	e^-	$+$	CH_4	$\rightarrow$	e^-	$+$	CH_4^*			(2)	[231]
Ionization	e^-	$+$	CH_4	$\rightarrow$	$2e^-$	$+$	CH_4^+				[232]
Dissociative Ionization	e^-	$+$	CH_4	$\rightarrow$	$2e^-$	$+$	CH_3^+	$+$	H		[232]
	e^-	$+$	CH_4	$\rightarrow$	$2e^-$	$+$	CH_2^+	$+$	H_2		[232]
Dissociation	e^-	$+$	CH_4	$\rightarrow$	e^-	$+$	CH_3	$+$	H		[233-234]
	e^-	$+$	CH_4	$\rightarrow$	e^-	$+$	CH_2	$+$	H_2		[233-234]
	e^-	$+$	CH_4	$\rightarrow$	e^-	$+$	CH	$+$	H_2	$+$ H	[233-234]
	e^-	$+$	CH_4	$\rightarrow$	e^-	$+$	C	$+$	$2H_2$		[233-234]
CH_3											
Ionization	e^-	$+$	CH_3	$\rightarrow$	$2e^-$	$+$	CH_3^+				[232]

Dissociative Ionization	e^-	+	CH_3	→	$2e^-$	+	CH_2^+	+	H		232
	e^-	+	CH_3	→	$2e^-$	+	CH^+	+	H_2		232
Dissociation	e^-	+	CH_3	→	e^-	+	CH_2	+	H		233-234
	e^-	+	CH_3	→	e^-	+	CH	+	H_2		233-234

CH_2

Ionization	e^-	+	CH_2	→	$2e^-$	+	CH_2^+				232
Dissociative Ionization	e^-	+	CH_2	→	$2e^-$	+	CH^+	+	H		232
	e^-	+	CH_2	→	$2e^-$	+	C^+	+	H_2		232
Dissociation	e^-	+	CH_2	→	e^-	+	CH	+	H		233-234

CH

Ionization	e^-	+	CH	→	$2e^-$	+	CH^+				232
Dissociative Ionization	e^-	+	CH	→	$2e^-$	+	C^+	+	H		232
Dissociation	e^-	+	CH	→	e^-	+	C	+	H		233-234

C

Ionization	e^-	+	C	→	$2e^-$	+	C^+				233-234

C_2H_6

Momentum Transfer	e^-	+	C_2H_6	→	e^-	+	C_2H_6				231
Vibrational Excitation	e^-	+	C_2H_6	→	e^-	+	$C_2H_6^*$		(3)		231
Ionization	e^-	+	C_2H_6	→	$2e^-$	+	$C_2H_6^+$				232
Dissociative Ionization	e^-	+	C_2H_6	→	$2e^-$	+	$C_2H_5^+$	+	H		232
	e^-	+	C_2H_6	→	$2e^-$	+	$C_2H_4^+$	+	H_2		232
	e^-	+	C_2H_6	→	$2e^-$	+	$C_2H_3^+$	+	H_2	+ H	232
	e^-	+	C_2H_6	→	$2e^-$	+	$C_2H_2^+$	+	$2H_2$		232

	e^-	+	C_2H_6	$\rightarrow$	$2e^-$	+	CH_3^+	+	CH_3	[232]
Dissociation	e^-	+	C_2H_6	$\rightarrow$	e^-	+	C_2H_5	+	H	[235-236]
	e^-	+	C_2H_6	$\rightarrow$	e^-	+	C_2H_4	+	H_2	[235-236]

C_2H_5

Ionization	e^-	+	C_2H_5	$\rightarrow$	$2e^-$	+	$C_2H_5^+$					[232]
Dissociative Ionization	e^-	+	C_2H_5	$\rightarrow$	$2e^-$	+	$C_2H_4^+$	+	H			[232]
	e^-	+	C_2H_5	$\rightarrow$	$2e^-$	+	$C_2H_3^+$	+	H_2			[232]
	e^-	+	C_2H_5	$\rightarrow$	$2e^-$	+	$C_2H_2^+$	+	H_2	+	H	[232]
Dissociation	e^-	+	C_2H_5	$\rightarrow$	e^-	+	C_2H_4	+	H			[235-236]
	e^-	+	C_2H_5	$\rightarrow$	e^-	+	C_2H_3	+	H_2			[235-236]

C_2H_4

Momentum Transfer	e^-	+	C_2H_4	$\rightarrow$	e^-	+	C_2H_4				[231]
Vibrational Excitation	e^-	+	C_2H_4	$\rightarrow$	e^-	+	$C_2H_4^*$		(2)		[231]
Ionization	e^-	+	C_2H_4	$\rightarrow$	$2e^-$	+	$C_2H_4^+$				[232]
Dissociative Ionization	e^-	+	C_2H_4	$\rightarrow$	$2e^-$	+	$C_2H_3^+$	+	H		[232]
	e^-	+	C_2H_4	$\rightarrow$	$2e^-$	+	$C_2H_2^+$	+	H_2		[232]
Dissociation	e^-	+	C_2H_4	$\rightarrow$	e^-	+	C_2H_3	+	H		[235-236]
	e^-	+	C_2H_4	$\rightarrow$	e^-	+	C_2H_2	+	H_2		[235-236]

C_2H_3

Ionization	e^-	+	C_2H_3	$\rightarrow$	$2e^-$	+	$C_2H_3^+$				[232]
Dissociative Ionization	e^-	+	C_2H_3	$\rightarrow$	$2e^-$	+	$C_2H_2^+$	+	H		[232]
	e^-	+	C_2H_3	$\rightarrow$	$2e^-$	+	C_2H^+	+	H_2		[232]
Dissociation	e^-	+	C_2H_3	$\rightarrow$	e^-	+	C_2H_2	+	H		[235-236]

	e^-	+	C_2H_3	$\rightarrow$	e^-	+	C_2H	+	H_2		235-236

C_2H_2										
Momentum Transfer	e^-	+	C_2H_2	$\rightarrow$	e^-	+	C_2H_2			231
Vibrational Excitation	e^-	+	C_2H_2	$\rightarrow$	e^-	+	$C_2H_2^*$		(3)	231
Ionization	e^-	+	C_2H_2	$\rightarrow$	$2e^-$	+	$C_2H_2^+$			232
Dissociation	e^-	+	C_2H_2	$\rightarrow$	e^-	+	C_2H	+	H	235-236
	e^-	+	C_2H_2	$\rightarrow$	e^-	+	C_2	+	H_2	235-236

C_2H									
Ionization	e^-	+	C_2H	$\rightarrow$	$2e^-$	+	C_2H^+		232
Dissociation	e^-	+	C_2H	$\rightarrow$	e^-	+	C_2	+	H	235-236
	e^-	+	C_2H	$\rightarrow$	e^-	+	C	+	CH	235-236

C_2									
Ionization	e^-	+	C_2	$\rightarrow$	$2e^-$	+	C_2^+		235-236
Dissociation	e^-	+	C_2	$\rightarrow$	e^-	+	C	+	C	235-236

C_3H_8										
Momentum Transfer	e^-	+	C_3H_8	$\rightarrow$	e^-	+	C_3H_8			231
Vibrational Excitation	e^-	+	C_3H_8	$\rightarrow$	e^-	+	$C_3H_8^*$		(2)	231
Dissociative Ionization	e^-	+	C_3H_8	$\rightarrow$	$2e^-$	+	$C_2H_5^+$	+	CH_3	232
	e^-	+	C_3H_8	$\rightarrow$	$2e^-$	+	$C_2H_4^+$	+	CH_4	232
Dissociation	e^-	+	C_3H_8	$\rightarrow$	e^-	+	C_3H_7	+	H	235-236
	e^-	+	C_3H_8	$\rightarrow$	e^-	+	C_3H_6	+	H_2	235-236
	e^-	+	C_3H_8	$\rightarrow$	e^-	+	C_2H_4	+	CH_4	235-236

C$_3$H$_7$										
Dissociative Ionization	e$^-$	+	C$_3$H$_7$	→	2e$^-$	+	C$_2$H$_5^+$	+	CH$_2$	235-236
	e$^-$	+	C$_3$H$_7$	→	2e$^-$	+	C$_2$H$_4^+$	+	CH$_3$	235-236
	e$^-$	+	C$_3$H$_7$	→	2e$^-$	+	C$_2$H$_3^+$	+	CH$_4$	235-236
	e$^-$	+	C$_3$H$_7$	→	2e$^-$	+	CH$_3^+$	+	C$_2$H$_4$	235-236
Dissociation	e$^-$	+	C$_3$H$_7$	→	e$^-$	+	C$_3$H$_6$	+	H	235-236
	e$^-$	+	C$_3$H$_7$	→	e$^-$	+	C$_3$H$_5$	+	H$_2$	235-236
	e$^-$	+	C$_3$H$_7$	→	e$^-$	+	C$_2$H$_4$	+	CH$_3$	235-236
	e$^-$	+	C$_3$H$_7$	→	e$^-$	+	C$_2$H$_3$	+	CH$_4$	235-236

C$_3$H$_6$										
Dissociative Ionization	e$^-$	+	C$_3$H$_6$	→	2e$^-$	+	C$_2$H$_5^+$	+	CH	235-236
	e$^-$	+	C$_3$H$_6$	→	2e$^-$	+	C$_2$H$_4^+$	+	CH$_2$	235-236
	e$^-$	+	C$_3$H$_6$	→	2e$^-$	+	C$_2$H$_3^+$	+	CH$_3$	235-236
	e$^-$	+	C$_3$H$_6$	→	2e$^-$	+	C$_2$H$_2^+$	+	CH$_4$	235-236
	e$^-$	+	C$_3$H$_6$	→	2e$^-$	+	CH$_3^+$	+	C$_2$H$_3$	235-236
Dissociation	e$^-$	+	C$_3$H$_6$	→	e$^-$	+	C$_3$H$_5$	+	H	235-236
	e$^-$	+	C$_3$H$_6$	→	e$^-$	+	C$_2$H$_2$	+	CH$_4$	235-236

C$_3$H$_5$										
Dissociative Ionization	e$^-$	+	C$_3$H$_5$	→	2e$^-$	+	C$_2$H$_3^+$	+	CH$_2$	235-236
	e$^-$	+	C$_3$H$_5$	→	2e$^-$	+	C$_2$H$_2^+$	+	CH$_3$	235-236
	e$^-$	+	C$_3$H$_5$	→	2e$^-$	+	CH$_3^+$	+	C$_2$H$_2$	235-236
Dissociation	e$^-$	+	C$_3$H$_5$	→	e$^-$	+	C$_2$H$_2$	+	CH$_3$	235-236

H$_2$								
Momentum Transfer	e$^-$	+	H$_2$	→	e$^-$	+	H$_2$	237

Vibrational Excitation	e^-	+	H_2		$\rightarrow$	e^-	+	H_2^*	(3)	238
Ionization	e^-	+	H_2		$\rightarrow$	$2e^-$	+	H_2^+		239
Dissociation	e^-	+	H_2		$\rightarrow$	e^-	+	$2H$		240
H										
Ionization	e^-	+	H		$\rightarrow$	$2e^-$	+	H^+		239
O_2										
Momentum Transfer	e^-	+	O_2		$\rightarrow$	e^-	+	O_2		195
Vibrational Excitation	e^-	+	O_2		$\rightarrow$	e^-	+	O_2^*	(4)	195
Electronic Excitation	e^-	+	O_2		$\rightarrow$	e^-	+	O_2^*	(4)	194-195
Ionization	e^-	+	O_2		$\rightarrow$	$2e^-$	+	O_2^+		194
Dissociative Ionization	e^-	+	O_2		$\rightarrow$	$2e^-$	+	O^+ + O		195
Attachment	e^-	+	O_2	+ O_2	$\rightarrow$	O_2^-	+	O_2	Energy dependent rate coefficient	241
Dissociative Attachment	e^-	+	O_2		$\rightarrow$	O^-	+	O		195
Ion-pair formation	e^-	+	O_2		$\rightarrow$	e^-	+	O^+ + O^-	Energy dependent rate coefficient	242
Dissociation	e^-	+	O_2		$\rightarrow$	e^-	+	$2O$	(2)	195
O										
Momentum Transfer	e^-	+	O		$\rightarrow$	e^-	+	O		243
Electronic Excitation	e^-	+	O		$\rightarrow$	e^-	+	O^*	(2)	244

Ionization	e^-	+	O			$\rightarrow$	$2e^-$	+	O^+				[244]
Attachment	e^-	+	O	+	O_2	$\rightarrow$	O^-	+	O_2			1.00×10^{-31} $cm^6 s^{-1}$	[195]

O_3

Dissociative Ionization	e^-	+	O_3			$\rightarrow$	$2e^-$	+	O_2^+	+	O			[195]
Attachment	e^-	+	O_3	+	O_2	$\rightarrow$	O_3^-	+	O_2				Energy dependent rate coefficient	[241]
Dissociative Attachment	e^-	+	O_3			$\rightarrow$	O^-	+	O_2					[245]
	e^-	+	O_3			$\rightarrow$	O_2^-	+	O					[245]
Ion-pair formation	e^-	+	O_3			$\rightarrow$	e^-	+	O^-	+	O^+	+ O		[195]
Dissociation	e^-	+	O_3			$\rightarrow$	e^-	+	O_2	+	O		Energy dependent rate coefficient	[195]

CO_2

Momentum Transfer	e^-	+	CO_2	$\rightarrow$	e^-	+	CO_2				[196]
Vibrational Excitation	e^-	+	CO_2	$\rightarrow$	e^-	+	CO_2^*		(3)		[196]
Electronic Excitation	e^-	+	CO_2	$\rightarrow$	e^-	+	CO_2^*		(2)		[246-247]
Ionization	e^-	+	CO_2	$\rightarrow$	$2e^-$	+	CO_2^+				[196]
Dissociative Attachment	e^-	+	CO_2	$\rightarrow$	O^-	+	CO				[196]
Dissociation	e^-	+	CO_2	$\rightarrow$	e^-	+	CO	+	O		[196]

CO

Momentum Transfer	e^- + CO	→	e^-	+	CO				[238]
Vibrational Excitation	e^- + CO	→	e^-	+	CO^*			(1)	[238]
Electronic Excitation	e^- + CO	→	e^-	+	CO^*			(5)	[246-247]
Ionization	e^- + CO	→	$2e^-$	+	CO^+				[248]
Dissociative Attachment	e^- + CO	→	O^-	+	C				[249]
Dissociation	e^- + CO	→	e^-	+	C	+	O		[248]

H_2O

Momentum Transfer	e^- + H_2O	→	e^-	+	H_2O				[250]
Vibrational Excitation	e^- + H_2O	→	e^-	+	H_2O^*			(2)	[250]
Ionization	e^- + H_2O	→	$2e^-$	+	H_2O^+				[250]
Dissociative Attachment	e^- + H_2O	→	H^-	+	OH				[250]
	e^- + H_2O	→	O^-	+	H_2				[250]
	e^- + H_2O	→	OH^-	+	H				[250]
Dissociation	e^- + H_2O	→	e^-	+	OH	+	H		[250]
	e^- + H_2O	→	e^-	+	O	+	H_2		[250]

OH

Ionization	e^- + OH	→	$2e^-$	+	OH^+			Energy dependent rate coefficient	[251]
Dissociation	e^- + OH	→	e^-	+	O	+	H	Energy dependent rate coefficient	[251]

Table A.2. Electron-ion recombination reactions included in the model. These reactions are treated by energy-dependent rate coefficients, and the references where these rate coefficients were adopted from, are also included.

e^-	+	CH_5^+	$\rightarrow$	CH_3	+	$2H$				[233, 252]
e^-	+	CH_5^+	$\rightarrow$	CH_2	+	H_2	+	H		[233, 252]
e^-	+	CH_4^+	$\rightarrow$	CH_3	+	H				[233, 252]
e^-	+	CH_4^+	$\rightarrow$	CH_2	+	$2H$				[233, 252]
e^-	+	CH_4^+	$\rightarrow$	CH	+	H_2	+	H		[233, 252]
e^-	+	CH_3^+	$\rightarrow$	CH_2	+	H				[233, 252]
e^-	+	CH_3^+	$\rightarrow$	CH	+	H_2				[233, 252]
e^-	+	CH_3^+	$\rightarrow$	CH	+	$2H$				[233, 252]
e^-	+	CH_3^+	$\rightarrow$	C	+	H_2	+	H		[233, 252]
e^-	+	CH_2^+	$\rightarrow$	CH	+	H				[233, 252]
e^-	+	CH_2^+	$\rightarrow$	C	+	H_2				[233, 252]
e^-	+	CH_2^+	$\rightarrow$	C	+	$2H$				[233, 252]
e^-	+	CH^+	$\rightarrow$	C	+	H				[233, 252]
e^-	+	$C_2H_6^+$	$\rightarrow$	C_2H_5	+	H				[236]
e^-	+	$C_2H_6^+$	$\rightarrow$	C_2H_4	+	$2H$				[236]
e^-	+	$C_2H_5^+$	$\rightarrow$	C_2H_4	+	H				[236]
e^-	+	$C_2H_5^+$	$\rightarrow$	C_2H_3	+	$2H$				[236]
e^-	+	$C_2H_5^+$	$\rightarrow$	C_2H_2	+	H_2	+	H		[236]
e^-	+	$C_2H_5^+$	$\rightarrow$	C_2H_2	+	$3H$				[236]
e^-	+	$C_2H_5^+$	$\rightarrow$	CH_3	+	CH_2				[236]
e^-	+	$C_2H_4^+$	$\rightarrow$	C_2H_3	+	H				[236]
e^-	+	$C_2H_4^+$	$\rightarrow$	C_2H_2	+	$2H$				[236]

e⁻	+	$C_2H_4^+$			→	C_2H	+	H_2	+	H	236
e⁻	+	$C_2H_3^+$			→	C_2H_2	+	H			236
e⁻	+	$C_2H_3^+$			→	C_2H	+	2H			236
e⁻	+	$C_2H_2^+$			→	C_2H	+	H			236
e⁻	+	$C_2H_2^+$			→	C_2	+	2H			236
e⁻	+	$C_2H_2^+$			→	2CH					236
e⁻	+	C_2H^+			→	C_2	+	H			236
e⁻	+	C_2H^+			→	CH	+	C			236
e⁻	+	C_2H^+			→	2C	+	H			236
e⁻	+	C_2^+			→	2C					236
e⁻	+	H_3^+			→	3H					252
e⁻	+	H_3^+			→	H_2	+	H			252
e⁻	+	H_2^+			→	2H					252
e⁻	+	O^+	+	O_2	→	O	+	O_2			241
e⁻	+	O_2^+			→	O	+	O			241
e⁻	+	O_2^+	+	O_2	→	O_2	+	O_2			241
e⁻	+	O_4^+			→	O_2	+	O_2			241
e⁻	+	CO_2^+			→	CO	+	O			252
e⁻	+	CO^+			→	C	+	O			252
e⁻	+	OH^+			→	O	+	H			252
e⁻	+	H_2O^+			→	OH	+	H			252
e⁻	+	H_2O^+			→	O	+	H_2			252
e⁻	+	H_2O^+			→	O	+	2H			252
e⁻	+	H_3O^+			→	H_2O	+	H			252
e⁻	+	H_3O^+			→	OH	+	H_2			252
e⁻	+	H_3O^+			→	OH	+	2H			252

Table A.3. Neutral-neutral reactions included in the model, as well as the corresponding rate coefficients at 300 K and the references where these data were adopted from. Note a means "estimated value"; b = "adjusted in the model for a three-body collision by dividing by 2.446 x 10^{19} cm^{-3}, i.e., the density of the inlet gas". M = CH_4 in pure CH_4, M = CH_4, CO_2, O_2 or H_2O in the CH_4/O_2 and CH_4/CO_2 gas mixtures and M = CO_2 or H_2 in the CO_2/H_2 gas mixtures. The rate coefficients are expressed in cm^3 s^{-1} and cm^6 s^{-1} for two-body and three-body reactions, respectively. Note that the values in Table A.3. and Table A.4. are defined with two decimal digits, as found in literature, however, this precision is not decisive for the output of the model considering the likely uncertainty of these values.

CH_4	+	CH_2			→	CH_3	+	CH_3	3.01×10^{-19}	[253]
CH_4	+	CH			→	C_2H_4	+	H	9.74×10^{-11}	[254]
CH_4	+	C_2H_5			→	C_2H_6	+	CH_3	1.83×10^{-24}	[253]
CH_4	+	C_2H_3			→	C_2H_4	+	CH_3	2.28×10^{-18}	[253]
CH_4	+	C_2H			→	C_2H_2	+	CH_3	1.31×10^{-12}	[253]
CH_4	+	C_3H_7			→	C_3H_8	+	CH_3	4.38×10^{-24}	[255]
CH_4	+	C_3H_5			→	C_3H_6	+	CH_3	2.02×10^{-31}	[256]
CH_4	+	H			→	CH_3	+	H_2	8.43×10^{-19}	[254]
CH_3	+	CH_3			→	C_2H_5	+	H	2.71×10^{-19}	[257]
CH_3	+	CH_3	+	M	→	C_2H_6	+	M	1.56×10^{-26}	[254]
CH_3	+	CH_2			→	C_2H_4	+	H	7.01×10^{-11}	[254]
CH_3	+	C_2H_6			→	C_2H_5	+	CH_4	7.21×10^{-21}	[254]
CH_3	+	C_2H_5			→	C_2H_4	+	CH_4	1.91×10^{-12}	[254]
CH_3	+	C_2H_5	+	M	→	C_3H_8	+	M	1.00×10^{-28}	[a]
CH_3	+	C_2H_4			→	C_2H_3	+	CH_4	1.94×10^{-21}	[253]

CH_3	+	C_2H_3			→	C_2H_2	+	CH_4	6.51×10^{-13} [253]
CH_3	+	C_2H_3	+	M	→	C_3H_6	+	M	1.20×10^{-10} [258]
									4.91×10^{-30} [b]
CH_3	+	C_2H_2			→	CH_4	+	C_2H	7.65×10^{-26} [253]
CH_3	+	C_3H_8			→	C_3H_7	+	CH_4	1.02×10^{-20} [255]
CH_3	+	C_3H_7			→	C_3H_6	+	CH_4	3.07×10^{-12} [255]
CH_3	+	C_3H_6			→	C_3H_5	+	CH_4	1.24×10^{-19} [256]
CH_3	+	H_2			→	CH_4	+	H	9.60×10^{-21} [254]
CH_3	+	H			→	CH_2	+	H_2	9.96×10^{-22} [254]
CH_3	+	H	+	M	→	CH_4	+	M	2.97×10^{-28} [254]
CH_2	+	CH_2			→	C_2H_2	+	2H	5.27×10^{-11} [254]
CH_2	+	C_2H_5			→	C_2H_4	+	CH_3	3.01×10^{-11} [253]
CH_2	+	C_2H_3			→	C_2H_2	+	CH_3	3.01×10^{-11} [253]
CH_2	+	C_2H			→	C_2H_2	+	CH	3.01×10^{-11} [253]
CH_2	+	C_3H_8			→	C_3H_7	+	CH_3	1.02×10^{-20} [255]
CH_2	+	C_3H_7			→	C_2H_4	+	C_2H_5	3.01×10^{-11} [255]
CH_2	+	C_3H_7			→	C_3H_6	+	CH_3	3.01×10^{-12} [255]
CH_2	+	C_3H_6			→	C_3H_5	+	CH_3	3.65×10^{-17} [256]
CH_2	+	H_2			→	CH_3	+	H	5.00×10^{-15} [253]
CH_2	+	H			→	CH	+	H_2	2.01×10^{-10} [254]
CH	+	C_2H_6	+	M	→	C_3H_7	+	M	2.78×10^{-10} [254]
									1.14×10^{-29} [b]
CH	+	H_2			→	CH_2	+	H	6.80×10^{-13} [254]
CH	+	H			→	C	+	H_2	1.00×10^{-10} [259]
C	+	H_2			→	CH	+	H	1.50×10^{-10} [260]
C_2H_6	+	C_2H_3			→	C_2H_5	+	C_2H_4	3.39×10^{-21} [253]

C_2H_6	+	C_2H			→	C_2H_2	+	C_2H_5	5.99×10^{-12} [253]
C_2H_6	+	C_3H_7			→	C_3H_8	+	C_2H_5	3.16×10^{-22} [255]
C_2H_6	+	C_3H_5			→	C_3H_6	+	C_2H_5	2.02×10^{-28} [256]
C_2H_6	+	H			→	C_2H_5	+	H_2	4.96×10^{-17} [254]
C_2H_5	+	C_2H_5			→	C_2H_6	+	C_2H_4	2.41×10^{-12} [254]
C_2H_5	+	C_2H_4			→	C_2H_6	+	C_2H_3	4.56×10^{-27} [253]
C_2H_5	+	C_2H_2			→	C_2H_6	+	C_2H	3.72×10^{-30} [253]
C_2H_5	+	C_2H			→	C_2H_4	+	C_2H_2	3.01×10^{-12} [253]
C_2H_5	+	C_3H_8			→	C_2H_6	+	C_3H_7	3.62×10^{-22} [255]
C_2H_5	+	C_3H_7			→	C_3H_8	+	C_2H_4	1.91×10^{-12} [255]
C_2H_5	+	C_3H_7			→	C_3H_6	+	C_2H_6	2.41×10^{-12} [255]
C_2H_5	+	C_3H_6			→	C_3H_5	+	C_2H_6	2.53×10^{-20} [256]
C_2H_5	+	C_3H_5			→	C_3H_6	+	C_2H_4	5.36×10^{-12} [256]
C_2H_5	+	H_2			→	C_2H_6	+	H	2.97×10^{-21} [253]
C_2H_5	+	H			→	CH_3	+	CH_3	5.99×10^{-11} [254]
C_2H_5	+	H			→	C_2H_4	+	H_2	3.01×10^{-12} [253]
C_2H_5	+	H	+	M	→	C_2H_6	+	M	2.25×10^{-10} [261] 9.20×10^{-30} b
C_2H_4	+	C_2H			→	C_2H_2	+	C_2H_3	1.40×10^{-10} [258]
C_2H_4	+	H			→	C_2H_3	+	H_2	4.92×10^{-21} [253]
C_2H_4	+	H	+	M	→	C_2H_5	+	M	3.66×10^{-30} [254]
C_2H_3	+	C_2H_3			→	C_2H_4	+	C_2H_2	1.60×10^{-12} [253]
C_2H_3	+	C_2H			→	C_2H_2	+	C_2H_2	1.60×10^{-12} [253]
C_2H_3	+	C_3H_8			→	C_2H_4	+	C_3H_7	3.40×10^{-21} [255]
C_2H_3	+	C_3H_7			→	C_3H_8	+	C_2H_2	2.01×10^{-12} [255]
C_2H_3	+	C_3H_7			→	C_3H_6	+	C_2H_4	2.01×10^{-12} [255]

C_2H_3	+	C_3H_6			→	C_3H_5	+	C_2H_4	6.58×10^{-19} [256]
C_2H_3	+	C_3H_5			→	C_3H_6	+	C_2H_2	8.00×10^{-12} [256]
C_2H_3	+	H_2			→	C_2H_4	+	H	9.78×10^{-20} [253]
C_2H_3	+	H			→	C_2H_2	+	H_2	2.01×10^{-11} [254]
C_2H_3	+	H	+	M	→	C_2H_4	+	M	2.02×10^{-10} [261]
									8.26×10^{-30} b
C_2H_2	+	C_2H			→	C_4H_2	+	H	1.50×10^{-10} [114]
C_2H_2	+	H			→	C_2H	+	H_2	6.12×10^{-27} [253]
C_2H_2	+	H	+	M	→	C_2H_3	+	M	2.81×10^{-31} [254]
C_2H	+	C_2H			→	C_2H_2	+	C_2	3.01×10^{-12} [253]
C_2H	+	C_3H_8			→	C_2H_2	+	C_3H_7	5.99×10^{-12} [255]
C_2H	+	C_3H_7			→	C_3H_6	+	C_2H_2	1.00×10^{-11} [255]
C_2H	+	C_3H_6			→	C_3H_5	+	C_2H_2	5.99×10^{-12} [256]
C_2H	+	H_2			→	C_2H_2	+	H	1.52×10^{-13} [253]
C_2H	+	H			→	C_2	+	H_2	1.66×10^{-31} [253]
C_2H	+	H	+	M	→	C_2H_2	+	M	2.31×10^{-10} [261]
									9.44×10^{-30} b
C_3H_8	+	C_3H_5			→	C_3H_6	+	C_3H_7	2.02×10^{-28} [256]
C_3H_8	+	H			→	C_3H_7	+	H_2	5.15×10^{-17} [255]
C_3H_7	+	C_3H_7			→	C_3H_6	+	C_3H_8	2.81×10^{-12} [255]
C_3H_7	+	C_3H_6			→	C_3H_5	+	C_3H_8	2.53×10^{-20} [256]
C_3H_7	+	C_3H_5			→	C_3H_6	+	C_3H_6	3.00×10^{-12} [256]
C_3H_7	+	H_2			→	C_3H_8	+	H	7.12×10^{-21} [255]
C_3H_7	+	H			→	C_3H_6	+	H_2	3.01×10^{-12} [255]
C_3H_7	+	H	+	M	→	C_3H_8	+	M	9.68×10^{-11} [261]
									3.96×10^{-30} b

C_3H_6	+	H			→	C_3H_5	+	H_2			6.94×10^{-15}	[256]
C_3H_6	+	H	+	M	→	C_3H_7	+	M			9.26×10^{-14}	[256]
											3.79×10^{-33}	[b]
C_3H_5	+	H_2			→	C_3H_6	+	H			2.05×10^{-27}	[256]
C_3H_5	+	H	+	M	→	C_3H_6	+	M			3.26×10^{-10}	[262]
											1.33×10^{-29}	[b]
H	+	H	+	M	→	H_2	+	M			6.00×10^{-33}	[254]
O_3	+	O			→	O_2	+	O_2			8.43×10^{-15}	[263]
O_3	+	O_2			→	O	+	O_2	+	O_2	2.29×10^{-26}	[263]
O	+	O_2	+	M	→	O_3	+	M			6.90×10^{-34}	[263]
O_3	+	O_3			→	O	+	O_2	+	O_3	5.18×10^{-26}	[263]
O	+	O	+	O	→	O_2	+	O			5.09×10^{-33}	[263]
O	+	O	+	M	→	O_2	+	M			7.19×10^{-33}	[263]
O	+	O_2	+	O	→	O_3	+	O			6.32×10^{-34}	[263]
O	+	O_2	+	O_3	→	O_3	+	O_3			1.52×10^{-33}	[263]
O_3	+	O			→	O	+	O_2	+	O	3.14×10^{-27}	[263]
CH4	+	O			→	CH_3	+	OH			5.54×10^{-18}	[254]
CH3	+	O			→	CH_2O	+	H			1.12×10^{-10}	[264]
CH3	+	O			→	CO	+	H_2	+	H	2.80×10^{-11}	[264]
CH_3	+	O_2	+	M	→	CH_3O_2	+	M			9.79×10^{-31}	[265]
CH_3	+	O_3			→	CH_3O	+	O_2			2.33×10^{-12}	[265]
CH_2	+	O			→	CO	+	H_2			5.53×10^{-11}	[264]
CH_2	+	O			→	CO	+	2H			8.29×10^{-11}	[264]
CH_2	+	O_2			→	CO_2	+	H_2			1.42×10^{-12}	[254, 266]
CH_2	+	O_2			→	CO	+	H_2O			1.42×10^{-12}	[254, 266]

CH_2	+	O_2			→	CH_2O	+	O		5.39×10^{-13}	[254, 266]
CH	+	O			→	CO	+	H		6.60×10^{-11}	[254]
CH	+	O_2			→	CO_2	+	H		1.20×10^{-11}	[264]
CH	+	O_2			→	CO	+	OH		8.00×10^{-12}	[264]
CH	+	O_2			→	CHO	+	O		8.00×10^{-12}	[264]
CH	+	O_2			→	CO	+	H	+ O	1.20×10^{-11}	[264]
C	+	O_2			→	CO	+	O		2.45×10^{-13}	[267]
C_2H_6	+	O			→	C_2H_5	+	OH		5.11×10^{-16}	[254]
C_2H_5	+	O			→	CH_3CHO	+	H		8.80×10^{-11}	[264]
C_2H_5	+	O			→	CH_2O	+	CH_3		6.60×10^{-11}	[264]
C_2H_5	+	O			→	C_2H_4	+	OH		4.40×10^{-11}	[264]
C_2H_5	+	O_2			→	C_2H_4	+	HO_2		3.80×10^{-15}	[265]
C_2H_5	+	O_2	+	M	→	$C_2H_5O_2$	+	M		5.75×10^{-29}	[265]
C_2H_4	+	O			→	CH_2CHO	+	H		2.63×10^{-13}	[264]
C_2H_4	+	O			→	CHO	+	CH_3		4.51×10^{-13}	[264]
C_2H_4	+	O_3			→	CH_2O	+	CO_2	+ H_2	7.06×10^{-19}	[265-266]
C_2H_4	+	O_3			→	CH_2O	+	CO	+ H_2O	7.06×10^{-19}	[265-266]
C_2H_4	+	O_3			→	$2CH_2O$	+	O		2.69×10^{-19}	[265-266]
C_2H_3	+	O			→	C_2H_2	+	OH		1.25×10^{-11}	[264]
C_2H_3	+	O			→	CO	+	CH_3		1.25×10^{-11}	[264]
C_2H_3	+	O			→	CHO	+	CH_2		1.25×10^{-11}	[264]
C_2H_3	+	O			→	CH_2CO	+	H		1.25×10^{-11}	[264]
C_2H_3	+	O_2			→	CH_2O	+	CHO		9.00×10^{-12}	[254]
C_2H_2	+	O			→	CH_2	+	CO		6.75×10^{-14}	[254]

									Rate	Ref
C_2H_2	+	O			→	C_2HO	+	H	6.75×10^{-14}	[254]
C_2H	+	O			→	CH	+	CO	1.70×10^{-11}	[254]
C_2H	+	O_2			→	CHO	+	CO	3.00×10^{-11}	[254]
C_2H	+	O_2			→	C_2HO	+	O	1.00×10^{-12}	[253]
C_3H_8	+	O			→	C_3H_7	+	OH	2.73×10^{-15}	[255]
H_2	+	O			→	OH	+	H	9.32×10^{-18}	[254]
H	+	O	+	M	→	OH	+	M	4.33×10^{-32}	[253]
H	+	O_2			→	OH	+	O	1.87×10^{-22}	[254]
H	+	O_2	+	M	→	HO_2	+	M	5.40×10^{-32}	[268]
H	+	O_3			→	OH	+	O_2	2.83×10^{-11}	[269]
CH_4	+	OH			→	CH_3	+	H_2O	6.62×10^{-15}	[265]
CH_4	+	HO_2			→	CH_3	+	H_2O_2	8.76×10^{-27}	[253]
CH_4	+	CHO			→	CH_3	+	CH_2O	6.07×10^{-30}	[253]
CH_4	+	CH_3O			→	CH_3OH	+	CH_3	9.42×10^{-20}	[253]
CH_4	+	CH_3O_2			→	CH_3	+	CH_3OOH	1.03×10^{-26}	[253]
CH_3	+	CO	+	M	→	CH_3CO	+	M	4.19×10^{-36}	[114]
CH_3	+	H_2O			→	CH_4	+	OH	1.82×10^{-25}	[253]
CH_3	+	OH			→	CH_2	+	H_2O	1.13×10^{-12}	[114]
CH_3	+	OH			→	CH_2OH	+	H	1.31×10^{-11}	[270]
CH_3	+	OH			→	CH_3O	+	H	1.60×10^{-10}	[270]
CH_3	+	OH	+	M	→	CH_3OH	+	M	2.30×10^{-27}	[114]
CH_3	+	HO_2			→	CH_3O	+	OH	3.00×10^{-11}	[254]
CH_3	+	HO_2			→	CH_4	+	O_2	5.99×10^{-12}	[253]
CH_3	+	CH_2O			→	CH_4	+	CHO	6.14×10^{-18}	[114]
CH_3	+	CHO			→	CH_4	+	CO	2.00×10^{-10}	[253]
CH_3	+	CH_3O			→	CH_4	+	CH_2O	4.00×10^{-11}	[253]

CH_3	+	CH_3CHO			→	CH_4	+	CH_3CO	4.95×10^{-18} [254]
CH_3	+	CH_3O_2			→	CH_3O	+	CH_3O	4.00×10^{-11} [253]
CH_2	+	CO_2			→	CH_2O	+	CO	3.90×10^{-14} [253]
CH_2	+	H_2O			→	CH_3	+	OH	1.60×10^{-16} [253]
CH_2	+	OH			→	CH_2O	+	H	3.00×10^{-11} [253]
CH_2	+	HO_2			→	CH_2O	+	OH	3.00×10^{-11} [253]
CH_2	+	CH_2O			→	CH_3	+	CHO	1.00×10^{-14} [253]
CH_2	+	CHO			→	CH_3	+	CO	3.00×10^{-11} [253]
CH_2	+	CH_3O			→	CH_3	+	CH_2O	3.00×10^{-11} [253]
CH_2	+	CH_3O_2			→	CH_2O	+	CH_3O	3.00×10^{-11} [253]
CH	+	CO_2			→	CHO	+	CO	9.68×10^{-13} [264]
CH	+	CO_2			→	$2CO$	+	H	9.68×10^{-13} [264]
CH	+	CO	+	M	→	C_2HO	+	M	4.04×10^{-30} [264]
C_2H_6	+	OH			→	C_2H_5	+	H_2O	2.46×10^{-13} [265]
C_2H_6	+	HO_2			→	C_2H_5	+	H_2O_2	6.36×10^{-24} [253]
C_2H_6	+	CHO			→	C_2H_5	+	CH_2O	2.19×10^{-26} [253]
C_2H_6	+	CH_3O			→	C_2H_5	+	CH_3OH	2.72×10^{-18} [253]
C_2H_6	+	CH_3O_2			→	C_2H_5	+	CH_3OOH	6.36×10^{-24} [253]
C_2H_6	+	$C_2H_5O_2$			→	C_2H_5	+	C_2H_5OOH	8.69×10^{-27} [271]
C_2H_5	+	H_2O			→	C_2H_6	+	OH	3.56×10^{-29} [253]
C_2H_5	+	OH			→	C_2H_4	+	H_2O	4.00×10^{-11} [253]
C_2H_5	+	HO_2			→	C_2H_6	+	O_2	5.00×10^{-13} [253]
C_2H_5	+	HO_2			→	C_2H_4	+	H_2O_2	5.00×10^{-13} [253]
C_2H_5	+	CH_2O			→	C_2H_6	+	CHO	4.47×10^{-18} [253]
C_2H_5	+	CHO			→	C_2H_6	+	CO	2.00×10^{-10} [253]
C_2H_5	+	CH_3O			→	C_2H_6	+	CH_2O	4.00×10^{-11} [253]

C_2H_5	+	CH_3O_2	$\rightarrow$	CH_3O	+	C_2H_5O			4.00×10^{-11}	[253]
C_2H_4	+	OH	$\rightarrow$	C_2H_3	+	H_2O			1.54×10^{-16}	[253]
C_2H_4	+	HO_2	$\rightarrow$	CH_3CHO	+	OH			1.62×10^{-20}	[253]
C_2H_3	+	H_2O	$\rightarrow$	C_2H_4	+	OH			1.82×10^{-25}	[253]
C_2H_3	+	OH	$\rightarrow$	C_2H_2	+	H_2O			5.00×10^{-11}	[253]
C_2H_3	+	CH_2O	$\rightarrow$	C_2H_4	+	CHO			4.41×10^{-18}	[253]
C_2H_3	+	CHO	$\rightarrow$	C_2H_4	+	CO			1.50×10^{-10}	[253]
C_2H_3	+	CH_3O	$\rightarrow$	C_2H_4	+	CH_2O			4.00×10^{-11}	[253]
C_2H_2	+	OH	$\rightarrow$	C_2H	+	H_2O			1.77×10^{-22}	[253]
C_2H_2	+	HO_2	$\rightarrow$	CH_2CO	+	OH			1.62×10^{-20}	[253]
C_2H	+	OH	$\rightarrow$	CH_2	+	CO			3.00×10^{-11}	[253]
C_2H	+	OH	$\rightarrow$	C_2H_2	+	O			3.00×10^{-11}	[253]
C_2H	+	HO_2	$\rightarrow$	C_2H_2	+	O_2			3.00×10^{-11}	[253]
C_2H	+	HO_2	$\rightarrow$	C_2HO	+	OH			3.00×10^{-11}	[253]
C_2H	+	CHO	$\rightarrow$	C_2H_2	+	CO			1.00×10^{-10}	[253]
C_2H	+	CH_3O	$\rightarrow$	C_2H_2	+	CH_2O			4.00×10^{-11}	[253]
C_2H	+	CH_3O_2	$\rightarrow$	CH_3O	+	C_2HO			4.00×10^{-11}	[253]
C_3H_8	+	OH	$\rightarrow$	C_3H_7	+	H_2O			3.76×10^{-15}	[255]
C_3H_8	+	HO_2	$\rightarrow$	C_3H_7	+	H_2O_2			1.58×10^{-25}	[255]
C_3H_8	+	CHO	$\rightarrow$	C_3H_7	+	CH_2O			1.95×10^{-26}	[255]
C_3H_8	+	CH_3O	$\rightarrow$	C_3H_7	+	CH_3OH			1.42×10^{-17}	[255]
C_3H_8	+	CH_3O_2	$\rightarrow$	C_3H_7	+	CH_3OOH			7.69×10^{-26}	[255]
C_3H_7	+	CH_2O	$\rightarrow$	C_3H_8	+	CHO			4.10×10^{-18}	[255]
C_3H_7	+	CHO	$\rightarrow$	C_3H_8	+	CO			1.00×10^{-10}	[255]
C_3H_7	+	CH_3O	$\rightarrow$	C_3H_8	+	CH_2O			4.00×10^{-11}	[255]
C_3H_7	+	CH_3O_2	$\rightarrow$	C_2H_5	+	CH_2O	+	CH_3O	5.99×10^{-11}	[255]

										Rate	Ref
H_2	+	OH				→	H	+	H_2O	7.02×10^{-15}	[268]
H_2	+	HO_2				→	H	+	H_2O_2	5.43×10^{-30}	[253]
H_2	+	CHO				→	H	+	CH_2O	2.78×10^{-26}	[253]
H_2	+	CH_3O_2				→	H	+	CH_3OOH	5.43×10^{-30}	[253]
H	+	CO_2				→	CO	+	OH	1.40×10^{-29}	[253]
H	+	CO	+	M		→	CHO	+	M	1.54×10^{-34}	[114]
H	+	H_2O				→	H_2	+	OH	5.86×10^{-26}	[254]
H	+	OH				→	H_2	+	O	1.05×10^{-16}	[253]
H	+	OH	+	M		→	H_2O	+	M	4.33×10^{-30}	[254]
H	+	HO_2				→	H_2	+	O_2	5.60×10^{-12}	[268]
H	+	HO_2				→	H_2O	+	O	2.40×10^{-12}	[268]
H	+	HO_2				→	OH	+	OH	7.20×10^{-11}	[268]
H	+	CH_2O				→	H_2	+	CHO	5.72×10^{-14}	[114]
H	+	CHO				→	H_2	+	CO	1.50×10^{-10}	[254]
H	+	CH_3O				→	H_2	+	CH_2O	2.32×10^{-11}	[264]
H	+	CH_3O				→	CH_3	+	OH	9.93×10^{-12}	[264]
H	+	CH_3CHO				→	H_2	+	CH_3CO	8.98×10^{-14}	[254]
H	+	CH_2CO				→	CH_3	+	CO	1.04×10^{-13}	[254]
H	+	C_2HO				→	CH_2	+	CO	2.50×10^{-10}	[254]
H	+	CH_3O_2				→	OH	+	CH_3O	1.60×10^{-10}	[253]
O	+	CO	+	M		→	CO_2	+	M	1.11×10^{-35}	[253]
O	+	H_2O				→	OH	+	OH	4.48×10^{-24}	[253]
O	+	OH				→	H	+	O_2	3.46×10^{-11}	[268]
O	+	HO_2				→	O_2	+	OH	5.70×10^{-11}	[268]
O	+	CH_2O				→	OH	+	CHO	1.73×10^{-13}	[254]
O	+	CHO				→	CO	+	OH	5.00×10^{-11}	[254]

O	+	CHO	→	H	+	CO_2			5.00×10^{-11}	254
O	+	CH_3O	→	CH3	+	O_2			2.20×10^{-11}	254
O	+	CH_3O	→	OH	+	CH_2O			3.00×10^{-12}	254
O	+	CH_3CHO	→	OH	+	CH_3CO			4.68×10^{-13}	254
O	+	CH_2CO	→	CH_2	+	CO_2			2.29×10^{-13}	254, 272
O	+	CH_2CO	→	CH_2O	+	CO			7.88×10^{-14}	254, 272
O	+	CH_2CO	→	CHO	+	CO	+	H	4.33×10^{-14}	254, 272
O	+	CH_2CO	→	CHO	+	CHO			4.33×10^{-14}	254, 272
O	+	C_2HO	→	CO	+	CO	+	H	1.60×10^{-10}	254
O	+	CH_3O_2	→	CH_3O	+	O_2			5.99×10^{-11}	253
O	+	CH_3OOH	→	CH_3O_2	+	OH			5.63×10^{-15}	264
O_2	+	CHO	→	CO	+	HO_2			5.10×10^{-12}	265
O_2	+	CH_3O	→	CH_2O	+	HO_2			1.97×10^{-15}	265
O_2	+	CH_2CHO	→	CH_2O	+	CO	+	OH	3.00×10^{-14}	254, 273-274
O_2	+	C_2HO	→	CO	+	CO	+	OH	6.46×10^{-13}	254
O_3	+	OH	→	O_2	+	HO_2			7.41×10^{-14}	268
O_3	+	HO_2	→	O_2	+	O_2	+	OH	2.05×10^{-15}	268
O_3	+	CH_3O_2	→	CH_3O	+	O_2	+	O_2	1.00×10^{-17}	275
CO	+	OH	→	CO_2	+	H			1.25×10^{-13}	254
CO	+	HO_2	→	CO_2	+	OH			1.49×10^{-27}	254
CO	+	CH_3O	→	CO_2	+	CH_3			6.56×10^{-20}	253
H_2O	+	CHO	→	CH_2O	+	OH			9.35×10^{-32}	253
H_2O	+	CH_3O	→	CH_3OH	+	OH			1.67×10^{-14}	276

OH	+	OH			→	H_2O	+	O		1.47×10^{-12} [268]
OH	+	OH	+	M	→	H_2O_2	+	M		6.86×10^{-31} [268]
OH	+	HO_2			→	O_2	+	H_2O		1.10×10^{-10} [268]
OH	+	CH_2O			→	H_2O	+	CHO		8.47×10^{-12} [265]
OH	+	CHO			→	CO	+	H_2O		1.70×10^{-10} [254]
OH	+	CH_3O			→	CH_2O	+	H_2O		3.00×10^{-11} [253]
OH	+	CH_3CHO			→	CH_3CO	+	H_2O		1.49×10^{-11} [265]
OH	+	CH_2CO			→	CO	+	CH_2OH		1.14×10^{-11} [254, 277]
OH	+	CH_3O_2			→	CH_3OH	+	O_2		1.00×10^{-10} [253]
HO_2	+	HO_2			→	H_2O_2	+	O_2		1.63×10^{-12} [268]
HO_2	+	CH_2O			→	CHO	+	H_2O_2		1.05×10^{-20} [253]
HO_2	+	CHO			→	OH	+	H	+ CO_2	5.00×10^{-11} [253]
HO_2	+	CH_3O			→	CH_2O	+	H_2O_2		5.00×10^{-13} [253]
HO_2	+	CH_3O_2			→	CH_3OOH	+	O_2		5.12×10^{-12} [265]
HO_2	+	$C_2H_5O_2$			→	C_2H_5OOH	+	O_2		7.63×10^{-12} [265]
CH_2O	+	CH_3O			→	CH_3OH	+	CHO		1.14×10^{-15} [253]
CH_2O	+	CH_3O_2			→	CHO	+	CH_3OOH		1.05×10^{-20} [253]
CHO	+	CHO			→	CH_2O	+	CO		5.00×10^{-11} [254]
CHO	+	CH_3O			→	CH_3OH	+	CO		1.50×10^{-10} [253]
CHO	+	CH_3O_2			→	CH_3O	+	H	+ CO_2	5.00×10^{-11} [253]
CH_3O	+	CH_3O			→	CH_2O	+	CH_3OH		1.00×10^{-10} [253]
CH_3O	+	CH_3O_2			→	CH_2O	+	CH_3OOH		5.00×10^{-13} [253]
CH_3O_2	+	CH_3O_2			→	CH_3OH	+	CH_2O	+ O_2	2.19×10^{-13} [265]
CH_3O_2	+	CH_3O_2			→	CH_3O	+	CH_3O	+ O_2	1.29×10^{-13} [265]
$C_2H_5O_2$	+	$C_2H_5O_2$			→	C_2H_5OH	+	CH_3CHO	+ O_2	2.43×10^{-14} [265]
$C_2H_5O_2$	+	$C_2H_5O_2$			→	C_2H_5O	+	C_2H_5O	+ O_2	3.97×10^{-14} [265]

CH_4	+	CH_3CO	→	CH_3CHO	+	CH_3	1.14×10^{-29} [253]
CH_4	+	CH_2OH	→	CH_3OH	+	CH_3	2.55×10^{-27} [278]
CH_3	+	H_2O_2	→	CH_4	+	HO_2	5.46×10^{-14} [253]
CH_3	+	CH_3OH	→	CH_4	+	CH_3O	1.01×10^{-20} [278]
CH_3	+	CH_3OH	→	CH_4	+	CH_2OH	2.66×10^{-20} [278]
CH_3	+	CH_2OH	→	CH_4	+	CH_2O	4.00×10^{-12} [278]
CH_3	+	C_2H_5OH	→	CH_4	+	C_2H_5O	3.11×10^{-19} [279]
CH_2	+	H_2O_2	→	CH_3	+	HO_2	1.00×10^{-14} [253]
CH_2	+	CH_3CO	→	CH_2CO	+	CH_3	3.00×10^{-11} [253]
CH_2	+	CH_3OH	→	CH_3O	+	CH_3	1.01×10^{-20} [278]
CH_2	+	CH_3OH	→	CH_2OH	+	CH_3	2.66×10^{-20} [278]
CH_2	+	CH_2OH	→	CH_2O	+	CH_3	2.00×10^{-12} [278]
CH_2	+	CH_2OH	→	C_2H_4	+	OH	4.00×10^{-11} [278]
C_2H_6	+	CH_3CO	→	CH_3CHO	+	C_2H_5	3.32×10^{-26} [253]
C_2H_6	+	CH_2OH	→	CH_3OH	+	C_2H_5	5.93×10^{-25} [278]
C_2H_5	+	H_2O_2	→	C_2H_6	+	HO_2	2.83×10^{-15} [253]
C_2H_5	+	CH_3OH	→	C_2H_6	+	CH_3O	3.50×10^{-22} [278]
C_2H_5	+	CH_3OH	→	C_2H_6	+	CH_2OH	9.49×10^{-22} [278]
C_2H_5	+	CH_2OH	→	C_2H_6	+	CH_2O	4.00×10^{-12} [278]
C_2H_5	+	CH_2OH	→	CH_3OH	+	C_2H_4	4.00×10^{-12} [278]
C_2H_3	+	H_2O_2	→	C_2H_4	+	HO_2	5.46×10^{-14} [253]
C_2H_3	+	CH_3OH	→	C_2H_4	+	CH_3O	1.01×10^{-20} [278]
C_2H_3	+	CH_3OH	→	C_2H_4	+	CH_2OH	2.66×10^{-20} [278]
C_2H_3	+	CH_2OH	→	C_2H_4	+	CH_2O	5.00×10^{-11} [278]
C_2H_3	+	CH_2OH	→	C_3H_5	+	OH	2.00×10^{-11} [278]
C_2H_2	+	CH_2OH	→	C_2H_3	+	CH_2O	3.32×10^{-19} [278]

C_2H	+	CH_3OH	→	C_2H_2	+	CH_3O	2.00×10^{-12} [278]
C_2H	+	CH_3OH	→	C_2H_2	+	CH_2OH	1.00×10^{-11} [278]
C_2H	+	CH_2OH	→	C_2H_2	+	CH_2O	5.99×10^{-11} [278]
C_3H_8	+	CH_3CO	→	CH_3CHO	+	C_3H_7	2.60×10^{-26} [255]
C_3H_8	+	CH_2OH	→	CH_3OH	+	C_3H_7	4.45×10^{-25} [255]
C_3H_7	+	OH	→	C_3H_6	+	H_2O	4.00×10^{-11} [255]
C_3H_7	+	H_2O_2	→	C_3H_8	+	HO_2	7.08×10^{-17} [255]
C_3H_7	+	CH_3OH	→	C_3H_8	+	CH_3O	3.51×10^{-22} [255]
C_3H_7	+	CH_3OH	→	C_3H_8	+	CH_2OH	8.45×10^{-22} [255]
C_3H_7	+	CH_2OH	→	C_3H_8	+	CH_2O	1.60×10^{-12} [255]
C_3H_7	+	CH_2OH	→	C_3H_6	+	CH_3OH	8.00×10^{-13} [255]
C_3H_6	+	O	→	C_3H_5	+	OH	8.15×10^{-16} [256]
C_3H_6	+	OH	→	C_3H_5	+	H_2O	7.69×10^{-13} [256]
C_3H_6	+	HO_2	→	C_3H_5	+	H_2O_2	3.24×10^{-24} [256]
C_3H_6	+	CHO	→	C_3H_5	+	CH_2O	3.72×10^{-25} [256]
C_3H_6	+	CH_3O	→	C_3H_5	+	CH_3OH	5.65×10^{-24} [256]
C_3H_6	+	CH_3O_2	→	C_3H_5	+	CH_3OOH	1.25×10^{-24} [256]
C_3H_6	+	CH_3CO	→	C_3H_5	+	CH_3CHO	1.18×10^{-24} [256]
C_3H_6	+	CH_2OH	→	C_3H_5	+	CH_3OH	3.79×10^{-24} [256]
C_3H_5	+	HO_2	→	C_3H_6	+	O_2	4.40×10^{-12} [264]
C_3H_5	+	H_2O_2	→	C_3H_6	+	HO_2	1.00×10^{-23} [256]
C_3H_5	+	CH_2O	→	C_3H_6	+	CHO	6.06×10^{-25} [256]
C_3H_5	+	CHO	→	C_3H_6	+	CO	1.00×10^{-10} [256]
C_3H_5	+	CH_3O	→	C_3H_6	+	CH_2O	5.00×10^{-11} [256]
C_3H_5	+	CH_3OH	→	C_3H_6	+	CH_2OH	5.43×10^{-29} [256]
C_3H_5	+	CH_2OH	→	C_3H_6	+	CH_2O	3.00×10^{-11} [256]

H_2	+	CH_3CO		→	CH_3CHO	+	H		3.29×10^{-26}	[253]
H_2	+	CH_2OH		→	CH_3OH	+	H		1.89×10^{-23}	[278]
H	+	H_2O_2		→	H_2O	+	OH		4.20×10^{-14}	[254]
H	+	H_2O_2		→	H_2	+	HO_2		5.15×10^{-15}	[254]
H	+	CH_3OH		→	CH_2OH	+	H_2		1.27×10^{-15}	[278]
H	+	CH_3OH		→	CH_3O	+	H_2		3.18×10^{-16}	[278]
H	+	CH_2OH		→	CH_2O	+	H_2		1.00×10^{-11}	[278]
H	+	CH_2OH		→	CH_3	+	OH		1.60×10^{-10}	[278]
H	+	CH_2OH + M	→	CH_3OH	+	M			2.89×10^{-10}	[280]
									1.18×10^{-29}	b
H	+	C_2H_5OH		→	H_2	+	C_2H_5O		2.52×10^{-17}	[281]
H	+	CH_3OOH		→	H_2O	+	CH_3O		5.88×10^{-15}	[282]
H	+	CH_3OOH		→	H_2	+	CH_3O_2		7.11×10^{-15}	[282]
O	+	H_2O_2		→	HO_2	+	OH		8.91×10^{-16}	[264]
O	+	H_2O_2		→	O_2	+	H_2O		8.91×10^{-16}	[264]
O	+	CH_3CO		→	OH	+	CH_2CO		8.75×10^{-11}	[264]
O	+	CH_3CO		→	CO_2	+	CH_3		2.63×10^{-10}	[264]
O	+	CH_3OH		→	OH	+	CH_2OH		1.12×10^{-14}	[283]
O	+	CH_3OH		→	OH	+	CH_3O		1.68×10^{-15}	[283]
O	+	CH_2OH		→	CH_2O	+	OH		7.00×10^{-11}	[278]
O	+	C_2H_5OOH		→	$C_2H_5O_2$	+	OH		5.19×10^{-14}	[264]
O_2	+	CH_2OH		→	CH_2O	+	HO_2		9.70×10^{-12}	[265]
O_2	+	C_2H_5O		→	CH_3CHO	+	HO_2		8.12×10^{-15}	[265]
OH	+	H_2O_2		→	HO_2	+	H_2O		1.70×10^{-12}	[268]
OH	+	CH_3CO		→	CH_2CO	+	H_2O		2.00×10^{-11}	[253]
OH	+	CH_3CO		→	CH_3	+	CO + OH		5.00×10^{-11}	[253]

OH	+	CH_3OH	→	H_2O	+	CH_2OH			7.67×10^{-13}	[265]
OH	+	CH_3OH	→	H_2O	+	CH_3O			1.35×10^{-13}	[265]
OH	+	CH_2OH	→	CH_2O	+	H_2O			4.00×10^{-11}	[278]
OH	+	C_2H_5OH	→	H_2O	+	C_2H_5O			1.60×10^{-13}	[265]
OH	+	CH_3OOH	→	H_2O	+	CH_3O_2			3.55×10^{-12}	[265]
OH	+	C_2H_5OOH	→	H_2O	+	$C_2H_5O_2$			2.83×10^{-12}	[254]
HO_2	+	CH_3CO	→	CH_3	+	CO_2	+	OH	5.00×10^{-11}	[253]
HO_2	+	CH_3OH	→	CH_2OH	+	H_2O_2			1.10×10^{-22}	[278]
HO_2	+	CH_2OH	→	CH_2O	+	H_2O_2			2.00×10^{-11}	[278]
CH_2O	+	CH_3CO	→	CH_3CHO	+	CHO			1.17×10^{-22}	[253]
CH_2O	+	CH_2OH	→	CH_3OH	+	CHO			4.22×10^{-18}	[278]
CHO	+	H_2O_2	→	CH_2O	+	HO_2			1.50×10^{-18}	[253]
CHO	+	CH_3CO	→	CH_3CHO	+	CO			1.50×10^{-11}	[253]
CHO	+	CH_3OH	→	CH_2O	+	CH_2OH			6.85×10^{-23}	[278]
CHO	+	CH_2OH	→	CH_2O	+	CH_2O			3.00×10^{-10}	[278]
CHO	+	CH_2OH	→	CH_3OH	+	CO			2.00×10^{-10}	[278]
CH_3O	+	CH_3CO	→	CH_3OH	+	CH_2CO			1.00×10^{-11}	[253]
CH_3O	+	CH_3OH	→	CH_3OH	+	CH_2OH			5.38×10^{-16}	[278]
CH_3O	+	CH_2OH	→	CH_2O	+	CH_3OH			4.00×10^{-11}	[278]
CH_3O_2	+	H_2O_2	→	CH_3OOH	+	HO_2			2.31×10^{-19}	[253]
CH_3O_2	+	CH_3CO	→	CH_3	+	CO_2	+	CH_3O	4.00×10^{-11}	[253]
CH_3O_2	+	CH_3OH	→	CH_2OH	+	CH_3OOH			3.08×10^{-22}	[278]
CH_3O_2	+	CH_2OH	→	CH_3O	+	OH	+	CH_2O	2.00×10^{-11}	[278]
H_2O_2	+	CH_3CO	→	CH_3CHO	+	HO_2			3.05×10^{-19}	[253]
H_2O_2	+	CH_2OH	→	CH_3OH	+	HO_2			6.56×10^{-17}	[278]
CH_3CO	+	CH_3OH	→	CH_3CHO	+	CH_2OH			2.22×10^{-22}	[278]

CH_3OH + CH_2OH → CH_3OH + CH_3O 2.12×10^{-23} [278]

CH_2OH + CH_2OH → CH_2O + CH_3OH 8.00×10^{-12} [278]

Table A.4. Ion-neutral and ion-ion reactions included in the model, as well as the corresponding rate coefficients and the references where these data were adopted from. The rate coefficients are expressed in cm^3 s^{-1} and cm^6 s^{-1} for two-body and three-body reactions, respectively.

CH_5^+	+	CH_2	→	CH_3^+	+	CH_4			9.60×10^{-10}	[284]
CH_5^+	+	CH	→	CH_2^+	+	CH_4			6.90×10^{-10}	[284]
CH_5^+	+	C	→	CH^+	+	CH_4			1.20×10^{-09}	[284]
CH_5^+	+	C_2H_6	→	$C_2H_5^+$	+	H_2	+	CH_4	2.25×10^{-10}	[285]
CH_5^+	+	C_2H_4	→	$C_2H_5^+$	+	CH_4			1.50×10^{-09}	[284]
CH_5^+	+	C_2H_2	→	$C_2H_3^+$	+	CH_4			1.60×10^{-09}	[284]
CH_5^+	+	C_2H	→	$C_2H_2^+$	+	CH_4			9.00×10^{-10}	[284]
CH_5^+	+	C_2	→	C_2H^+	+	CH_4			9.50×10^{-10}	[284]
CH_5^+	+	H	→	CH_4^+	+	H_2			1.50×10^{-10}	[284]
CH_5^+	+	O	→	H_3O^+	+	CH_2			2.20×10^{-10}	[284]
CH_5^+	+	H_2O	→	H_3O^+	+	CH_4			3.70×10^{-09}	[284]
CH_5^+	+	OH	→	H_2O^+	+	CH_4			7.00×10^{-10}	[284]
CH_4^+	+	CH_4	→	CH_5^+	+	CH_3			1.50×10^{-09}	[284]
CH_4^+	+	C_2H_6	→	$C_2H_4^+$	+	CH_4	+	H_2	1.91×10^{-09}	[285]
CH_4^+	+	C_2H_4	→	$C_2H_5^+$	+	CH_3			4.23×10^{-10}	[284]
CH_4^+	+	C_2H_4	→	$C_2H_4^+$	+	CH_4			1.38×10^{-09}	[284]
CH_4^+	+	C_2H_2	→	$C_2H_3^+$	+	CH_3			1.23×10^{-09}	[284]
CH_4^+	+	C_2H_2	→	$C_2H_2^+$	+	CH_4			1.13×10^{-09}	[284]
CH_4^+	+	H_2	→	CH_5^+	+	H			3.30×10^{-11}	[284]
CH_4^+	+	H	→	CH_3^+	+	H_2			1.00×10^{-11}	[284]
CH_4^+	+	O	→	CH_3^+	+	OH			1.00×10^{-09}	[284]
CH_4^+	+	O_2	→	O_2^+	+	CH_4			3.90×10^{-10}	[284]

CH_4^+	+	H_2O	→	H_3O^+	+	CH_3			2.60×10^{-09}	[284]
CH_3^+	+	CH_4	→	CH_4^+	+	CH_3			1.36×10^{-10}	[286]
CH_3^+	+	CH_4	→	$C_2H_5^+$	+	H_2			1.20×10^{-09}	[284]
CH_3^+	+	CH_2	→	$C_2H_3^+$	+	H_2			9.90×10^{-10}	[284]
CH_3^+	+	CH	→	$C_2H_2^+$	+	H_2			7.10×10^{-10}	[284]
CH_3^+	+	C	→	C_2H^+	+	H_2			1.20×10^{-09}	[284]
CH_3^+	+	C_2H_6	→	$C_2H_5^+$	+	CH_4			1.48×10^{-09}	[284]
CH_3^+	+	C_2H_4	→	$C_2H_3^+$	+	CH_4			3.50×10^{-10}	[284]
CH_3^+	+	C_2H_3	→	$C_2H_3^+$	+	CH_3			3.00×10^{-10}	[284]
CH_2^+	+	CH_4	→	CH_3^+	+	CH_3			1.38×10^{-10}	[81]
CH_2^+	+	CH_4	→	$C_2H_5^+$	+	H			3.60×10^{-10}	[284]
CH_2^+	+	CH_4	→	$C_2H_4^+$	+	H_2			8.40×10^{-10}	[284]
CH_2^+	+	CH_4	→	$C_2H_3^+$	+	H_2	+	H	2.31×10^{-10}	[81]
CH_2^+	+	CH_4	→	$C_2H_2^+$	+	$2H_2$			3.97×10^{-10}	[81]
CH_2^+	+	C	→	C_2H^+	+	H			1.20×10^{-09}	[284]
CH_2^+	+	H_2	→	CH_3^+	+	H			1.60×10^{-09}	[284]
CH^+	+	CH_4	→	$C_2H_4^+$	+	H			6.50×10^{-11}	[284]
CH^+	+	CH_4	→	$C_2H_3^+$	+	H_2			1.09×10^{-09}	[284]
CH^+	+	CH_4	→	$C_2H_2^+$	+	H_2	+	H	1.43×10^{-10}	[284]
CH^+	+	CH_2	→	C_2H^+	+	H_2			1.00×10^{-09}	[284]
CH^+	+	CH	→	C_2^+	+	H_2			7.40×10^{-10}	[284]
CH^+	+	C	→	C_2^+	+	H			1.20×10^{-09}	[284]
CH^+	+	H_2	→	CH_2^+	+	H			1.20×10^{-09}	[284]
CH^+	+	H	→	C^+	+	H_2			7.50×10^{-10}	[284]
CH^+	+	O	→	CO^+	+	H			3.50×10^{-10}	[284]
CH^+	+	O_2	→	CO^+	+	OH			1.00×10^{-11}	[284]

CH^+	+	O_2	$\rightarrow$	O^+	+	CHO	1.00×10^{-11} [284]
CH^+	+	H_2O	$\rightarrow$	H_3O^+	+	C	5.80×10^{-10} [284]
CH^+	+	OH	$\rightarrow$	CO^+	+	H_2	7.50×10^{-10} [284]
C^+	+	CH_4	$\rightarrow$	$C_2H_3^+$	+	H	1.10×10^{-09} [284]
C^+	+	CH_4	$\rightarrow$	$C_2H_2^+$	+	H_2	4.00×10^{-10} [284]
C^+	+	CH_3	$\rightarrow$	$C_2H_2^+$	+	H	1.30×10^{-09} [284]
C^+	+	CH_3	$\rightarrow$	C_2H^+	+	H_2	1.00×10^{-09} [284]
C^+	+	CH_2	$\rightarrow$	CH_2^+	+	C	5.20×10^{-10} [284]
C^+	+	CH_2	$\rightarrow$	C_2H^+	+	H	5.20×10^{-10} [284]
C^+	+	CH	$\rightarrow$	CH^+	+	C	3.80×10^{-10} [284]
C^+	+	CH	$\rightarrow$	C_2^+	+	H	3.80×10^{-10} [284]
C^+	+	C_2H_6	$\rightarrow$	$C_2H_5^+$	+	CH	2.31×10^{-10} [284]
C^+	+	C_2H_6	$\rightarrow$	$C_2H_4^+$	+	CH_2	1.16×10^{-10} [284]
C^+	+	C_2H_6	$\rightarrow$	$C_2H_3^+$	+	CH_3	4.95×10^{-10} [284]
C^+	+	C_2H_6	$\rightarrow$	$C_2H_2^+$	+	CH_4	8.25×10^{-11} [284]
C^+	+	C_2H_5	$\rightarrow$	$C_2H_5^+$	+	C	5.00×10^{-10} [284]
C^+	+	C_2H_4	$\rightarrow$	$C_2H_4^+$	+	C	1.70×10^{-11} [284]
C^+	+	C_2H_4	$\rightarrow$	$C_2H_3^+$	+	CH	8.50×10^{-11} [284]
C^+	+	O_2	$\rightarrow$	O^+	+	CO	6.20×10^{-10} [284]
C^+	+	O_2	$\rightarrow$	CO^+	+	O	3.80×10^{-10} [284]
C^+	+	OH	$\rightarrow$	CO^+	+	H	7.70×10^{-10} [284]
C^+	+	CO_2	$\rightarrow$	CO^+	+	CO	1.10×10^{-09} [284]
C^+	+	H^-	$\rightarrow$	C	+	H	2.30×10^{-07} [284]
$C_2H_6^+$	+	C_2H_4	$\rightarrow$	$C_2H_4^+$	+	C_2H_6	1.15×10^{-09} [284]
$C_2H_6^+$	+	C_2H_2	$\rightarrow$	$C_2H_5^+$	+	C_2H_3	2.47×10^{-10} [284]
$C_2H_6^+$	+	H	$\rightarrow$	$C_2H_5^+$	+	H_2	1.00×10^{-10} [284]

$C_2H_6^+$	+	H_2O	→	H_3O^+	+	C_2H_5	2.95×10^{-09}	[284]
$C_2H_5^+$	+	H	→	$C_2H_4^+$	+	H_2	1.00×10^{-11}	[284]
$C_2H_5^+$	+	H_2O	→	H_3O^+	+	C_2H_4	1.40×10^{-09}	[284]
$C_2H_4^+$	+	C_2H_3	→	$C_2H_5^+$	+	C_2H_2	5.00×10^{-10}	[284]
$C_2H_4^+$	+	C_2H_3	→	$C_2H_3^+$	+	C_2H_4	5.00×10^{-10}	[284]
$C_2H_4^+$	+	H	→	$C_2H_3^+$	+	H_2	3.00×10^{-10}	[284]
$C_2H_4^+$	+	O	→	CH_3^+	+	CHO	1.08×10^{-10}	[284]
$C_2H_3^+$	+	C_2H_6	→	$C_2H_5^+$	+	C_2H_4	2.91×10^{-10}	[284]
$C_2H_3^+$	+	C_2H_4	→	$C_2H_5^+$	+	C_2H_2	8.90×10^{-10}	[284]
$C_2H_3^+$	+	C_2H_3	→	$C_2H_5^+$	+	C_2H	5.00×10^{-10}	[284]
$C_2H_3^+$	+	C_2H	→	$C_2H_2^+$	+	C_2H_2	3.30×10^{-10}	[284]
$C_2H_3^+$	+	H	→	$C_2H_2^+$	+	H_2	6.80×10^{-11}	[284]
$C_2H_3^+$	+	H_2O	→	H_3O^+	+	C_2H_2	1.11×10^{-09}	[284]
$C_2H_2^+$	+	CH_4	→	$C_2H_3^+$	+	CH_3	4.10×10^{-09}	[81]
$C_2H_2^+$	+	C_2H_6	→	$C_2H_5^+$	+	C_2H_3	1.31×10^{-10}	[285]
$C_2H_2^+$	+	C_2H_6	→	$C_2H_4^+$	+	C_2H_4	2.48×10^{-10}	[284]
$C_2H_2^+$	+	C_2H_4	→	$C_2H_4^+$	+	C_2H_2	4.14×10^{-10}	[284]
$C_2H_2^+$	+	C_2H_3	→	$C_2H_3^+$	+	C_2H_2	3.30×10^{-10}	[284]
$C_2H_2^+$	+	H_2	→	$C_2H_3^+$	+	H	1.00×10^{-11}	[284]
$C_2H_2^+$	+	H_2O	→	H_3O^+	+	C_2H	2.20×10^{-10}	[284]
C_2H^+	+	CH_4	→	$C_2H_2^+$	+	CH_3	3.74×10^{-10}	[284]
C_2H^+	+	CH_2	→	CH_3^+	+	C_2	4.40×10^{-10}	[284]
C_2H^+	+	CH	→	CH_2^+	+	C_2	3.20×10^{-10}	[284]
C_2H^+	+	H_2	→	$C_2H_2^+$	+	H	1.10×10^{-09}	[284]
C_2^+	+	CH_4	→	$C_2H_2^+$	+	CH_2	1.82×10^{-10}	[284]
C_2^+	+	CH_4	→	C_2H^+	+	CH_3	2.38×10^{-10}	[284]

C_2^+	+	CH_2	$\rightarrow$	CH_2^+	+	C_2	4.50×10^{-10} [284]
C_2^+	+	CH	$\rightarrow$	CH^+	+	C_2	3.20×10^{-10} [284]
C_2^+	+	C	$\rightarrow$	C^+	+	C_2	1.10×10^{-10} [284]
C_2^+	+	H_2	$\rightarrow$	C_2H^+	+	H	1.10×10^{-09} [284]
C_2^+	+	O	$\rightarrow$	CO^+	+	C	3.10×10^{-10} [284]
C_2^+	+	O_2	$\rightarrow$	CO^+	+	CO	8.00×10^{-10} [284]
C_2^+	+	H_2O	$\rightarrow$	C_2H^+	+	OH	4.40×10^{-10} [284]
C_2^+	+	OH	$\rightarrow$	OH^+	+	C_2	6.50×10^{-10} [284]
H_3^+	+	CH_4	$\rightarrow$	CH_5^+	+	H_2	2.40×10^{-09} [284]
H_3^+	+	CH_3	$\rightarrow$	CH_4^+	+	H_2	2.10×10^{-09} [284]
H_3^+	+	CH_2	$\rightarrow$	CH_3^+	+	H_2	1.70×10^{-09} [284]
H_3^+	+	CH	$\rightarrow$	CH_2^+	+	H_2	1.20×10^{-09} [284]
H_3^+	+	C	$\rightarrow$	CH^+	+	H_2	2.00×10^{-09} [284]
H_3^+	+	C_2H_6	$\rightarrow$	$C_2H_5^+$	+	$2H_2$	2.40×10^{-09} [284]
H_3^+	+	C_2H_5	$\rightarrow$	$C_2H_6^+$	+	H_2	1.40×10^{-09} [284]
H_3^+	+	C_2H_4	$\rightarrow$	$C_2H_5^+$	+	H_2	1.15×10^{-09} [284]
H_3^+	+	C_2H_4	$\rightarrow$	$C_2H_3^+$	+	$2H_2$	1.15×10^{-09} [284]
H_3^+	+	C_2H_3	$\rightarrow$	$C_2H_4^+$	+	H_2	2.00×10^{-09} [284]
H_3^+	+	C_2H_2	$\rightarrow$	$C_2H_3^+$	+	H_2	3.50×10^{-09} [284]
H_3^+	+	C_2H	$\rightarrow$	$C_2H_2^+$	+	H_2	1.70×10^{-09} [284]
H_3^+	+	C_2	$\rightarrow$	C_2H^+	+	H_2	1.80×10^{-09} [284]
H_3^+	+	O	$\rightarrow$	OH^+	+	H_2	8.40×10^{-10} [284]
H_3^+	+	O	$\rightarrow$	H_2O^+	+	H	3.60×10^{-10} [284]
H_3^+	+	OH	$\rightarrow$	H_2O^+	+	H_2	1.30×10^{-09} [284]
H_3^+	+	H_2O	$\rightarrow$	H_3O^+	+	H_2	5.90×10^{-09} [284]
H_3^+	+	H^-	$\rightarrow$	H_2	+	H_2	2.30×10^{-07} [284]

H_2^+	+	CH_4	→	CH_5^+	+	H			1.14×10^{-10}	[284]
H_2^+	+	CH_4	→	CH_4^+	+	H_2			1.40×10^{-09}	[284]
H_2^+	+	CH_4	→	CH_3^+	+	H_2	+	H	2.30×10^{-09}	[284]
H_2^+	+	CH_2	→	CH_3^+	+	H			1.00×10^{-09}	[284]
H_2^+	+	CH_2	→	CH_2^+	+	H_2			1.00×10^{-09}	[284]
H_2^+	+	CH	→	CH_2^+	+	H			7.10×10^{-10}	[284]
H_2^+	+	CH	→	CH^+	+	H_2			7.10×10^{-10}	[284]
H_2^+	+	C	→	CH^+	+	H			2.40×10^{-09}	[284]
H_2^+	+	C_2H_6	→	$C_2H_6^+$	+	H_2			2.94×10^{-10}	[284]
H_2^+	+	C_2H_6	→	$C_2H_5^+$	+	H_2	+	H	1.37×10^{-09}	[284]
H_2^+	+	C_2H_6	→	$C_2H_4^+$	+	$2H_2$			2.35×10^{-09}	[284]
H_2^+	+	C_2H_6	→	$C_2H_3^+$	+	$2H_2$	+	H	6.86×10^{-10}	[285]
H_2^+	+	C_2H_6	→	$C_2H_2^+$	+	$3H_2$			1.96×10^{-10}	[285]
H_2^+	+	C_2H_4	→	$C_2H_4^+$	+	H_2			2.21×10^{-09}	[284]
H_2^+	+	C_2H_4	→	$C_2H_3^+$	+	H_2	+	H	1.81×10^{-09}	[284]
H_2^+	+	C_2H_4	→	$C_2H_2^+$	+	$2H_2$			8.82×10^{-10}	[284]
H_2^+	+	C_2H_2	→	$C_2H_3^+$	+	H			4.80×10^{-10}	[284]
H_2^+	+	C_2H_2	→	$C_2H_2^+$	+	H_2			4.82×10^{-09}	[284]
H_2^+	+	C_2H	→	$C_2H_2^+$	+	H			1.00×10^{-09}	[284]
H_2^+	+	C_2H	→	C_2H^+	+	H_2			1.00×10^{-09}	[284]
H_2^+	+	C_2	→	C_2H^+	+	H			1.10×10^{-09}	[284]
H_2^+	+	C_2	→	C_2^+	+	H_2			1.10×10^{-09}	[284]
H_2^+	+	H_2	→	H_3^+	+	H			2.08×10^{-09}	[284]
H_2^+	+	H	→	H^+	+	H_2			6.40×10^{-10}	[284]
H_2^+	+	O	→	OH^+	+	H			1.50×10^{-09}	[284]
H_2^+	+	O_2	→	O_2^+	+	H_2			8.00×10^{-10}	[284]

H_2^+	+	OH	$\rightarrow$	OH^+	+	H_2		7.60×10^{-10}	[284]
H_2^+	+	OH	$\rightarrow$	H_2O^+	+	H		7.60×10^{-10}	[284]
H_2^+	+	H_2O	$\rightarrow$	H_2O^+	+	H_2		3.90×10^{-09}	[284]
H_2^+	+	H_2O	$\rightarrow$	H_3O^+	+	H		3.40×10^{-09}	[284]
H_2^+	+	CO	$\rightarrow$	CO^+	+	H_2		6.44×10^{-10}	[284]
H_2^+	+	H^-	$\rightarrow$	H_2	+	H		2.30×10^{-07}	[284]
H^+	+	CH_4	$\rightarrow$	CH_4^+	+	H		1.50×10^{-09}	[284]
H^+	+	CH_4	$\rightarrow$	CH_3^+	+	H_2		2.30×10^{-09}	[284]
H^+	+	CH_3	$\rightarrow$	CH_3^+	+	H		3.40×10^{-09}	[284]
H^+	+	CH_2	$\rightarrow$	CH_2^+	+	H		1.40×10^{-09}	[284]
H^+	+	CH_2	$\rightarrow$	CH^+	+	H_2		1.40×10^{-09}	[284]
H^+	+	CH	$\rightarrow$	CH^+	+	H		1.90×10^{-09}	[284]
H^+	+	C_2H_6	$\rightarrow$	$C_2H_5^+$	+	H_2		1.30×10^{-09}	[285]
H^+	+	C_2H_6	$\rightarrow$	$C_2H_4^+$	+	H_2 + H		1.40×10^{-09}	[284]
H^+	+	C_2H_6	$\rightarrow$	$C_2H_3^+$	+	$2H_2$		2.80×10^{-09}	[284]
H^+	+	C_2H_5	$\rightarrow$	$C_2H_4^+$	+	H_2		1.65×10^{-09}	[284]
H^+	+	C_2H_5	$\rightarrow$	$C_2H_3^+$	+	H_2 + H		3.06×10^{-09}	[284]
H^+	+	C_2H_4	$\rightarrow$	$C_2H_4^+$	+	H		1.00×10^{-09}	[284]
H^+	+	C_2H_4	$\rightarrow$	$C_2H_3^+$	+	H_2		3.00×10^{-09}	[284]
H^+	+	C_2H_4	$\rightarrow$	$C_2H_2^+$	+	H_2 + H		1.00×10^{-09}	[284]
H^+	+	C_2H_3	$\rightarrow$	$C_2H_3^+$	+	H		2.00×10^{-09}	[284]
H^+	+	C_2H_3	$\rightarrow$	$C_2H_2^+$	+	H_2		2.00×10^{-09}	[284]
H^+	+	C_2H_2	$\rightarrow$	$C_2H_2^+$	+	H		5.40×10^{-10}	[284]
H^+	+	C_2H	$\rightarrow$	C_2H^+	+	H		1.50×10^{-09}	[284]
H^+	+	C_2H	$\rightarrow$	C_2^+	+	H_2		1.50×10^{-09}	[284]
H^+	+	C_2	$\rightarrow$	C_2^+	+	H		3.10×10^{-09}	[284]

H^+	+	O	→	O^+	+	H		3.44×10^{-10}	284
H^+	+	O_2	→	O_2^+	+	H		2.00×10^{-09}	284
H^+	+	OH	→	OH^+	+	H		2.10×10^{-09}	284
H^+	+	H_2O	→	H_2O^+	+	H		6.90×10^{-09}	284
H^+	+	H^-	→	H	+	H		2.30×10^{-07}	284
H^-	+	CH_3	→	CH_4	+	e^-		1.00×10^{-09}	284
H^-	+	CH_2	→	CH_3	+	e^-		1.00×10^{-09}	284
H^-	+	CH	→	CH_2	+	e^-		1.00×10^{-10}	284
H^-	+	C	→	CH	+	e^-		1.00×10^{-09}	284
H^-	+	C_2H	→	C_2H_2	+	e^-		1.00×10^{-09}	284
H^-	+	C_2	→	C_2H	+	e^-		1.00×10^{-09}	284
H^-	+	H	→	H_2	+	e^-		1.30×10^{-09}	284
H^-	+	O	→	OH	+	e^-		1.00×10^{-09}	284
H^-	+	OH	→	H_2O	+	e^-		1.00×10^{-10}	284
H^-	+	H_2O	→	OH^-	+	H_2		3.80×10^{-09}	284
H^-	+	O^+	→	H	+	O		2.30×10^{-07}	284
H^-	+	H_3O^+	→	H_2	+	OH	+ H	2.30×10^{-07}	284
H^-	+	H_3O^+	→	H_2O	+	H_2		2.30×10^{-07}	284
O^+	+	CH_4	→	CH_4^+	+	O		8.90×10^{-10}	284
O^+	+	CH_4	→	CH_3^+	+	OH		1.10×10^{-10}	284
O^+	+	CH_2	→	CH_2^+	+	O		9.70×10^{-10}	284
O^+	+	CH	→	CH^+	+	O		3.50×10^{-10}	284
O^+	+	CH	→	CO^+	+	H		3.50×10^{-10}	284
O^+	+	C_2H_4	→	$C_2H_4^+$	+	O		7.00×10^{-11}	284
O^+	+	C_2H_4	→	$C_2H_3^+$	+	OH		2.10×10^{-10}	284
O^+	+	C_2H_4	→	$C_2H_2^+$	+	H_2O		1.12×10^{-09}	284

O^+	+	C_2H_2			→	$C_2H_2^+$	+	O	3.90×10^{-11}	[284]
O^+	+	C_2H			→	C_2H^+	+	O	4.60×10^{-10}	[284]
O^+	+	C_2H			→	CO^+	+	CH	4.60×10^{-10}	[284]
O^+	+	C_2			→	C_2^+	+	O	4.80×10^{-10}	[284]
O^+	+	C_2			→	CO^+	+	C	4.80×10^{-10}	[284]
O^+	+	H_2			→	OH^+	+	H	1.70×10^{-09}	[284]
O^+	+	H			→	H^+	+	O	5.82×10^{-10}	[284]
O^+	+	O	+	O_2	→	O_2^+	+	O_2	1.00×10^{-29}	[195]
O^+	+	O_2			→	O_2^+	+	O	2.00×10^{-11}	[195]
O^+	+	O_3			→	O_2^+	+	O_2	1.00×10^{-10}	[241]
O^+	+	OH			→	OH^+	+	O	3.60×10^{-10}	[284]
O^+	+	OH			→	O_2^+	+	H	3.60×10^{-10}	[284]
O^+	+	H_2O			→	H_2O^+	+	O	3.20×10^{-09}	[284]
O^+	+	CO_2			→	O_2^+	+	CO	9.40×10^{-10}	[284]
O^+	+	CO			→	CO^+	+	O	1.15×10^{-18}	[284]
O^+	+	O^-			→	O	+	O	4.00×10^{-08}	[287]
O^+	+	O^-	+	O	→	O_2	+	O	2.00×10^{-25}	[195]
O^+	+	O^-	+	O_2	→	O_2	+	O_2	2.00×10^{-25}	[195]
O^+	+	O_2^-			→	O	+	O_2	2.70×10^{-07}	[287]
O^+	+	O_2^-	+	O_2	→	O_3	+	O_2	2.00×10^{-25}	[195]
O^+	+	O_3^-			→	O_3	+	O	1.00×10^{-07}	[195]
O_2^+	+	CH_2			→	CH_2^+	+	O_2	4.30×10^{-10}	[284]
O_2^+	+	CH			→	CH^+	+	O_2	3.10×10^{-10}	[284]
O_2^+	+	C			→	CO^+	+	O	5.20×10^{-11}	[284]
O_2^+	+	C			→	C^+	+	O_2	5.20×10^{-11}	[284]
O_2^+	+	C_2H_4			→	$C_2H_4^+$	+	O_2	6.80×10^{-10}	[284]

O_2^+	+	C_2H_2			→	$C_2H_2^+$	+	O_2		1.11×10^{-09}	284
O_2^+	+	C_2			→	C_2^+	+	O_2		4.10×10^{-10}	284
O_2^+	+	C_2			→	CO^+	+	CO		4.10×10^{-10}	284
O_2^+	+	O_2	+	O_2	→	O_4^+	+	O_2		2.40×10^{-30}	241
O_2^+	+	O^-			→	O	+	O_2		2.60×10^{-08}	287
O_2^+	+	O^-			→	O	+	O	+ O	2.60×10^{-08}	287
O_2^+	+	O^-	+	O_2	→	O_3	+	O_2		2.00×10^{-25}	195
O_2^+	+	O_2^-			→	O_2	+	O_2		2.00×10^{-07}	287
O_2^+	+	O_2^-			→	O_2	+	O	+ O	1.00×10^{-07}	195
O_2^+	+	O_2^-	+	O_2	→	O_2	+	O_2	+ O_2	2.00×10^{-25}	195
O_2^+	+	O_3^-			→	O_2	+	O_3		2.00×10^{-07}	195
O_2^+	+	O_3^-			→	O	+	O	+ O_3	1.00×10^{-07}	195
O_4^+	+	O			→	O_2^+	+	O_3		3.00×10^{-10}	241
O_4^+	+	O_2			→	O_2^+	+	O_2	+ O_2	1.73×10^{-13}	241
O^-	+	CH_4			→	OH^-	+	CH_3		1.00×10^{-10}	284
O^-	+	C			→	CO	+	e^-		5.00×10^{-10}	284
O^-	+	H_2			→	H_2O	+	e^-		7.00×10^{-10}	284
O^-	+	H_2			→	OH^-	+	H		3.00×10^{-11}	284
O^-	+	H			→	OH	+	e^-		5.00×10^{-10}	284
O^-	+	O			→	O_2	+	e^-		2.30×10^{-10}	287
O^-	+	O_2			→	O	+	O_2	+ e^-	$k = f(E/N)$	195
O^-	+	O_2			→	O_2^-	+	O		$k = f(E/N)$	195
O^-	+	O_2			→	O_3	+	e^-		5.00×10^{-15}	195
O^-	+	O_2	+	O_2	→	O_3^-	+	O_2		1.10×10^{-30}	195
O^-	+	O_3			→	O_3^-	+	O		5.30×10^{-10}	195
O^-	+	O_3			→	O_2	+	O_2	+ e^-	3.00×10^{-10}	288

O^-	+	CO			$\rightarrow$	CO_2	+	e^-		6.50×10^{-10}	[284]
O_2^-	+	O			$\rightarrow$	O^-	+	O_2		3.30×10^{-10}	[195]
O_2^-	+	O			$\rightarrow$	O_3	+	e^-		3.30×10^{-10}	[287]
O_2^-	+	O_2			$\rightarrow$	O_2	+	O_2	+ e^-	2.18×10^{-18}	[195]
O_2^-	+	O_2	+	O_2	$\rightarrow$	O_4^-	+	O_2		3.50×10^{-31}	[241]
O_2^-	+	O_3			$\rightarrow$	O_3^-	+	O_2		4.00×10^{-10}	[195]
O_3^-	+	O			$\rightarrow$	O^-	+	O_3		1.00×10^{-13}	[288]
O_3^-	+	O			$\rightarrow$	O_2	+	O_2	+ e^-	3.00×10^{-10}	[241]
O_3^-	+	O			$\rightarrow$	O_2^-	+	O_2		3.20×10^{-10}	[241]
O_3^-	+	O_2			$\rightarrow$	O_3	+	O_2	+ e^-	2.30×10^{-11}	[195]
O_3^-	+	O_3			$\rightarrow$	O_2	+	O_2	+ O_2 + e^-	1.00×10^{-12}	[288]
O_4^-	+	O			$\rightarrow$	O_3^-	+	O_2		4.00×10^{-10}	[241]
O_4^-	+	O			$\rightarrow$	O^-	+	O_2	+ O_2	3.00×10^{-10}	[241]
O_4^-	+	O_2			$\rightarrow$	O_2^-	+	O_2	+ O_2	3.08×10^{-12}	[241]
CO_2^+	+	CH_4			$\rightarrow$	CH_4^+	+	CO_2		5.50×10^{-10}	[284]
CO_2^+	+	C_2H_4			$\rightarrow$	$C_2H_4^+$	+	CO_2		1.50×10^{-10}	[284]
CO_2^+	+	C_2H_2			$\rightarrow$	$C_2H_2^+$	+	CO_2		7.30×10^{-10}	[284]
CO_2^+	+	O_2			$\rightarrow$	O_2^+	+	CO_2		5.30×10^{-11}	[284]
CO_2^+	+	O			$\rightarrow$	O_2^+	+	CO		1.64×10^{-10}	[284]
CO_2^+	+	O			$\rightarrow$	O^+	+	CO_2		9.62×10^{-11}	[284]
CO_2^+	+	H_2O			$\rightarrow$	H_2O^+	+	CO_2		2.04×10^{-09}	[284]
CO^+	+	CH_4			$\rightarrow$	CH_4^+	+	CO		7.93×10^{-10}	[284]
CO^+	+	CH_2			$\rightarrow$	CH_2^+	+	CO		4.30×10^{-10}	[284]
CO^+	+	CH			$\rightarrow$	CH^+	+	CO		3.20×10^{-10}	[284]
CO^+	+	C			$\rightarrow$	C^+	+	CO		1.10×10^{-10}	[284]
CO^+	+	C_2H			$\rightarrow$	C_2H^+	+	CO		3.90×10^{-10}	[284]

CO^+	+	C_2	$\rightarrow$	C_2^+	+	CO		8.40×10^{-10} [284]
CO^+	+	H	$\rightarrow$	H^+	+	CO		7.50×10^{-10} [284]
CO^+	+	O_2	$\rightarrow$	O_2^+	+	CO		1.20×10^{-10} [284]
CO^+	+	O	$\rightarrow$	O^+	+	CO		1.40×10^{-10} [284]
CO^+	+	CO_2	$\rightarrow$	CO_2^+	+	CO		1.00×10^{-9} [284]
CO^+	+	H_2O	$\rightarrow$	H_2O^+	+	CO		1.72×10^{-09} [284]
CO^+	+	OH	$\rightarrow$	OH^+	+	CO		3.10×10^{-10} [284]
H_3O^+	+	CH_2	$\rightarrow$	CH_3^+	+	H_2O		9.40×10^{-10} [284]
H_3O^+	+	CH	$\rightarrow$	CH_2^+	+	H_2O		6.80×10^{-10} [284]
H_3O^+	+	C_2H_3	$\rightarrow$	$C_2H_4^+$	+	H_2O		2.00×10^{-09} [284]
H_3O^+	+	C_2	$\rightarrow$	C_2H^+	+	H_2O		9.20×10^{-10} [284]
H_2O^+	+	CH_4	$\rightarrow$	H_3O^+	+	CH_3		1.40×10^{-09} [284]
H_2O^+	+	CH_2	$\rightarrow$	CH_3^+	+	OH		4.70×10^{-10} [284]
H_2O^+	+	CH_2	$\rightarrow$	CH_2^+	+	H_2O		4.70×10^{-10} [284]
H_2O^+	+	CH	$\rightarrow$	CH_2^+	+	OH		3.40×10^{-10} [284]
H_2O^+	+	CH	$\rightarrow$	CH^+	+	H_2O		3.40×10^{-10} [284]
H_2O^+	+	C	$\rightarrow$	CH^+	+	OH		1.10×10^{-09} [284]
H_2O^+	+	C_2H_6	$\rightarrow$	H_3O^+	+	C_2H_5		1.33×10^{-09} [284]
H_2O^+	+	C_2H_6	$\rightarrow$	$C_2H_6^+$	+	H_2O		6.40×10^{-11} [284]
H_2O^+	+	C_2H_6	$\rightarrow$	$C_2H_4^+$	+	H_2O + H_2		1.92×10^{-10} [284]
H_2O^+	+	C_2H_4	$\rightarrow$	$C_2H_4^+$	+	H_2O		1.50×10^{-09} [284]
H_2O^+	+	C_2H_2	$\rightarrow$	$C_2H_2^+$	+	H_2O		1.90×10^{-09} [284]
H_2O^+	+	C_2H	$\rightarrow$	$C_2H_2^+$	+	OH		4.40×10^{-10} [284]
H_2O^+	+	C_2H	$\rightarrow$	C_2H^+	+	H_2O		4.40×10^{-10} [284]
H_2O^+	+	C_2	$\rightarrow$	C_2H^+	+	OH		4.70×10^{-10} [284]
H_2O^+	+	C_2	$\rightarrow$	C_2^+	+	H_2O		4.70×10^{-10} [284]

H_2O^+	+	H_2	$\rightarrow$	H_3O^+	+	H		6.40×10^{-10}	284
H_2O^+	+	O_2	$\rightarrow$	O_2^+	+	H_2O		4.60×10^{-10}	284
H_2O^+	+	O	$\rightarrow$	O_2^+	+	H_2		4.00×10^{-11}	284
H_2O^+	+	H_2O	$\rightarrow$	H_3O^+	+	OH		2.10×10^{-09}	284
H_2O^+	+	OH	$\rightarrow$	H_3O^+	+	O		6.90×10^{-10}	284
OH^+	+	CH_4	$\rightarrow$	CH_5^+	+	O		1.95×10^{-10}	284
OH^+	+	CH_4	$\rightarrow$	H_3O^+	+	CH_2		1.31×10^{-09}	284
OH^+	+	CH_2	$\rightarrow$	CH_3^+	+	O		4.80×10^{-10}	284
OH^+	+	CH_2	$\rightarrow$	CH_2^+	+	OH		4.80×10^{-10}	284
OH^+	+	CH	$\rightarrow$	CH_2^+	+	O		3.50×10^{-10}	284
OH^+	+	CH	$\rightarrow$	CH^+	+	OH		3.50×10^{-10}	284
OH^+	+	C	$\rightarrow$	CH^+	+	O		1.20×10^{-09}	284
OH^+	+	C_2H_6	$\rightarrow$	H_3O^+	+	C_2H_4		1.60×10^{-10}	284
OH^+	+	C_2H_6	$\rightarrow$	$C_2H_6^+$	+	OH		4.80×10^{-11}	284
OH^+	+	C_2H_6	$\rightarrow$	$C_2H_5^+$	+	H_2 + O		3.20×10^{-10}	284
OH^+	+	C_2H_6	$\rightarrow$	$C_2H_4^+$	+	H_2 + OH		1.04×10^{-09}	284
OH^+	+	C_2H	$\rightarrow$	$C_2H_2^+$	+	O		4.50×10^{-10}	284
OH^+	+	C_2H	$\rightarrow$	C_2H^+	+	OH		4.50×10^{-10}	284
OH^+	+	C_2	$\rightarrow$	C_2H^+	+	O		4.80×10^{-10}	284
OH^+	+	C_2	$\rightarrow$	C_2^+	+	OH		4.80×10^{-10}	284
OH^+	+	H_2	$\rightarrow$	H_2O^+	+	H		1.01×10^{-09}	284
OH^+	+	O_2	$\rightarrow$	O_2^+	+	OH		5.90×10^{-10}	284
OH^+	+	O	$\rightarrow$	O_2^+	+	H		7.10×10^{-10}	284
OH^+	+	H_2O	$\rightarrow$	H_2O^+	+	OH		1.59×10^{-09}	284
OH^+	+	H_2O	$\rightarrow$	H_3O^+	+	O		1.30×10^{-09}	284
OH^+	+	OH	$\rightarrow$	H_2O^+	+	O		7.00×10^{-10}	284

OH$^-$	+	CH$_3$	$\rightarrow$	CH$_3$OH	+	e$^-$	1.00×10^{-09}	[284]
OH$^-$	+	CH	$\rightarrow$	CH$_2$O	+	e$^-$	5.00×10^{-10}	[284]
OH$^-$	+	C	$\rightarrow$	CHO	+	e$^-$	5.00×10^{-10}	[284]
OH$^-$	+	H	$\rightarrow$	H$_2$O	+	e$^-$	1.40×10^{-09}	[284]

Bibliography

(1)   http://www.iea.org

(2)   International Energy Agency *World Energy Outlook 2014*; Paris, 2014.

(3)   International Energy Agency *World Energy Outlook 2015*; Paris, 2015.

(4)   International Energy Agency *World Energy Outlook 2008*; Paris, 2008.

(5)   World Energy Council *World Energy Resources 2013 Survey*; London, 2013.

(6)   http://www.worldenergy.org

(7)   World Energy Council *Survey of Energy Resources 2007*; London, 2007.

(8)   Intergovernmental Panel on Climate Change *Climate Change 2014: Synthesis Report*; Geneva, Switzerland, 2014.

(9)   http://www.ipcc.ch

(10)   http://www.icca-chem.org

(11)   http://www.cefic.org

(12)   Lunsford, J. H. Catalytic Conversion of Methane to More Useful Chemicals and Fuels: A Challenge for the 21st Century. *Catal. Today* **2000**, *63*, 165-174.

(13)   Aghamir, F. M.; Matin, N. S.; Jalili, A. H.; Esfarayeni, M. H.; Khodagholi, M. A.; Ahmadi, R. Conversion of Methane to Methanol in an AC Dielectric Barrier Discharge. *Plasma Sources Sci. Technol.* **2004**, *13*, 707-711.

(14)   Zou, J. J.; Zhang, Y. P.; Liu, C. J.; Li, Y.; Eliasson, B. Starch-Enhanced Synthesis of Oxygenates from Methane and Carbon Dioxide Using Dielectric-Barrier Discharges. *Plasma Chem. Plasma Process.* **2003**, *23*, 69-82.

(15)   Roth, J. F. Evolving Nature of Industrial Catalysis. *Appl. Catal. A-Gen.* **1994**, *113*, 131-140.

(16)   European Seventh Framework Programme *A Vision for Smart CO$_2$ Transformation in Europe*; 2015.

(17)   Intergovernmental Panel on Climate Change *Ipcc Special Report on Carbon Dioxide Capture and Storage*; Cambridge University Press, Cambridge, United Kingdom and New York, NY, USA, 2005.

(18)   Damiani, D.; Litynski, J. T.; McIlvried, H. G.; Vikara, D. M.; Srivastava, R. D. The US Department of Energy's R&D Program to Reduce Greenhouse Gas Emissions through Beneficial Uses of Carbon Dioxide. *Greenhouse Gases: Science and Technology* **2012**, *2*, 9-16.

(19)   International Energy Agency *Technology Roadmap: Energy and Ghg Reductions in the Chemical Industry Via Catalytic Processes*; Paris, 2013.

(20)   Zhou, L. M.; Xue, B.; Kogelschatz, U.; Eliasson, B. Nonequilibrium Plasma Reforming of Greenhouse Gases to Synthesis Gas. *Energ. Fuel.* **1998**, *12*, 1191-1199.

(21)   Zhang, K.; Kogelschatz, U.; Eliasson, B. Conversion of Greenhouse Gases to Synthesis Gas and Higher Hydrocarbons. *Energ. Fuel.* **2001**, *15*, 395-402.

(22)   Mills, G. A. Status and Future Opportunities for Conversion of Synthesis Gas to Liquid Fuels. *Fuel* **1994**, *73*, 1243-1279.

(23)   http://www.linde-gas.com

(24)   Jadhav, S. G.; Vaidya, P. D.; Bhanage, B. M.; Joshi, J. B. Catalytic Carbon Dioxide Hydrogenation to Methanol: A Review of Recent Studies. *Chem. Eng. Res. Des.* **2014**, *92*, 2557-2567.

(25)   Agiral, A.; Nozaki, T.; Nakase, M.; Yuzawa, S.; Okazaki, K.; Gardeniers, J. G. E. Gas-to-Liquids Process Using Multi-Phase Flow, Non-Thermal Plasma Microreactor. *Chem. Eng. J.* **2011**, *167*, 560-566.

(26)   Bogaerts, A.; Neyts, E.; Gijbels, R.; van der Mullen, J. Gas Discharge Plasmas and Their Applications. *Spectrochim. Acta B* **2002**, *57*, 609-658.

(27)   Martens, T. Numerical Simulations of Dielectric Barrier Discharges. PhD Thesis, University of Antwerp, Antwerpen, 2010.

(28)   Conrads, H.; Schmidt, M. Plasma Generation and Plasma Sources. *Plasma Sources Sci. Technol.* **2000**, *9*, 441-454.

(29)   Wagner, H. E.; Brandenburg, R.; Kozlov, K. V.; Sonnenfeld, A.; Michel, P.; Behnke, J. F. The Barrier Discharge: Basic Properties and Applications to Surface Treatment. *Vacuum* **2003**, *71*, 417-436.

(30)   Kogelschatz, U. Dielectric-Barrier Discharges: Their History, Discharge Physics, and Industrial Applications. *Plasma Chem. Plasma Process.* **2003**, *23*, 1-46.

(31)   Eliasson, B.; Kogelschatz, U. Modeling and Applications of Silent Discharge Plasmas. *IEEE Trans. Plasma Sci.* **1991**, *19*, 309-323.

(32)   Kogelschatz, U.; Eliasson, B.; Egli, W. From Ozone Generators to Flat Television Screens: History and Future Potential of Dielectric-Barrier Discharges. *Pure Appl. Chem.* **1999**, *71*, 1819-1828.

(33)   Gibalov, V. I.; Pietsch, G. J. The Development of Dielectric Barrier Discharges in Gas Gaps and on Surfaces. *J. Phys. D: Appl. Phys.* **2000**, *33*, 2618-2636.

(34)   Kogelschatz, U. Filamentary, Patterned, and Diffuse Barrier Discharges. *IEEE Trans. Plasma Sci.* **2002**, *30*, 1400-1408.

(35)   Kim, H. H. Nonthermal Plasma Processing for Air-Pollution Control: A Historical Review, Current Issues, and Future Prospects. *Plasma Process. Polym.* **2004**, *1*, 91-110.

(36)   Chang, J. S. Physics and Chemistry of Plasma Pollution Control Technology. *Plasma Sources Sci. Technol.* **2008**, *17*, 045004.

(37)   Xu, X. J. Dielectric Barrier Discharge - Properties and Applications. *Thin Solid Films* **2001**, *390*, 237-242.

(38)   Ozkan, A.; Dufour, T.; Silva, T.; Britun, N.; Snyders, R.; Bogaerts, A.; Reniers, F. The Influence of Power and Frequency on the Filamentary Behavior of a Flowing DBD-Application to the Splitting of CO_2. *Plasma Sources Sci. Technol.* **2016**, *25*, 025013.

(39)   Eliasson, B.; Kogelschatz, U. Nonequilibrium Volume Plasma Chemical Processing. *IEEE Trans. Plasma Sci.* **1991**, *19*, 1063-1077.

(40)   Eliasson, B.; Egli, W.; Kogelschatz, U. Modeling of Dielectric Barrier Discharge Chemistry. *Pure Appl. Chem.* **1994**, *66*, 1275-1286.

(41)   Jie, Y. X.; Xu, X. J. Study on the Breakdown Process in Dielectric Barrier Discharge with a Magnetohydrodynamic Method. *Phys. Scr.* **1996**, *53*, 212-215.

(42)   Hagelaar, G. J. M. Modeling of Microdischarges for Display Technology. PhD Thesis, Eindhoven University of Technology, Eindhoven, 2000.

(43)   Gogolides, E.; Sawin, H. H. Continuum Modeling of Radiofrequency Glow-Discharges. I. Theory and Results for Electropositive and Electronegative Gases. *J. Appl. Phys.* **1992**, *72*, 3971-3987.

(44)   van Dijk, J.; Peerenboom, K.; Jimenez, M.; Mihailova, D.; van der Mullen, J. The Plasma Modelling Toolkit Plasimo. *J. Phys. D: Appl. Phys.* **2009**, *42*, 194012.

(45)   http://plasimo.phys.tue.nl

(46)   Hagelaar, G. J. M.; Kroesen, G. M. W.; van Slooten, U.; Schreuders, H. Modeling of the Microdischarges in Plasma Addressed Liquid Crystal Displays. *J. Appl. Phys.* **2000**, *88*, 2252-2262.

(47)   Hagelaar, G. J. M.; Kroesen, G. M. W. Speeding up Fluid Models for Gas Discharges by Implicit Treatment of the Electron Energy Source Term. *J. Comput. Phys.* **2000**, *159*, 1-12.

(48)   Hagelaar, G. J. M.; de Hoog, F. J.; Kroesen, G. M. W. Boundary Conditions in Fluid Models of Gas Discharges. *Phys. Rev. E* **2000**, *62*, 1452-1454.

(49)   Brok, W. J. M.; van Dijk, J.; Bowden, M. D.; van der Mullen, J. J. A. M.; Kroesen, G. M. W. A Model Study of Propagation of the First Ionization Wave During Breakdown in a Straight Tube Containing Argon. *J. Phys. D: Appl. Phys.* **2003**, *36*, 1967-1979.

(50)   Brok, W. J. M.; Gendre, M. F.; van der Mullen, J. J. A. M. Model Study of DC Ignition of Fluorescent Tubes. *J. Phys. D: Appl. Phys.* **2007**, *40*, 156-162.

(51)   Brok, W. J. M.; Gendre, M. F.; Haverlag, M.; van der Mullen, J. J. A. M. Numerical Description of High Frequency Ignition of Fluorescent Tubes. *J. Phys. D: Appl. Phys.* **2007**, *40*, 3931-3936.

(52)   Brok, W. J. M.; Bowden, M. D.; van Dijk, J.; van der Mullen, J. J. A. M.; Kroesen, G. M. W. Numerical Description of Discharge Characteristics of the Plasma Needle. *J. Appl. Phys.* **2005**, *98*, 013302.

(53)   Wagenaars, E.; Brandenburg, R.; Brok, W. J. M.; Bowden, M. D.; Wagner, H. E. Experimental and Modelling Investigations of a Dielectric Barrier Discharge in Low-Pressure Argon. *J. Phys. D: Appl. Phys.* **2006**, *39*, 700-711.

(54)   Martens, T.; Bogaerts, A.; Brok, W.; van Dijk, J. Computer Simulations of a Dielectric Barrier Discharge Used for Analytical Spectrometry. *Anal. Bioanal. Chem.* **2007**, *388*, 1583-1594.

(55)   Martens, T.; Bogaerts, A.; Brok, W. J. M.; van der Mullen, J. J. A. M. Modeling Study on the Influence of the Pressure on a Dielectric Barrier Discharge Microplasma. *J. Anal. Atom. Spectrom.* **2007**, *22*, 1033-1042.

(56)   Martens, T.; Mihailova, D.; van Dijk, J.; Bogaerts, A. Theoretical Characterization of an Atmospheric Pressure Glow Discharge Used for Analytical Spectrometry. *Anal. Chem.* **2009**, *81*, 9096-9108.

(57)   Meyyappan, M.; Kreskovsky, J. P. Glow-Discharge Simulation through Solutions to the Moments of the Boltzmann Transport-Equation. *J. Appl. Phys.* **1990**, *68*, 1506-1512.

(58)   Passchier, J. D. P.; Goedheer, W. J. A 2-Dimensional Fluid Model for an Argon Rf Discharge. *J. Appl. Phys.* **1993**, *74*, 3744-3751.

(59)   Meunier, J.; Belenguer, P.; Boeuf, J. P. Numerical-Model of an Ac Plasma Display Panel Cell in Neon-Xenon Mixtures. *J. Appl. Phys.* **1995**, *78*, 731-745.

(60)   Punset, C.; Boeuf, J. P.; Pitchford, L. C. Two-Dimensional Simulation of an Alternating Current Matrix Plasma Display Cell: Cross-Talk and Other Geometric Effects. *J. Appl. Phys.* **1998**, *83*, 1884-1897.

(61)   Mihailova, D.; Grozeva, M.; Hagelaar, G. J. M.; van Dijk, J.; Brok, W. J. M.; van der Mullen, J. J. A. M. A Flexible Platform for Simulations of Sputtering

Hollow Cathode Discharges for Laser Applications. *J. Phys. D: Appl. Phys.* **2008**, *41*, 245202.

(62)   Schneider, G. E.; Zedan, M. A Modified Strongly Implicit Procedure for the Numerical Solution of Field Problems. *Numer. Heat Tr. A-Appl.* **1981**, *4*, 1-19.

(63)   Bogaerts, A.; Wang, W.; Berthelot, A.; Guerra, V. Modeling Plasma-Based CO_2 Conversion: Crucial Role of the Dissociation Cross Section. *Plasma Sources Sci. Technol.* **2016**, *25*, 055016.

(64)   Larkin, D. W.; Caldwell, T. A.; Lobban, L. L.; Mallinson, R. G. Oxygen Pathways and Carbon Dioxide Utilization in Methane Partial Oxidation in Ambient Temperature Electric Discharges. *Energ. Fuel.* **1998**, *12*, 740-744.

(65)   Larkin, D. W.; Zhou, L. M.; Lobban, L. L.; Mallinson, R. G. Product Selectivity Control and Organic Oxygenate Pathways from Partial Oxidation of Methane in a Silent Electric Discharge Reactor. *Ind. Eng. Chem. Res.* **2001**, *40*, 5496-5506.

(66)   Larkin, D. W.; Lobban, L. L.; Mallinson, R. G. The Direct Partial Oxidation of Methane to Organic Oxygenates Using a Dielectric Barrier Discharge Reactor as a Catalytic Reactor Analog. *Catal. Today* **2001**, *71*, 199-210.

(67)   Larkin, D. W.; Lobban, L. L.; Mallinson, R. G. Production of Organic Oxygenates in the Partial Oxidation of Methane in a Silent Electric Discharge Reactor. *Ind. Eng. Chem. Res.* **2001**, *40*, 1594-1601.

(68)   Paulussen, S.; Verheyde, B.; Tu, X.; De Bie, C.; Martens, T.; Petrovic, D.; Bogaerts, A.; Sels, B. Conversion of Carbon Dioxide to Value-Added Chemicals in Atmospheric Pressure Dielectric Barrier Discharges. *Plasma Sources Sci. Technol.* **2010**, *19*, 034015.

(69)   Reid, R. C.; Prausnitz, J. M.; Poling, B. E., *The Properties of Gases and Liquids*, 4th ed.: New York, 1987.

(70)   Herrebout, D.; Bogaerts, A.; Yan, M.; Gijbels, R.; Goedheer, W.; Dekempeneer, E. One-Dimensional Fluid Model for an RF Methane Plasma of Interest in Deposition of Diamond-Like Carbon Layers. *J. Appl. Phys.* **2001**, *90*, 570-579.

(71)   National Aeronautics and Space Administration *Estimated Viscosities and Thermal Conductivities of Gases at High Temperatures*; Washington D.C., 1962.

(72)   Mcdaniel, E. W.; Mason, E. A., *The Mobility and Diffusion of Ions in Gases*: New York, 1973.

(73)   Böttcher, C. J. F.; Bordewijk, P., *Theory of Electric Polarization*, 2nd ed.; Elsevier Scientific Publishing Company: Amsterdam, 1978; Vol. 2 Dielectrics in Time-Dependent Fields.

(74)   Hagelaar, G. J. M.; Pitchford, L. C. Solving the Boltzmann Equation to Obtain Electron Transport Coefficients and Rate Coefficients for Fluid Models. *Plasma Sources Sci. Technol.* **2005**, *14*, 722-733.

(75)   Bohmeyer, W.; Naujoks, D.; Markin, A.; Arkhipov, I.; Koch, B.; Schroder, D.; Fussmann, G. Transport and Deposition of Injected Hydrocarbons in Plasma Generator Psi-2. *J. Nucl. Mater.* **2005**, *337-339*, 89-93.

(76)   Eckert, M.; Neyts, E.; Bogaerts, A. Molecular Dynamics Simulations of the Sticking and Etch Behavior of Various Growth Species of (Ultra)Nanocrystalline Diamond Films. *Chem. Vapor Depos.* **2008**, *14*, 213-223.

(77)   Liu, C. J.; Eliasson, B.; Xue, B. Z.; Li, Y.; Wang, Y. Q. Zeolite-Enhanced Plasma Methane Conversion Directly to Higher Hydrocarbons Using Dielectric-Barrier Discharges. *React. Kinet. Catal. L.* **2001**, *74*, 71-77.

(78)   Yang, Y. Direct Non-Oxidative Methane Conversion by Non-Thermal Plasma: Experimental Study. *Plasma Chem. Plasma Process.* **2003**, *23*, 283-296.

(79)   Kim, S. S.; Lee, H.; Choi, J. W.; Na, B. K.; Song, H. K. Methane Conversion to Higher Hydrocarbons in a Dielectric-Barrier Discharge Reactor with Pt/gamma-Al2O3 Catalyst. *Catal. Commun.* **2007**, *8*, 1438-1442.

(80)   Indarto, A. Hydrogen Production from Methane in a Dielectric Barrier Discharge Using Oxide Zinc and Chromium as Catalyst. *J. Chin. Inst. Chem. Eng,* **2008**, *39*, 23-28.

(81)   Tachibana, K.; Nishida, M.; Harima, H.; Urano, Y. Diagnostics and Modeling of a Methane Plasma Used in the Chemical Vapor-Deposition of Amorphous-Carbon Films. *J. Phys. D: Appl. Phys.* **1984**, *17*, 1727-1742.

(82)   Gogolides, E.; Buteau, C.; Rhallabi, A.; Turban, G. Radiofrequency Glow-Discharges in Methane Gas: Modeling of the Gas-Phase Physics and Chemistry. *J. Phys. D: Appl. Phys.* **1994**, *27*, 818-825.

(83)   Gogolides, E.; Mary, D.; Rhallabi, A.; Turban, G. Rf Plasmas in Methane: Prediction of Plasma Properties and Neutral Radical Densities with Combined Gas-Phase Physics and Chemistry Model. *Jpn. J. Appl. Phys. 1* **1995**, *34*, 261-270.

(84)   Masi, M.; Cavallotti, C.; Carra, S. Different Approaches for Methane Plasmas Modeling. *Chem. Eng. Sci.* **1998**, *53*, 3875-3886.

(85)   Zhou, L. M.; Xue, B.; Kogelschatz, U.; Eliasson, B. Partial Oxidation of Methane to Methanol with Oxygen or Air in a Nonequilibrium Discharge Plasma. *Plasma Chem. Plasma Process.* **1998**, *18*, 375-393.

(86)   Bugaev, S. P.; Kozyrev, A. V.; Kuvshinov, V. A.; Sochugov, N. S.; Khryapov, P. A. Plasma-Chemical Conversion of Lower Alkanes with Stimulated Condensation of Incomplete Oxidation Products. *Plasma Chem. Plasma Process.* **1998**, *18*, 247-261.

(87)   Fan, W. Y.; Knewstubb, P. F.; Kaning, M.; Mechold, L.; Ropcke, J.; Davies, P. B. A Diode Laser and Modeling Study of Mixed (CH4-H-2-O-2) AC Plasmas. *J. Phys. Chem. A* **1999**, *103*, 4118-4128.

(88)   Herrebout, D.; Bogaerts, A.; Yan, M.; Gijbels, R.; Goedheer, W.; Vanhulsel, A. Modeling of a Capacitively Coupled Radio-Frequency Methane Plasma: Comparison between a One-Dimensional and a Two-Dimensional Fluid Model. *J. Appl. Phys.* **2002**, *92*, 2290-2295.

(89)   Kraus, M.; Egli, W.; Haffner, K.; Eliasson, B.; Kogelschatz, U.; Wokaun, A. Investigation of Mechanistic Aspects of the Catalytic CO_2 Reforming of Methane in a Dielectric-Barrier Discharge Using Optical Emission Spectroscopy and Kinetic Modeling. *Phys. Chem. Chem. Phys.* **2002**, *4*, 668-675.

(90)   Yoon, S. F.; Tan, K. H.; Rusli; Ahn, J. Modeling and Analysis of Hydrogen-Methane Plasma in Electron Cyclotron Resonance Chemical Vapor Deposition of Diamond-Like Carbon. *J. Appl. Phys.* **2002**, *91*, 40-47.

(91)   Herrebout, D.; Bogaerts, A.; Gijbels, R.; Goedheer, W. J.; Vanhulsel, A. A One-Dimensional Fluid Model for an Acetylene RF Discharge: A Study of the Plasma Chemistry. *IEEE Trans. Plasma Sci.* **2003**, *31*, 659-664.

(92)   Yang, Y. Direct Non-Oxidative Methane Conversion by Non-Thermal Plasma: Modeling Study. *Plasma Chem. Plasma Process.* **2003**, *23*, 327-346.

(93)   Hwang, B.; Yeo, Y.; Na, B. Conversion of CH_4 and CO_2 to Syngas and Higher Hydrocarbons Using Dielectric Barrier Discharge. *Korean J. Chem. Eng.* **2003**, *20*, 631-634.

(94)   Wang, J. G.; Liu, C. J.; Eliassion, B. Density Functional Theory Study of Synthesis of Oxygenates and Higher Hydrocarbons from Methane and Carbon Dioxide Using Cold Plasmas. *Energ. Fuel.* **2004**, *18*, 148-153.

(95)   Jiang, C. Q.; Mohamed, A. A. H.; Stark, R. H.; Yuan, J. H.; Schoenbach, K. H. Removal of Volatile Organic Compounds in Atmospheric Pressure Air by Means of Direct Current Glow Discharges. *IEEE Trans. Plasma Sci.* **2005**, *33*, 1416-1425.

(96)   Kovacs, T.; Deam, R. T. Methane Reformation Using Plasma: An Initial Study. *J. Phys. D: Appl. Phys.* **2006**, *39*, 2391-2400.

(97)   Istadi, I.; Amin, N. A. S. Modelling and Optimization of Catalytic-Dielectric Barrier Discharge Plasma Reactor for Methane and Carbon Dioxide Conversion Using Hybrid Artificial Neural Network - Genetic Algorithm Technique. *Chem. Eng. Sci.* **2007**, *62*, 6568-6581.

(98)   Naidis, G. V. Modelling of Transient Plasma Discharges in Atmospheric-Pressure Methane-Air Mixtures. *J. Phys. D: Appl. Phys.* **2007**, *40*, 4525-4531.

(99)   Nair, S. A.; Nozaki, T.; Okazaki, K. Methane Oxidative Conversion Pathways in a Dielectric Barrier Discharge Reactor - Investigation of Gas Phase Mechanism. *Chem. Eng. J.* **2007**, *132*, 85-95.

(100)   Pintassilgo, C. D.; Jaoul, C.; Loureiro, J.; Belmonte, T.; Czerwiec, T. Kinetic Modelling of a N-2 Flowing Microwave Discharge with CH4 Addition in the Post-Discharge for Nitrocarburizing Treatments. *J. Phys. D: Appl. Phys.* **2007**, *40*, 3620-3632.

(101)   Matin, N. S.; Whitehead, J. C. A Chemical Model for the Atmospheric Pressure Plasma Reforming of Methane with Oxygen. *28th ICPIG, July 15-20, 2007, Prague, Czech Republic* **2007**, 983-986.

(102)   Agiral, A.; Trionfetti, C.; Lefferts, L.; Seshan, K.; Gardeniers, J. G. E. Propane Conversion at Ambient Temperatures C-C and C-H Bond Activation

Using Cold Plasma in a Microreactor. *Chem. Eng. Technol.* **2008**, *31*, 1116-1123.

(103)   Indarto, A.; Coowanitwong, N.; Choi, J.-W.; Lee, H.; Song, H. K. Kinetic Modeling of Plasma Methane Conversion in a Dielectric Barrier Discharge. *Fuel Process. Technol.* **2008**, *89*, 214-219.

(104)   Luche, J.; Aubry, O.; Khacef, A.; Cormier, J. M. Syngas Production from Methane Oxidation Using a Non-Thermal Plasma: Experiments and Kinetic Modeling. *Chem. Eng. J.* **2009**, *149*, 35-41.

(105)   Goujard, V.; Nozaki, T.; Yuzawa, S.; Ağiral, A.; Okazaki, K. Plasma-Assisted Partial Oxidation of Methane at Low Temperatures: Numerical Analysis of Gas-Phase Chemical Mechanism. *J. Phys. D: Appl. Phys.* **2011**, *44*, 274011.

(106)   Zhou, J.; Xu, Y.; Zhou, X.; Gong, J.; Yin, Y.; Zheng, H.; Guo, H. Direct Oxidation of Methane to Hydrogen Peroxide and Organic Oxygenates in a Double Dielectric Plasma Reactor. *ChemSusChem* **2011**, *4*, 1095-1098.

(107)   Goujard, V.; Tatibouet, J. M.; Batiot-Dupeyrat, C. Carbon Dioxide Reforming of Methane Using a Dielectric Barrier Discharge Reactor: Effect of Helium Dilution and Kinetic Model. *Plasma Chem. Plasma Process.* **2011**, *31*, 315-325.

(108)   Machrafi, H.; Cavadias, S.; Amouroux, J. CO_2 Valorization by Means of Dielectric Barrier Discharge. *J. Phys.: Conf. Ser.* **2011**, *275*, 012016.

(109)   Snoeckx, R.; Aerts, R.; Tu, X.; Bogaerts, A. Plasma-Based Dry Reforming: A Computational Study Ranging from the Nanoseconds to Seconds Time Scale. *J. Phys. Chem. C* **2013**, *117*, 4957-4970.

(110)   Farouk, T.; Farouk, B.; Gutsol, A.; Fridman, A. Atmospheric Pressure Methane-Hydrogen DC Micro-Glow Discharge for Thin Film Deposition. *J. Phys. D: Appl. Phys.* **2008**, *41*, 175202.

(111)   Kozak, T.; Bogaerts, A. Splitting of CO_2 by Vibrational Excitation in Non-Equilibrium Plasmas: A Reaction Kinetics Model. *Plasma Sources Sci. Technol.* **2014**, *23*, 045004.

(112)   Bogaerts, A.; Kozak, T.; van Laer, K.; Snoeckx, R. Plasma-Based Conversion of CO_2: Current Status and Future Challenges. *Faraday Discuss.* **2015**, *183*, 217-232.

(113)   Morgan, W. L. A Critical-Evaluation of Low-Energy Electron-Impact Cross-Sections for Plasma Processing Modeling .2. Cf4, Sih4, and Ch4. *Plasma Chem. Plasma Process.* **1992**, *12*, 477-493.

(114)   Baulch, D. L.; Cobos, C. J.; Cox, R. A.; Frank, P.; Hayman, G.; Just, T.; Kerr, J. A.; Murrells, T.; Pilling, M. J.; Troe, J., et al. Evaluated Kinetic Data for Combustion Modeling - Supplement-1. *J. Phys. Chem. Ref. Data* **1994**, *23*, 847-1033.

(115)   Laufer, A. H.; Gardner, E. P.; Kwok, T. L.; Yung, Y. L. Computations and Estimates of Rate Coefficients for Hydrocarbon Reactions of Interest to the Atmospheres of the Outer Solar System. *Icarus* **1983**, *56*, 560-567.

(116)   Martens, T.; Brok, W. J. M.; van Dijk, J.; Bogaerts, A. On the Regime Transitions During the Formation of an Atmospheric Pressure Dielectric Barrier Glow Discharge. *J. Phys. D: Appl. Phys.* **2009**, *42*, 122002.

(117)   De Bleecker, K.; Bogaerts, A.; Goedheer, W. Detailed Modeling of Hydrocarbon Nanoparticle Nucleation in Acetylene Discharges. *Phys. Rev. E* **2006**, *73*, 026405.

(118)   De Bleecker, K.; Bogaerts, A.; Goedheer, W. Aromatic Ring Generation as a Dust Precursor in Acetylene Discharges. *Appl. Phys. Lett.* **2006**, *88*, 151501.

(119)   Mao, M.; Benedikt, J.; Consoli, A.; Bogaerts, A. New Pathways for Nanoparticle Formation in Acetylene Dusty Plasmas: A Modelling Investigation and Comparison with Experiments. *J. Phys. D: Appl. Phys.* **2008**, *41*, 225201.

(120)   Liu, C. J.; Marafee, A.; Mallinson, R.; Lobban, L. Methane Conversion to Higher Hydrocarbons in a Corona Discharge over Metal Oxide Catalysts with OH Groups. *Appl. Catal. A-Gen.* **1997**, *164*, 21-33.

(121)   Okumoto, M.; Mizuno, A. Conversion of Methane for Higher Hydrocarbon Fuel Synthesis Using Pulsed Discharge Plasma Method. *Catal. Today* **2001**, *71*, 211-217.

(122)   Okumoto, M.; Kim, H. H.; Takashima, K.; Katsura, S.; Mizuno, A. Reactivity of Methane in Nonthermal Plasma in the Presence of Oxygen and Inert Gases at Atmospheric Pressure. *IEEE Trans. Ind. Appl.* **2001**, *37*, 1618-1624.

(123)   Cho, W.; Baek, Y.; Moon, S. K.; Kim, Y. C. Oxidative Coupling of Methane with Microwave and RF Plasma Catalytic Reaction over Transitional Metals Loaded on ZSM-5. *Catal. Today* **2002**, *74*, 207-223.

(124)   Pietruszka, B.; Anklam, K.; Heintze, M. Plasma-Assisted Partial Oxidation of Methane to Synthesis Gas in a Dielectric Barrier Discharge. *Appl. Catal. A-Gen.* **2004**, *261*, 19-24.

(125)   Heintze, M.; Pietruszka, B. Plasma Catalytic Conversion of Methane into Syngas: The Combined Effect of Discharge Activation and Catalysis. *Catal. Today* **2004**, *89*, 21-25.

(126)   Nozaki, T.; Hattori, A.; Okazaki, K. Partial Oxidation of Methane Using a Microscale Non-Equilibrium Plasma Reactor. *Catal. Today* **2004**, *98*, 607-616.

(127)   Indarto, A.; Choi, J. W.; Lee, H.; Song, H. K.; Palgunadi, J. Partial Oxidation of Methane with Sol-Gel Fe/Hf/YSZ Catalyst in Dielectric Barrier Discharge: Catalyst Activation by Plasma. *J. Rare Earth.* **2006**, *24*, 513-518.

(128)   Sreethawong, T.; Thakonpatthanakun, P.; Chavadej, S. Partial Oxidation of Methane with Air for Synthesis Gas Production in a Multistage Gliding Arc Discharge System. *Int. J. Hydrogen Energ.* **2007**, *32*, 1067-1079.

(129)   Indarto, A.; Lee, H.; Choi, J. W.; Song, H. K. Partial Oxidation of Methane with Yttria-Stabilized Zirconia Catalyst in a Dielectric Barrier Discharge. *Energ. Sources Part A* **2008**, *30*, 1628-1636.

(130)   Indarto, A.; Yang, D. R.; Palgunadi, J.; Choi, J. W.; Lee, H.; Song, H. K. Partial Oxidation of Methane with Cu-Zn-Al Catalyst in a Dielectric Barrier Discharge. *Chem. Eng. Process.* **2008**, *47*, 780-786.

(131)   Matin, N. S.; Savadkoohi, H. A.; Feizabadi, S. Y. Methane Conversion to C-2 Hydrocarbons Using Dielectric-Barrier Discharge Reactor: Effects of System Variables. *Plasma Chem. Plasma Process.* **2008**, *28*, 189-202.

(132)   Wang, B. W.; Zhang, X.; Liu, Y. W.; Xu, G. H. Conversion of CH_4, Steam and O_2 to Syngas and Hydrocarbons Via Dielectric Barrier Discharge. *J. Nat. Gas Chem.* **2009**, *18*, 94-97.

(133)   Nozaki, T.; AgIral, A.; Yuzawa, S.; Han Gardeniers, J. G. E.; Okazaki, K. A Single Step Methane Conversion into Synthetic Fuels Using Microplasma Reactor. *Chem. Eng. J.* **2011**, *166*, 288-293.

(134)   Nozaki, T.; Goujard, V.; Yuzawa, S.; Moriyama, S.; Ağıral, A.; Okazaki, K. Selective Conversion of Methane to Synthetic Fuels Using Dielectric Barrier Discharge Contacting Liquid Film. *J. Phys. D: Appl. Phys.* **2011**, *44*, 274010.

(135)   Eliasson, B.; Liu, C. J.; Kogelschatz, U. Direct Conversion of Methane and Carbon Dioxide to Higher Hydrocarbons Using Catalytic Dielectric-Barrier Discharges with Zeolites. *Ind. Eng. Chem. Res.* **2000**, *39*, 1221-1227.

(136)   Huang, A. M.; Xia, G. G.; Wang, J. Y.; Suib, S. L.; Hayashi, Y.; Matsumoto, H. CO_2 Reforming of CH_4 by Atmospheric Pressure AC Discharge Plasmas. *J. Catal.* **2000**, *189*, 349-359.

(137)   Kozlov, K. V.; Michel, P.; Wagner, H. E. Synthesis of Organic Compounds from Mixtures of Methane with Carbon Dioxide in Dielectric-Barrier Discharges at Atmospheric Pressure. *Plasmas Polym.* **2000**, *5*, 129-150.

(138)   Yao, S. L.; Ouyang, F.; Nakayama, A.; Suzuki, E.; Okumoto, N.; Mizuno, A. Oxidative Coupling and Reforming of Methane with Carbon Dioxide Using a High-Frequency Pulsed Plasma. *Energ. Fuel.* **2000**, *14*, 910-914.

(139)   Kraus, M.; Eliasson, B.; Kogelschatz, U.; Wokaun, A. CO_2 Reforming of Methane by the Combination of Dielectric-Barrier Discharges and Catalysis. *Phys. Chem. Chem. Phys.* **2001**, *3*, 294-300.

(140)   Liu, C. J.; Xue, B. Z.; Eliasson, B.; He, F.; Li, Y.; Xu, G. H. Methane Conversion to Higher Hydrocarbons in the Presence of Carbon Dioxide Using Dielectric-Barrier Discharge Plasmas. *Plasma Chem. Plasma Process.* **2001**, *21*, 301-310.

(141)   Yao, S. L.; Okumoto, M.; Nakayama, A.; Suzuki, E. Plasma Reforming and Coupling of Methane with Carbon Dioxide. *Energ. Fuel.* **2001**, *15*, 1295-1299.

(142) Jiang, T.; Li, Y.; Liu, C. J.; Xu, G. H.; Eliasson, B.; Xue, B. Z. Plasma Methane Conversion Using Dielectric-Barrier Discharges with Zeolite A. *Catal. Today* **2002**, *72*, 229-235.

(143) Li, Y.; Liu, C. J.; Eliasson, B.; Wang, Y. Synthesis of Oxygenates and Higher Hydrocarbons Directly from Methane and Carbon Dioxide Using Dielectric-Barrier Discharges: Product Distribution. *Energ. Fuel.* **2002**, *16*, 864-870.

(144) Zhang, X. L.; Dai, B.; Zhu, A. M.; Gong, W. M.; Liu, C. H. The Simultaneous Activation of Methane and Carbon Dioxide to C_2 Hydrocarbons under Pulse Corona Plasma over La_2O_3/gamma-Al_2O_3 Catalyst. *Catal. Today* **2002**, *72*, 223-227.

(145) Zhang, K.; Eliasson, B.; Kogelschatz, U. Direct Conversion of Greenhouse Gases to Synthesis Gas and C_4 Hydrocarbons over Zeolite HY Promoted by a Dielectric-Barrier Discharge. *Ind. Eng. Chem. Res.* **2002**, *41*, 1462-1468.

(146) Zhang, J. Q.; Zhang, J. S.; Yang, Y. J.; Liu, Q. Oxidative Coupling and Reforming of Methane with Carbon Dioxide Using a Pulsed Microwave Plasma under Atmospheric Pressure. *Energ. Fuel.* **2003**, *17*, 54-59.

(147) Zhang, Y. P.; Li, Y.; Wang, Y.; Liu, C. J.; Eliasson, B. Plasma Methane Conversion in the Presence of Carbon Dioxide Using Dielectric-Barrier Discharges. *Fuel Process. Technol.* **2003**, *83*, 101-109.

(148) Song, H. K.; Choi, J. W.; Yue, S. H.; Lee, H.; Na, B. K. Synthesis Gas Production Via Dielectric Barrier Discharge over Ni/gamma-Al_2O_3 Catalyst. *Catal. Today* **2004**, *89*, 27-33.

(149) Song, H. K.; Lee, H.; Choi, J.-W.; Na, B.-k. Effect of Electrical Pulse Forms on the CO_2 Reforming of Methane Using Atmospheric Dielectric Barrier Discharge. *Plasma Chem. Plasma Process.* **2004**, *24*, 57-72.

(150) Indarto, A.; Choi, J.-W.; Lee, H.; Song, H. K. Effect of Additive Gases on Methane Conversion Using Gliding Arc Discharge. *Energy* **2006**, *31*, 2986-2995.

(151) Istadi, I.; Amin, N. A. S. Co-Generation of Synthesis Gas and C_{2+} Hydrocarbons from Methane and Carbon Dioxide in a Hybrid Catalytic-Plasma Reactor: A Review. *Fuel* **2006**, *85*, 577-592.

(152) Li, M. W.; Tian, Y. L.; Xu, G. H. Characteristics of Carbon Dioxide Reforming of Methane Via Alternating Current (AC) Corona Plasma Reactions. *Energ. Fuel.* **2007**, *21*, 2335-2339.

(153) Li, D. H.; Li, X.; Bai, M. G.; Tao, X. M.; Shang, S. Y.; Dai, X. Y.; Yin, Y. X. CO_2 Reforming of CH_4 by Atmospheric Pressure Glow Discharge Plasma: A High Conversion Ability. *Int. J. Hydrogen Energ.* **2009**, *34*, 308-313.

(154) Wang, Q.; Yan, B. H.; Jin, Y.; Cheng, Y. Dry Reforming of Methane in a Dielectric Barrier Discharge Reactor with Ni/Al_2O_3 Catalyst: Interaction of Catalyst and Plasma. *Energ. Fuel.* **2009**, *23*, 4196-4201.

(155) Wang, Q.; Yan, B. H.; Jin, Y.; Cheng, Y. Investigation of Dry Reforming of Methane in a Dielectric Barrier Discharge Reactor. *Plasma Chem. Plasma Process.* **2009**, *29*, 217-228.

(156) Wang, Q.; Cheng, Y.; Jin, Y. Dry Reforming of Methane in an Atmospheric Pressure Plasma Fluidized Bed with $Ni/gamma-Al_2O_3$ Catalyst. *Catal. Today* **2009**, *148*, 275-282.

(157) Rico, V. J.; Hueso, J. L.; Cotrino, J.; Gonzalez-Elipe, A. R. Evaluation of Different Dielectric Barrier Discharge Plasma Configurations as an Alternative Technology for Green C_1 Chemistry in the Carbon Dioxide Reforming of Methane and the Direct Decomposition of Methanol. *J. Phys. Chem. A* **2010**, *114*, 4009-4016.

(158) Sentek, J.; Krawczyk, K.; Mlotek, M.; Kalczewska, M.; Kroker, T.; Kolb, T.; Schenk, A.; Gericke, K. H.; Schmidt-Szalowski, K. Plasma-Catalytic Methane Conversion with Carbon Dioxide in Dielectric Barrier Discharges. *Appl. Catal. B-Environ.* **2010**, *94*, 19-26.

(159) Seyed-Matin, N.; Jalili, A. H.; Jenab, M. H.; Zekordi, S. M.; Afzali, A.; Rasouli, C.; Zamaniyan, A. DC-Pulsed Plasma for Dry Reforming of Methane to Synthesis Gas. *Plasma Chem. Plasma Process.* **2010**, *30*, 333-347.

(160) Yan, B. H.; Wang, Q.; Jin, Y.; Cheng, Y. Dry Reforming of Methane with Carbon Dioxide Using Pulsed DC Arc Plasma at Atmospheric Pressure. *Plasma Chem. Plasma Process.* **2010**, *30*, 257-266.

(161) Pinhão, N. R.; Janeco, A.; Branco, J. B. Influence of Helium on the Conversion of Methane and Carbon Dioxide in a Dielectric Barrier Discharge. *Plasma Chem. Plasma Process.* **2011**, *31*, 427-439.

(162)   Scarduelli, G.; Guella, G.; Ascenzi, D.; Tosi, P. Synthesis of Liquid Organic Compounds from CH_4 and CO_2 in a Dielectric Barrier Discharge Operating at Atmospheric Pressure. *Plasma Process. Polym.* **2011**, *8*, 25-31.

(163)   Schmidt-Szalowski, K.; Krawczyk, K.; Sentek, J.; Ulejczyk, B.; Gorska, A.; Mlotek, M. Hybrid Plasma-Catalytic Systems for Converting Substances of High Stability, Greenhouse Gases and VOC. *Chem. Eng. Res. Des.* **2011**, *89*, 2643-2651.

(164)   Tu, X.; Gallon, H. J.; Twigg, M. V.; Gorry, P. A.; Whitehead, J. C. Dry Reforming of Methane over a Ni/Al_2O_3 Catalyst in a Coaxial Dielectric Barrier Discharge Reactor. *J. Phys. D: Appl. Phys.* **2011**, *44*, 274007.

(165)   Wang, Q.; Shi, H. L.; Yan, B. H.; Jin, Y.; Cheng, Y. Steam Enhanced Carbon Dioxide Reforming of Methane in DBD Plasma Reactor. *Int. J. Hydrogen Energ.* **2011**, *36*, 8301-8306.

(166)   Gallon, H. J.; Tu, X.; Whitehead, J. C. Effects of Reactor Packing Materials on H_2 Production by CO_2 Reforming of CH_4 in a Dielectric Barrier Discharge. *Plasma Process. Polym.* **2012**, *9*, 90-97.

(167)   Kim, T. K.; Lee, W. G. Reaction between Methane and Carbon Dioxide to Produce Syngas in Dielectric Barrier Discharge System. *J. Ind. Eng. Chem.* **2012**, *18*, 1710-1714.

(168)   Kolb, T.; Kroker, T.; Voigt, J. H.; Gericke, K. H. Wet Conversion of Methane and Carbon Dioxide in a DBD Reactor. *Plasma Chem. Plasma Process.* **2012**, *32*, 1139-1155.

(169)   Tu, X.; Whitehead, J. C. Plasma-Catalytic Dry Reforming of Methane in an Atmospheric Dielectric Barrier Discharge: Understanding the Synergistic Effect at Low Temperature. *Appl. Catal. B-Environ.* **2012**, *125*, 439-448.

(170)   Zhang, X. M.; Cha, M. S. Electron-Induced Dry Reforming of Methane in a Temperature-Controlled Dielectric Barrier Discharge Reactor. *J. Phys. D: Appl. Phys.* **2013**, *46*, 415205.

(171)   Chung, W. C.; Pan, K. L.; Lee, H. M.; Chang, M. B. Dry Reforming of Methane with Dielectric Barrier Discharge and Ferroelectric Packed-Bed Reactors. *Energ. Fuel.* **2014**, *28*, 7621-7631.

(172)   Krawczyk, K.; Mlotek, M.; Ulejczyk, B.; Schmidt-Szalowski, K. Methane Conversion with Carbon Dioxide in Plasma-Catalytic System. *Fuel* **2014**, *117*, 608-617.

(173)   Martini, L. M.; Dilecce, G.; Guella, G.; Maranzana, A.; Tonachini, G.; Tosi, P. Oxidation of CH_4 by CO_2 in a Dielectric Barrier Discharge. *Chem. Phys. Lett.* **2014**, *593*, 55-60.

(174)   Pan, K. L.; Chung, W. C.; Chang, M. B. Dry Reforming of CH_4 with CO_2 to Generate Syngas by Combined Plasma Catalysis. *IEEE Trans. Plasma Sci.* **2014**, *42*, 3809-3818.

(175)   Scapinello, M.; Martini, L. M.; Tosi, P. CO_2 Hydrogenation by CH_4 in a Dielectric Barrier Discharge: Catalytic Effects of Nickel and Copper. *Plasma Process. Polym.* **2014**, *11*, 624-628.

(176)   Tu, X.; Whitehead, J. C. Plasma Dry Reforming of Methane in an Atmospheric Pressure AC Gliding Arc Discharge: Co-Generation of Syngas and Carbon Nanomaterials. *Int. J. Hydrogen Energ.* **2014**, *39*, 9658-9669.

(177)   Abd Allah, Z.; Whitehead, J. C. Plasma-Catalytic Dry Reforming of Methane in an Atmospheric Pressure AC Gliding Arc Discharge. *Catal. Today* **2015**, *256*, 76-79.

(178)   Janeco, A.; Pinhao, N. R.; Guerra, V. Electron Kinetics in $He/CH_4/CO_2$ Mixtures Used for Methane Conversion. *J. Phys. Chem. C* **2015**, *119*, 109-120.

(179)   Kameshima, S.; Tamura, K.; Ishibashi, Y.; Nozaki, T. Pulsed Dry Methane Reforming in Plasma-Enhanced Catalytic Reaction. *Catal. Today* **2015**, *256*, 67-75.

(180)   Ozkan, A.; Dufour, T.; Arnoult, G.; De Keyzer, P.; Bogaerts, A.; Reniers, F. CO_2-CH_4 Conversion and Syngas Formation at Atmospheric Pressure Using a Multi-Electrode Dielectric Barrier Discharge. *J. CO2 Util.* **2015**, *9*, 74-81.

(181)   Snoeckx, R.; Zeng, Y. X.; Tu, X.; Bogaerts, A. Plasma-Based Dry Reforming: Improving the Conversion and Energy Efficiency in a Dielectric Barrier Discharge. *RSC Advances* **2015**, *5*, 29799-29808.

(182)   Zeng, Y. X.; Zhu, X. B.; Mei, D. H.; Ashford, B.; Tu, X. Plasma-Catalytic Dry Reforming of Methane over gamma-Al_2O_3 Supported Metal Catalysts. *Catal. Today* **2015**, *256*, 80-87.

(183)   Zheng, X. G.; Tan, S. Y.; Dong, L. C.; Li, S. B.; Chen, H. M. Plasma-Assisted Catalytic Dry Reforming of Methane: Highly Catalytic Performance of Nickel Ferrite Nanoparticles Embedded in Silica. *J. Power Sources* **2015**, *274*, 286-294.

(184)   Scapinello, M.; Martini, L. M.; Dilecce, G.; Tosi, P. Conversion of CH_4/CO_2 by a Nanosecond Repetitively Pulsed Discharge. *J. Phys. D: Appl. Phys.* **2016**, *49*, 075602.

(185)   Liu, C. J.; Mallinson, R.; Lobban, L. Nonoxidative Methane Conversion to Acetylene over Zeolite in a Low Temperature Plasma. *J. Catal.* **1998**, *179*, 326-334.

(186)   Gordon, C. L.; Lobban, L. L.; Mallinson, R. G. Ethylene Production Using a Pd and Ag-Pd-Y-Zeolite Catalyst in a DC Plasma Reactor. *Catal. Today* **2003**, *84*, 51-57.

(187)   Nozaki, T.; Muto, N.; Kadio, S.; Okazaki, K. Dissociation of Vibrationally Excited Methane on Ni Catalyst - Part 2. Process Diagnostics by Emission Spectroscopy. *Catal. Today* **2004**, *89*, 67-74.

(188)   Snoeckx, R.; Setareh, M.; Aerts, R.; Simon, P.; Maghari, A.; Bogaerts, A. Influence of N_2 Concentration in a CH_4/N_2 Dielectric Barrier Discharge Used for CH_4 Conversion into H_2. *Int. J. Hydrogen Energ.* **2013**, *38*, 16098-16120.

(189)   Matsumoto, H.; Tanabe, S.; Okitsu, K.; Hayashi, Y.; Suib, S. L. Selective Oxidation of Methane to Methanol and Formaldehyde with Nitrous Oxide in a Dielectric-Barrier Discharge - Plasma Reactor. *J. Phys. Chem. A* **2001**, *105*, 5304-5308.

(190)   Rueangjitt, N.; Akarawitoo, C.; Sreethawong, T.; Chavadej, S. Reforming of CO_2-Containing Natural Gas Using an AC Gliding Arc System: Effect of Gas Components in Natural Gas. *Plasma Chem. Plasma Process.* **2007**, *27*, 559-576.

(191)   Rueangjitt, N.; Sreethawong, T.; Chavadej, S. Reforming of CO_2-Containing Natural Gas Using an AC Gliding Arc System: Effects of Operational Parameters and Oxygen Addition in Feed. *Plasma Chem. Plasma Process.* **2008**, *28*, 49-67.

(192)   Huang, L. A.; Zhang, X. W.; Chen, L.; Lei, L. C. Direct Oxidation of Methane to Methanol over Cu-Based Catalyst in an AC Dielectric Barrier Discharge. *Plasma Chem. Plasma Process.* **2011**, *31*, 67-77.

(193)   *Inerting or Purging*; University of Missouri-Rolla: Rolla, 2000.

(194)   Lawton, S. A.; Phelps, A. V. Excitation of B1-Sigma-G+ State of O_2 by Low-Energy Electrons. *J. Chem. Phys.* **1978**, *69*, 1055-1068.

(195)   Eliasson, B.; Hirth, M.; Kogelschatz, U. Ozone Synthesis from Oxygen in Dielectric Barrier Discharges. *J. Phys. D: Appl. Phys.* **1987**, *20*, 1421-1437.

(196)   Itikawa, Y. Cross Sections for Electron Collisions with Carbon Dioxide. *J. Phys. Chem. Ref. Data* **2002**, *31*, 749-767.

(197)   Aerts, R.; Somers, W.; Bogaerts, A. Carbon Dioxide Splitting in a Dielectric Barrier Discharge Plasma: A Combined Experimental and Computational Study. *ChemSusChem* **2015**, *8*, 702-716.

(198)   Tsuji, M.; Tanoue, T.; Nakano, K.; Nishimura, Y. Decomposition of CO_2 into CO and O in a Microwave-Excited Discharge Flow of CO_2/He or CO_2/Ar Mixtures. *Chem. Lett.* **2001**, *30*, 22-23.

(199)   Wen, Y. Z.; Jiang, X. Z. Decomposition of CO_2 Using Pulsed Corona Discharges Combined with Catalyst. *Plasma Chem. Plasma Process.* **2001**, *21*, 665-678.

(200)   Mikoviny, T.; Kocan, M.; Matejcik, S.; Mason, N. J.; Skalny, J. D. Experimental Study of Negative Corona Discharge in Pure Carbon Dioxide and Its Mixtures with Oxygen. *J. Phys. D: Appl. Phys.* **2004**, *37*, 64-73.

(201)   Indarto, A.; Choi, J.-W.; Lee, H.; Song, H. K. Conversion of CO_2 by Gliding Arc Plasma. *Environ. Eng. Sci.* **2006**, *23*, 1033-1043.

(202)   Indarto, A.; Yang, D. R.; Choi, J. W.; Lee, H.; Song, H. K. Gliding Arc Plasma Processing of CO_2 Conversion. *J. Hazard. Mater.* **2007**, *146*, 309-315.

(203)   Horvath, G.; Skalny, J. D.; Mason, N. J. FTIR Study of Decomposition of Carbon Dioxide in DC Corona Discharges. *J. Phys. D: Appl. Phys.* **2008**, *41*, 225207.

(204)   Spencer, L.; Gallimore, A. D.; Nguyen, S. V. T. Dissociation of CO_2 in a Radio-Frequency Plasma Source. *4th International Congress on Cold Atmospheric Pressure Plasmas: Sources and Applications, Proceedings* **2009**, 130-133.

(205)   Nunnally, T.; Gutsol, K.; Rabinovich, A.; Fridman, A.; Gutsol, A.; Kemoun, A. Dissociation of CO_2 in a Low Current Gliding Arc Plasmatron. *J. Phys. D: Appl. Phys.* **2011**, *44*, 274009.

(206)   Spencer, L. F.; Gallimore, A. D. Efficiency of CO_2 Dissociation in a Radio-Frequency Discharge. *Plasma Chem. Plasma Process.* **2011**, *31*, 79-89.

(207)   Vesel, A.; Mozetic, M.; Drenik, A.; Balat-Pichelin, M. Dissociation of CO_2 Molecules in Microwave Plasma. *Chem. Phys.* **2011**, *382*, 127-131.

(208)   Aerts, R.; Martens, T.; Bogaerts, A. Influence of Vibrational States on CO_2 Splitting by Dielectric Barrier Discharges. *J. Phys. Chem. C* **2012**, *116*, 23257-23273.

(209)   Wang, S.; Zhang, Y.; Liu, X.; Wang, X. Enhancement of CO_2 Conversion Rate and Conversion Efficiency by Homogeneous Discharges. *Plasma Chem. Plasma Process.* **2012**, *32*, 979-989.

(210)   Yu, Q. Q.; Kong, M.; Liu, T.; Fei, J. H.; Zheng, X. M. Characteristics of the Decomposition of CO_2 in a Dielectric Packed-Bed Plasma Reactor. *Plasma Chem. Plasma Process.* **2012**, *32*, 153-163.

(211)   Spencer, L. F.; Gallimore, A. D. CO_2 Dissociation in an Atmospheric Pressure Plasma/Catalyst System: A Study of Efficiency. *Plasma Sources Sci. Technol.* **2013**, *22*, 015019.

(212)   Van Laer, K.; Bogaerts, A. Improving the Conversion and Energy Efficiency of Carbon Dioxide Splitting in a Zirconia-Packed Dielectric Barrier Discharge Reactor. *Energy Technology* **2015**, *3*, 1038-1044.

(213)   Yap, D.; Tatibouet, J. M.; Batiot-Dupeyrat, C. Carbon Dioxide Dissociation to Carbon Monoxide by Non-Thermal Plasma. *J. CO2 Util.* **2015**, *12*, 54-61.

(214)   Belov, I.; Paulussen, S.; Bogaerts, A. Appearance of a Conductive Carbonaceous Coating in a CO_2 Dielectric Barrier Discharge and Its Influence

on the Electrical Properties and the Conversion Efficiency. *Plasma Sources Sci. Technol.* **2016**, *25*, 015023.

(215) Chen, G. X.; Georgieva, V.; Godfroid, T.; Snyders, R.; Delplancke-Ogletree, M. P. Plasma Assisted Catalytic Decomposition of CO_2. *Appl. Catal. B-Environ.* **2016**, *190*, 115-124.

(216) Mei, D. H.; Zhu, X. B.; Wu, C. F.; Ashford, B.; Williams, P. T.; Tu, X. Plasma-Photocatalytic Conversion of CO_2 at Low Temperatures: Understanding the Synergistic Effect of Plasma-Catalysis. *Appl. Catal. B-Environ.* **2016**, *182*, 525-532.

(217) Ponduri, S.; Becker, M. M.; Welzel, S.; van de Sanden, M. C. M.; Loffhagen, D.; Engeln, R. Fluid Modelling of CO_2 Dissociation in a Dielectric Barrier Discharge. *J. Appl. Phys.* **2016**, *119*, 093301.

(218) Ray, D.; Subrahmanyam, C. CO_2 Decomposition in a Packed DBD Plasma Reactor: Influence of Packing Materials. *RSC Advances* **2016**, *6*, 39492-39499.

(219) Eliasson, B.; Kogelschatz, U.; Xue, B. Z.; Zhou, L. M. Hydrogenation of Carbon Dioxide to Methanol with a Discharge-Activated Catalyst. *Ind. Eng. Chem. Res.* **1998**, *37*, 3350-3357.

(220) Hayashi, N.; Yamakawa, T.; Baba, S. Effect of Additive Gases on Synthesis of Organic Compounds from Carbon Dioxide Using Non-Thermal Plasma Produced by Atmospheric Surface Discharges. *Vacuum* **2006**, *80*, 1299-1304.

(221) Kano, M.; Satoh, G.; Iizuka, S. Reforming of Carbon Dioxide to Methane and Methanol by Electric Impulse Low-Pressure Discharge with Hydrogen. *Plasma Chem. Plasma Process.* **2012**, *32*, 177-185.

(222) Zeng, Y.; Tu, X. Plasma-Catalytic CO_2 Hydrogenation at Low Temperatures. *IEEE Trans. Plasma Sci.* **2016**, *44*, 405-411.

(223) Liu, C. J.; Xu, G. H.; Wang, T. M. Non-Thermal Plasma Approaches in CO_2 Utilization. *Fuel Process. Technol.* **1999**, *58*, 119-134.

(224) Belov, I.; Vanneste, J.; Aghaee, M.; Paulussen, S.; Bogaerts, A. Synthesis of Micro- and Nanomaterials in CO_2 and CO Dielectric Barrier Discharges. *Plasma Process. Polym.* **2016**, *DOI: 10.1002/ppap.201600065*.

(225)   Snoeckx, R.; Ozkan, A.; Reniers, F.; Bogaerts, A. The Quest for Value-Added Products from CO_2 and H_2O in a Dielectric Barrier Discharge Plasma: A Chemical Kinetics Study. *ChemSusChem* **2016**, *DOI: 10.1002/cssc.201601234*.

(226)   Neyts, E. C.; Ostrikov, K.; Sunkara, M. K.; Bogaerts, A. Plasma Catalysis: Synergistic Effects at the Nanoscale. *Chem. Rev.* **2015**, *115*, 13408-13446.

(227)   Aerts, R. Experimental and Computational Study of Dielectric Barrier Discharges for Environmental Applications. University of Antwerp, Antwerpen, 2014.

(228)   Aerts, R.; Snoeckx, R.; Bogaerts, A. In-Situ Chemical Trapping of Oxygen in the Splitting of Carbon Dioxide by Plasma. *Plasma Process. Polym.* **2014**, *11*, 985-992.

(229)   Snoeckx, R.; Heijkers, S.; Van Wesenbeeck, K.; Lenaerts, S.; Bogaerts, A. CO_2 Conversion in a Dielectric Barrier Discharge Plasma: N_2 in the Mix as a Helping Hand or Problematic Impurity? *Energ. Environ. Sci.* **2016**, *9*, 999-1011.

(230)   Van Laer, K.; Bogaerts, A. Fluid Modelling of a Packed Bed Dielectric Barrier Discharge Plasma Reactor. *Plasma Sources Sci. Technol.* **2016**, *25*, 015002.

(231)   Janev, R. K., *Atomic and Molecular Processes in Fusion Edge Plasmas*; Plenum Press: New York, USA, 1995.

(232)   National Institute for Fusion Science (NIFS) of Japan *Cross Sections and Rate Coefficients for Electron-Impact Ionization of Hydrocarbon Molecules*; Toki, Gifu, Japan, 2001.

(233)   Janev, R. K.; Reiter, D. Collision Processes of Chy and Chy+ Hydrocarbons with Plasma Electrons and Protons. *Phys. Plasmas* **2002**, *9*, 4071-4081.

(234)   Janev, R. K.; Reiter, D. Collision Processes of Hydrocarbon Species in Hydrogen Plasmas. Part 1. The Methane Family. *ChemInform* **2003**, *34*.

(235)   Janev, R. K.; Reiter, D. Collision Processes of Hydrocarbon Species in Hydrogen Plasmas. Part 2. The Ethane and Propane Families. *ChemInform* **2003**, *34*.

(236)   Janev, R. K.; Reiter, D. Collision Processes of C2,3hy and C2,3hy+ Hydrocarbons with Electrons and Protons. *Phys. Plasmas* **2004**, *11*, 780-829.

(237)   Engelhardt, A. G.; Phelps, A. V. Elastic and Inelastic Collision Cross Sections in Hydrogen and Deuterium from Transport Coefficients. *Phys. Rev.* **1963**, *131*, 2115-2128.

(238)   Trajmar, S.; Register, D. F.; Chutjian, A. Electron-Scattering by Molecules .2. Experimental Methods and Data. *Phys. Rep.* **1983**, *97*, 221-356.

(239)   Tawara, H.; Kato, T. Total and Partial Ionization Cross Sections of Atoms and Ions by Electron Impact. *Atom. Data Nucl. Data* **1987**, *36*, 167-353.

(240)   Corrigan, S. J. B. Dissociation of Molecular Hydrogen by Electron Impact. *J. Chem. Phys.* **1965**, *43*, 4381-4386.

(241)   Kossyi, I. A.; Kostinsky, A. Y.; Matveyev, A. A.; Silakov, V. P. Kinetic Scheme of the Non-Equilibrium Discharge in Nitrogen-Oxygen Mixtures. *Plasma Sources Sci. Technol.* **1992**, *1*, 207-220.

(242)   Gudmundsson, J. T.; Kouznetsov, I. G.; Patel, K. K.; Lieberman, M. A. Electronegativity of Low-Pressure High-Density Oxygen Discharges. *J. Phys. D: Appl. Phys.* **2001**, *34*, 1100-1109.

(243)   Joshipura, K. N.; Patel, P. M. Cross-Sections of E--O Scattering at Intermediate and High-Energies (E(I) = 8.7-1000 Ev). *Phys. Rev. A* **1993**, *48*, 2464-2467.

(244)   Laher, R. R.; Gilmore, F. R. Updated Excitation and Ionization Cross Sections for Electron Impact on Atomic Oxygen. *J. Phys. Chem. Ref. Data* **1990**, *19*, 277-305.

(245)   Matejcik, S.; Kiendler, A.; Cicman, P.; Skalny, J.; Stampfli, P.; Illenberger, E.; Chu, Y.; Stamatovic, A.; Mark, T. D. Electron Attachment to Molecules and Clusters of Atmospheric Relevance: Oxygen and Ozone. *Plasma Sources Sci. Technol.* **1997**, *6*, 140-146.

(246)   http://www.kinema.com

(247)   http://www.lxcat.laplace.univ-tlse.fr

(248)   McConkey, J. W.; Malone, C. P.; Johnson, P. V.; Winstead, C.; McKoy, V.; Kanik, I. Electron Impact Dissociation of Oxygen-Containing Molecules - a Critical Review. *Phys. Rep.* **2008**, *466*, 1-103.

(249)   Rapp, D.; Briglia, D. D. Total Cross Sections for Ionization and Attachment in Gases by Electron Impact .2. Negative-Ion Formation. *J. Chem. Phys.* **1965**, *43*, 1480-1489.

(250)   Itikawa, Y.; Mason, N. Cross Sections for Electron Collisions with Water Molecules. *J. Phys. Chem. Ref. Data* **2005**, *34*, 1-22.

(251)   Riahi, R.; Teulet, P.; Ben Lakhdar, Z.; Gleizes, A. Cross-Section and Rate Coefficient Calculation for Electron Impact Excitation, Ionisation and Dissociation of H-2 and OH Molecules. *Eur. Phys. J. D* **2006**, *40*, 223-230.

(252)   Florescu-Mitchell, A. I.; Mitchell, J. B. A. Dissociative Recombination. *Phys. Rep.* **2006**, *430*, 277-374.

(253)   Tsang, W.; Hampson, R. F. Chemical Kinetic Data Base for Combustion Chemistry. Part I. Methane and Related Compounds. *J. Phys. Chem. Ref. Data* **1986**, *15*, 1087-1279.

(254)   Baulch, D. L.; Cobos, C. J.; Cox, R. A.; Esser, C.; Frank, P.; Just, T.; Kerr, J. A.; Pilling, M. J.; Troe, J.; Walker, R. W., et al. Evaluated Kinetic Data for Combustion Modeling. *J. Phys. Chem. Ref. Data* **1992**, *21*, 411-734.

(255)   Tsang, W. Chemical Kinetic Data Base for Combustion Chemistry. Part 3: Propane. *J. Phys. Chem. Ref. Data* **1988**, *17*, 887-951.

(256)   Tsang, W. Chemical Kinetic Data-Base for Combustion Chemistry .5. Propene. *J. Phys. Chem. Ref. Data* **1991**, *20*, 221-273.

(257)   Stewart, P. H.; Larson, C. W.; Golden, D. M. Pressure and Temperature-Dependence of Reactions Proceeding Via a-Bound Complex .2. Application to 2ch3->C2h5+H. *Combust. Flame* **1989**, *75*, 25-31.

(258)   Laufer, A. H.; Fahr, A. Reactions and Kinetics of Unsaturated C-2 Hydrocarbon Radicals. *Chem. Rev.* **2004**, *104*, 2813-2832.

(259)   Harding, L. B.; Guadagnini, R.; Schatz, G. C. Theoretical-Studies of the Reactions H+Ch->C+H2 and C+H2->Ch2 Using an Abinitio Global Ground-State Potential Surface for Ch2. *J. Phys. Chem.* **1993**, *97*, 5472-5481.

(260)   Lin, S. Y.; Guo, H. Case Study of a Prototypical Elementary Insertion Reaction: C(D-1)+H-2 -> Ch+H. *J. Phys. Chem. A* **2004**, *108*, 10066-10071.

(261)   Harding, L. B.; Georgievskii, Y.; Klippenstein, S. J. Predictive Theory for Hydrogen Atom - Hydrocarbon Radical Association Kinetics. *J. Phys. Chem. A* **2005**, *109*, 4646-4656.

(262)   Harding, L. B.; Klippenstein, S. J.; Georgievskii, Y. On the Combination Reactions of Hydrogen Atoms with Resonance-Stabilized Hydrocarbon Radicals. *J. Phys. Chem. A* **2007**, *111*, 3789-3801.

(263)   Hadj-Ziane, S.; Held, B.; Pignolet, P.; Peyrous, R.; Coste, C. Ozone Generation in an Oxygen-Fed Wire-to-Cylinder Ozonizer at Atmospheric-Pressure. *J. Phys. D: Appl. Phys.* **1992**, *25*, 677-685.

(264)   Baulch, D. L.; Bowman, C. T.; Cobos, C. J.; Cox, R. A.; Just, T.; Kerr, J. A.; Pilling, M. J.; Stocker, D.; Troe, J.; Tsang, W., et al. Evaluated Kinetic Data for Combustion Modeling: Supplement Ii. *J. Phys. Chem. Ref. Data* **2005**, *34*, 757-1397.

(265)   Atkinson, R.; Baulch, D. L.; Cox, R. A.; Crowley, J. N.; Hampson, R. F.; Hynes, R. G.; Jenkin, M. E.; Rossi, M. J.; Troe, J. Evaluated Kinetic and Photochemical Data for Atmospheric Chemistry: Volume Ii - Gas Phase Reactions of Organic Species. *Atmos. Chem. Phys.* **2006**, *6*, 3625-4055.

(266)   Fang, D. C.; Fu, X. Y. Casscf and Cas+1+2 Studies on the Potential Energy Surface and the Rate Constants for the Reactions between Ch2 and O-2. *J. Phys. Chem. A* **2002**, *106*, 2988-2993.

(267)   Dean, A. J.; Davidson, D. F.; Hanson, R. K. A Shock-Tube Study of Reactions of C Atoms with H-2 and O2 Using Excimer Photolysis of C3o2 and C Atom Atomic Resonance-Absorption Spectroscopy. *J. Phys. Chem.* **1991**, *95*, 183-191.

(268)   Atkinson, R.; Baulch, D. L.; Cox, R. A.; Crowley, J. N.; Hampson, R. F.; Hynes, R. G.; Jenkin, M. E.; Rossi, M. J.; Troe, J. Evaluated Kinetic and Photochemical Data for Atmospheric Chemistry: Volume I - Gas Phase Reactions of O-X, Hox, Nox and Sox Species. *Atmos. Chem. Phys.* **2004**, *4*, 1461-1738.

(269)   Atkinson, R.; Baulch, D. L.; Cox, R. A.; Hampson, R. F.; Kerr, J. A.; Troe, J. Evaluated Kinetic and Photochemical Data for Atmospheric Chemistry .3.

Iupac Subcommittee on Gas Kinetic Data Evaluation for Atmospheric Chemistry. *J. Phys. Chem. Ref. Data* **1989**, *18*, 881-1097.

(270) Pereira, R. D.; Baulch, D. L.; Pilling, M. J.; Robertson, S. H.; Zeng, G. Temperature and Pressure Dependence of the Multichannel Rate Coefficients for the Ch3+OH System. *J. Phys. Chem. A* **1997**, *101*, 9681-9693.

(271) Carstensen, H. H.; Dean, A. M. Rate Constants for the Abstraction Reactions Ro2 + C2h6; R = H, Ch3, and C2h5. *P. Combust. Inst.* **2005**, *30*, 995-1003.

(272) Sun, H.; Tang, Y. Z.; Wang, Z. L.; Pan, X. M.; Li, Z. S.; Wang, R. S. Dft Investigation of the Mechanism of Ch2co+O(P-3) Reaction. *Int. J. Quantum Chem.* **2005**, *105*, 527-532.

(273) Kuwata, K. T.; Hasson, A. S.; Dickinson, R. V.; Petersen, E. B.; Valin, L. C. Quantum Chemical and Master Equation Simulations of the Oxidation and Isomerization of Vinoxy Radicals. *J. Phys. Chem. A* **2005**, *109*, 2514-2524.

(274) Delbos, E.; Fittschen, C.; Hippler, H.; Krasteva, N.; Olzmann, M.; Viskolcz, B. Rate Coefficients and Equilibrium Constant for the Ch2cho+O-2 Reaction System. *J. Phys. Chem. A* **2006**, *110*, 3238-3245.

(275) Tyndall, G. S.; Wallington, T. J.; Ball, J. C. FTIR Product Study of the Reactions Ch3o2+Ch3o2 and Ch3o2+O-3. *J. Phys. Chem. A* **1998**, *102*, 2547-2554.

(276) Jodkowski, J. T.; Rayez, M. T.; Rayez, J. C.; Berces, T.; Dobe, S. Theoretical Study of the Kinetics of the Hydrogen Abstraction from Methanol. 3. Reaction of Methanol with Hydrogen Atom, Methyl, and Hydroxyl Radicals. *J. Phys. Chem. A* **1999**, *103*, 3750-3765.

(277) Hou, H.; Wang, B. S.; Gu, Y. S. Mechanism of the OH+Ch2co Reaction. *Phys. Chem. Chem. Phys.* **2000**, *2*, 2329-2334.

(278) Tsang, W. Chemical Kinetic Data Base for Combustion Chemistry. Part 2. Methanol. *J. Phys. Chem. Ref. Data* **1987**, *16*, 471-508.

(279) Xu, Z. F.; Park, J.; Lin, M. C. Thermal Decomposition of Ethanol. Iii. A Computational Study of the Kinetics and Mechanism for the Ch3+C2h5oh Reaction. *J. Chem. Phys.* **2004**, *120*, 6593-6599.

(280)   Jasper, A. W.; Klippenstein, S. J.; Harding, L. B.; Ruscic, B. Kinetics of the Reaction of Methyl Radical with Hydroxyl Radical and Methanol Decomposition. *J. Phys. Chem. A* **2007**, *111*, 3932-3950.

(281)   Park, J.; Xu, Z. F.; Lin, M. C. Thermal Decomposition of Ethanol. Ii. A Computational Study of the Kinetics and Mechanism for the H+C2h5oh Reaction. *J. Chem. Phys.* **2003**, *118*, 9990-9996.

(282)   Slemr, F.; Warneck, P. Kinetics of Reaction of Atomic-Hydrogen with Methyl Hydroperoxide. *Int. J. Chem. Kinet.* **1977**, *9*, 267-282.

(283)   Lu, C. W.; Chou, S. L.; Lee, Y. P.; Xu, S. C.; Xu, Z. F.; Lin, M. C. Experimental and Theoretical Studies of Rate Coefficients for the Reaction O(P-3)+Ch3oh at High Temperatures. *J. Chem. Phys.* **2005**, *122*, 244314.

(284)   Woodall, J.; Agúndez, M.; Markwick-Kemper, A. J.; Millar, T. J. The Umist Database for Astrochemistry 2006. *Astron. Astrophys.* **2007**, *466*, 1197-1204.

(285)   Kim, Y. H.; Fox, J. L. The Chemistry of Hydrocarbon Ions in the Jovian Ionosphere. *Icarus* **1994**, *112*, 310-325.

(286)   Tahara, H.; Minami, K.; Murai, A.; Yasui, T.; Yoshikawa, T. Diagnostic Experiment and Kinetic-Model Analysis of Microwave Ch4/H-2 Plasmas for Deposition of Diamond-Like Carbon-Films. *Jpn. J. Appl. Phys. 1* **1995**, *34*, 1972-1979.

(287)   Gudmundsson, J. T.; Thorsteinsson, E. G. Oxygen Discharges Diluted with Argon: Dissociation Processes. *Plasma Sources Sci. Technol.* **2007**, *16*, 399-412.

(288)   Ionin, A. A.; Kochetov, I. V.; Napartovich, A. P.; Yuryshev, N. N. Physics and Engineering of Singlet Delta Oxygen Production in Low-Temperature Plasma. *J. Phys. D: Appl. Phys.* **2007**, *40*, R25-R61.